1991

WAVE OVERTOPPING: A COMPARISON OF PHYSICAL AND NUMERICAL STUDIES

Murton, Gary John

WAVE OVERTOPPING:

A COMPARISON OF PHYSICAL AND NUMERICAL STUDIES

GARY JOHN MURTON B.Sc.(Hons)

Submitted to the Council for National Academic Awards in partial fulfilment for the Degree of Doctor of Philosophy.

Sponsoring Establishment:

POLYTECHNIC SOUTH WEST
Department of Civil and Structural Engineering

June 1991

WAVE OVERTOPPING: A COMPARISON OF PHYSICAL AND NUMERICAL METHODS

by

GARY JOHN MURTON

The overtopping of low-crested breakwater is investigated by means of hydraulic and mathematical models.

A conventional laboratory wavemaker with a wedge-type paddle is converted into an absorbing wavemaker so that it can be used to investigate accurately wave overtopping of reflective coastal structures. The absorption system is achieved by use of a feedback loop added to the control circuit. The design criteria and implementation of the circuit are presented in detail. Enhanced control software is used to generate different 'random' sea states with the same statistical properties.

The absorption system is validated by an extensive series of tests made possible by the development of automated data acquisition and analysis software. Particular attention is given to the derivation of incident and reflected wave spectra. The results show over 90% success in reducing reflected waves. It is also possible to establish stable standing wave patterns over a wide frequency range. The results show significant improvement over similar existing wavemakers and in effect create an open-ended channel in the sense that the test structure hardly influences incident wave conditions.

A closely controlled series of overtopping tests was carried out using the absorption system to prevent any re-reflections. Equipment and software were designed to quantify the overtopping rates for the structures used. The design and implementation of all aspects of the tests is fully described.

Overtopping tests were carried out on breakwaters with smooth 1:1 and 1:2 seaward slopes. The results are tabulated and plotted in a dimensionless form which permits comparison with earlier work carried out at Hydraulics Research Ltd. The range of available data is extended and the new data for fully-developed sea states shown to be compatible with a linear extrapolation of the earlier results. It is believed that the earlier results were obtained using fully developed sea states but this is not known for certain. The importance of rigorously defining and publishing both test conditions and analysis techniques is highlighted.

In the numerical study the 1-D mass and continuity equations were solved by a hybrid finite element/finite difference scheme. Whilst a good comparison is achieved between the physical and numerical tests for breakwater slopes of 1:2 and less, realistic results are not achieved for steeper slopes. The reasons for this are discussed and the results presented.

Both sets of model tests add valuable data to an area presently lacking detailed information.

ACKNOWLEDGEMENTS

I would like to thank all the people who helped in the work described in this thesis and its preparation. In particular, thanks go to Dr. G.N. Bullock for his continual guidance and patience; the staff at Hydraulic Research Ltd; and to all my family and friends for their continual support and encouragement.

CONTENTS

List of Tables
List of Figures
List of Plates

1. INTRODUCTION

1.1 Introduction 1
1.2 Scope of Work 2
1.3 Review of Previously Related Work 4

2. LABORATORY WAVE GENERATION SYSTEM

2.1 Introduction 20
2.2 Wave Paddle 22
2.3 Spending Beach 22
2.4 Wave Gauges 23
2.5 Paddle Control Signal 24
2.6 Data Acquisition 28

3. ANALYSIS THEORY

3.1 Introduction 30
3.2 Linear Wave Theory 30
3.3 Regular Waves - A Wave Envelope Analysis 34
3.4 Random Waves - Energy Spectra 39
3.5 Statistics from Spectrum 45
3.6 Random Waves - Frequency Response Function Method 46
3.7 Programming Considerations 50

4. SOFTWARE DEVELOPMENT

4.1 Introduction 51
4.2 Data Acquisition 51
4.3 Wave Data Processing 53
4.4 Wave Data Analysis 54
4.5 Graphics 55
4.6 Regular Wave Reflection Progam 55
4.7 Programming Considerations 55
4.8 Program Flowcharts 56
4.9 Quality Assurance 56

5. CALIBRATION AND OPTIMISATION OF THE PADDLE

5.1 Introduction 60
5.2 Paddle Dynamic Characteristics 60
5.3 Conventions 60
5.4 Test Procedure 61
5.5 Results 61
5.6 Theoretical Transfer Function 69
5.7 Hydraulic System Problems 73

6. A WAVE ABSORPTION SYSTEM

6.1 Introduction 74
6.2 Design Criteria for a Wave Absorption System 74
6.3 Wave Absorption Theory 76
6.4 Practical Implementation 80
6.5 Physical Implementation 82
6.6 Operation of Absorption System 83
6.7 Calibration and Optimisation 84
6.8 Sensitivity 85
6.9 Appraisal of Wave Absorption System 85

7. TESTS ON WAVE ABSORPTION SYSTEM

7.1 Introduction 87
7.2 Wavescreens 87
7.3 Regular Wave Tests 89
7.4 Random Wave Tests 96
7.5 Conclusions 115
7.6 Recommendations to improve Wave Absorption system 115

8. WAVE OVERTOPPING

8.1 Introduction 116
8.2 Factors Influencing the Overtopping Discharge 117
8.3 Maximum Overtopping Discharge 120
8.4 Design of breakwater and Overtopping Measurement Equipment 122
8.5 A Count of Overtopping Waves 125
8.6 Incident and Reflected Spectra 126
8.7 Wave Spectrum Generation 127
8.8 Tests on Wave Absorption System 128
8.9 Test Procedure 129

9. WAVE OVERTOPPING TEST RESULTS

9.1 Introduction 130
9.2 Breakwaters 130
9.3 Results 132
9.4 Wave Absorption 159
9.5 Summary and Conclusions 162

10. NUMERICAL OVERTOPPING MODEL

10.1 Introduction 165
10.2 Governing Equations 166
10.3 The Finite Element Method 166
10.4 Problem Domain 173
10.5 Solution System - Space Domain 174
10.6 Time Integration 179
10.7 The Forcing Function 181
10.8 Boundary Conditions 182
10.9 Element Splitting 182
10.10 Weir Function 188
10.11 Programming Considerations 188

11. NUMERICAL OVERTOPPING RESULTS

11.1 Introduction 192
11.2 Regular Wave Tests 193
11.3 Reflections 201
11.4 The Effect of Choice of Numerical Parameters on the Overtopping Results 202
11.5 Ill-Conditioning 203
11.6 Validation,Calibration and Accuracy of the Model 204
11.7 Possible Improvements to Model 205
11.8 Conclusions 206

12. SUMMARY AND CONCLUSIONS

12.1 Conclusions 207
12.2 Recommendations for Future Work 217

Appendices

A Computer Output 219
B Frequency Response Function Method 233
C Wave Gauge Spacing 239
D Spectral Equations 242
E Vertical Acceleration Term 247

References 253

LIST OF TABLES

3.1 Energy Spectrum Parameters

5.1 Measured Paddle Transfer Function
5.2 Comparison of Measured and Theoretical Transfer Function

7.1 Wavescreen Combinations
7.2 Notations used on Figure 7.4
7.3 Random Wave Parameters
7.4 Results from Single Gauge Analysis
7.5 Random Wave Test Results

8.1 Feedback Connections

9.1 Reflection Coefficient Values for 1:1 Slope
9.2 Reflection Coefficient Values for 1:2 Slope
9.3 Wave Statistics from 3 Gauges, 1:1 Slope
9.4 Wave Statistics from 3 Gauges, 1:2 Slope
9.5 A Comparison of the Dimensionless Parameters calculated at the Breakwater Toe and 1.98m Offshore
9.6 Overtopping Discharge from 1:1 Slope Breakwater
9.7 Overtopping Discharge from 1:2 Slope Breakwater
9.8 A Comparison of Overtopping Discharge Measured over a Sharp-Crested Weir and Volumetrically over the Breakwater
9.9 A Comparison of Overtopping Discharge from two different spectra
9.10 Summary of Regular Wave Test Results
9.11 The Effect of Wave Absorption on Overtopping Discharge 1:1 slope
9.12 The Effect of Wave Absorption on Overtopping Discharge 1:2 slope

10.1 Numerical Model Subroutines

11.1 Range of Regular Wave Tests for Numerical Model
11.2 Comparison of Discharge
11.3 Example Velocity Results
11.4 Comparison of Surface Elevations for Various Time-Steps
11.5 Results up to Run-time Error 'divide by zero'

A.1 Statistics Menu
A.2 Data File Handling Programs

C.1 Wave Gauge Spacings for Frequency Response Analysis

LIST OF FIGURES

1.1 'Side-splitters' to reduce reflection
1.2 Lax-wendroff mesh

2.1 Plan and Elevation of Laboratory
2.2 Laboratory Equipment Arrangements

3.1 Anti-node at Vertical Barrier
3.2 Anti-node at Paddle Front
3.3 Node at Paddle Front
3.4 Section of Wave Envelope
3.5 Example of Wave Envelope for 0.5Hz Waves
3.6 Regular Wave Test Data Sheet
3.7 Mean Zero Up-crossing Period
3.8 Variance Density Spectrum - Cosine Window
3.9 Variance Density Spectrum - No Window
3.10 Schemitisation of Laboratory Reflections

4.1 Data Acquisition Flowchart
4.2 Analysis Suite Flowchart
4.3 Frequency Response Function Flowchart

5.1 Reflection Coefficient in 1.0m
5.2 Reflection Coefficient in 0.8m
5.3 Reflection Coefficient in 0.6m
5.4 Transfer Function in 1.0m
5.5 Transfer Function in 0.8m
5.6 Transfer Function in 0.6m
5.7 Theoretical Transfer Function - Definitions
5.8 Theoretical Transfer Functions
5.9 Comparison of Theoretical and Measured Transfer Functions

6.1 Schematic Representation of Absorbing Wave Maker
6.2 Block Diagram of Wave Maker Systems
6.3 Absorption Filter-Loop Gain
6.4 Filter Characteristics
6.5 Absorption Filter-Block Diagram

7.1 Transfer Function with and without Absorption
7.2 Reflection Characteristics - No Wavescreen
7.3 Transfer Function - Full Wavescreen
7.4 Transfer Function - Full Wavescreen
7.5 Reflection Characteristics - No Wavescreen
7.6 Paddle Stroke Variation
7.7 Paddke Stroke Variation
7.8 Wave Amplitude/Paddle Stroke Amplitude vs Frequency
7.9 - 7.20 Regular Wave Spectra
7.21 'Point' Spectrum
7.22 'Point' Spectrum
7.23 20 Second Wave Record
7.24 - 7.30 Frequency Response Function Graphical Output
7.31 - 7.34 Incident Spectra

8.1 A Typical Breakwater Profile
8.2 Test Breakwater Profile
8.3 Coefficients A for Overtopping Discharge
8.4 Coefficients B for Overtopping Discharge
8.5 Side Panels
8.6 Breakwater Construction Details
8.7 Profiled Discharge Weir
8.8 Wave Gauge Location

9.1 P-M Spectrum
9.2 - 9.5 Frequency Response Function Test Results
9.6 Test Spectra Overlain
9.7 Incident Spectra
9.8 Reflected Spectra
9.9 Incident Specrrum - Newman
9.10 Reflected Spectrum - Newman
9.11 Theoretical Newman Comparison
9.12 Reflection Coefficients 1:1 Slope
9.13 Reflection Coefficients 1:2 Slope
9.14 Comparison of Reflection Coefficients
9.15- 9.18 Wave Records
9.19- 9.20 Breakwater Gauge Wave Records
9.21 Dimensionless Overtopping
9.22 Dimensionless Overtopping
9.23 Comparison of PM and Newman Spectra
9.24 Percentage Waves Overtopping
9.25 Percentage Waves Overtopping
9.26 Incident Spectra
9.27 Incident Spectra
9.28 Comparison of 'Point' Spectra
9.29 Comparison of 'Point' Spectra

10.1 Linear Shape Functions
10.2 Assembly of Line Elements
10.3 Spatial Discretisation
10.4 Predictor-Corrector Scheme
10.5 Sinusoidal Wave
10.6 Moving Downstream Boundary
10.7 Water Profile and End-Element at Time t
10.8 Water Profile and End-Element at Time t+Δt
10.9 Position at Time t
10.10 Position at Time (t+Δt)
10.11 Element Splitting at Time (t+Δt)
10.12 Downstream Condition at Time t and (t+Δt)
10.13 Numerical Model Flowchart

11.1 Dimensionless Discharge and Freeboard
11.2 Dimensionless Discharge and Freeboard
11.3- 11.6 Run-Up Profiles
11.7 Superimposition of Run-Up for Successive Time Steps

D.1 Cosine Taper Window Function

LIST OF PLATES

2.1 Wave Paddle
2.2 Spending Beach

6.1 Paddle Wave Gauge

7.1 Wavescreens
7.2 Wavescreens

8.1 1:1 Breakwater
8.2 1:2 Breakwater
8.3 Overtopping Weir
8.4 Calibrated Weir and Collection Sump

GLOSSARY

A-D	-	Analogue to Digital. The conversion of a continuous signal to a series of discrete points.
Berm	-	Flat central portion on some breakwaters.
Compiled	-	Computer code translated from a programming language to machine instructions.
D-A	-	Digital to Analogue. The opposite of A-D conversion.
EPROM	-	Erasable Programmable Read Only Memory. A computer chip used for software or data storage.
FFT	-	Fast Fourier Transform.
Freeboard	-	The level of a breakwater crest above still water level.
Gain	-	Voltage amplitude supplied to wave generator.
IEEE	-	Institution of Electric and Electronic Engineers. An IEEE-488 is an industry standard computer connection.
Primary Address	-	Numeric value by which the computer can recognise any connected peripherals.
Secondary Address	-	Additional numeric value by which the computer can recognise sub-divisions of the peripheral called by its primary address.
Softkey	-	A key on the computer terminal keyboard programmed to perform a defined task.
Spending Beach	-	An absorbent slope used to minimise reflections in a laboratory wave channel.
Wavescreen	-	A flexible system of vertical slabs to produce varying degrees of reflection in the wave channel.

NOTATION

a_i	-	A water surface elevation - Incident Waves
A_i	-	Laplace Transform of a_i
a_r	-	A water surface elevation - Reflected Waves
A_r	-	Laplace Transform of a_r
a_m	-	Mean acceleration at top of Run-up
a_T	-	Lagrangian acceleration at top of Run-up
b	-	Submergence of paddle front at mid-stroke
c	-	Real part of cross-spectrum s_{xy}
C	-	Wave celerity
d	-	Water depth
d_B	-	Berm depth
D_t	-	Sampling Interval
$\bar{E}$	-	Mean Energy
E_I	-	Incident Energy
E_R	-	Reflected Energy
f	-	Frequency
f_m	-	Peak (or modal) frequency
F_x	-	Vertical acceleration term
g	-	Acceleration due to gravity
G_k	-	Variance Density
h	-	Peak to trough wave height
$\bar{H}_S$	-	Significant wave height
H_I	-	Incident wave height
H_R	-	Reflected wave height
H	-	Frequency response operator
H_{si}	-	Incident significant wave height
k	-	Wave number = $2\pi/L$
$k_{r(\rho)}$	-	Reflection coefficient
l	-	Element length
L	-	Wave length
L_o	-	Deep water wave length = $gT^2/2\pi$
L	-	Differential operator
M	-	Breakwater slope as 1:M
M_o	-	Zeroth moment of spectrum (σ)
N_i	-	Galerkin trial function
P	-	Number of degrees of freedom
q	-	Imaginary part of cross-spectrum S_{xy}
Q	-	Overtopping discharge
Q^+	-	Dimensionless overtopping

R	–	Run-up parameter
R^+	–	Dimensionless freeboard
R_c	–	Crest elevation
$\bar{R}$	–	Weighted residual
s	–	paddle stroke
$S(f)$	–	Spectral density
S	–	Wave steepness
S_{ii}	–	Incident spectrum
S_{rr}	–	Reflected spectrum
S_{xx}	–	Spectrum at x
S_{yy}	–	Spectrum at y
S_{xy}	–	Cross-spectrum
S_{11}	–	Spectrum at location 1
S_{12}	–	Incident spectrum between 1 and 2 (etc)
S_{22}	–	Spectrum at location 2
S_{33}	–	Spectrum at location 3
t	–	Time
T_r	–	Time slice
T	–	Wave period
T_z	–	Zero-crossing period
U	–	Horizontal water particle velocity
V_c	–	Paddle control signal
V_f	–	Filtered paddle control signal
W_b	–	Berm width
$x(t)$	–	Paddle displacement
x,y,z	–	Cartesion co-ordinates
$*$	–	Complex conjugate
$*$	–	Dimensionless parameter
o	–	Time derivative
$_1$	–	Space derivative
ϵ	–	Surf similarity parameter
ϵ_r	–	Normalised standard error
θ	–	Breakwater slope $\tan\theta = 1/M$
ρ	–	Density
ρ^2	–	Reflection coefficient
η	–	Water surface elevation
Φ	–	Transfer function of reflected wave
Φ	–	Numeric variable
w	–	Angular frequency

CHAPTER 1

1.1 Introduction

Waves incident on a structure such as a breakwater or sea wall are usually subject to a significant amount of reflection. In the field the reflected waves generally propagate back out to sea and are eventually lost to the coastal system. The system in effect has an open or absorbent seaward boundary.

In a conventional laboratory wave channel the situation is quite different due to the 'seaward' boundary being closed by some type of wave paddle. The typical paddle is highly reflective so that, in this closed system, waves reflected by a model structure are re-reflected back towards it. This establishes an unnatural system of positive feedback in which the waves incident on the model are the sum of the new input from the paddle and the re-reflected waves. The characteristics of the incident waves are changed in an uncontrolled way with the wave height increasing until losses in the system dissipate energy, possibly through an increase of wave breaking, at a rate equal to the primary input from the paddle. The resonance resulting from the combination of high reflection and low losses can lead to water being thrown from the channel.

Recently, due to advances in electronics, it has become possible to detect this positive feedback and by means of a suitable filter system to modify the primary control signal in order to remove or 'absorb' the re-reflected part of the wave train.

An 'absorbing' paddle of this type will allow more controlled or accurate laboratory model tests than the conventional paddle.

Few breakwater overtopping model studies have been carried out and of these fewer still used a randomly generated sea to conduct the tests.

An accurate assessment of the likely wave overtopping of a particular breakwater is of prime importance to the coastal engineer at the design stage. The degree of overtopping permitted will depend upon the use for which the breakwater is to be designed.

Practical full-scale measurement has so far proved to be a very difficult proposition and the engineer is thus very dependent upon results obtained from laboratory model studies. Use of an absorption system as outlined above will allow a more controlled approach to the measurement problem and as a result much better data should result.

The other problem which confronts the design engineer is, unlike in many other branches of engineering, the lack of good, well verified numerical solutions to the problem of wave overtopping.

Mathematical solutions have been derived for the closely related run-up problem, although these are generally for the more mild 'beach' type slope, rather than the steeper breakwater slope. The development of a reliable suite of computer programs would reduce the need for costly model studies as well as increase the knowledge base of what is still a largely unknown area.

1.2 Scope of Work

The work described in this thesis deals with some of the problems outlined above.

A 2-D laboratory wave channel with a wedge type paddle, with random wave generator capabilities at one end, was installed and calibrated. The calibration was performed with regular waves in order to obtain a paddle transfer function of wave amplitude to control signal voltage. Once the dynamic characteristics of the paddle were known it was possible to design an appropriate filter circuit to incorporate into an absorption system as mentioned above. Concurrent with the development of the absorption system a micro-computer based data acquisition and analysis system was developed.

A fully compatible suite of programs was written to collect wave data from up to 6 gauges simultaneously; calibrate the data collected; store the data and perform a variety of analysis options on the data.

The data was collected from resistance wire wave gauges and passed through a 12 bit A-D converter for calibration and storage by the computer.

The analysis package included all the conventional wave data processing functions such as spectral analyses from fourier transforms and general statistical analyses for mean, standard deviation etc. In addition to the analyses mentioned above, a program was developed to determine the incident and reflected spectra from a composite wave train. For this process it was necessary to simultaneously measure the wave train in at least two different locations in the channel.

A program of this type was essential to evaluate the performance of the wave absorption system in a random wave environment.

Once the wave absorption system had been optimised and fully tested the facility was used to measure irregular wave overtopping rates over 'low-crested' breakwaters. In this case 'low-crested' refers to breakwaters with crests at or just above still water level. The breakwaters tested had seaward slopes of 1:1 and 1:2.

A system was designed and built to accurately measure the quantity of wave which 'overtopped'. The tests were all repeated for various combinations of wave trains which had the same statistical properties. The random-wave generation software was modified as part of the project to allow this to be carried out.

The results obtained were compared in a dimensionless form to results from earlier studies on similar, although not identical, geometric arrangements. The wave absorption system in use allowed much more operational control over the tests and the incident and reflected spectra software provided a much more realistic assessment of the wave conditions present during each test.

A 1-D (in space) numerical model of the overtopping process was developed to provide a comparison with the physical data. The model was a space-time discretisation of the problem with finite elements used to solve the space dimension and a finite difference scheme to provide the time step iterations.

The model was developed on the same micro-computer as was used for the model tests data acquisition and analysis. This multiple use of a single computer emphasises the flexibility of such a machine and thus its suitability in a small design office or research establishment.

1.3 Review of Previous Related Work

1.3.1 Random Wave Generation

The techniques of laboratory wave generation have been widely documented elsewhere (Salter 1984, Buhr Hansen 1975 and others) and the intention here is not to dwell upon the physical designs of laboratory wavemakers but to concentrate on the random wave signal generation techniques.

Until fairly recently the 'normal' practice in hydraulic modelling was to use regular waves - usually sinewaves - to investigate coastal phenomena. For example, a number of investigations into run-up and overtopping have been carried out with regular waves (Allsop and Ojo 1982, Seelig 1979, Sollit and Debok 1976) but very limited work has applied random waves to the problem. It is generally considered that a regular wave study, whilst useful, cannot hope to provide accurate data for a comprehensive understanding of coastal phenomena. (Kimura and Iwagaki 1976). In 1980 Ploeg and Funke carried out a survey of wave generation techniques in hydraulics laboratories and found that more than twice as many were using regular wave generators rather than random. A main factor for this was the lack of suitable, economic computers to produce an appropriate paddle control signal.

An early random wave synthesiser was developed at the Hydraulics Research Station (Thompson and Shuttler 1972) based upon the addition of sixteen sinusoids at discrete frequencies and preset phase relationships. The system was satisfactory although limited in application and it failed to reproduce accurately extreme maxima since the maximum wave height was limited to that given by the sinusoids in phase. Goda (1970) demonstrated that for accurate simulation up to 50 components sinewaves were required.

The present Hydraulics Research Station (now Hydraulics Research Limited) method of random wave generation has evolved from an electro-mechanical system to an analogue signal generator and then to a hybrid analogue/digital system to the technique now used of a digital synthesiser based around a BBC microcomputer. It is an advanced form of the digital synthesizer which is used in the work presented here and its configuration and implementation are described fully in Chapter 2.

Funke (1974) describes a similar system used to produce a JONSWAP spectrum. Other systems developed for 'random' or pseudo-random' wave generation include the preparation of a command signal on digital tape from an analogue signal generator (Webber and Christian 1974). Whilst this system worked satisfactorily it lacks the versatility of the on-line computer methods now employed. Gravesen et al (1974) recorded a wave record from the ocean and replayed it in their hydraulic model tests but found that whilst long period waves were correctly reproduced short period waves were probably not.

Salter (1984) used superposition of sinewaves claiming that it allows the user more creativity in the choice of spectrum. The comb spectrum method allows the generation of bizarre spectra not possible with the shift-register synthesiser although of how much practical use in hydraulic modelling these are must be in serious doubt. Kimura and Iwagakai (1976) used the Goda method of superposition of 50 composite sinewaves with analogue band-pass filters with the gain to equal the power of the output signal. A later development of this was to use a numerical filter and fourier transforms using the monte-carlo technique for random number generation.

Recently (Tucker 1982) has demonstrated that the composite sinewave method is 'inherently incorrect' since the spectrum produced does not model a random Gaussian surface and the variance of the signal may be less than the theory suggests. It is possible to generate the Gaussian probability field with random numbers and pass them through linear filters where frequency response is calculated to give the correct spectrum (similar to the Kimura and Iwagakai methods). This proves very expensive in computer time. For a solution to the problem it is suggested that it is advisable to work in the time and not the frequency domain.

1.3.2 Random Wave Analysis

The spectral analysis of a random sea has proceeded in two stages. Initially a generalised spectral analysis procedure for the spectrum at a single measurement point was developed. More recently the emphasis has shifted to the determination of directional spectra. In a channel facility it is possible to resolve the wave record into incident and reflected spectra from a composite wave train, with measurement at two or more locations. The spectral analysis of a wave record at a point has been comprehensively dealt with in the past and is itself the subject of papers, reports and theses (Tucker 1979, Chae 1976, Wilson et al 1974) and others. The intention here is to concentrate more on the estimation of directional spectra as related to the present project.

The analysis of wave records based on a spectral approach originated in the late 1940's and 1950's (Tucker 1957, Deacon 1955) and others. However, the extreme jaggedness of the resultant spectra led to many uncertainties of interpretation and difficulties remained until Tukey (1949) developed methods used in communications for use with ocean wave data.

It has always been apparent that interpretation of results will be open to confusion since all the methods are based on statistical processes and approximations. The rediscovery of the Fast Fourier Transform (FFT) was introduced by Cooley and Tukey (1965). The FFT is computationally much faster than the conventional covariance method but has more leakage (Wilson et al 1974). The covariance function may be obtained from the FFT procedure (Bingham et al 1967). However, no matter what methods are employed, they are all influenced by a degree of subjectivity that enters the analysis from a conflict between degrees of confidence and resolution. It is possible for two analysts to report different results from identical data sets simply based upon a choice of certain parameters.

The above subjective interpretation is a large factor in the availability today of a number of different analysis procedures all pertaining to produce an energy spectrum which is supposedly 'correct'. As a result of this no standard notation, nomenclature or 'standard' procedure has developed and the choice of analysis seems largely dependent upon what the user requires as results!

All the analysis procedures are based on determination of the mean energy:

$$\overline{E} = (\rho g) \int_0^\infty [A(f)^2/2]\, df$$

The spectral energy density is then:

$$S(f) = A(f)^2/T_r \text{ where } T_r = N\Delta t$$

The most common analysis procedure is by use of the FFT algorithm.

See Chapter 3 for the analysis procedure used in this project.

Other methods have been primarily developed for directional spectra applications and include such data adaptive methods as the Maximum Likelihood Method (MLM) and Maximum Entropy Method (MEM). It is also possible to determine low frequency components with a 201 point kaiser filter operating on the data in the time domain (Mansard and Funke 1986).

The analysis of directional spectra has developed due to the problems of reflections and the need to determine incident wave conditions more rigorously (Sand 1982).

1.3.3 Reflections in Random Waves

The problem of reflections in laboratory overtopping work has caused numerous problems in the accurate estimation of the overtopping discharge for tests using both monochromatic and random waves. Rayner (1983) found that the overtopping rate was a function largely dependent upon the degree of reflection allowed. The partial solution in the above case and others (Owen 1980)(Allsop 1983) was to

use side splitters in the channel and to only utilise part of the width of channel for the model tests. Whether this method works and how efficiently is a research area on its own.

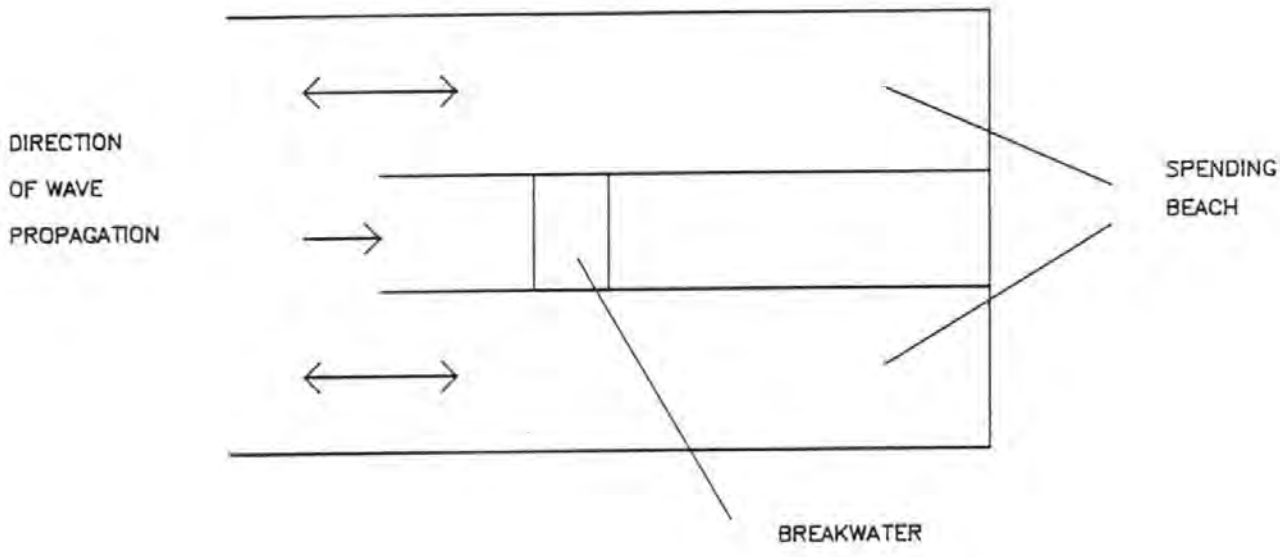

Fig.1.1 'Side splitters' to reduce reflections.

In order to prevent re-reflection from the wave maker Raichen and Hammack (1974) investigated wave run-up with test lengths of only 5 waves to avoid the problem and in a different solution based on the same principles, Hamer and Hamer (1982) used a test length of 30 seconds which was short enough to prevent any re-reflection reaching the test structure. Not only is the procedure laborious, but also the test waves are deficient in the spectral component of high frequency band due to the wave dispersion, unless a special wave generation technique is employed.

In other work (Seelig 1983, Ouellett 1982) an attempt has been made to quantify the reflection coefficient of a test structure and so make allowances in the generated sea. The reflection coefficient method is more suitable for wave run-up problems and breakwater stability tests rather than the measurement of overtopping quantities.

Other workers have concentrated on the determination of incident and reflected spectra from wave measurement arrays all measuring composite wave trains. The analysis procedures used can discriminate between incident and reflected wave energy but no account is made for re-reflected waves.

Various analysis techniques have been proposed. The Maximum Likelihood Method (MLM) has been widely used (Jefferys et al 1981, Clarke and Gelding 1981) for directional wave properties and determination of incident and reflected spectra. The MLM supposes that the wave amplitude is small and that the water surface elevation can be expressed as the superposition of component waves with wave number, k, and angular frequency, w. The water surface elevation, η, at the point x and at the time t is expressed as:

$$\eta(x,t) = \int_w \int_k e^{i(kx-wt)} z(dk,dw)$$

The wave number - frequency spectrum s(k,w) is defined as

$$S(k,w)dk\ dw = Z(Dk,dw)Z^*(Dk,dw)$$

where * denotes complex conjugate.

The estimation of direction is made from records at two points as described by Panicker and Borgman (1974) who also used the Maximum Entropy Method (MEM). The MLM has the highest resolution power for the estimation of directional spectrum but was applicable to wave gauge arrays only. Isobe et al (1984) presented an extension of the method(EMLM) which could be used with mixed instrument arrays. The MLM is simple to implement and economic with respect to time but it is better suited to 3-D directional applications rather than the

determination of incident and reflected spectra. The MEM (Briggs 1984) is a non-linear data adaptive method of spectral analysis which is capable of generating higher resolution spectral estimates from shorter data records than conventional FFT methods. Entropy is a measure of the information content contained in a signal. Maximising entropy, therefore, maximises the information transmitted in a signal. The concept involves finding a spectral estimate which corresponds to the most random or unpredictable time series whose extended correlation function satisfies the constraint that it agrees with known values.

Since the MEM is data adaptive like the MLM, there is no 'bias vs variance' trade off due to finite record length requirements as in FFT procedures.

The MEM spectral estimate is given by:

$$S(f) = |A(f)|^2 Sw(f)$$

where $w^2(L)$ or $Sw(f)/2\Delta$ is the white noise variance where Δ is the time increment.

The MEM spectrum is much less peaked than the FFT spectrum with a slightly shifted peak frequency.

The other main analaysis technique is based upon the Fourier transform method. Kajima (1969) first proposed the method, however, it has been adapted and improved since. Goda and Suzuki (1976) employed FFT's to determine incident and reflected spectra from two wave gauges separated by a length ΔL. The incident and reflected wave heights are then estimated from the composite wave heights by energy considerations. Goda and Suzuki showed that the method was effective in the range outside the condition of the gauge spacing being even half integers of wavelengths at the peak frequency. They proposed that for maximum resolution the spacing was chosen using the guidelines shown overleaf:

fmin: $\Delta L/L_{max} = 0.05$

fmax: $\Delta L/L_{min} = 0.45$

where L_{max} and L_{min} are the wavelengths corresponding to f_{min} and f_{max} respectively.

Gaillard et al (1980) derive the same relationships for the spacing to give maximum resolution.

The overall coefficient of reflection is given by:

$$k_R = \sqrt{(E_R/E_I)}$$

where E_I and E_R are the energies of the resolved incident and reflected waves.

The wave heights can then be evaluated by: (Goda and Suzuki 1980)

$$H_I = \frac{1}{\sqrt{(1+K_R^2)}} \bar{H}_S$$

$$H_R = \frac{K_R}{\sqrt{(1+K_R^2)}} \bar{H}_S$$

Where $\bar{H}_S$ is the mean of the significant wave height taken from the composite waves at the two gauge locations. For a good estimation of incident and reflected wave heights the wave gauges are required to be away from both the test structure and the wave paddle. (This is because the composite wave height, $\bar{H}_S$, used in the above equations fluctuates in the neighbourhood of a reflective boundary.

Mansard and Funke (1980) extended this method to use more than 2 wave gauges for more accurate estimates by use of a least squares method. The least squares method supposes superposition of components of phase and amplitude.

Gilbert and Thompson (1978) proposed a Frequency Response Function type approach to Kajima's theory. It is this method which has been adopted here since it lends itself to compatibility with the other analysis procedures which were used. The method is described fully in Chapter 3.

1.3.4 Wave Absorption

There are several flap-type paddles with a wave absorption system fitted. These include a system at Edinburgh University (Salter 1981 and 1984) and the 3-D wave basin at the Danish Hydraulic Institute (Aage and Sand 1984). Less common is an absorption system fitted to a wedge-type paddle.

A wave absorption system was developed in 1970 by Milgram. The system used a wave gauge to sense the wave as it approached the paddle which then moved to absorb the wave. The only crucial difference between this system and the one used in the present work is that the waves for Milgram's system were generated at the opposite end of his flume from his absorber. A system like this is of no use for breakwater tests.

The Edinburgh wave absorber uses force sensing for the feedback. The force sensor will be free from the contaminations in the water that affects resistance type wave gauges. Force transducers will also average across the width of the channel. The water surface elevation technique used in Plymouth has overcome the problem of averaged readings by use of two long probes across the paddle front. The water surface elevation measurement requires no transfer of pressure record to wave heights, it is simpler to calibrate and has a much faster frequency response to reflections.

1.3.5 Hydraulic Overtopping

Accurately estimating the amount of water which will wash over a coastal structure can be vital to design engineers. Building seawalls high enough to completely prevent overtopping is often unacceptable because of aesthetics and costs. Situations also arise where water on the lee side of a breakwater is perfectly acceptable, such as outfall protection breakwaters for power stations.

Overtopping is an extremely complex coastal phenomenon. Variables include structure characteristics (shape, weight, slope, roughness, porosity, berm width, offshore slopes etc.) wave characterics (height, period etc.) water depth, wind speed etc. Most overtopping investigations have ignored winds and wave direction in order to concentrate on the more significant variables.

Related to the investigation of wave overtopping is the phenomenon of wave run-up. Nagaki and Takoda (1982) investigated the correlation between run-up and overtopping and found that the correlation was good. Recent work has concentrated on random wave environments but earlier tests used monochromatic waves which can only provide an approximation to the random wave situation. Roos and Battjes (1976) conducted an experimental study of periodic wave run-up compared with Hunts formula for run-up height defined as:

$$R = \sqrt{HL_o}\ \mathrm{Tan}\alpha$$

where R = run-up height
α = slope
H = Wave height

from $L_o = gT^2/2\pi$
$R = 4T\sqrt{gH}\ \mathrm{Tan}\alpha$

This predicts run-up depends only upon wave height and wave period.

Ouellett (1982) proposed that other factors important in run-up are the storm duration and the structural shape of the breakwater. He predicted that significant overtopping will occur when SWL $\geq$ 60% of breakwater height. Hamer and Hamer (1982) also concluded that the freeboard height was the most significant factor to differentiate run-up from overtopping. They tested the hypothesis that the amount of wave transmission due to overtopping is determined by the ratio:

(Actual run-up, R_C)/(Theoretical run-up,R)

The calculation of theoretical run-up was based on Hunts formula. The structures tested had a smooth slope of 1:4. Other run-up/overtopping related work includes Sutherland et al (1976) who found that an offshore bar would reduce run-up height. Raichlen and Hammack (1974), Carlsen (1984) and Mase and Iwagaki (1984) who were primarily concerned with gentle slopes up to 1:5 which is beyond the scope of this work. Ahrens (1983) measured run-up on an idealised structure up to 1:1 in both regular and random waves and made an estimate of the incident spectrum from Goda's method (1976).

Many studies of run-up and overtopping have been conducted as part of tests on checks on stability of breakwater armour units designed in accordance with Hudson's formula as given in the Shore Protection Manual.

Kimura and Seyama (1984) investigated the statistical properties of short-term overtopping and made the following assumptions to simplify the investigation:

1) "Characteristics of an overtopping of zero up-crossing wave from a sea wall can be approximated by an existing theory for periodic waves".

2) "The characteristic of an overtopping is not affected by neighbouring waves but can be evaluated only by properties of an individual wave".

3) "The statistical distribution of wave height can be approximated as the Rayleigh distribution".

This model was over simplified as Shi Igai et al (1977) had previously shown that overtopping is a highly non-linear and discontinuous phenomenon regarding wave height. This is because the reflected wave energy decreases after a large amount of overtopping thus the wave height near the sea wall also decreases, hence a larger subsequent wave is needed for more overtopping and vice versa. Thus the effects of wave group action should be considered in the measurement of overtopping discharge.

Douglass (1984) has produced a paper in which he compares the most significant recent random wave overtopping experiments of Owen (1980), Goda (1971) and Battjes (1974) with the design criterion recommended in the Shore Protection Manual.

The Owen method is based upon the experimental derivation of dimensionless coefficients to quantify the overtopping discharge depending on a number of variables discussed in Chapter 7. An example of the design procedure from Owens work will also be found in Chapter 7.

The one thing that is clear from all the overtopping work so far carried out is that much more data is required to produce accurate design charts.

1.3.6 Numerical Modelling

To numerically model the effects of wave overtopping in random seas accurately, a good model of the sea is first required. This is used as the generating function for the overtopping processes to follow. A regular sea is simply defined with a sinewave generating function but a random sea is harder to define.

Larsen et al (1984) describe the use of boundary integral equation and 'sponge-layer' techniques to generate a directional sea in deep water. The 'sponge-layer' is to absorb reflections along the model boundaries. The technique uses a finite difference scheme to solve the deep water equations in vertical and horizontal cartesian co-ordinates. Pinkster (1984) reviews this and other similar techniques with a directional application.

All the techniques are based on the assumption that the real sea surface elevation is a zero mean, stationary, ergodic, random Gaussian process. The statisitcal properties are independent of time. On all the models the assumption is made of non-breaking waves since breaking is known to be a non-conservative process and breaking point is a mathematical singularity (Wang and Purpura 1974).

Any numerical model of overtopping is likely to be an extension of the closely related run-up problem. Jennings (1978) modelled the run-up of constant form sinewaves with the method of characteristics. The method of characteristics is based on a simplified solution to the Shallow Water Equations given by:

$$\text{Momentum} \quad \frac{\partial u}{\partial t} + U\frac{\partial u}{\partial x} = -g\frac{\partial \eta}{\partial x}$$

$$\text{Continuity} \quad \frac{\partial[u(\eta + \eta)]}{\partial x} = \frac{-\partial \eta}{\partial t}$$

The simplifying assumptions for the method of characteristics are:

1. that the vertical acceleleration of the fluid particles is negligible;

2. that the velocity distribution of the horizontal water particle velocity is uniform;

3. that the bed friction forces are negligible.

The above equations readily lend themselves to adoption for a finite-difference analysis.

A solution of the equations leads to the formation of +ve, C+, and -ve, C-, characteristic lines of constant depth.

The disadvantages of the method are:-

1. It is based on an irregular grid therefore there is a need for interpolation;

2. The need to determine node positions;

3. A slope approximation is made.

The theory of characteristics does, however, give information on grid spacing for a finite difference method. Alternative finite difference methods allow for the inclusion of slope, inflow and coriolis terms. (Katapodes 1979).

Three different mesh techniques are available:

1. A regular mesh which uses characteristic equations;

2. A staggered mesh which uses shallow water equations;

3. A two-step regular mesh known as the Lax-Wendroff method.

The Lax-Wendroff method uses the shallow water equations in the following form:(Lax-Wendroff 1960)

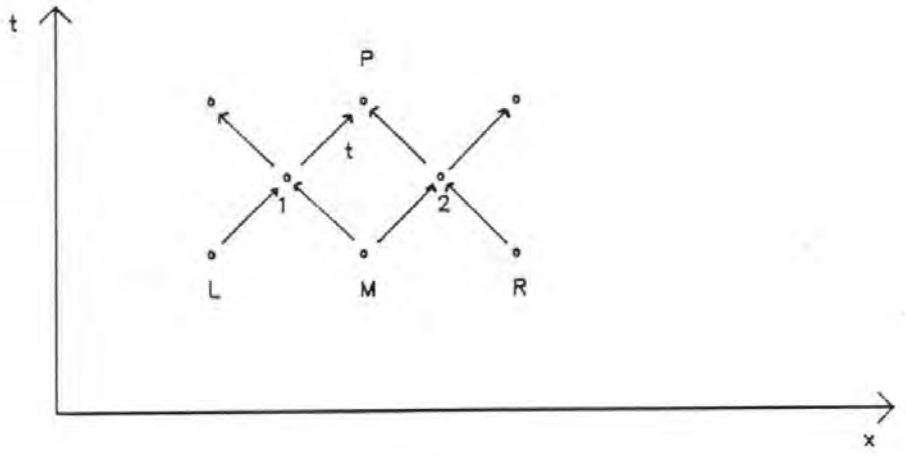

Figure 1.2 Lax-Wendroff Mesh

$$\frac{\partial y}{\partial t} + \frac{\partial Q}{\partial x} = 0$$

$$\frac{\partial v}{\partial t} + \frac{\partial E}{\partial x} = V$$

where $Q = Vy$

$E = V^2/2 + gy$

$v = g(S_o - S_f)$ where S_f is the bed slope.

The solution of the equations is as follows:

$$\frac{g - Y(Y_1 - Y_M)}{Y\Delta t} + \frac{Q_M - Q_L}{\Delta x} = 0$$

The calculation is performed for Y_1, as all the other variables are known.

Similarly for Y_2

$$\frac{V_1 - \frac{1}{2}(V_L - V_M)}{Y\Delta t} + \frac{E_L - E_M}{\Delta x} = Y_2 (V_L + V_M)$$

and for V_2

$$\frac{V_2 - \frac{1}{2}(V_M - V_R)}{Y\Delta t} + \frac{E_M - E_R}{\Delta x} = Y_2 (V_M + V_R)$$

Thus V_1 and Y_1 are used to calculate Q_1, E_1, V_1 and V_2 and Y_2 are used to calculate Q_2, E, V_2 then:

$$\frac{Y_p - Y_M}{\Delta t} + \frac{Q_L - Q_M}{\Delta x} = 0 \qquad \ldots\ldots\ldots 1$$

$$\frac{V_p - V_M}{\Delta t} + \frac{E_2 - E_1}{\Delta x} = Y_2 (V_1 + V_2) \qquad \ldots\ldots\ldots 2$$

Y_p and V_p are the two unknowns and can be calculated from 1 and 2.

The method is easily adapted for irregular profiles as:

$$\frac{dA}{dt} + \frac{d}{dx}(AV) = 0$$

$$\frac{dv}{dt} + \frac{d}{dx}(YV^2 + g^2) = -g^2 f_1$$

$$\frac{d\eta}{dx} = \frac{dy}{dx} - So$$

The above shallow water techniques have been used in a number of run-up studies including Haugel et al (1984) who used a finite element solution and Zielke (1984) who modelled short waves with Boussinesq equations.

The other main analysis technique used to date is to model the Navier-Stokes equations. The Navier-Stokes equations govern the flow of incompressible fluids with reasonably constant viscosity. In the cartesian co-ordinate system Newton's 2nd Law of Motion applied to a unit mass of fluid element gives 3 equations in x,y and z directions.

Navier-Stokes models have been developed by Daubert et al (1984) who used a finite different scheme for 2-D flow with non-breaking waves. Austin and Schleuler (1982) also used the Navier-Stokes equations with a hydrodynamic code for impacts on coastal structures.

All the previously mentioned methods and others such as Finite Amplitude Waves (Packwood 1982)(Yamaguchi and Tsuchuya 1976) show very good results on mild or shallow slopes. The situation of breakwater overtopping differs in one important respect. The slopes of the breakwaters to be considered are not shallow, and the traditionally used shallow water equations cannot be applied to regions where vertical accelerations become significant. Such accelerations are significant when water moves over fairly steep slopes - above 1:10.

In 1980 Gopalakrishnan and Tung presented a finite element model for use on steep slopes by making an allowance for the vertical accelerations whilst a 1-D problem was retained. It is an extension of this method which will be presented later.

CHAPTER 2

LABORATORY WAVE GENERATION SYSTEM

2.1 Introduction

All the laboratory work described here has been carried out in the wave channel in the Department of Civil Engineering at Polytechnic South West. The facility consists of twin channels 20.72m long, 0.90m wide and 1.22m deep. Both channels are equipped with a wedge type wave paddle controlled with an electro-hydraulic system supplied by Keelavite Ltd. At the opposite end of the channel there is a spending beach which consists of a 2 inch layer of hair-lock material fixed onto a plywood slope of 1:4½. Mounted on rails which run the length of the channel is a motorised trolley upon which wave gauges can be fixed for traverses etc.

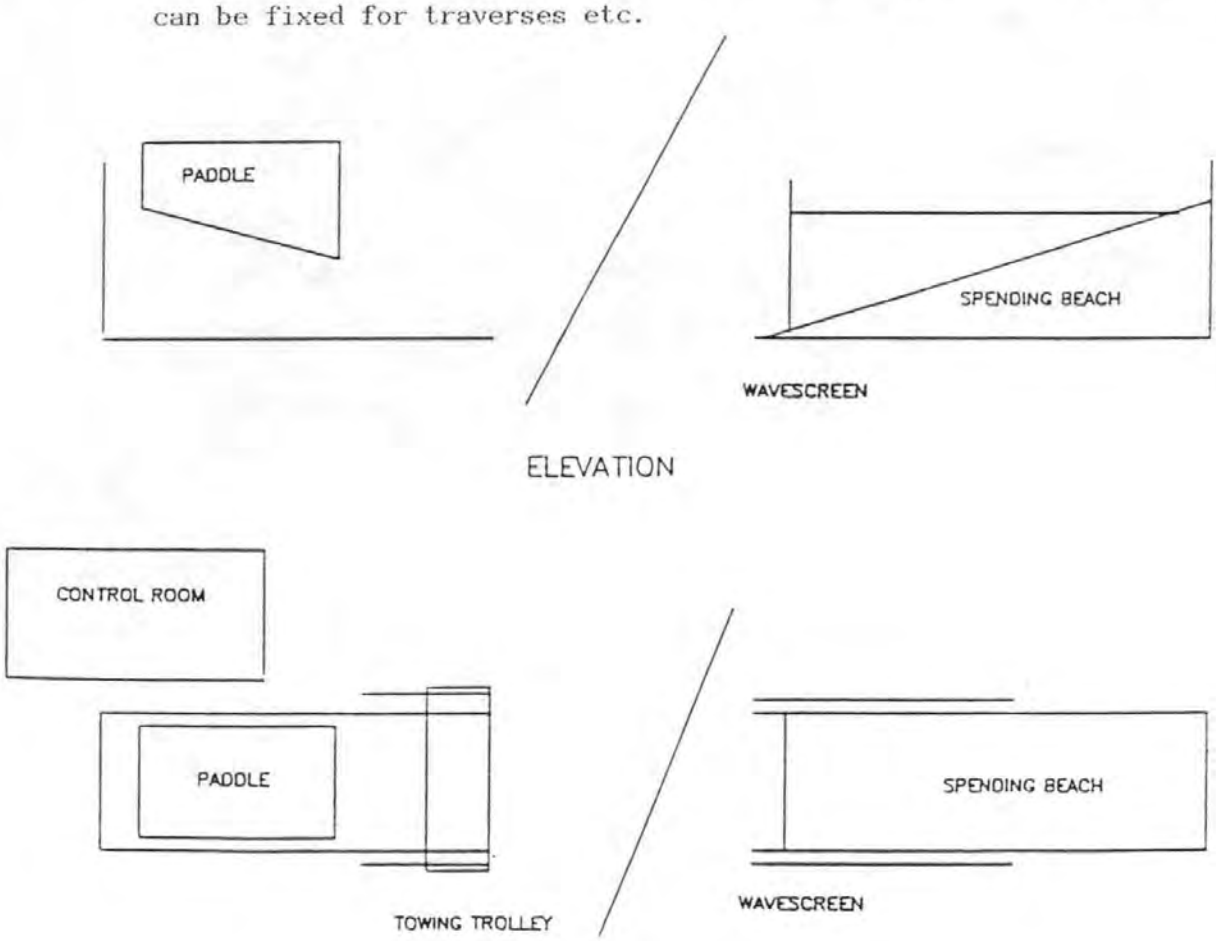

Figure 2.1 Plan and Elevation of Laboratory

The paddle control signal is produced by a BBC model B microcomputer running wave generation programs written at Hydraulics Research Ltd. The programs can produce either a regular or 'random' wave signal as required.

On line wave data analysis is available via a Hewlett-Packard 9816S microcomputer connected to a Biodata Microlink high speed data logger. The data logger accepts an analogue voltage signal from a Churchill Controls Wave Monitor. The analogue signal is converted to a digital record for analysis.

Other equipment used includes a high speed chart recorder to record wave records, a digital storage oscilloscope and a Hewlett-Packard Spectrum Analyser. The general arrangement is shown in Figure 2.2.

The transfer function for the chart recorder was measured at the start of the project and used in the calculation of incident wave heights from wave envelopes (Chapter 3). The transfer function was determined by measuring the recorder's response to sinusoidal signals of known amplitude at each frequency used in the regular wave tests. The transfer function relates measured voltage to actual voltage at each frequency.

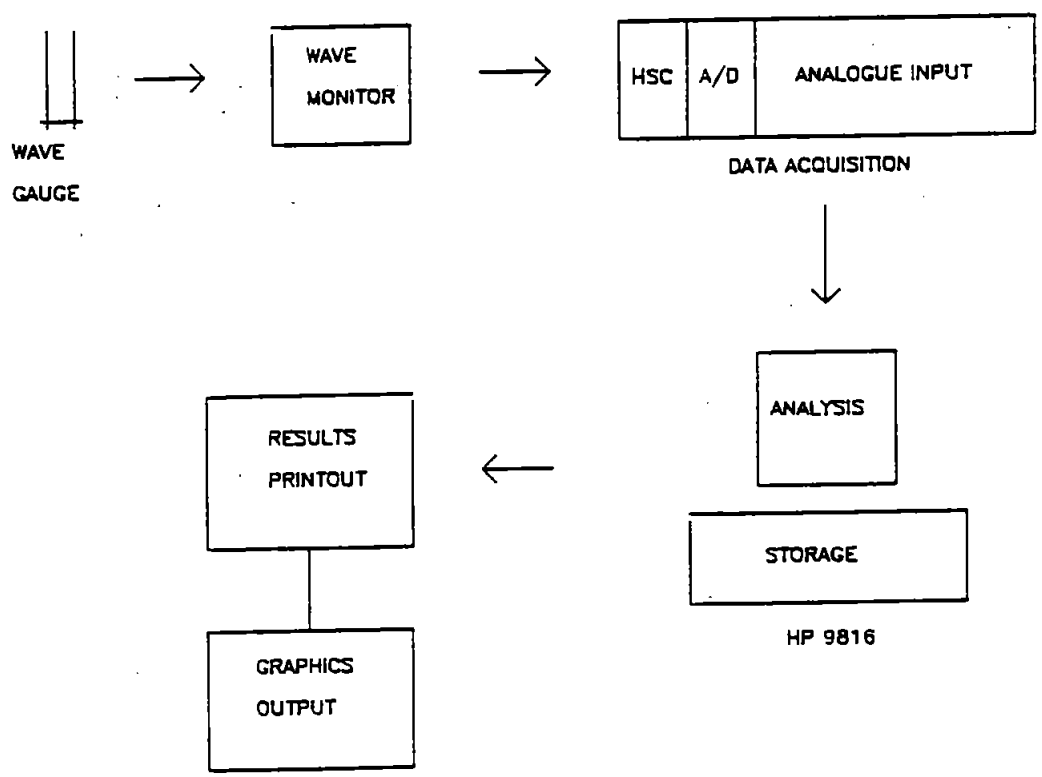

Figure 2.2 Laboratory Equipment Arrangement

2.2 Wave Paddle (Plate 2.1)

The wedge shaped wave paddle is constructed from aluminium channel sections with a marine plywood shell. The paddle runs on a single chrome plated bar 150mm in diameter. A guide rail beneath the paddle prevents any lateral displacement. The paddle is driven by a double ended hydraulic actuator with a maximum stroke of 500mm. The movement of the actuator is controlled by a Moog Servovalve and the position of the actuator is monitored by a LVDT (Linear Voltage Displacement Transducer).

The actuator is supplied with hydraulic oil at a pressure of 1800 psi via an accumulator charged to 90 psi. The accumulator acts as a reserve when a sudden large demand is required.

The advantage of a wedge type paddle is that no waves are generated in the region behind the paddle, thus avoiding the need for a rear spending beach. A hydraulic system has certain advantages over an electrical system, for example, interference is less, an important consideration especially when the absorption circuit came to be tested. The response to high power requirements is also better supplied by hydraulics.

The high noise levels normally associated with a hydraulic system have been eliminated by locating the pump and hydraulic oil reservoir in a separate room adjacent to the laboratory.

2.3 Spending Beach (Plate 2.2)

The Spending Beach is a low cost solution to the need to absorb as much wave energy as possible. The slope of 1:4½ was chosen as a compromise between the degree of reflection permissible and the need to make full use of the channel space available. Waves with frequencies between 0.5 - 0.7 Hz produce 5-8% reflection.

2.4 Wave Gauges

The wave gauge system used in the project is based around a Churchill Controls Wave Monitor. The Wave Monitor is used to drive wave gauges positioned in the channel. The gauges work by measuring the current flowing in a probe which consists of a pair of parallel wires. The probes used in the channel consists of a pair of stainless steel wires 1.5mm in diameter, 300mm long and separated by a 12.5mm gap. The probe is energised with a high frequency square wave voltage to avoid polarisation effects at the water surface. Each probe can be energised with a different frequency signal so that the gauges may be used close together with no risk of interference between gauges. The wires dip into the water and the current that flows between them is proportional to the depth of immersion. The current is sensed by an electronic circuit which provides an output voltage proportional to the instantaneous depth of immersion. The voltage is used to drive a chart recorder and/or data logger.

The output voltage can be calibrated in terms of wave height by varying the depth of immersion of the probe in still water. The calibration was done in measured increments (10mm) with a record made of the variation in output signal. When the data logger was used the probe was calibrated over an 80mm range with a least squares regression analysis. This enabled the 12 bit output from the A/D converter to be scaled to mm of wave height.

The gauges were calibrated for each series of tests and remained linear over the whole length of probe provided they were kept clean. An example of a record taken with a gauge when oil was present in the channel is given in Figure 2.3. This variation can be attributed to changes in the electrical conductivity of the water due to temperature changes and/or water contamination. The variation of calibrations over a single days testing was negligible.

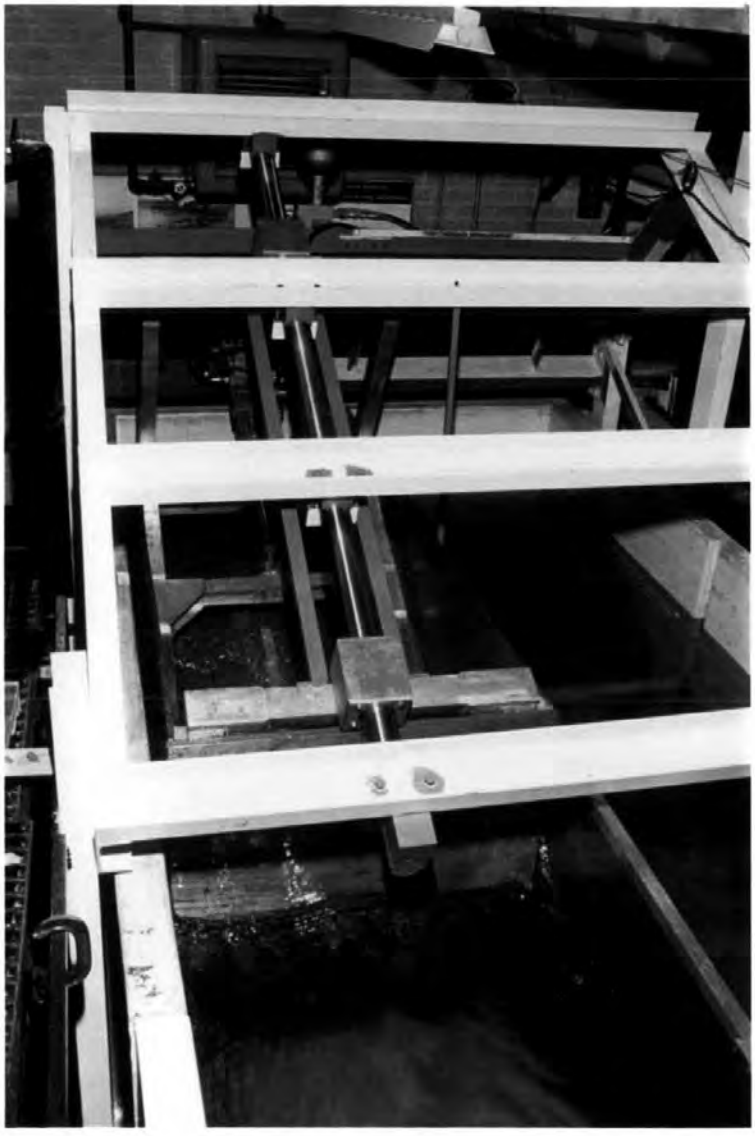

PLATE 3.1 WAVE PADDLE

PLATE 2.2 SPENDING BEACH

2.5 Paddle Control Signal

The paddle control signal is generated by programs installed in the BBC computer in the form of EPROMS (see Glossary). Regular wave generation is a relatively straightforward procedure. For a sinewave the required frequency is entered and the program uses a 'look up' table to determine the correct output signal. A user-defined regular wave requires the user to input specified ordinates which correctly define the shape of the required wave.

2.5.1 Pseudo-Random Wave Generation

2.5.2 Introduction

'Random' wave generation takes the form of a computer controlled synthesiser (Thompson and Shuttler 1972).

The synthesiser consists essentially of a digital white noise generator with a variable digital filter which creates pseudo-random output with an energy spectrum that is pre-set by the user. There is a program to Fourier transform the required spectrum and derive the coefficients for the filter and other information needed to set up the synthesiser. All the calculated information to set up the synthesiser is saved in a file by the Fourier transform program, for later retrieval by the wave generation program.

The signal is pseudo-random in that it eventually repeats itself. However, it can be regarded as truly random when the repetition period is made long compared with the duration of any test. Alternatively it may be experimentally convenient to use and record data over a short repetition period so that the spectrum can be calculated without statistical uncertainty.

The repeatability of the signal has the advantage of giving the user close operational control over the test programme, in that individual tests can be carried out at different times or on different experimental arrangements with exactly the same input signals. Direct comparison between test results is then possible.

The spectrum synthesiser can be considered to consist of two separate blocks:

a. The noise source

b. A variable filter which controls the shape of the noise spectrum

The noise is generated by using a pseudo-random binary sequence (PRBS) generator based on a shift register with logical feedback of bits (Binary Digits). The signal is completely deterministic and will be identical every time the noise source is started with the same bit pattern in the shift register, and is cyclic with a repetition period which can be determined at will by changing the logical feedback. During the repetition period it generates a binary sequence which sweeps out a completely representative sample of the probability space appropriate to that sequence length and has sufficient of the properties of random noise to be treated as such for most purposes. A spectrum in which the repetition period is equal to the test length will be defined as a 'full length' spectrum.

The variable filter acts on the PRBS to produce a digital output signal with the required spectrum, which is passed to a digital to analogue (D/A) converter to produce an analogue output. The filter is of finite impulse response (F.I.R.) non-recursive design which interfaces to the PRBS generator with great ease, since the 65 stage shift register which forms the basis of the PRBS generator inherently retains the required delayed signals. The weightings are thus applied to the outputs of each shift register stage and the results summed to produce the filtered signal.

The impulse response defined by the weightings is anti-symmetric; the weightings on stages 1,33 and 65 are zero and the others are taken in symmetrical pairs of opposite sign (the weighting of Stage 2 is equal and opposite to that of Stage 64, 3 with 63 etc). Thus 31 weight values are required to define the filter's response.

The final stage of the synthesiser is a three-pole low pass 'reconstruction' filter to remove high frequency components resulting from the sampling process; the cut-off frequency is switchable to suit the spectrum being generated.

2.5.3 The PRBS Generator

A software implemented 65 stage shift register is used to generate the 65 delayed versions of the PRBS; it also forms part of the PRBS generator.

There are certain preferred combinations of feedback stages which produce PRB sequences with statistical properties which most nearly approximate those of a true random signal; these are known as m-sequences. For a truly RBS the auto-correlation function is zero except for zero delay, when it is unity. An m-sequence has unit auto-correlation function for delays of $2^n - 1$ clock pulses, where n is the number of active shift register stages used in the production of the sequence. The auto-correlation function reduces linearly to zero within one clock period on either side of these points and remains at zero for all other delays. The sequence repeats itself after $2^n - 1$ clock pulses and this figure is called the sequence length (in bits). The sequence duration is $T=2^n - 1$ t seconds where t is the clock period. Every possible state but one of the active length of the shift register occurs exactly once in each m-sequence. The one forbidden state depends on the feedback logic used; in the spectrum synthesiser used here it is all zeros, which is a self sustaining state. For this reason at least one '1' must be preset to the active length (first n stages) of the shift register before the sequence is started.

2.5.4 Program Configuration

The pseudo-random wave generation is achieved by means of two BASIC programs; NEWSYN and USERN. Program USERN is used to produce the paddle control signals but before it can be successfully run a file of spectral parameters must have been created by NEWSYN. To produce parameters, NEWSYN must know the paddle transfer function (Wave Amplitude/Input Voltage). The transfer function was determined during the initial calibration and setting up the system (see Chapter 5). Once the transfer function has been entered it may be saved in a file so that it may be automatically retrieved for subsequent runs of the program.

2.5.5 Defining a spectrum

The first step in creating a file of spectral parameters is to enter all relevant parameters such as water depth and model scale a choice of spectra is then presented:

Moskowitz
Jonswap
Darbyshire
Newman
ISSC
User-defined

The defining equations for the above spectra can be found in Appendix D.

NEWSYN calculates the peak frequency, fm, of the chosen spectrum and then uses a frequency interval of fm/8. 16 ordinates are calculated with the maximum frequency at 2fm. The first 3 ordinates are set to zero.

After selection of a spectrum the transfer function is entered manually or from disc and the program calculates the parameters required by USERN (filter weightings etc). The calculated parameters are stored to disc and the model and prototype parameters can be displayed on the screen. NEWSYN was modified to NEWSYNP to suit the needs of this project, so that the model and prototype parameters could be output to a line printer (see Appendix A) to produce hard copy output.

2.5.6 Spectrum Generation

USERN is "Loaded" and "Run" to generate the spectrum. It will ask for a filename created by NEWSYN and display the parameters.

The shift register must now be initialised. A choice of shift register length and initial state is offered. The default state is all zeros except the first stage. Any state is available and hence it is possible to start and restart a sequence from any position.

The signal can now be started with the Gain control and filter set at the positions indicated on the display.

2.5.7 Software Modifications

In the course of the absorption and overtopping tests various modifications and improvements were made to the wave generation programs. In the spectrum general program NEWSYN a routine was added to calculate the optimum probe spacings for the frequency response analysis used. The spacings were calculated based on the theoretical peak frequency from the spectral definition and by means of a 'look-up' table for wavelengths.

The other major alteration was to develop a routine in USERN to allow any possible feedback connection sequence to be chosen for the given sequence length. The choice of feedback connection allows different full length sequences to be used for comparison in the overtopping tests (see Chapter 7). Each 'full length' sequence of the same length will have the same statistical and spectral properties but will produce a different time series record.

2.6 Data Acquisition

The data collection is achieved with a Biodata Microlink. The analogue output voltage from the Wave Monitor is sent to the Microlink where it is converted to a digital record and passed to the Hewlett-Packard for storage and analysis. Various routines and programs were developed for data acquisition. The software development is described in Chapter 4.

The Microlink is a modular system with a main frame containing the circuitry necessary for complete IEEE-488 bus operation and a number of modules which transfer data between the bus and the input devices.

The analogue voltage signal from each channel of the Wave Monitor is sent to a single ended input module known as an AN-1 module. The modules have continuously variable Gain and Offset controls allowing accurate calibration to the signal source. The AN-1 has a full scale of 10.0 volts (i.e. 0-10V, ±5v etc).

Each AN-1 module has a different SECONDARY ADDRESS (see Glossary) associated with it which is set with switches on the AN-1's circuit board. The SECONDARY ADDRESS allows each module to be uniquely defined. Hence individual modules can be addressed from the computer within the data collection program. Each module must be sent a SKIP or RETURN flag bit from the computer to determine whether or not it is included in the data collection routine.

A SKIP flag implies that the module is to be excluded from data collection. A RETURN flag indicates that this module is the final module in the scan. (Means that SKIP flags need not be sent to modules to the right of a RETURN module). If no SKIP or RETURN flag is sent the system default is to include the module in any scan.

The analogue signal is converted to a 12 bit digital record by an A/D converter module. The digital signal is passed to the computer via the IEEE interface bus.

The rate of data acquisition is software controlled. the user can choose any logging rate from 32μs to 255s. The data is sent to a software buffer prior to storage on disc. The acquisition rate is controlled by a High Speed Clock (HSC) module. The HSC module has a Trigger Facility which enables data acquisition to commence by activating a switch which can be remote from the computer and Microlink. The trigger facility is especially useful during calibration of the wave gauges. It also allows the user to observe the whole length of the channel and commence data acquisition simultaneously.

CHAPTER 3

ANALYSIS THEORY

3.1 Introduction

In this chapter the theory is presented and developed for the analysis of regular and random waves. Regular as well as random waves were used in the optimisation and calibration of the paddle and the absorption circuit. Random waves were also used in the trials of the absorption circuit. The majority of the overtopping tests were carried out with random waves.

3.2 Linear Wave Theory

To predict and interpret the behaviour of the paddle with and without wave absorption when a highly reflective barrier (wavescreen) was present in the channel, linear wave theory was used.

The variation in water surface elevation $\eta(x,t)$ is assumed to be sinusoidal in both space and time. The elevation may be expressed as:

$$\eta(x,t) = \frac{h}{2} \cos 2\pi \left\{ \frac{x}{L} - \frac{t}{T} \right\}$$

where h = Wave height (Peak to trough)

L = $2\pi/k$ wave length

T = $2\pi/w$ wave period

By assuming that $H \ll L$ and $H \ll d$ where d is the depth of water, it may be shown that the wave celerity, C, is given by:

$$C = L/T = w/k$$

$$= \frac{gT}{2\pi} \text{ Tanh } \frac{2\pi d}{L}$$

$$\therefore L = \frac{gT^2}{2\pi} \text{ Tanh } \left\{ \frac{2\pi d}{L} \right\} \qquad \ldots\ldots\ldots\ldots\ldots\ldots \quad (3.1)$$

Equation 3.1 was used to calculate the wave lengths of the sinewaves used in the regular wave tests. The calculation was performed by a program "WAVELEN", written to calculate wave lengths and wave numbers by an iterative technique to determine the wavelengths which caused nodes or antinodes to be formed at the paddle front.

Approximations for Deep Water:

Equation 3.1 shows the influence the relative depth d/L has on the propagation of waves. The application of the adjective "deep" or "shallow" to gravity waves depends upon the length of the wave being transmitted.

The approximation "deep" is governed by the following test:

$$\text{If } d/L \geqslant 0.5 \text{ then } \operatorname{Tanh}\left\{\frac{2\pi d}{L}\right\} \simeq 1$$

$$\therefore L = \frac{gT^2}{2\pi} \quad \ldots\ldots\ldots\ldots \text{ deep water approximation } \ldots\ldots\ldots \quad (3.2)$$

3.2.1 Fluid Particle Motion

These are two methods of following the motion of fluid particles. The Eulerian approach is to concentrate on a fixed point in space and note the changes in time. The Lagrangian approach is to travel with the fluid particles and record their spatial variations. The lagrangian equations will be used here.

The horizontal, x', and vertical, y', displacements of a particle about its mean position $(\bar{x}, \bar{y})$ are given by:

$$x' = \frac{-h}{2} \frac{\operatorname{Cosh}\left[2\pi\left(\bar{y}+d\right)/L\right]}{\operatorname{Sinh}\left(2\pi d/L\right)} \operatorname{Sin}\left[2\pi\left[\frac{\bar{x}}{L} - \frac{t}{T}\right]\right] \quad (3.3)$$

$$y' = \frac{-h}{2} \frac{\operatorname{Sinh}\left[2\pi\left(\bar{y}+d\right)/L\right]}{\operatorname{Sinh}\left(2\pi d/L\right)} \operatorname{Cos}\left[2\pi\left[\frac{\bar{x}}{L} - \frac{t}{T}\right]\right] \quad (3.4)$$

Thus in deep water the water particles move in closed circular orbits. This is only a first order approximation and higher order theories predict open orbits in which the particles slowly progress in the direction of wave propagation. This is known as Mass Transport.

3.2.2 Effects of Wavescreen

When regular waves travel towards a vertical impermeable barrier an anti-node must be formed at the barrier. The wavescreen (see Chapter 6) forms a vertical barrier in the wave channel at the opposite end to the wave paddle.

The effect of the wavescreens used to test the wave absorption system board (Chapter 6) was to increase reflection. When the full wavescreen (No 1) was used standing wave patterns were produced.

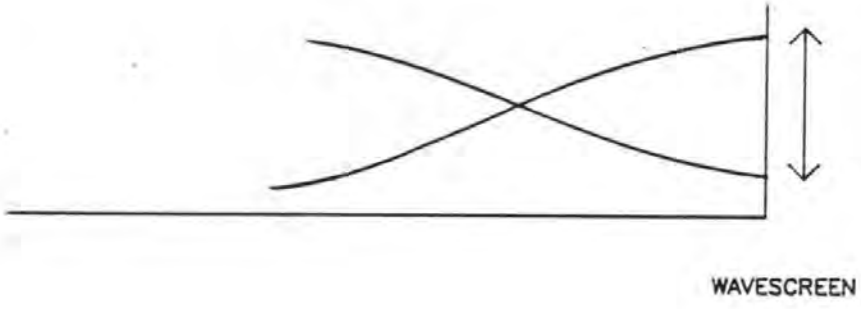

Figure 3.1 Anti-node at Vertical Barrier

At an anti-node there is maximum vertical water displacement with zero horizontal displacement. At a node there is maximum horizontal water displacement and zero vertical displacement.

Given that there will always be an antinode (full or partial) at the wavescreen, there will also be an antinode at the paddle if:

$$L_R = IL_n \tag{3.5}$$

where I = 1,2,3, ... N

L_n = half the the distance from the mid-stroke of the paddle to the wavescreen

and L_R = wavelength of generated wave.

A node will be formed at the paddle if

$$L_R = IL_n - \frac{L_n}{2} \tag{3.6}$$

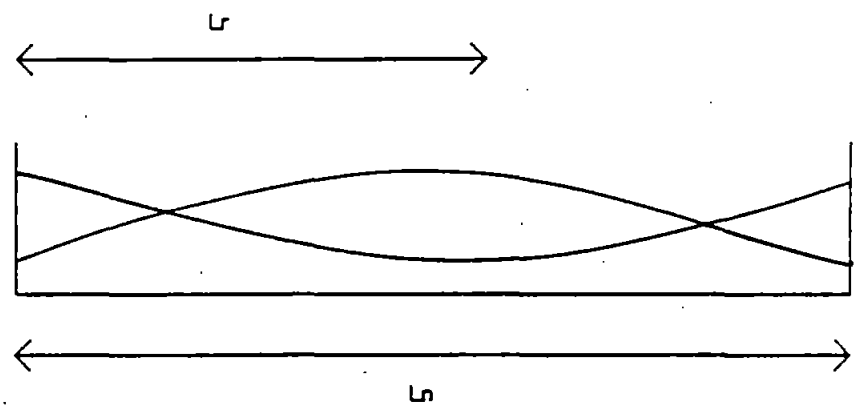

Figure 3.2 Antinode at Paddle Front

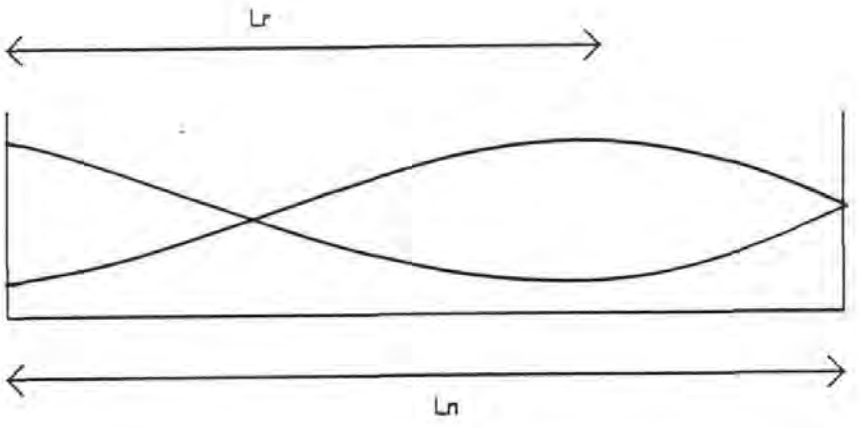

Figure 3.3 Node at Paddle Front

The test frequencies for the regular wave tests were chosen to introduce the two above effects. For the purposes of analysis the paddle to wavescreen distance was calculated with the paddle at its mid-stroke position.

When no attempt is made to prevent the re-reflections from the paddle (as in a conventional system) the wave action between two antinodes will cause resonance. The waves increase in size until no measurement is possible. In the present investigation the wavescreen used was not 100% reflective, due to small gaps between some of the slats. In this case the increase of wave height caused by the resonance was partially offset by the wave transmission through these gaps. As will be seen later, the wave absorption system completely changed the situation.

3.3 Regular Waves - A Wave Envelope Analysis

The incident and reflected wave heights in the regular wave tests were evaluated by examination of wave envelopes. The results were used to determine the dynamic characteristics of the paddle and to help assess the potential of the absorption circuit.

trace recorded with the high speed chart recorder. Later a computer program was developed to analyse the record digitally. Both the manual analysis and the computer program use the same logic to evaluate an incident wave height, a reflected wave height and the reflection coefficient.

3.3.1 Reflections of Regular Waves

The spending beach installed in the channel absorbs most of the wave energy. However, a significant portion is reflected back towards the paddle. The degree of reflection is frequency dependent. The reflected wave train is superimposed on the incident wave train.

If a wave gauge mounted on a slow moving trolley traverses over a length of the channel then a wave envelope is produced. The wave envelope (Fig.3.4) is a result of positive and negative interference from the incident and reflected waves. The analysis of the wave envelope is based upon the following interpretation. The theory was discussed by Sandstrom (1974).

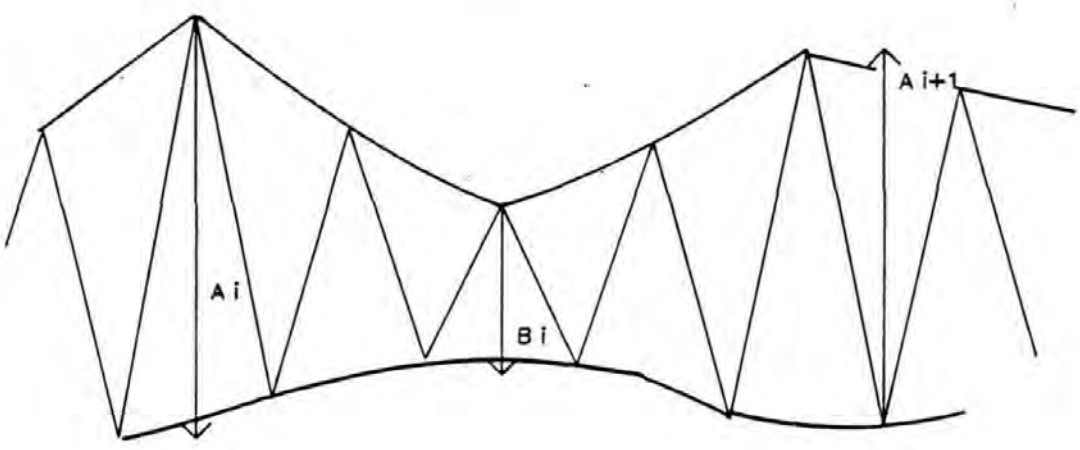

Figure 3.4 Section of Wave Envelope

$\bar{A} = (A_1 + A_2 + \ldots\ldots\ldots\ldots A_m)/m$ over the whole record.

$\bar{B} = (B_1 + B_2 + \ldots\ldots\ldots\ldots B_n)/n$ over the whole record

where A_i are the maxima taken from the wave envelope and B_i are the minima taken from the wave envelope then:

Incident wave height $H_I = (\bar{A} + \bar{B})/2$ (3.7)

Reflected wave height $H_R = (\bar{A} - \bar{B})/2$ (3.8)

Reflection Coefficient $\rho = (H_R/H_I) \times 100$ (3.9)

When the chart recorder was used the results were scaled by the chart recorder transfer function as described in Chapter 2.

3.3.2 Free Second Harmonic Wave

The procedure described above is a simplification of the real situation. The waves produced by a sinusoidal paddle motion do not have the ideal constant form which would be expected. As the waves propagate they slowly change form in a periodic way, which depends on both the wave steepness H/L, the relative water depth d/L, and the undisturbed water depth. There is then a temporal variation of the surface elevation at different points along the channel. One reason for the irregularities is that a paddle cannot exactly produce the variation of the particle motion which corresponds to a progressive wave of constant form.

This phenomenon has been investigated by a number of people including Goda (1967), Le Méhauté et al (1968) and Iwagaki and Sakai (1970).

An analysis of the changing wave profile suggests as a crude explanation that a smaller wave is travelling down the channel superimposed on the main wave, but with a somewhat smaller speed. Theoretical considerations show (Fontanet 1961) that to the lowest approximation the period of this wave is T/2 (where T is the period of the main wave). This wave is called the 'free second harmonic wave'.

Including all terms to second order the surface elevation η can be written as the superposition of a second order Stokes wave and a free second harmonic wave.

$$\eta = a_1 \cos (wt-kx) + a_2 \cos 2(wt-kx) + a_{22} \cos (2wt-k_{22} x + \alpha_{22}) \quad (3.10)$$

Analysis of the above equation shows that the water surface elevation varies with distance but not time.

The existence of the free second harmonic waves requires that care must be exhibited when measuring the maxima and minima in the wave envelope. It is important to measure between adjacent waves rather than absolute maxima and minima. The computer program is designed to calculate successive wave heights rather than absolute maxima and minima.

Figure 3.6 is an example of the data sheet used for a regular wave test.

An example of a wave envelope is shown below.

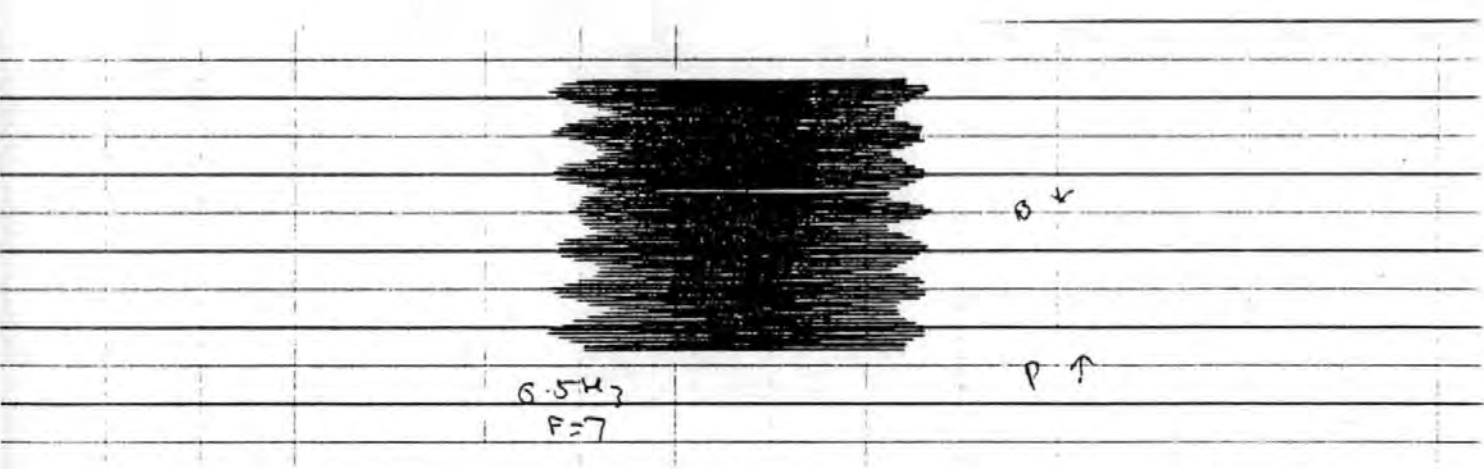

Figure 3.5 Example of a Wave Envelope for 0.5Hz waves.

REGULAR WAVE TEST

DATE = 4−12−84

WATER DEPTH = 1.00 m

WAVE GAUGE−SET OUTPUT = 5.00

PEN RECORDER RANGE = 50 mV

GENERATOR SETTINGS

FREQUENCY = 0.7 Hz

FILTER = 6

GAIN = 0.80

WAVE ABSORPTION IN OUT

ENVELOPE MAX (Hmax '')

4.0,4.0,3.9,4.0,4.1/4.0,4.0,4.0,3.9,4.0

Hmax= 3.99 Smax= 0.05

ENVELOPE MIN (Hmin '')

3.5,3.5,3.5,3.5,3.4/3.5,3.5,3.5,3.5,3.5

Hmin= 3.49 Smin= 0.03

PEN TRANSFER SCALE

HI=(3.99 + 3.49)/2* 0.961 * 15.58 = 56.00 mm

HR=(3.99− 3.49)/2* 0.961 * 15.58 = 3.74 mm

REFLECTION COEFFCIENT=HR/HI*100 = 6.7 %

WAVE HEIGHT(HI)/INPUT VOLTAGE= 0.07 m/Volt

FIG 3.6 REGULAR WAVE TEST DATA SHEET

3.4 Random Waves : The Energy Spectrum

3.4.1 Introduction

The analysis of a random wave record is a more complicated procedure than the regular wave analysis. Over the years no definitive approach to nomenclature and procedure has been developed. The intention here is to adopt the convention used at the Institute of Oceanographic Sciences (IOS) and by Bendat and Piersol (1971).

There are two basic types of analysis for random wave records. The wave by wave approach or analysis by energy spectrum. The former is the more straightforward but limited in applications. Since the advent of 'cheap' computing the energy spectrum approach has gained almost universal use and all the information available from a wave by wave analysis is available via the energy spectrum. The wave by wave record is a good check on the coding for the energy spectrum approach and can provide a quick 'first impression' before a more detailed analysis is undertaken.

3.4.2 Wave Record - Time Domain

A wave by wave analysis of the record only yields limited data but is very quick. The available information and definitions are given below:

Mean zero up-crossing period T_z

The time between successive up-crossings of mean water level (MWL).

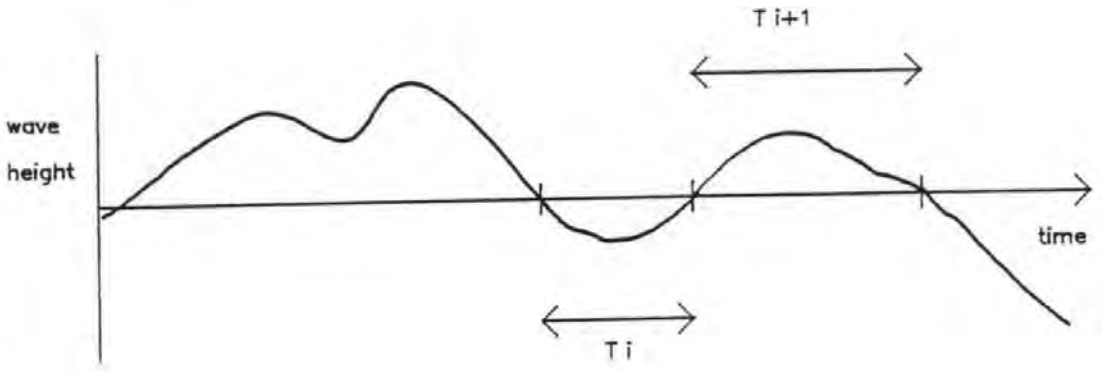

Figure 3.7 Mean zero up-crossing period

$$\tilde{T}_z = \sum_{i=1}^{n} T_i/n-1$$

The computer program calculates this by searching for each successive up-crossing in the digital wave record and calculating the mean.

Significant Wave Height $\bar{H}_S$

The mean of the highest 1/3 of all the waves in the record. $\bar{H}_S$ approximates to the visual estimate of wave height that would be obtained by an experienced observer. The program finds $\bar{H}_S$ by calculating all the wave heights in the record and sorting them to ascending order. The highest 1/3 of the values can then be averaged. The sort for significant wave height makes it straightforward to calculate other percentiles. The values calculated by the program at present are the mean highest 10% and 1%. In addition the maximum and minimum wave heights are output.

Wave Steepness

The parameters calculated can also be used to calculate a value for wave steepness defined as:

Wave Steepness = Wave height/wave length

3.4.3 Energy Spectrum

The study of wave statistics connected with the energy spectrum of surface elevation is made on the assumption that sea waves are a random Gaussian process. The many approaches to producing an energy spectrum were discussed in Chapter 1. The technique used here was to produce a variance density spectrum via a Fast Fourier Transform (FFT). The FFT algorithm was taken from the HP Numerical Analysis programs and adapted to accept up to 4k (4096) of data instead of the 1k (1024) for which it was written. A full description of the FFT process and the energy spectrum has been produced by Tucker (1979).

The variance density spectrum, calculated from data recorded at one location within the channel, will be referred to as a 'point' spectrum.

3.4.3.1 Fast Fourier Transform

The FFT algorithm used is a Radix-2 FFT. In this the sequence length is given by:

$$N = 2^t$$

where N is the number of data points and t is an integer. For a 4k data set t = 12.

The data set is split into two complimentary arrays. The even points (i.e. the 2nd data point, 4th....) are put into the real array and the odd points into the imaginary array.

The FFT is defined as $X(F_k,T) = \bar{X}_k = \sum_{m=0}^{n/2-1} x_{2m} \quad W^{2nk} - W^k \sum_{m=0}^{n/2-1} x_{2m+1}$ (3.11)

For k = 0 to N/2-1

and $W=e^{-i2\pi/n}$ $\quad i = \sqrt{-1}$

The values are returned as a real and imaginary pair with a frequency interval of

$\Delta f = 1/(N \times Dt)$ where Dt is the sampling interval.

It is common to apply some kind of window function to the data to produce a smooth estimate. The window function used here is the Cosine Taper Window. The equations for this window and others can be found in Appendix D. The effect of the window is to reduce the variance of the tapered data relative to the original data. The smooth estimates should be multiplied by 1/0.085 to retain the correct variance. Examples of spectra from the same data set with and without windowing can be seen in Figs 3.8 and 3.9.

In order to remove the energy at 0 Hz it is usual to transform the data to have a mean value of zero.

The cut-off frequency is defined as

$$F_{cut} = (\Delta f \times N)/2$$

3.4.3.2 Variance Density Spectrum

The variance density $\tilde{G}_k$ is defined as

$$\tilde{G}_k = G_x(F_x) = \frac{2}{N \times D_t} \mid X(f_{t1}T) \mid^2$$

$$= \frac{2Dt}{N} \mid X_k \mid^2 = \frac{2Dt}{N} \mid X_k^* X_k \mid \qquad (3.12)$$

where $k = n\Delta f$ and X_k^* is the complex conjugate of X_k.

The raw estimates of variance density need to be smoothed in some manner since successive values are essentially uncorrelated.

3.4.4 Smoothing

There are two types of smoothing available. Frequency smoothing or segment averaging. The method used here is segment averaging. In this case q slices of a time slice of length, T_r', are averaged together such that $T_r = n\ qT_r'$ where T_r is the original record length. The final smooth estimate is then given by:

$$\tilde{G}_k = \frac{1}{q} \left[\hat{G}_{k1}, + \hat{G}_{k2}, \quad .....\hat{G}_{kq} \right] \tag{3.13}$$

where $\hat{G}_k$, q is the raw estimate at frequency f_k of the qth time slice.

The bandwidth will be approximately $1/T_r'$.

The normalised standard error in calculating the spectrum, ϵr, is given by:

$$\epsilon r = \sqrt{1/q} \tag{3.14}$$

3.4.5 Variance Density Algorithm

The main steps in the algorithm used for calculating a variance density spectrum are listed below:

1. Transform data to have mean value zero.
2. Taper the data using the cosine taper data window.
3. Compute X_k using the FFT routine
4. Compute G_k.
5. Adjust estimates by 1/0.875 to correct for tapering.
6. Smooth estimates by segment averaging.

Examples of Variance Density Spectrum are given in Figures 3.8 and 3.9.

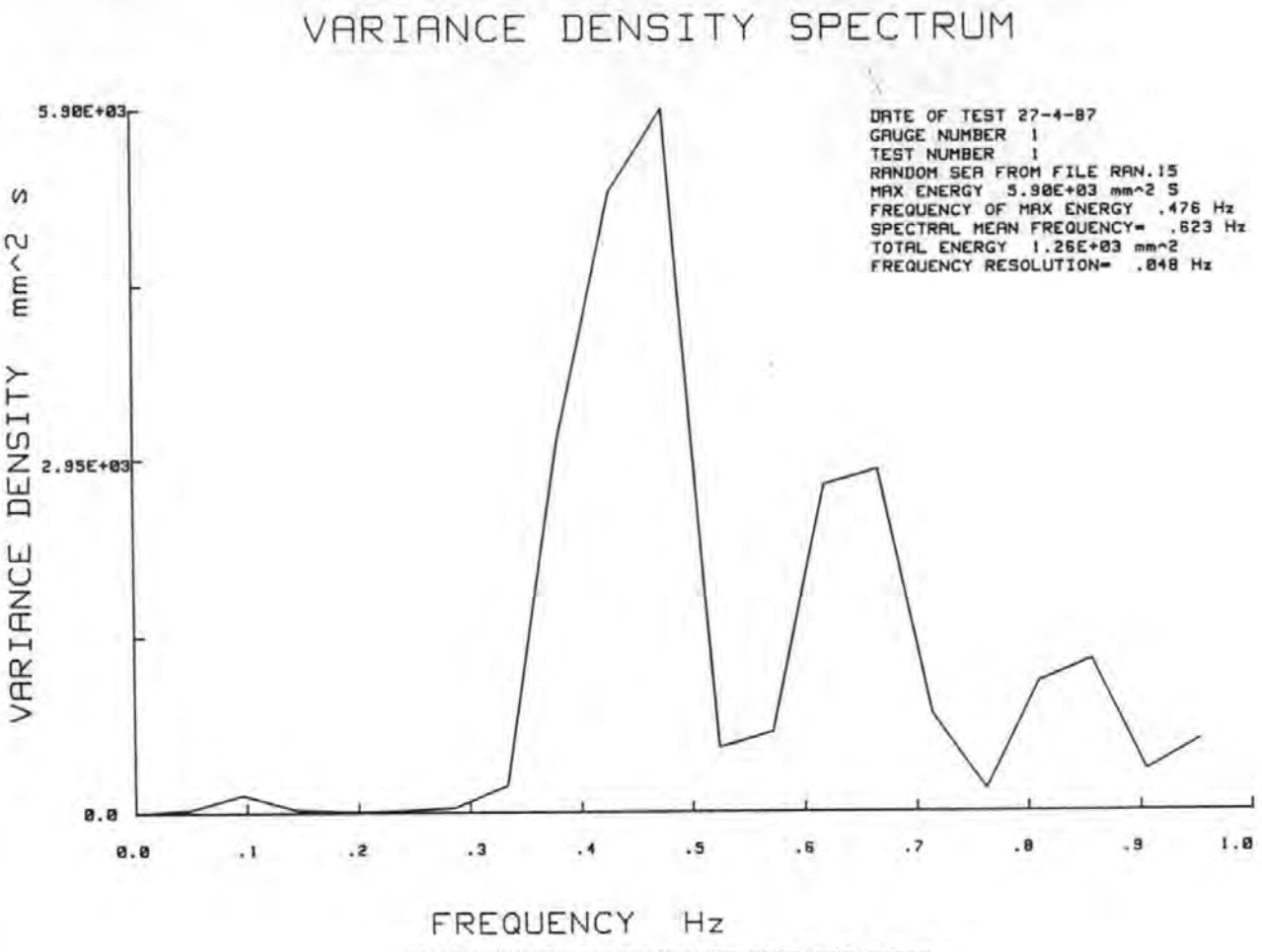

FIG 3.8 VARIANCE DENSITY SPECTRUM WITH COSINE TAPER APPLIED

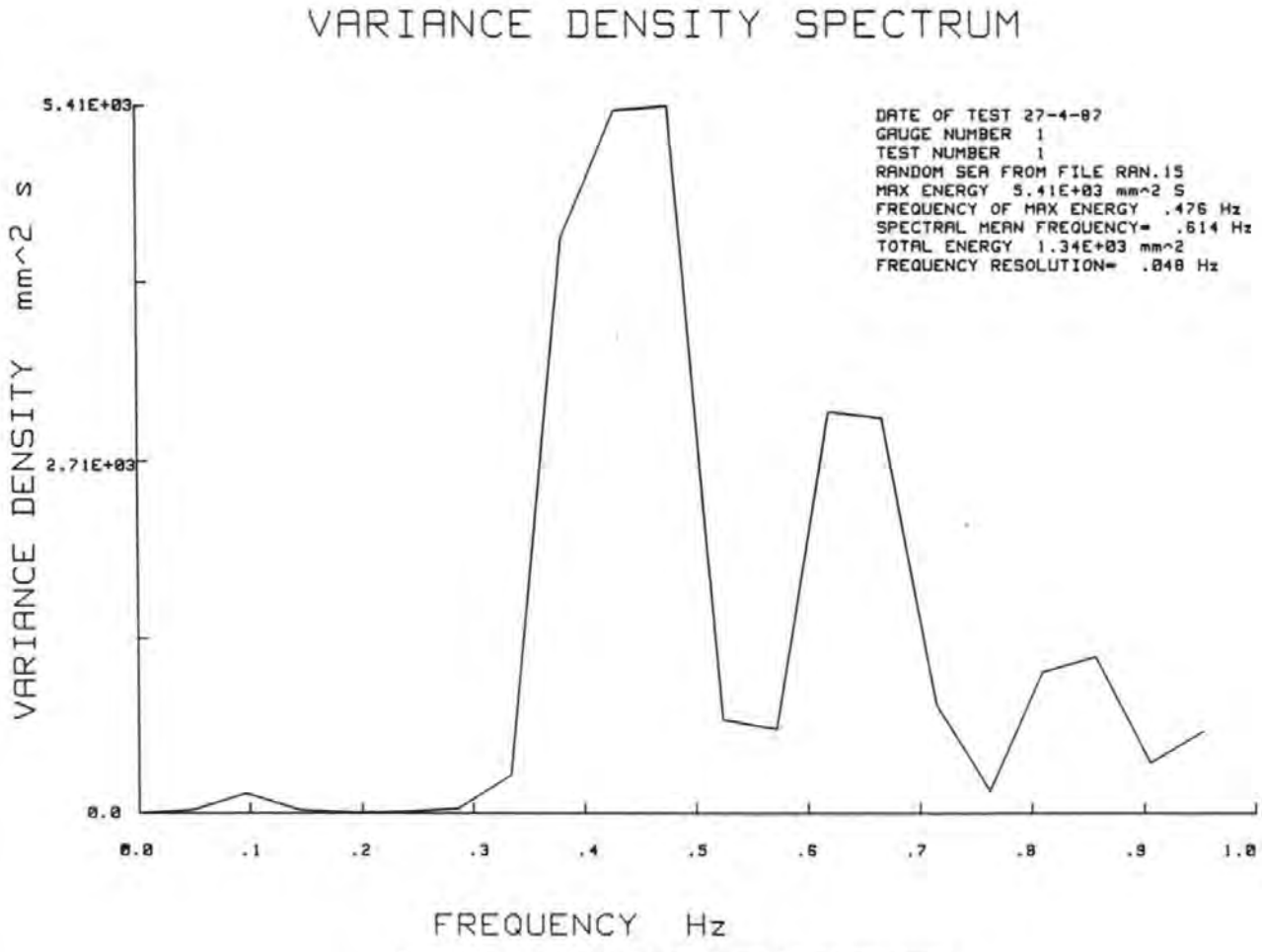

FIG 3.9 VARIANCE DENSITY SPECTRUM WITH NO COSINE TAPER APPLIED

3.5 Statistics from Spectrum

It is possible to estimate various wave statistics from the spectrum. The significant wave height $\bar{H}_S$ is the most statistically stable of these and is given by:

$$\bar{H}_S = 4\sigma = 4\sqrt{M_0} \qquad (3.15)$$

where σ is the variance of the spectral estimates.

If higher order statistics are calculated then an estimate of the zero-crossing period can be obtained, although it has been found (Goda 1974) that this can be up to 20% too low compared to the physical situation.

Other statistics calculated include:

$$\text{Spectral width parameter} = \sqrt{(M_0 M_4 - M_2^2)(M_0 M_4)}$$

where M_0, M_2 and M_4 are Spectral Moments defined by:

$$Mn = \int_0^\infty f^n \, G(t) \, df$$

where M_n denotes the nth moment and n is an integer

$$\text{Spectral peakedness parameter} = \frac{2}{m_0^2} \int_0^\infty f[G(t)]^2 \, df$$

Spectral mean frequency = centroid of spectrum

The following list is a list of typical input parameters and parameters calculated for a variance density spectrum:

Record Size	4096
Sampling Interval	0.1 S
Record Length	409.6 S
Cut off Frequency	5 Hz
Discrete frequency interval	0.00244 Hz
Normalised Standard Error	15.6%
Bandwidth	0.1001 Hz
No. of raw estimates in smooth estimate	41
Frequency Resolution	0.049 Hz

Table 3.1 Energy Spectrum Parameters

3.6 Random Waves : Frequency Response Function Method (FRFM)

3.6.1 Introduction

As previously mentioned, in a laboratory wave channel a proportion of the energy of the waves is reflected back along the channel towards the wave generator. Hence, in random waves, it is necessary to have a means of measuring the incident wave spectrum and the reflection coefficient. This can be done by simultaneously recording the water surface elevations at two points x and y separated by a distance, s, in the direction of wave propagation and calculating the cross-spectrum. A number of techniques were reviewed in Chapter 1. The incident spectrum and reflection coefficient can be calculated from the cross-spectrum. This approach was used by Kajima. The calculations are achieved with a FFT in preference to the correlation functions originally used.

3.6.2 Cross-spectrum

The cross-spectrum is given by:

$$G_{xy}(f) = \frac{2\Delta f}{N} \left| X_k^* \, Y_k \right| \qquad (3.15)$$

where X_k^* is the complex conjugate of X_k.

Thus it is possible to obtain the cross-spectrum from FFT's of the two data sets at x and y.

The cross spectrum will be a complex pair often written as

$$S_{xy} = c + iq \qquad (3.16)$$

For the subsequent analysis the spectra at x and y, S_{xx} and S_{yy} are calculated in the same way as described in the previous section and S_{xy} is calculated as above.

3.6.3 Frequency Response Function

For waves in a channel the frequency response function, H, is given by:

$$H=e^{-ks} = \cos(ks)-i\sin(ks) \qquad (3.17)$$

where k is the wave number: $k = 2\pi/L$

since a particular wave component only undergoes a phase change of ks radians between x and y.

3.6.4 Incident and Reflected Spectra

The situation is represented schematically below:

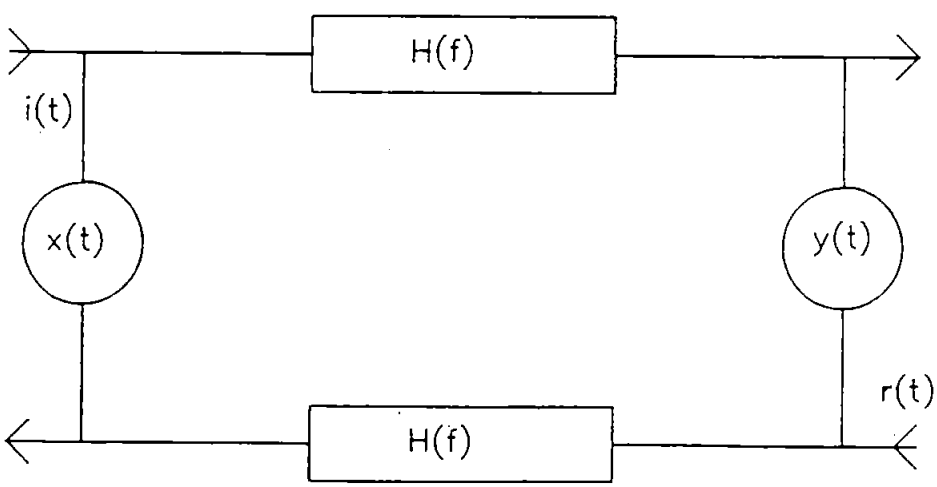

Fig.3.10 Schematisation of Laboratory Reflections

No assumption has been made about any correlation between the waves in the two directions. If I, R, X and Y are the fourier transforms of the waves in the two directions and of the waves recorded at x and y then:

$$X = I + HR \tag{3.18}$$

$$Y = HI + R \tag{3.19}$$

That is the transform at x is equal to the transform of the incident spectrum at x added to the frequency response of the transform of the reflected spectrum at Y.

A full expansion of all the following complex algebra can be found in Appendix B.

From (3.17), (3.18) and (3.19)

$$I*I = (X-HY)*(X-HY)/(1-H^2)(1-H^2) \tag{3.20}$$

$$R*R = (Y-HX)*(Y-HX)/(1-H^2)(1-H^2) \tag{3.21}$$

Hence

$$S_{ii} = (S_{xx} + S_{yy} - 2c\ \mathrm{Cos}(ks) - 2q\ \mathrm{Sin}\ (ks)/4\ \mathrm{Sin}^2(ks) \tag{3.22}$$

$$S_{rr} = (S_{xx} + S_{yy} - 2c\ \mathrm{Cos}(ks) + 2q\ \mathrm{Sin}\ (ks)/4\ \mathrm{Sin}^2(ks) \tag{3.23}$$

The reflection coefficient $\rho(t)$ is given by

$$\rho^2(f) = S_{rr}/S_{ii} \tag{3.24}$$

The functions S_{ii} and S_{rr} are singular at

$$k = n\pi\ ,\quad n = 0,1.2\ .....$$

Equations (3.22) and (3.23) are those used in the computer program to derive incident and reflected spectra.

3.6.5 Measurement

The physical measurement of incident and reflected spectra is made by three wave gauges located in the channel. The three gauges measure water surface elevation simultaneously. The spacing of the gauges must be known and an optimum spacing strategy can be used to obtain maximum resolution around the point of most interest (modal frequency). The strategy used is outlined below.

3.6.6 Wave Gauge Separation

The gauges must be separated so that the peak frequency does not occur when $ks = n\pi$, $n=0,1,2 \ldots$ since at these values $\sin^2(ks)$ tends to infinity.

For maximum resolution around the peak frequency the spacing of two of the gauges (gauges 1 and 2 were used) was chosen as $ks = \frac{n\pi}{2}$

Hence $s = \frac{n\pi}{2k}$

The spacing of gauges 2 and 3 was chosen so that $\sin\left(\frac{2\pi}{2k}\right) \geq \frac{1}{2}$ in all cases.

The third spacing (gauges 1-3) is the sum of the other two spacings and hence a check on the data and the assumptions made about the separations could be kept.

An example calculation for the wave gauge separations for the random seas produced can be found in Appendix C.

The theory and subsequent computer program have been thoroughly tested with the random wave tests on the absorption circuit board.

The effects of different spacings and the resolution of the technique is fully described in Chapter 6 where results from the absorption tests are presented.

3.7 Program Configuration

The program, in addition to calculating variance density spectra at x and y, incident and reflected spectra and a reflection coefficient, also offers substantial graphical output.

All four spectra can be plotted singly or in any desired combination and a reflection coefficient graph may be plotted if required.

A brief description of the program can be found in the next chapter.

Program output can be found in Appendix A.

CHAPTER 4

SOFTWARE DEVELOPMENT

4.1 Introduction

In order to analyse and interpret the results from the physical overtopping studies and to aid the development of the absorption system a comprehensive set of wave data collection and analysis routines was written. The programs were written to be flexible enough to cope with a variety of different test configurations and to be sufficiently 'user-friendly' to allow any number of users rapid access to the interpretations. For this purpose, a comprehensive documentation of all programs, together with sets of instructions, has been compiled.

The programs have been written for the Hewlett-Packard 9816S in HP BASIC 2.0 with extensions AP2.1. The advantage of a microcomputer based system over a mainframe lies in the mobility of the equipment and the ease to which data acquisition and analysis can be implemented.

Wherever possible use was made of the screen defined softkeys. Up to 10 possible answers may be displayed and labelled on the screen and a single key press is all that is required to select an option. For example two keys could be labelled 'Yes' and 'No' and when the questions is displayed a positive answer is given by a single press of the 'Yes' key rather than typing YES 'ENTER'. Use of the softkey facility greatly increases efficiency and reduces the possibility of typing errors.

4.2 Data Acquisition

The data acquisition program was written in a very general form which will allow it compatibility with a wide range of possible data types, provided that the data is logged by a MICROLINK data logger. The program has software control over both the sampling interval and the size of sample required. In addition, it can select any number of modules from the MICROLINK as required and control the multiplexing (simultaneous scanning of all active modules) facility.

Throughout the development of the software the aim has been to eliminate the possibility of any ambiguity in the interpretation of results. From each test, a Masterfile is created by the program. All useful data acquisition parameters such as the date, logging rates, etc, are stored in this file on disc. When the analysis is performed, the analysis program input is only the Masterfile. In this way data entry errors can be eliminated, and analysis proceeds much quicker.

The digital data is collected sequentially in either 8 or 12 bit form (i.e. 0-255 or 0-4095 respectively). The collection starts from the left side of the Microlink and scans all the active modules (see Chapter 2) from left to right up to the last active module. The data is collected by the computer in a sequential buffer file. Thus, if five gauges are being used to each collect 2048 data points the buffer will hold 2048 x 5 = 10240 data points of which the points from module one, for example, will be every fifth starting at one, i.e. 1, 6, 11 etc. and so on for each module.

Once data collection has finished the data is calibrated and stored onto disc in separate data files for the data from each wavegauge. The calibration relates the digital record to the analogue input by an appropriate scale factor (see below).

With this system once all parameters (logging rate, data file names, etc) have been entered and the data acquisition started with the trigger switch (see Chapter 2) no user interaction is required until a data analysis is required.

It is possible that the analogue input signal may have gone beyond the range of the analogue input module (The AN-1, see Chapter 2) and hence the A/D converter. The AN-1 modules have a 10 volt full scale range, adjustable as required, i.e. 0-10V,±5V etc.

An error trap routine has been incorporated within the acquisition program which will note all occurrences where the data may have been clipped at either end of the scale. Thus, with 12 bit conversion if a 0 or 4095 is recorded a message will appear on the printed output to indicate the extent of any truncation. It is then up to the user to decide whether this truncation is acceptable or not with regards to the analysis to be performed on the data.

To help users not familiar with either the Hewlett-Packard or the Microlink, a 'Help' routine has been included in the program which provides 4 pages of instructions and hints for the data acquisition. Any part of 'Help' routine may be printed out on request. A copy of 'Help' is included in Appendix A.

4.2.1 Wave Data Acquisition

When the data acquisition program is used to collect wave data the analogue input modules are connected to the Churchill Controls Wave Monitor (see Chapter 2). Each wave gauge needs to be calibrated separately - as described earlier - to establish a relationship between mm wave height and the digital signal. The calibration of the digital record to mm wave height is in the form of a least squares regression analysis. For each gauge, 8 readings are taken, in 10mm increments from -30mm to + 40mm with 0mm at still water level. The least squares regression analysis of the digital output compared to the theoretical values of mm of surface elevation provides the calibration to mm wave height as well as checking the linearity of the probe.

4.3 Wave Data Processing

Since all the data acquisition and analysis is performed on the same machine very little data processing is required. The data acquisition program stores the data as a digital record of the surface displacement in mm from the still water level. The wave data analysis routines can use the data in this form. However, a library of data processing routines have been written to allow the user some flexibility in data types and rapid access to certain pieces of information.

The programs in the library include programs to; perform spectral analysis on voltage rather than wave height records, read and/or print data files, edit the contents of masterfiles and calibration routines for the wave gauges. Appendix A details a more comprehensive list of data processing programs.

4.4 Wave Data Analysis

All the routines written for the menu-driven wave data analysis software package can process up to a 4k (i.e. 4096) data set. A 4k data is seen as a sufficiently long record for accurate analysis. (Bendat and Piersol 1971).

As a pre-requisite to all the more advanced statistics offered, a general statistical analysis is carried out. The statistics calculated are: mean, variance, standard deviation, root mean square, skewness and kurtosis. A brief glance at such values as the mean can highlight any possible errors in the data and avoid wasting time with a detailed analysis.

Other more advanced statistical routines are then made available (see Appendix A for details of statistics available).

A 'point' spectral analysis routine as described in Chapter 3 is also available in the package although its function is duplicated as part of the main Frequency Response Function analysis.

The Frequency Response Function method was also fully described in Chapter 3. The program written, in addition to computing the incident and reflected spectra also produces the 'point' spectra for both gauge locations. Use of the program provides nearly all the required information for detailed interpretation.

Other programs which are on the same menu are the program to calculate the overtopping discharge from the breakwater tests (see Chapter 7) and a program to calculate the times and number of overtopping waves in a test.

4.5 Graphics

Whenever possible, use has been made of the excellent graphics capabilities of the HP system and a number of graphics routines have been written to aid the interpretation of results. A further menu is used to determine the location of the output; screen, plotter, etc. Presentation quality is available.

4.6 Regular Wave Reflection Program

A program, the logic for which was described in Chapter 3, was written to help analyse the results of the regular wave tests. The regular wave tests were used both to calibrate the paddle and then to test the absorption system. The program calculated a wave envelope from the digital record. To try and eliminate any unwanted values which may be in the data, such as from mains spikes, values outside 30% of the mean of maxima and minima were discarded. The 30% value was chosen after careful scrutiny of chart records.

The results from the program were compared to a manual analysis of a chart record and found to be within ± 1mm.

4.7 Programming Considerations

In order to keep the dynamic memory (i.e. array memory) as large as possible, all the analysis programs are written as subroutines which are loaded into memory from disc if required, and removed once they have been used. Careful allocation of array space was also maintained.

The graphics programs are written is a combination of HP BASIC and HPGL (Hewlett Packard Graphics Language).

For the more complex programs 'HELP' routines have been built in, the routines can be called if a user is uncertain as to the program's operation or function. Pages from the 'HELP' routines can be output on the printer if required.

Although BASIC is a non-compiled language the analysis is fairly quick. The results are all presented in a non-ambiguous form on the printer with clear labels and all the input information such as date, test number etc. clearly shown. Large quantities of data can thus be processed with no problem of confusion of data.

The 'HELP' routines are given in Appendix A, together with the statistics offered and the execution times of the main programs.

4.8 Program Flowcharts

Simplified flow diagrams are given in Figures 4.1 - 4.3 for the main data acquisition and analysis programs. Where necessary a brief description of subroutine function is also given.

4.9 Quality Assurance

All the programs have been extensively tested and wherever possible the results compared to a manual analysis. Checks were made at all stages of the development with diagnostic information printed out if necessary. All the program output contains details of the input parameters to provide a check on the results.

Cross-checking of results wherever possible also helps verify the computer analysis. The extensive graphical output also helped to validate the results of some of the more complex programs such as the Frequency Response analysis.

A comprehensive wave data acquisition and analysis suite has now been compiled with a high degree of confidence in the software. The system is also very user-friendly.

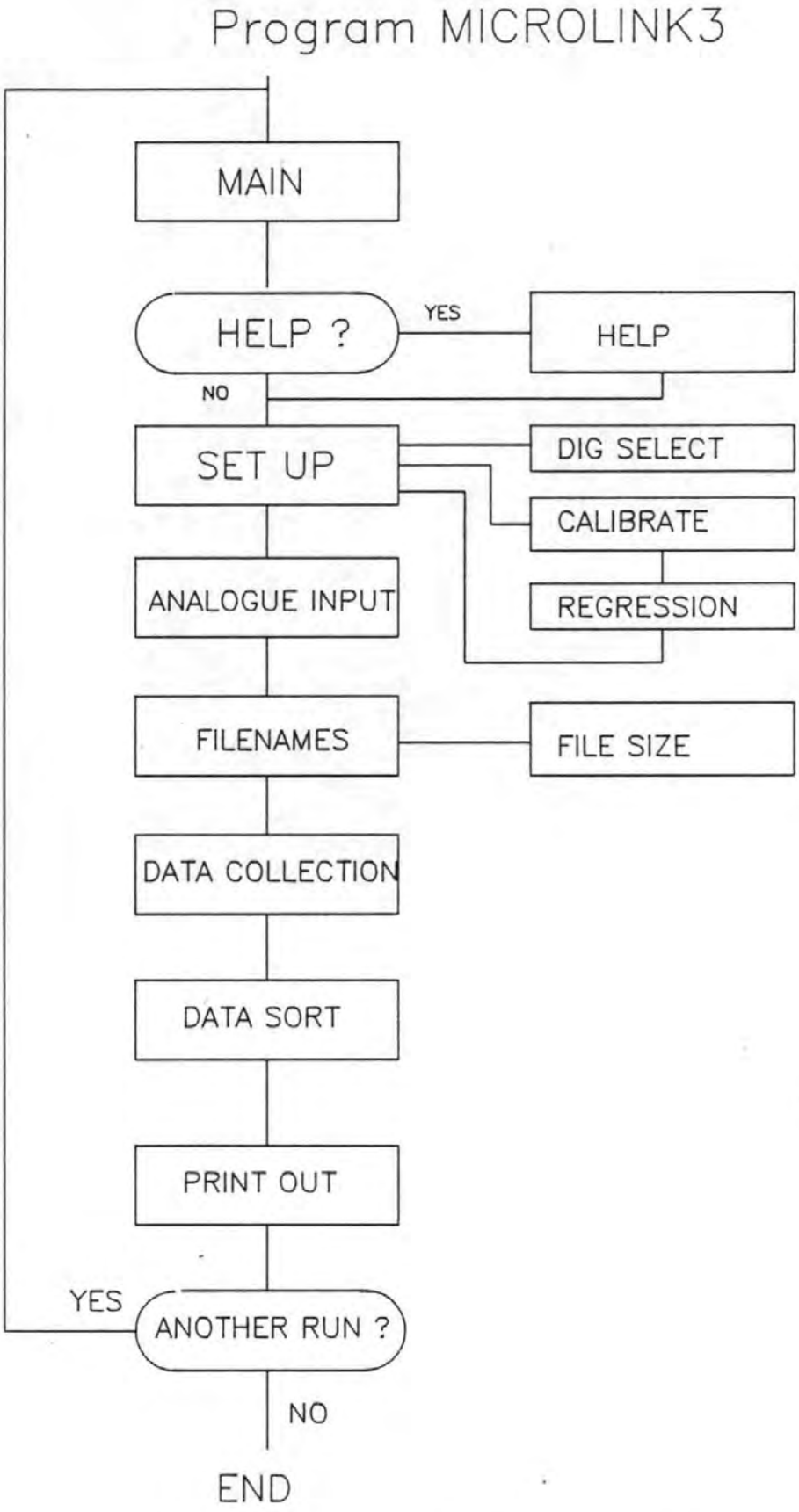

FIG 4.1 FLOW CHART FOR DATA ACQUISITION PROGRAM

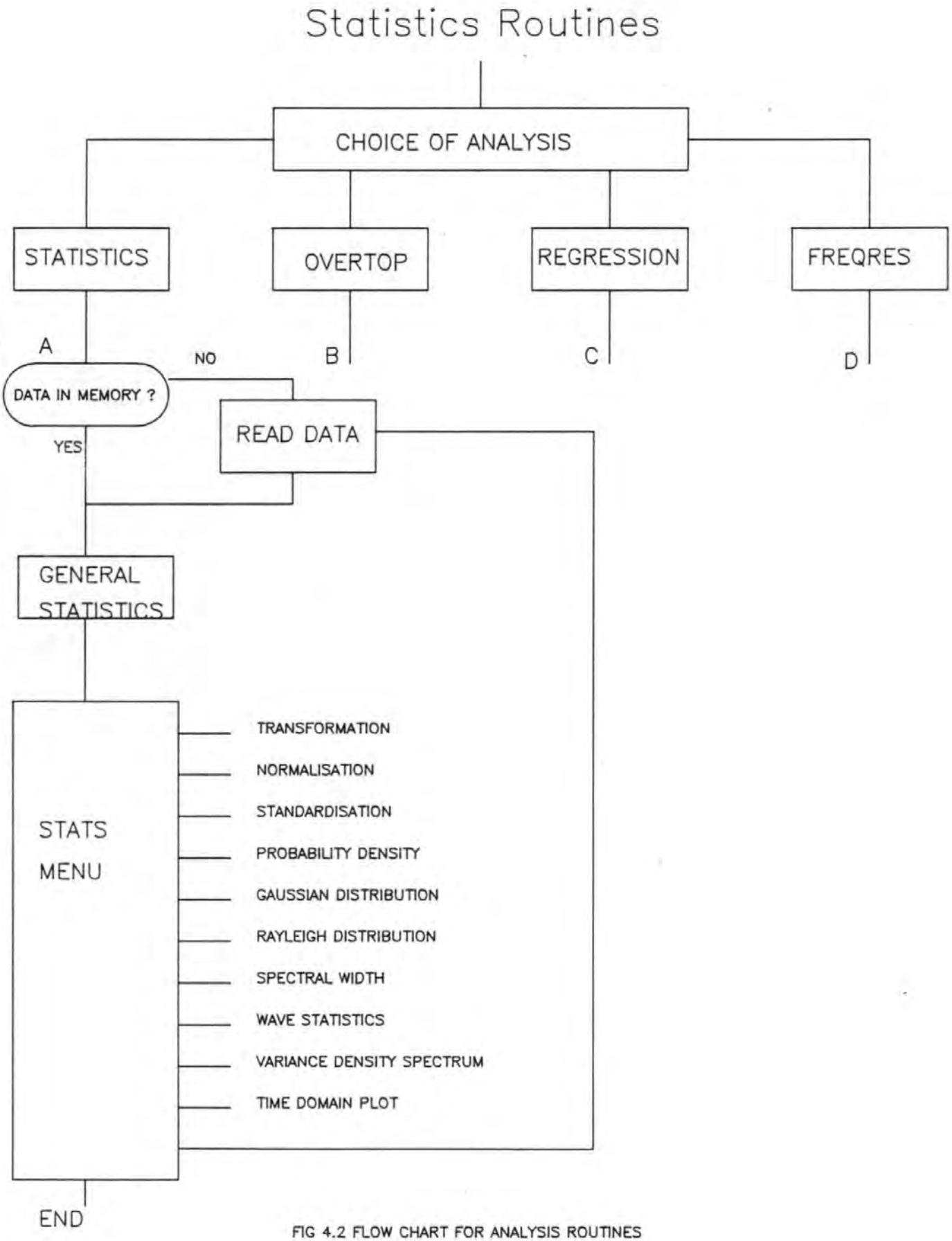

FIG 4.2 FLOW CHART FOR ANALYSIS ROUTINES

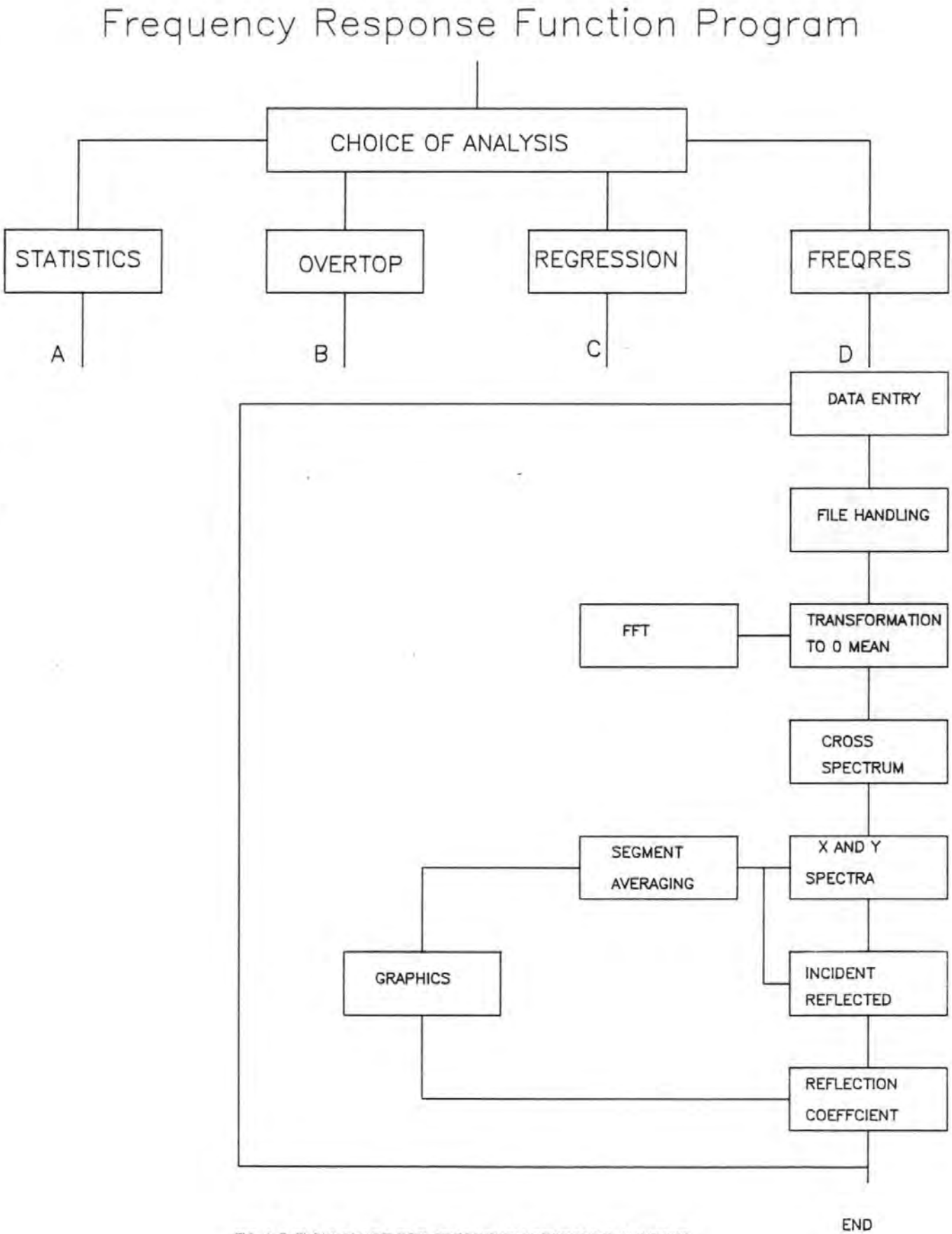

FIG 4.3 FLOW CHART FOR FREQUENCY RESPONSE ANALYSIS

CHAPTER 5

CALIBRATION AND OPTIMISATION OF THE PADDLE

5.1 Introduction

Only basic construction of the wedge wave paddle and channel facility had been completed at the onset of the project. Initially, a calibration and optimisation of the paddle was undertaken and over the first 8 months or so a number of operating problems were encountered and snags in the system ironed out.

5.2 Paddle Dynamic Characteristics

The dynamic characteristics of the paddle need to be known for the generation of random waves as mentioned earlier. The procedure is to determine a Transfer Function of wave amplitude to input voltage. [Equations (5.1 to 5.3)]. The simplest procedure is to produce a whole series of monochromatic waves with different input voltages for various depths of water in the channel. The results from each test series can be then used to produce the Transfer Functions needed for random wave generation (see Chapter 2). For the purpose of this investigation the following conventions were used. This convention avoids the ambiguities in changing from amplitude to height present in the regular and random Hydraulics Research software.

5.3 Conventions

The amplitude in volts of the sinusoidal paddle control signal is known as an input voltage, defined as the voltage amplitude i.e. Input voltage = 2 means a ±2V signal.

The input voltage is related to Wave Amplitude where the wave amplitude is half the total peak-trough height.

The Stroke Length used to calculate the theoretical transfer function and used in the absorption circuit board tests is half stroke or stroke amplitude (see also Chapter 7).

5.4 Test Procedure

The method of analysis to determine incident and reflected wave heights from a wave envelope has already been discussed (Chapter 3). The practical test procedure was to mount a wave gauge onto the trolley above the channel. The envelope of the wave motion was produced by a slow moving traverse forward i.e. in the direction of wave propagation, and back over a 11m section of channel. The results were recorded to a chart recorder for subsequent analysis. Later a computer program was written to analyse the wave record.

Sinewaves with frequencies from 0.1 Hz up to that frequency which caused the waves to break were generated, incremented in steps of 0.1 Hz. For each test series the wave gauge was calibrated to provide a relationship between m wave height in the channel and inches on the chart recorder (inches were used simply because the chart paper was scaled in inches). A typical test series would require 1½ hours of laboratory work and a further 1½ hours manual analysis time. The computer analysis reduced the analysis time to a couple of minutes.

To determine the dynamic characteristics of the paddle the tests were repeated with 5 different input voltages (gain) and 3 different water depths. The gains used (see Glossary and Chapter 2) were 0.40, 0.80, 1.00, 2.00 and 3.00 which cover the expected range of random wave heights up to 220mm.

The test were all carried out with the spending beach at the opposite end of the channel to the wave paddle. The spending beach was described in chapter 2.

5.5 Results

A complete set of results from all the tests can be found in a separate report.

A comparison of the Frequency vs. Reflection Coefficient graphs (Figures 5.1, 5.2, 5.3), where the Reflection Coefficient is given as a percentage and measured with the wave envelope theory described in Chapter 3, shows that the overall characteristics of the channel are very similar at all depths of water.

The transfer function graphs of Frequency vs Wave Amplitude (Figures 5.4, 5.5, 5.6) suggest that within the range of general scatter of the results the paddle characteristics for a given depth of water are linear. The transfer function curves all reach a peak at around 1.0 Hz and then a higher frequency wave appears to produce no increase of wave height. The upper limit of any particular test series was determined by wave breaking.

The transfer function curves at 1.00m and 0.80m water depth give very similar results, but the 0.60m depth curve, although the same shape shows waves of much smaller amplitude. This is attributable to the smaller area of paddle front immersed in the water at a lower depth, since all tests were conducted with the paddle moving about its mid-stroke position.

The results were used to produce the following Transfer Function for the generation of random waves in 1.0m and 0.8m of water.

Frequency Hz	Transfer Function m/v
0.1	.003
0.2	.0055
0.3	.010
0.4	.013
0.5	.016
0.6	.023
0.7	.031
0.8	.036
0.9	.038
1.0	.040
⋮	⋮
2.0	.040

Table 5.1 Measured Paddle Transfer Function

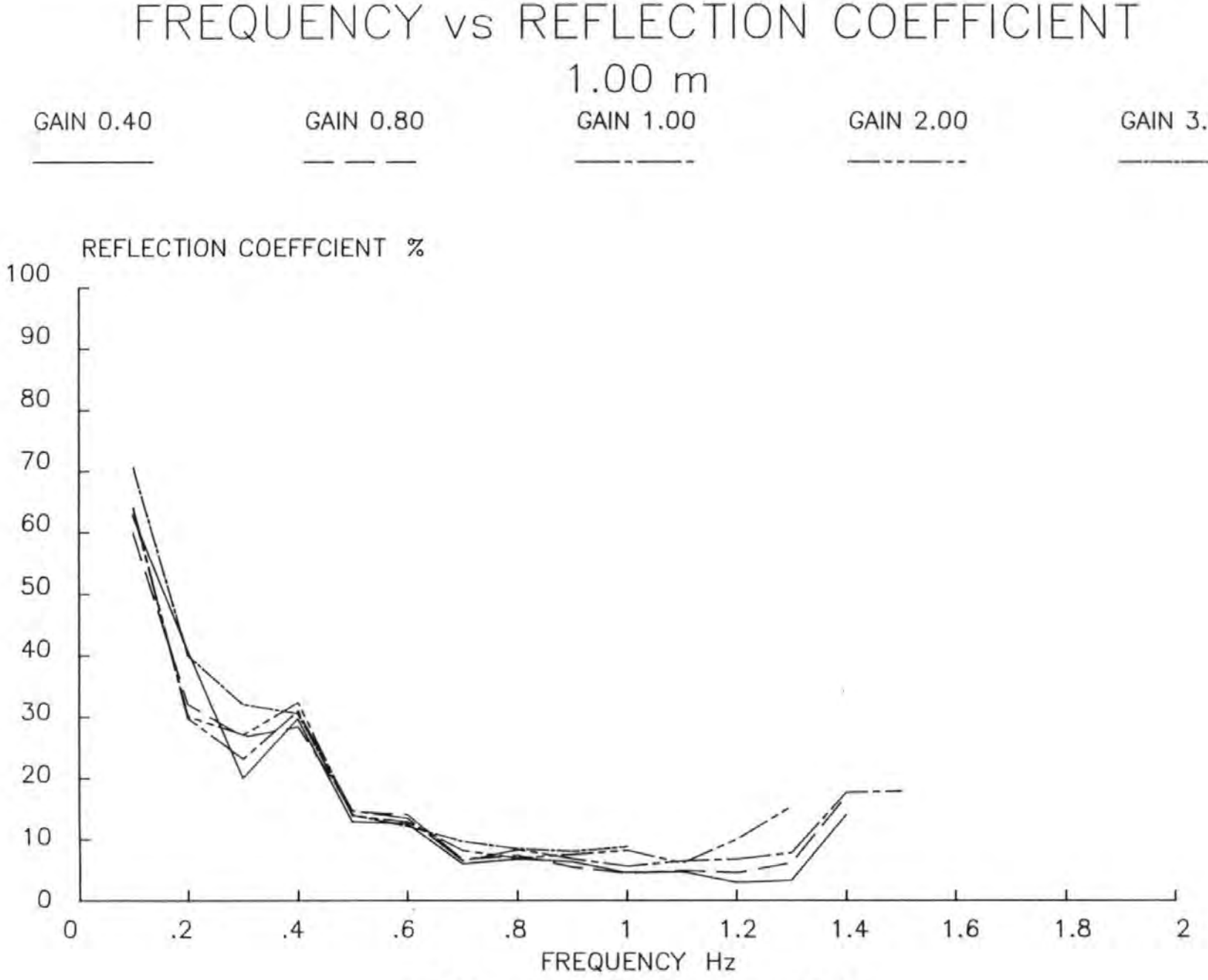

FIG 5.1 CHANNEL REFLECTION CHARACTERISTICS 1.00 m

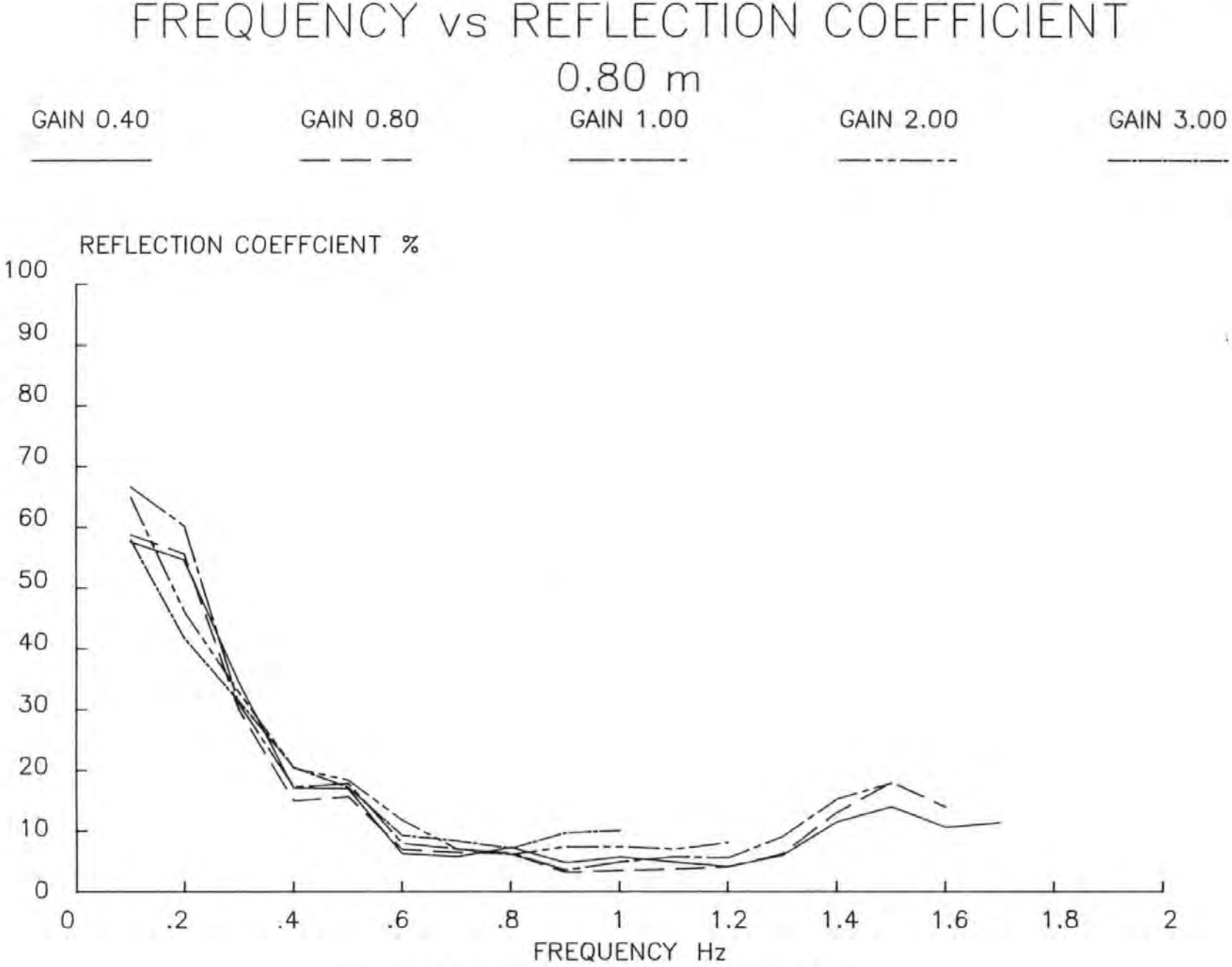

FIG 5.2 CHANNEL REFLECTION CHARACTERISTICS 0.80 m

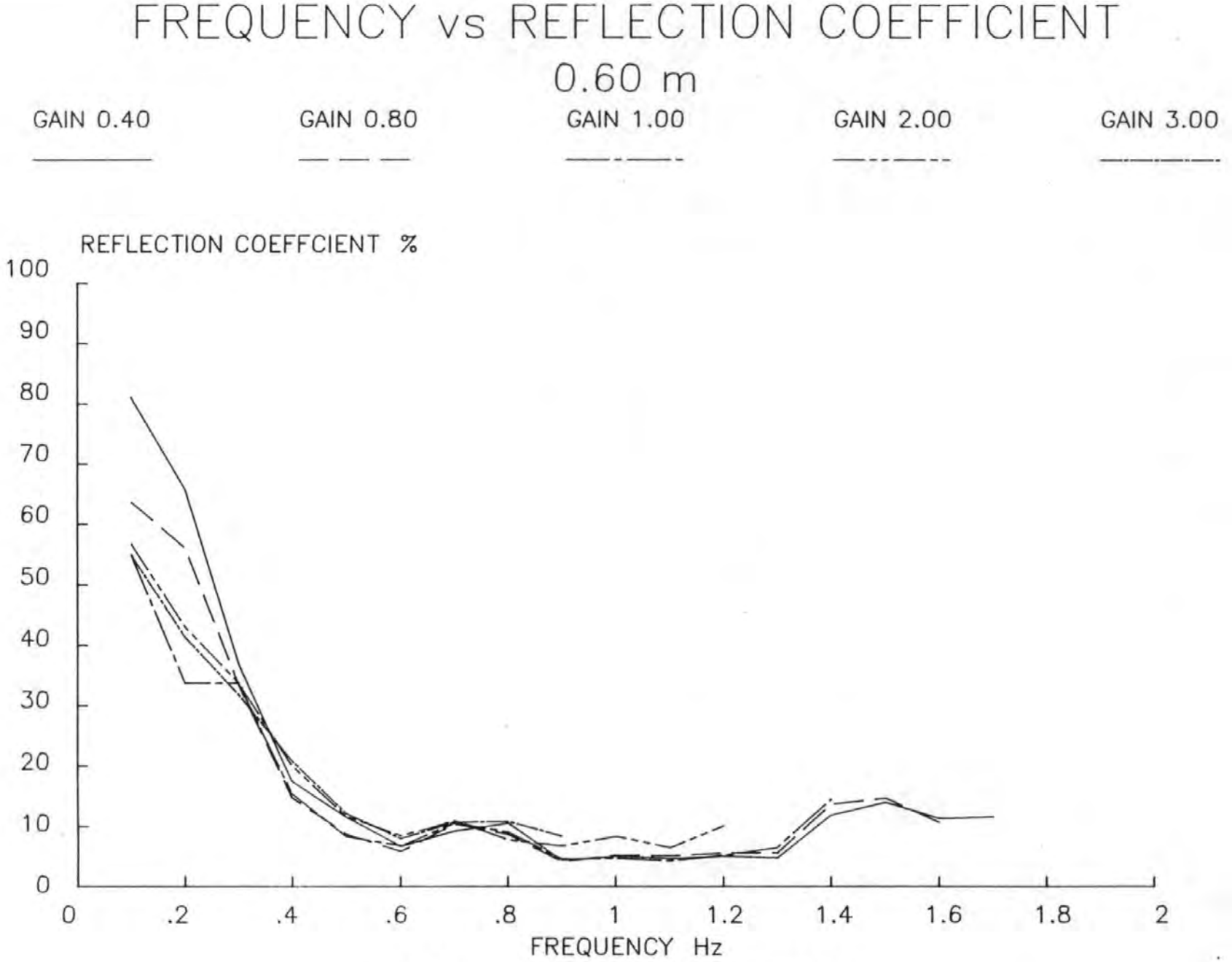

FIG 5.3 CHANNEL REFLECTION CHARACTERISTICS 0.60 m

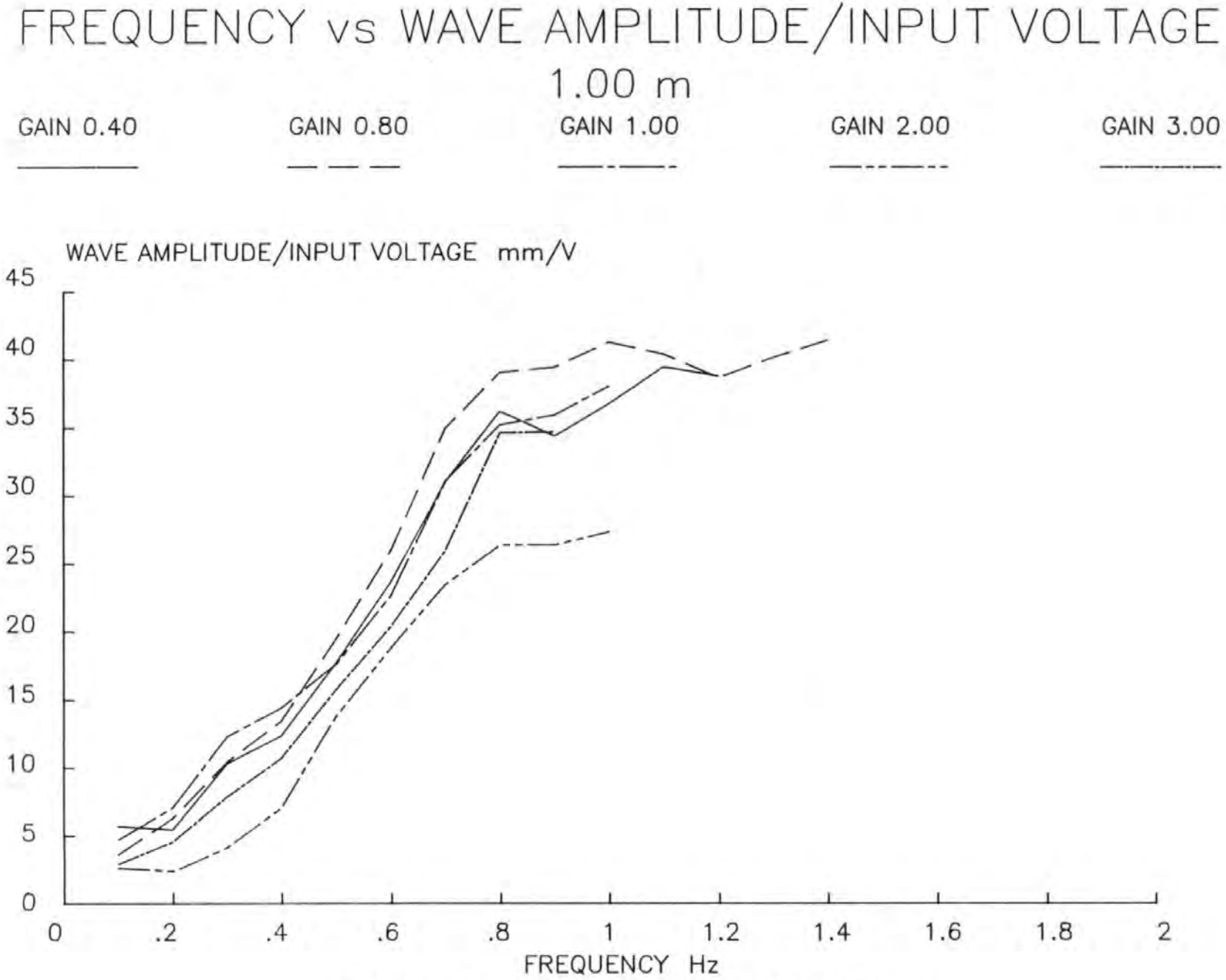

FIG 5.4 PADDLE TRANSFER CHARACTERISTICS AT 1.00 m WATER DEPTH

FREQUENCY vs WAVE AMPLITUDE/INPUT VOLTAGE

0.80 m

GAIN 0.40 ——— GAIN 0.80 — — — GAIN 1.00 —·—·— GAIN 2.00 —··—·— GAIN 3.00 ———·———

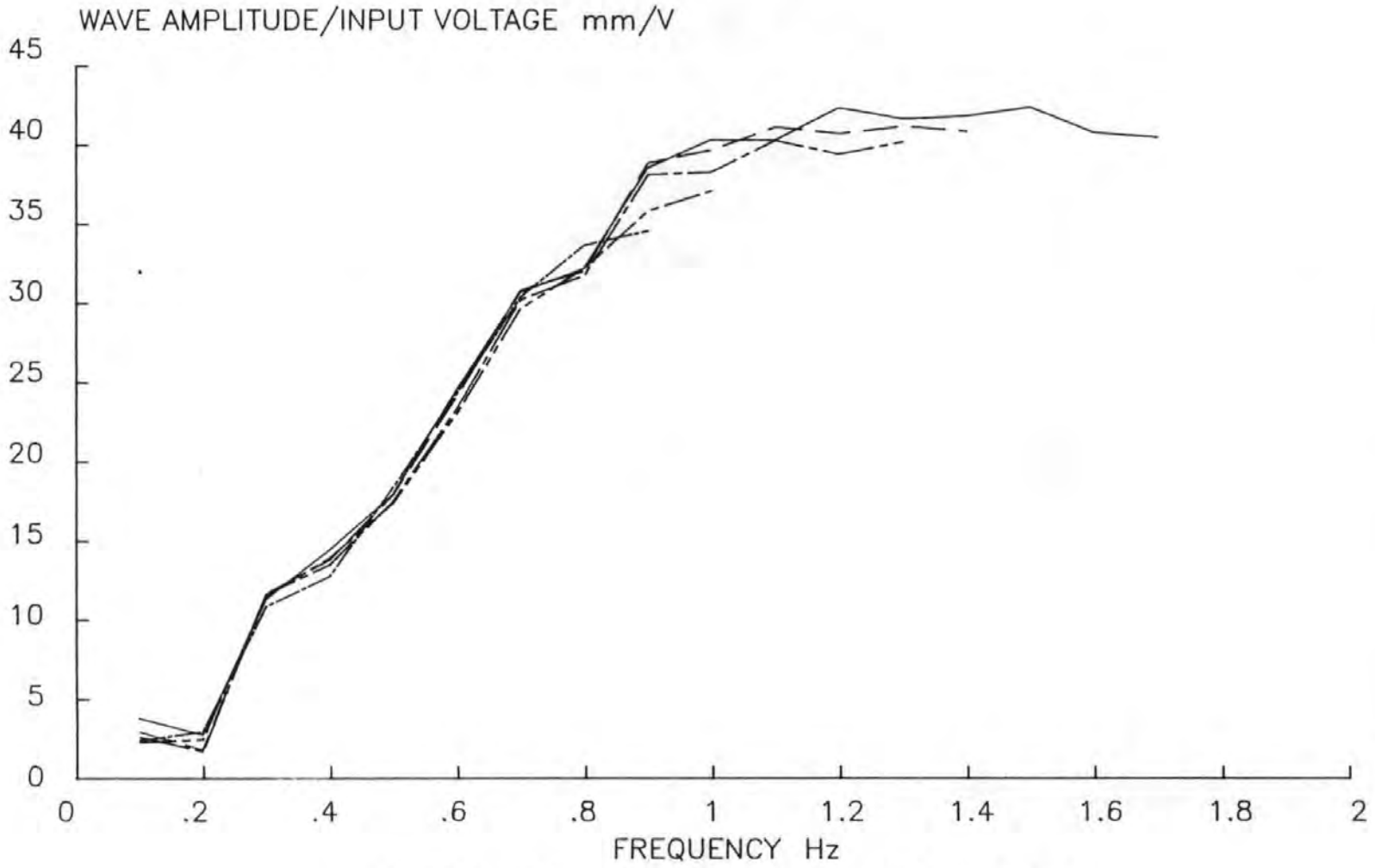

FIG 5.5 PADDLE TRANSFER CHARACTERISTICS AT 0.80 m WATER DEPTH

FREQUENCY vs WAVE AMPLITUDE/INPUT VOLTAGE

0.60 m

GAIN 0.40 ——— GAIN 0.80 — — — GAIN 1.00 —·—·— GAIN 2.00 —··—·· GAIN 3.00 ———·———

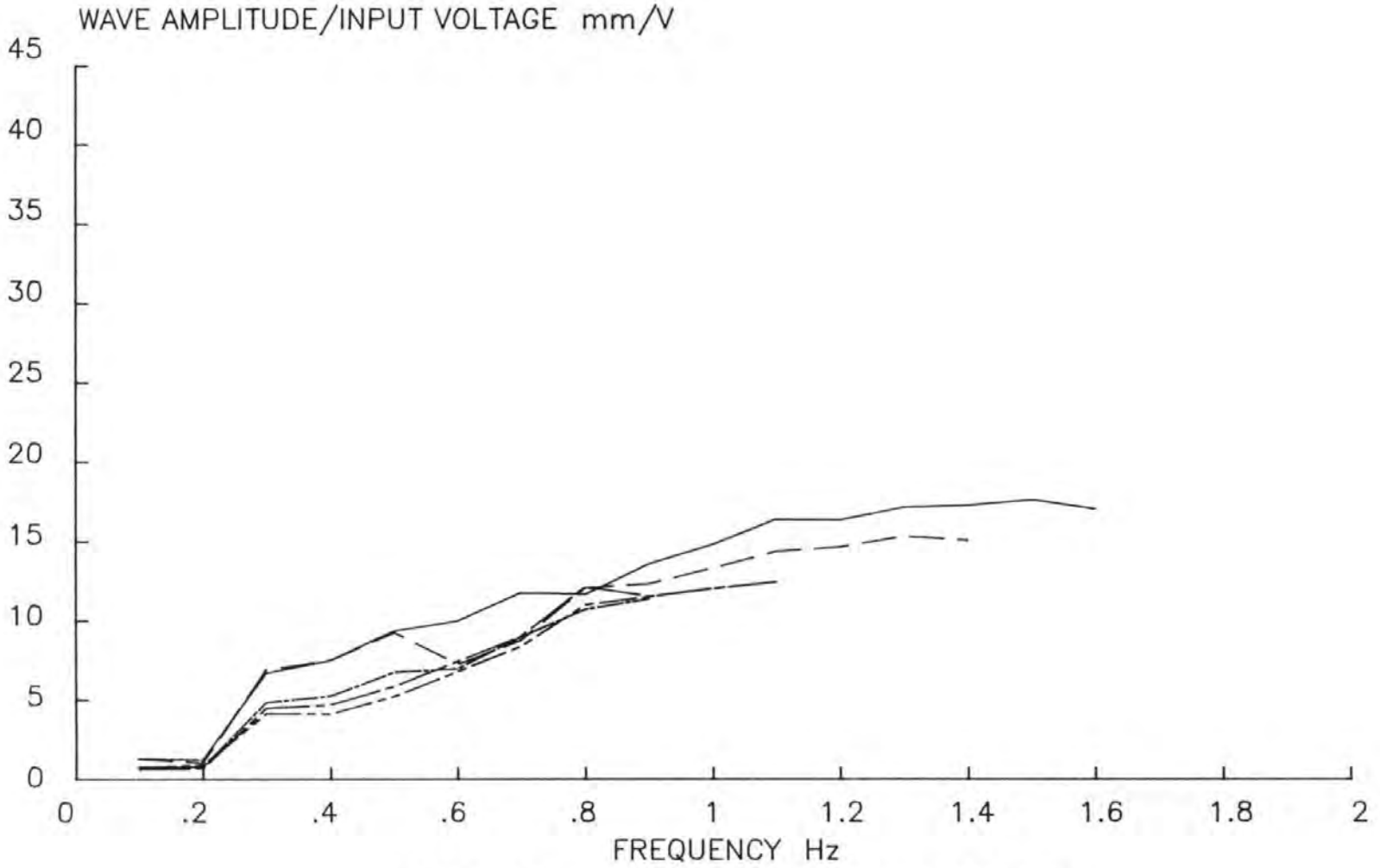

FIG 5.6 PADDLE TRANSFER CHARACTERISTICS AT 0.60 m WATER DEPTH

The transfer function values, once entered into the wave generation program NEWSYN, (see Chapter 2) are stored on disc. The 0.8m depth of water Transfer Function is stored with a filename of 'TRANS8'. For subsequent spectrum generation only the filename needs to be entered and the program will calculate the spectral parameters. Wave generation was more fully described in Chapter 2.

The results of the monochromatic wave tests were presented to Hydraulics Research Limited for a determination of the characteristics necessary to design an effective wave absorption filter as described in the next chapter.

5.6 Theoretical Transfer Function

In addition to the measurement of the Transfer Function with monochromotic waves it is possible to determine the Transfer Function analytically (Thompson et al 1970).

The Transfer Function for the wedge-type paddle in use here has been derived and a comparison shown below and on Figure 5.9.

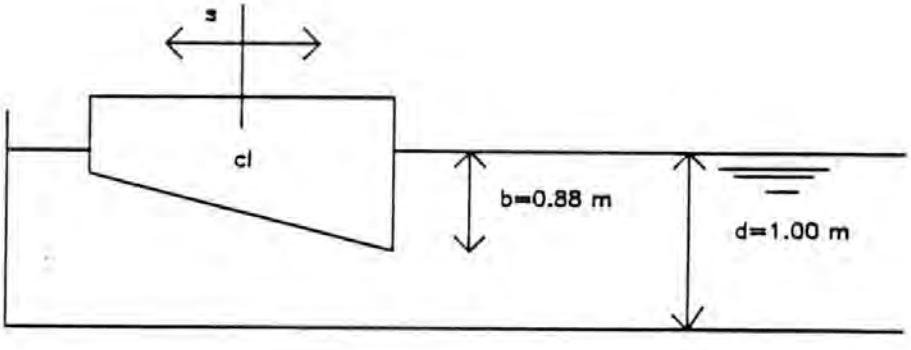

Figure 5.7 Theoretical Transfer Function - Definitions

$W = d/b$ where b - submergence of paddle at mid-stroke
d - water depth (5.1)

$G_2 = H/s$ where H - wave height
s - paddle stroke (5.2)

$\pi = H/gT^2$ where g - acceleration due to gravity = 9.81 m/s^2
T - wave period (5.3)

For a ±1v signal s = 0.02 m
so here W = 0.88/1 = 0.88

The values of G_2 are found from Figure 5.8.

This leads to the following results:

Frequency	% π	G_2	Theoretical h/m	Measured h/m
.1	.001	.18	.0036	.003
.2	.004	.37	.0074	.0055
.3	.009	.60	.012	.010
.4	.016	.80	.016	.013
.5	.025	1.10	.022	.016
.6	.037	1.50	.030	.023
.7	.050	1.70	.034	.031
.8	.065	1.90	.038	.036
.9	.083	1.95	.039	.078
1.0	.102	2.00	.040	.040
2.0	.102	2.00	.040	.046

Table 5.2 Comparison of Measured and Theoretical Transfer Function

The measured transfer function is lower than the theoretical for all frequencies below 1.0 Hz. At 1.0 Hz and above the two are identical. The lower measured transfer function can be in part attributed to the non-perfect frequency response of the paddle to the demand signal. The theory also does not account for losses due to leakage around the paddle. The diffference is, however, small and not unexpected for the reasons mentioned above.

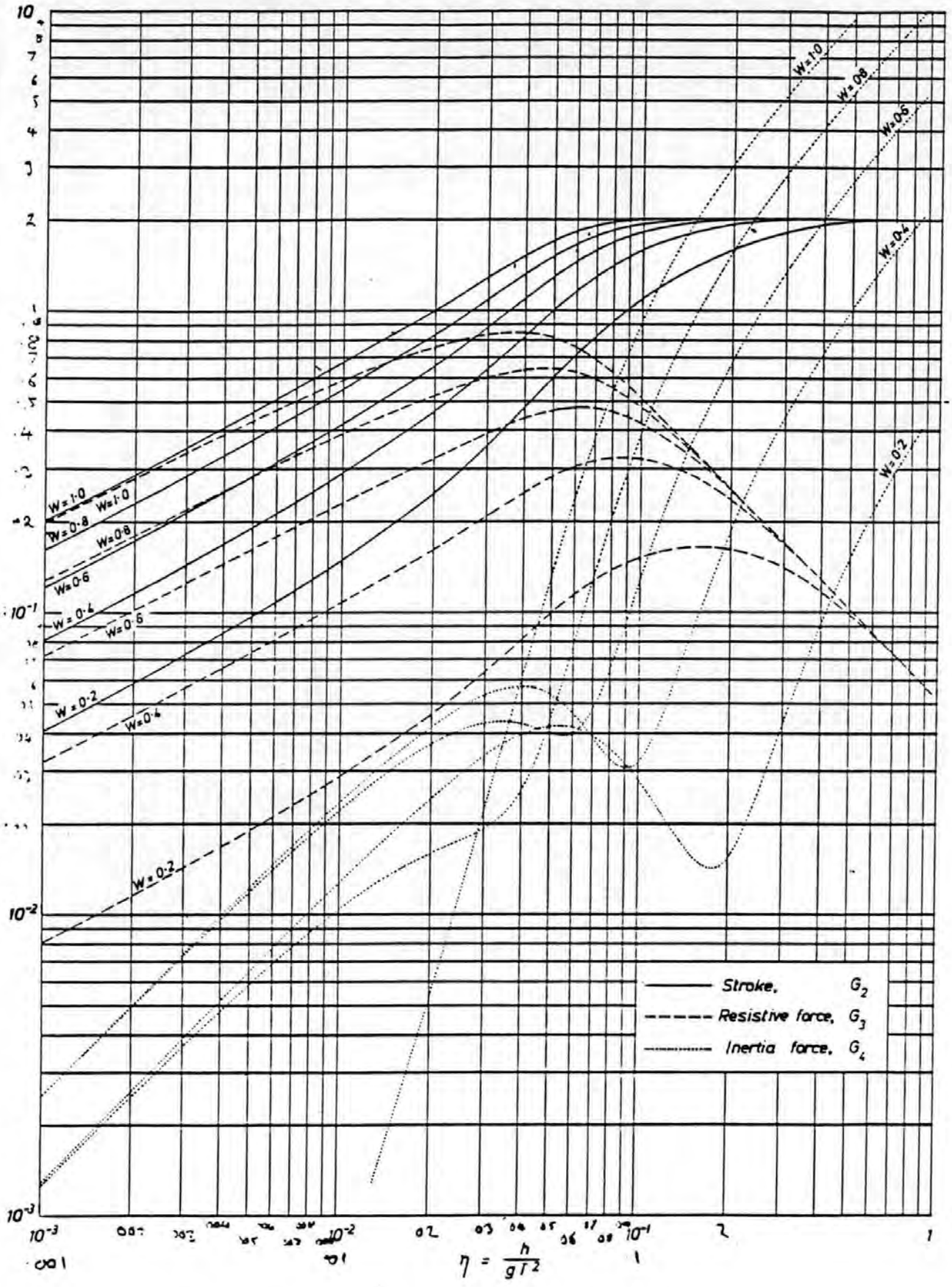

PISTON AND WEDGE REGULAR WAVE GENERATORS

FIG 5.8 THEORETICAL TRANSFER FUNCTION – DESIGN CURVES

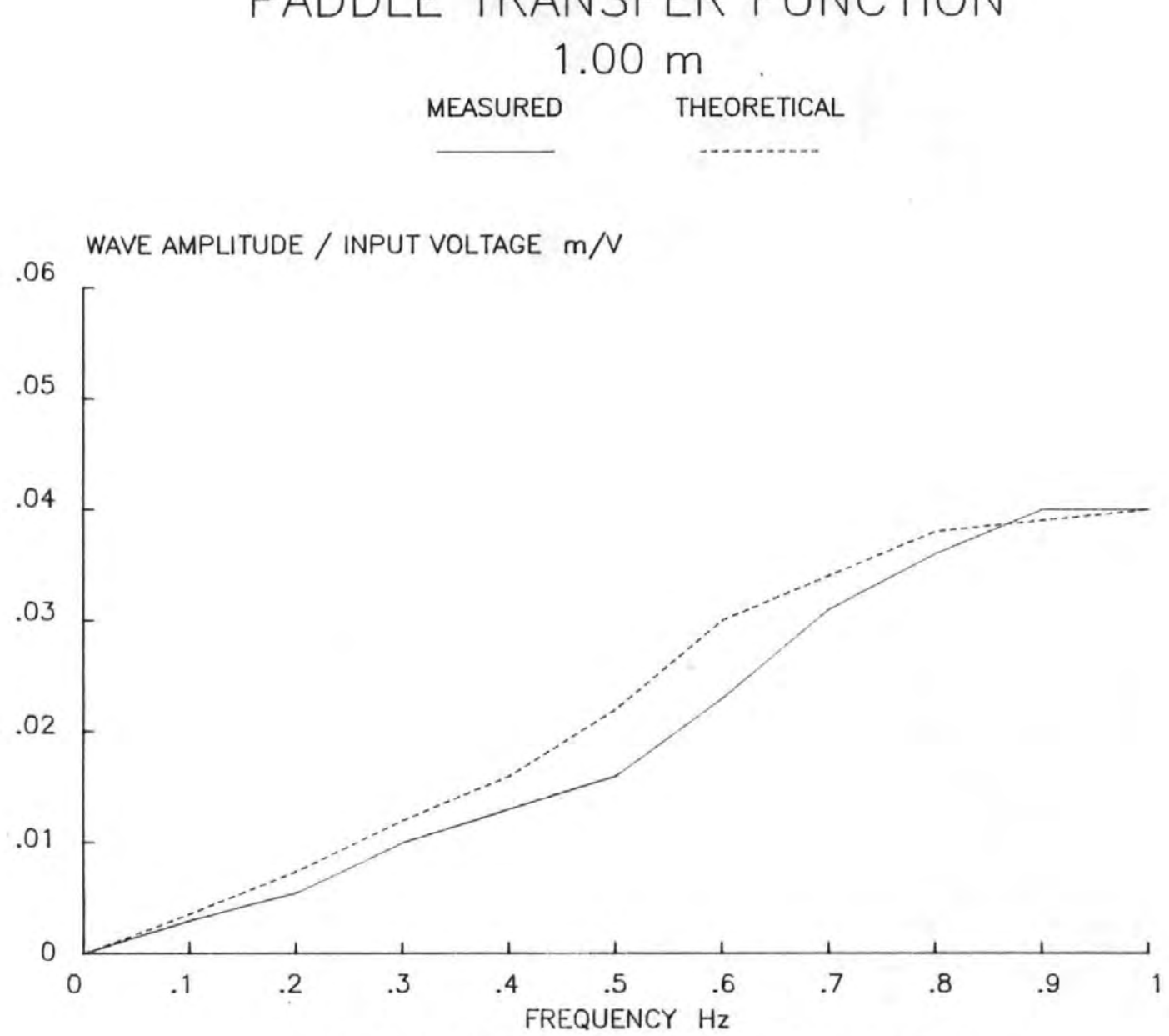

FIG 5.9 COMPARISON OF MEASURED AND THEORETICAL TRANSFER FUNCTION

5.7 Hydraulic System Problems

Whilst the determination of the dynamic characteristics of the paddle were under way a number of technical problems arose with both the hydraulics and the wave paddle. The main problem was the tendency at the paddle to not run smoothly on its bearings at low amplitudes and frequencies. The effect of this was to cause ripples in the tank which in some cases were larger than the waves the paddle motion produced.

At first it was thought that the problem was one of insufficient lubrication, but, whilst increased lubrication eased the problem it did not solve it. The final solution was to substantially increase the stiffness of the paddle by the addition of extra bracing. The structural mounts for the bearing shaft were also increased in size and the support frame for the whole system stiffened.

The increased stiffness of the system almost completely solved the problem and now it is possible to run the paddle smoothly for all but the smallest wave amplitudes (<10mm). A solution to the problem whilst time consuming, was important for an efficient system, especially when the absorption circuit board came to be installed and tested, as small movements were typical of adjustments to account for wave reflections.

Additional problems with faulty valves and a broken pump also occurred. The replacement or repair of a valve, although simple, was time consuming. All the problems together interrupted the smooth flow of work and introduced a slight mistrust of the equipment which took a while to dispel. The system has since given many months trouble-free operation and hopefully all the initial problems have been ironed out.

CHAPTER 6

A WAVE ABSORPTION SYSTEM

6.1 Introduction

The problems associated with the hydraulic modelling of waterwaves in a laboratory channel have been discussed in some detail by Svendsen (1985), so difficult is it to reproduce accurately a particular set of conditions that experimental data must be interpreted with great care. Phenomena which give rise to experimental errors include: transients, mass-transport, free second harmonics, instabilities and reflections. Another cause of errors in hydraulic models is that re-reflection can make it impossible to test a highly reflective structure in a conventional wave channel. Where tests are possible the results may be highly misleading. Traditional methods of dealing with re-reflections were reviewed in Chapter 1.

Recently, as a result of advances in electronic measurement and control, it has become possible to equip a laboratory wave channel with an absorption system. In addition to generating the required incident waves, the paddle has an additional feedback loop to cause it to move in such a way to cancel out or absorb any reflected waves which reach it. The paddle is then, in effect, making waves equal and opposite to the reflected waves. Two such systems were reviewed in Chapter 1.

A different system, based on water level detection at the paddle front has been designed and used in this project. This system is ideal for conversion of an existing, conventional wave generation system.

6.2 Design Criteria for a Wave Absorption System

The theoretical basis for the absorption system was outlined by Gilbert (1978) and summarised below. The essential physical requirements are:-

i. A means of detecting the reflected waves as they approach the paddle.

ii. A means of making the paddle generate waves that are, in effect, equal and opposite to the reflected waves to cancel out the reflected waves at the paddle front. The paddle must also maintain the capability to generate the incident waves.

The first requirement is met by mounting a wave gauge on the paddle front. The design of the paddle wave gauge is discussed later. The second requirement is met by incorporating a second feedback loop in the control system, as represented schematically in Figure 6.1.

The physical characteristics of the paddle measured as part of the initial calibration of the wavemaker system were used to design the filter characteristics of the absorption system.

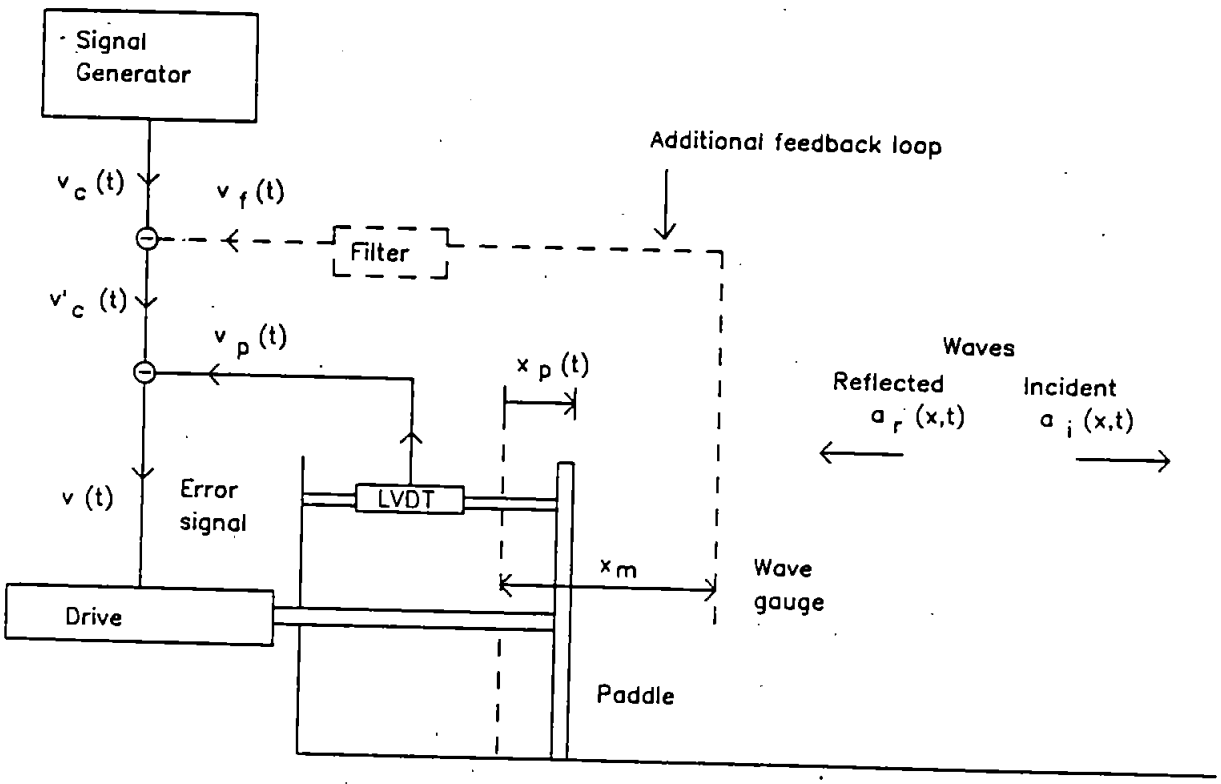

Figure 6.1 Schematic Representation of Absorbing Wavemaker

6.3 Wave Absorption Theory

In a conventional wavemaker the primary control signal $v_c(t)$ is supplied directly to the servo system (i.e. $v_c(t) = v_c'(t)$) so that the paddle displacement $x_p(t)$ is effectively proportional to $v_c(t)$ over the frequency range of interest (0-1 Hz). To incorporate absorption $v_c(t)$ is compared with the filtered output from a wave gauge $v_f(t)$ and the difference signal $v_c'(t)$ supplied to the servo system. Figure 6.2 summarises wavemaker systems.

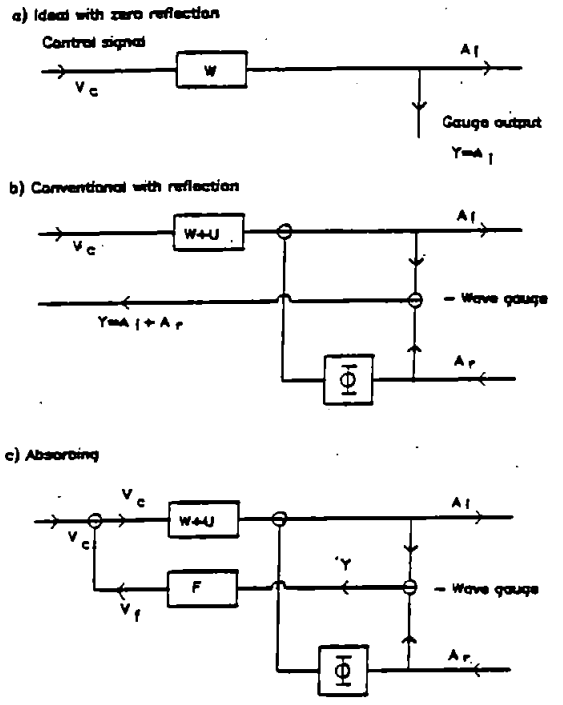

Figure 6.2 Block Diagrams of Wavemaker Systems

6.3.1 Design of the Filter

The dynamic characteristics of a constant parameter linear system can be described by a weighting function. If f(y) represents the weighting function of the filter and y(t) is the input variation in water surface elevation, as measured by a gauge located at $x=x_m$, the output from the filter is defined by the convolution integral:

$$V_f(t) = \int_0^\infty f(\tau)\, y(t-\tau)\, d\tau \qquad (6.1)$$

For present purposes it is more conventional to describe the filter in terms of its transfer function F(s) where F(s) is the Laplace transform of $f(\tau)$ (Lynn 1982).

That is:

$$F(p) = \int_0^\infty f(\tau)e^{-s\tau}\, d\tau \qquad (6.2)$$

where s is the 'complex frequency'. The filter will be stable only when F(s) has no poles in the right hand half of the complex s plane.

Transfer functions provide a conventional link between the input and output of any linear system. Thus for the filter:

$$V_f(s) = F(s)\ Y(s) \qquad (6.3)$$

where $V_f(s)$ and Y(s) are the Laplace transforms of $v_f(t)$ and y(t) respectively. With more complex expressions, greater clarity can be achieved if dependance on the parameter s is assumed. Following the convention that capitals denote functions of the complex variable s rather than of time, equation (6.3) reduces to:-

$$V_f = FY \qquad (6.4)$$

Similar relationships can be used to describe the overall performance of the wavemaker. If $a_i(x_m,t)$ represents the temporal variation in water surface elevation at x_m due to incident waves as they propagate away from the paddle, with an ideal conventional wavemaker and no wave reflection or re-reflection:

$$A_i = WV_c \qquad (6.5)$$

where W is the transfer function of the servo-controlled paddle system relative to the point x_m. In these circumstances a wave gauge at x_m would simply record:-

$$y(t) = a_i(x_m,t) \qquad (6.6)$$

See Figure 6.2a.

In practice the paddle motion is unlikely to match the precise water particle motion beneath the required waves and this will lead to the generation of a complex mixture of unwanted wave components. These include the free second-harmonics previously mentioned (Chapter 3) and a disturbance in the immediate vicinity of the paddle which increases in magnitude in proportion to the degree of mismatch between the actual and ideal paddle motions. Typically, the situation is further complicated by the presence of reflected waves $a_r(x,t)$ so that a gauge at x_m records:

$$y(t) = a_i(x_m,t) + a_r(x_m,t) \tag{6.7}$$

or $$Y = A_i + A_r \tag{6.8}$$

where a_i and A_i incorporate both the unwanted components and the re-reflections of reflected waves from the paddle. Thus, to give a more realistic description of a conventional wavemaker, equation (6.5) should be extended to:

$$A_i = (W + U)V_c + \Phi A_r \tag{6.9}$$

where U represents that part of the conventional wavemaker's transfer function that produces the unwanted waves and displacements, and Φ is a transfer function which takes account of the phase delay between a reflected wave at x_m and its re-reflection getting back to that point.

In an absorbing wavemaker linked to a wavegauge, the input to the filter is defined by equations (6.7) and (6.8). The output from the filter is used to modify the input to the conventional paddle control system (Figures 6.1 and 6.2). Thus V_c is equation (6.9) changes to V_c', where:

$$\begin{aligned} V_c &= V_c - V_f \\ &= V_c - FY \\ &= V_c - F(A_i + A_r) \end{aligned} \tag{6.10}$$

To achieve the desired absorption characteristics, the value of F in equation (6.10) must make A_i independent of A_r when the resulting value of V_c' is substituted in equation (6.9). By carrying out the substitution it may be shown that:

$$A_i = \frac{(W + U)V_c + [\Phi - F(W + U)]\ A_r}{1 + F(W + U)} \qquad (6.11)$$

Thus, the incident waves will be independent of the reflected waves if:

$$\Phi - F(W + U) = 0 \qquad (6.12)$$

i.e. if:

$$F = \frac{\Phi}{W + U} \qquad (6.13)$$

Substituting this value of F in equation (6.11) gives:

$$A_i = \frac{(W + U)V_c}{1 + \Phi} \qquad (6.14)$$

To avoid zeros in the denominator of equation (6.14) the distance x_m to the wave gauge should be less than a quarter wave-length of the highest frequency wave. The ideal solution is to make x_m zero which, in practical terms, means mounting the wave gauge on the face of the paddle. When $x_m = 0$, $\Phi = 1$ so that:-

$$A_i = \frac{(W + U)V_c}{2} \qquad (6.15)$$

By comparison to equation (6.9), which is the corresponding expression for a conventional wavemaker, it can be seen that not only has A_r been eliminated as required, but the output, A_i, for a given input, V_c, has been halved. The absorption system used here was modified at the output stage to double A_i to correspond to the conventional system. In this way it was possible to switch absorption 'in' or 'out' without a change in the paddle's performance. The effect of wave absorption on paddle characteristics can be seen in the next chapter.

6.4 Practical Implementation

The dynamic characteristics of the paddle at 3 depths (1.0m, 0.8m, 0.6m) were determined in the previous chapter. The design of the filter for the absorption feedback loop was based on those results. The values obtained were for $|W(f)|$ at the three depths at 0.1 Hz frequency intervals from 0.1 Hz to the limit imposed by wave breaking. It is clear from the scatter of the results that the design of the filter must of necessity be something of a compromise. The strategy adopted in the investigation was to neglect any influence of U not embraced by the empirically determined W(f), which included an assessment of phase lags, and to design the filter on the basis that:

$$FW = 1 \tag{6.16}$$

Equation (6.16) was obtained by substitution of $\Phi = 1$ and $U = 0$ into equation (6.13).

The output level of the filter could be adjusted by means of a gain control on the circuit board. This enables the characteristics to be matched empirically.

The estimated loop gain $|F(f)\ W(t)|$ of the absorption circuit with the filter adjusted to give optimum performance at 0.6 Hz is shown in Figure 6.3, where each curve is based on the measured $|F(t)|$ of the filter and the average $|W(t)|$ for a particular combination of f and d. Given that the objective was to achieve a loop gain of unity at all frequencies, Figure 6.3 clearly indicates that the filter characteristic was far from ideal. Some of the likely effects of this lack of perfection can be predicted by substitution of $\Phi = 1$ and $U = 0$ in equation (6.11) and rearranging to give:

$$A_i = \left[\frac{W}{1 + FW}\right] V_c + \left[\frac{1 - FW}{1 + FW}\right] A_r \tag{6.17}$$

With perfect absorption FW=1 and equation (6.17) effectively reduces to equation (6.15). If, as in the present investigation, the circuit is modified to avoid the 'halving' introduced by perfect absorption, equation (6.17) can be changed to:

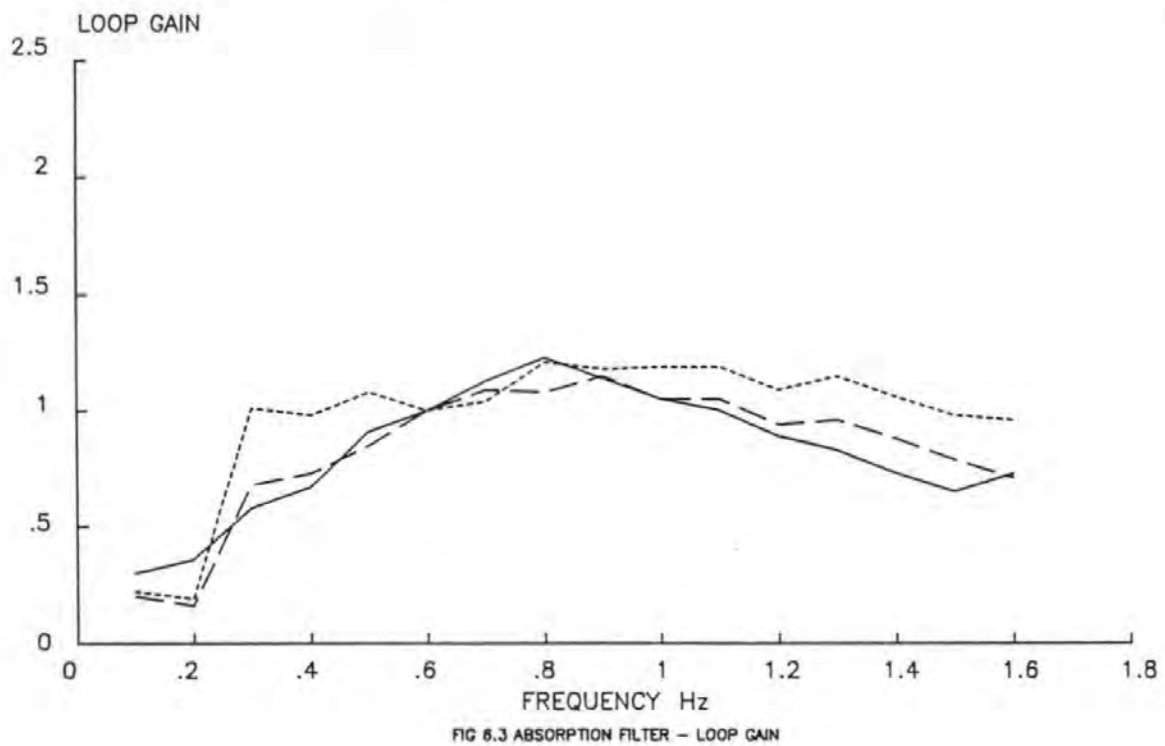

FIG 6.3 ABSORPTION FILTER – LOOP GAIN

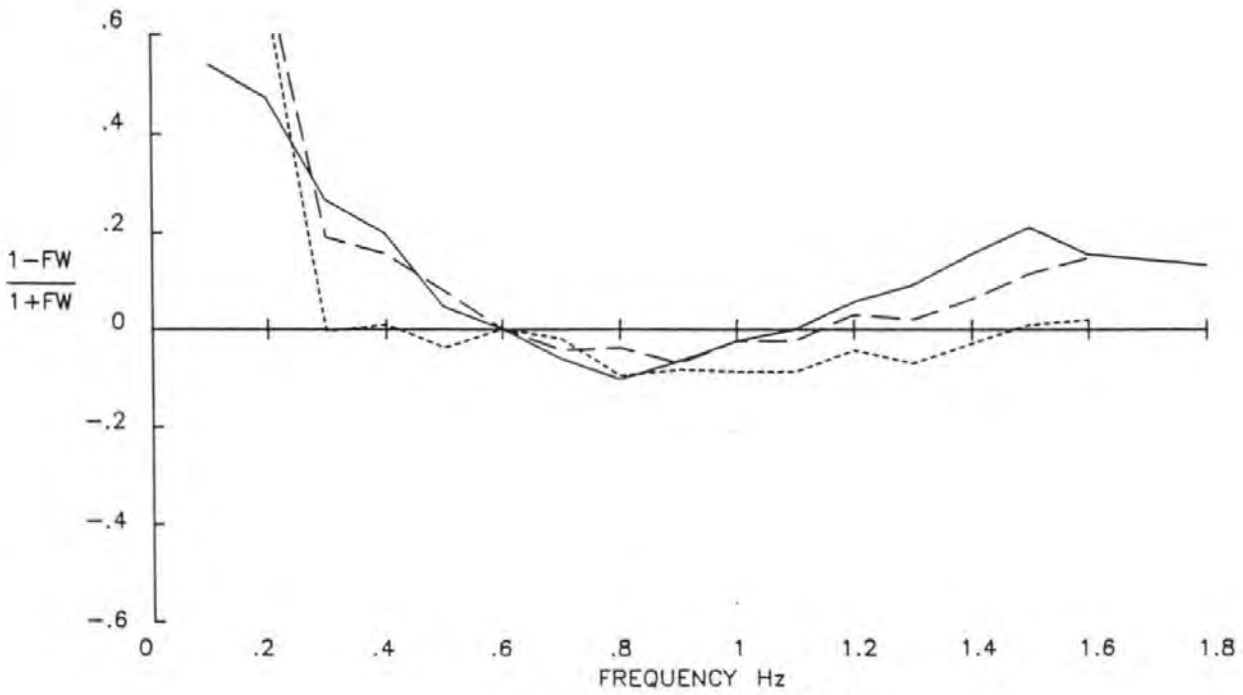

FIG 6.4 ABSORPTION FILTER CHARACTERISTICS

$$A_i = \left[\frac{2W}{1 + FW} \right] V_c + \left[\frac{1 - FW}{1 + FW} \right] A_r \qquad (6.18)$$

In either case, the first term on the right hand side of equations (6.17) or (6.18) defines the primary input from the wavemaker. If FW > 1 the contribution will be smaller than with perfect absorption.

The second term on the right hand side of equations (6.17) or (6.18) defines the proportion of A_r that is re-reflected by the paddle. If FW < 1 the paddle will not fully absorb the reflected waves. Conversely, if FW > 1 the paddle will over compensate for the reflected waves so that A_i effectively contains a negative re-reflection of A_r. Estimates of $|(1-FW)/(1+FW)|$ based on the data given in Figure (6.3) and neglecting small phase errors are shown in Figure (6.4). These indicate that in the present case, for frequencies from 0.5 Hz to 1.3 Hz and the three depths of water considered, the height of a re-reflected wave component might be expected to be less than 10% of the corresponding reflected wave height. Thus, even with the less than ideal loop gain defined by equation (6.5), the absorption system can be more than 90% effective in amplitude terms and more than 99% effective in energy terms over a significant frequency range. To retain the full benefit of this performance, the primary input from the wavemaker must be defined by equation (6.18) rather than (6.19).

The above analysis is incomplete due to the neglect of U, non-linear effects and various small phase errors. All the tests using the wavemaker fall into the 0.5 Hz to 1.3 Hz range and the performance of this 'first trial' absorption filter can be seen in the next chapter. No insuperable problems are foreseeen in the event of a need to improve the filter characteristics. To prevent HF stability problems a lowpass filter was incorporated in the circuit. The filter is shown in Figure 6.5. The relatively flat top indicates that this filter is unlikely to alter the system's performance.

6.5 Physical Implementation

Implementation of the absorption system involved mounting a wave gauge on the face of the paddle. Twin wire resistance gauges linked to the wave monitor were used (Chapter 2). So that the gauge would average out at least some of the variation in water surface elevation

which might occur across the width of the channel, two probes connected in series were used. (Plate 6.1). The probes were mounted one third the way across the channel from both walls. Each probe was constructed from two 500mm lengths of 1.5mm diameter stainless steel wire separated by a 15mm gap.

All the wires were supported by a common frame which caused them to project vertically down through the water surface in a plane from the face of the paddle. The combined signal from the two probes was fed to the standard wave monitoring equipment.

A slight complication arises from the use of a wedge-type paddle in that the motion of the paddle face has both horizontal and vertical components. Thus, if a wave gauge is rigidly attached to the paddle, steps must be taken to ensure that the vertical movement of the gauge is not interpreted as a reflected wave component. This problem was overcome by mounting the gauge support frame on wheels which ran along the top of the channel sides. The frame was attached to a pair of vertical rails fixed to the paddle face which allowed the gauge to move horizontally with the paddle without change of elevation.

6.6 Operation of Absorption System

The filter and 'mixer' circuits needed for the wave absorption system are contained on a printed circuit board. Modifications were made to the original design to adjust the performance of the filter to match equation (6.18) rather than equation (6.17).

The absorption circuit board is located in the Keelavite Hydraulics control box. It is switched 'in' and 'out' via a contact switch on the front control panel. When it is switched 'out' the circuit is completely bypassed and the absorption circuitry has no effect on the control system. When absorption is switched 'in' the demand voltage is 'mixed' with the feedback voltage from the wave gauge and the 'corrected' voltage used to drive the paddle.

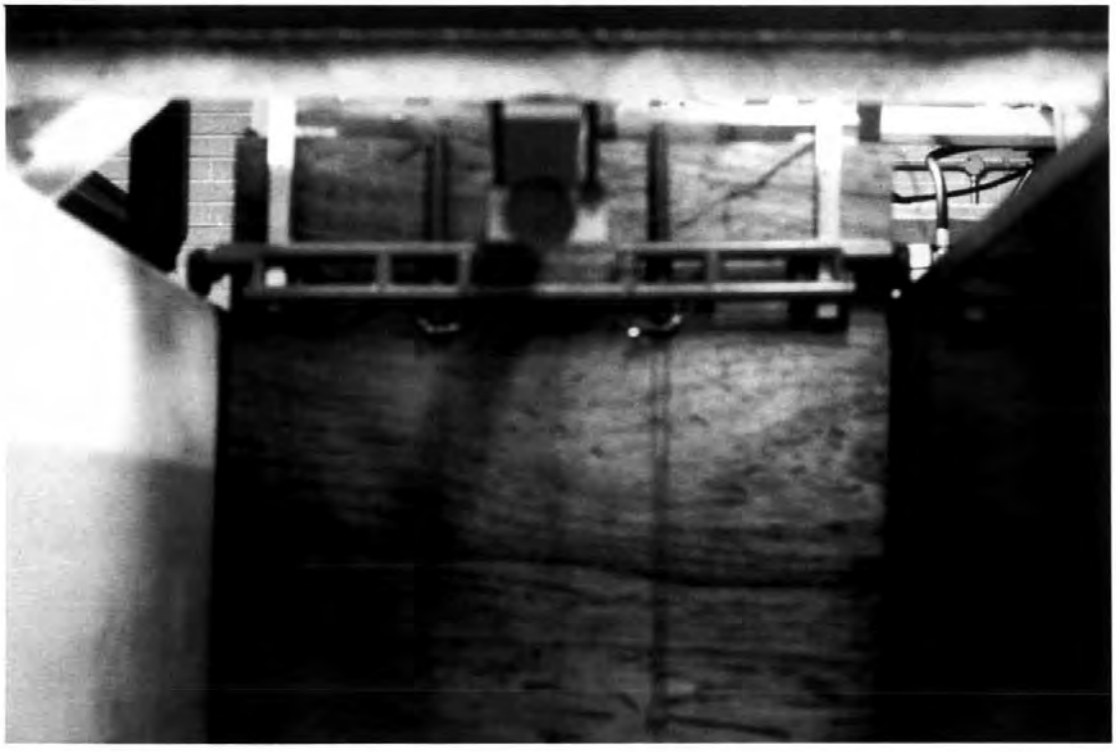

PLATE 1.1 PADDLE WAVE GAUGE

It is not advisable to switch the wave absorption 'in' when an external control signal is present. The inclusion of a feedback signal at this time may well require the paddle position to be radically different from the existing position. This would cause the paddle to jump to its new position in the shortest possible time. The sudden, violent movement could cause serious damage to the system.

To use the wave absorption facility the paddle must be stopped at the mid-stroke position. With the wave monitor output set to the correct level (see next section) the absorption can now be switched 'in'. The paddle can now be used in the conventional manner. To switch 'out' the wave absorption the opposite procedure must be adopted. Turn the external signal to zero, wait for the paddle to stop moving (this will occur when the water calms) and switch absorption 'out'.

6.7 Calibration and Optimisation

The present wave absorption system is not provided with any means of direct, analytical calibration. Although whilst under test this is perhaps not critical, for general purpose use this does impose certain limitations on the system.

At present, to set up the system for optimum performance, the output level of the filter gain is increased until the paddle becomes unstable. The instability is caused by too great a feedback signal (see above). A level just less than instability is used as the optimum setting. Although this direct procedure produces the correct calibration it is unrealistic to expect to have to carry out this procedure every time the absorption system is used.

Once the system has been set up, the need for further adjustment is only likely to arise due to a change in the voltage output from the paddle wave gauge. Any change in voltage signal will affect the absorption systems efficiency in one of the two ways described above.

6.7.1 Calibration

Since any variation in calibration is likely to be related to changes in the wave gauge output this is the best area to obtain a calibration. A logical way to calibrate the absorption system is to run the system as described above, but with the output level of the Wave Monitor below its maximum. From a still water calibration of the paddle wave gauge a datum point can be obtained. For subsequent use a repeat calibration can be performed and any necessary adjustment to the Wave Monitor output level made. The correct adjustment will return the level of the wave gauge output signal to that measured for the original calibration. This level is relatively easy to obtain, and with a little experience can be achieved quite quickly.

During the optimisation of the absorption system a gauge calibration was carried out which established the following relationship:

Wave Monitor Output level 8.00 (Range 0-10.00)
10mm water level change ≡ 0.300 v Wave Monitor output.

6.8 Sensitivity

A check on the sensitivity of the wave absorption system to changes in wave gauge voltage was made. An assessment of how critical the calibration of the system is could then be made.

For a regular wave of constant voltage gain, the 'set-output' control on the Wave Monitor was decreased in steps. The effect on wave height in the channel was then noted. As would be expected a decrease of, for example, 20% of the Wave Monitor voltage output corresponded to a 20% increase in wave height. This is consistent with the theory outlined above.

6.9 Appraisal of Wave Absorption System

To test the effectiveness or otherwise of the system a comprehensive test program was conducted. Regular and random waves were used. The results of these tests are presented in the next chapter.

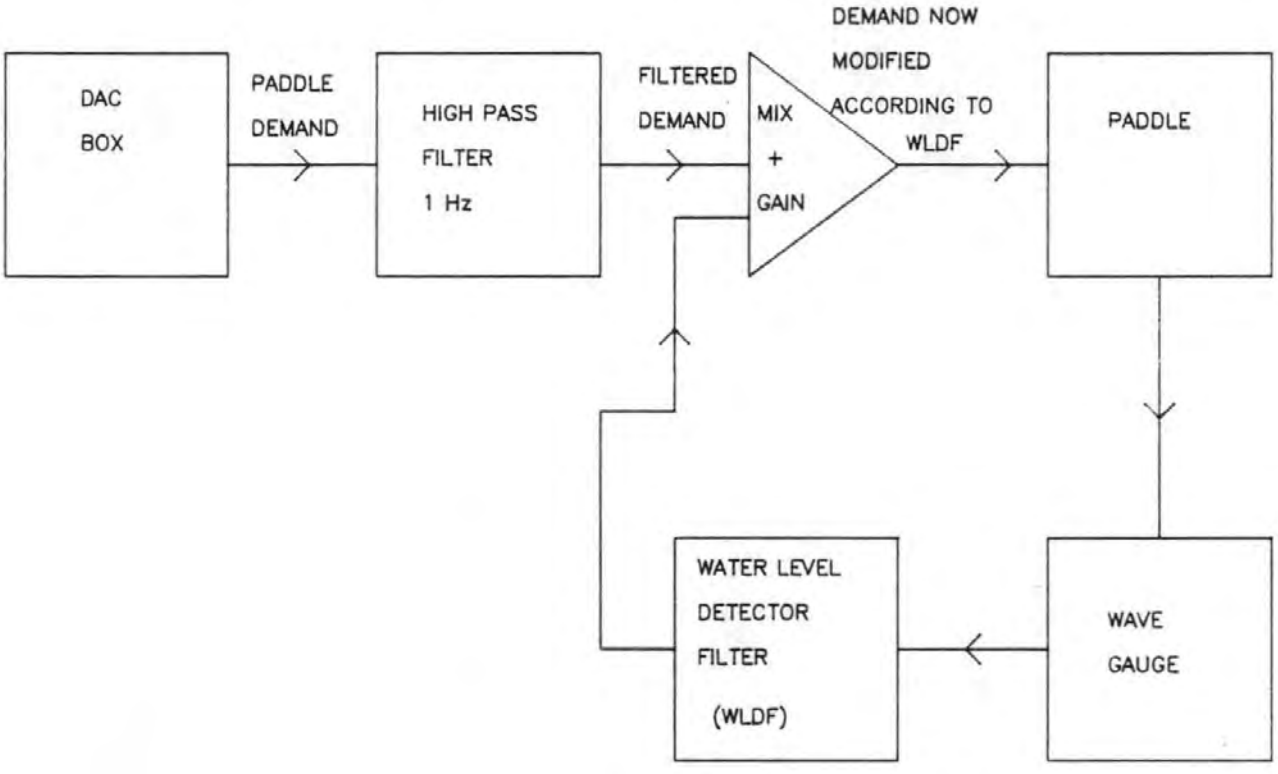

FIG 6.5 BLOCK DIAGRAM OF WAVE ABSORPTION SYSTEM

CHAPTER 7

TESTS ON WAVE ABSORPTION SYSTEM

7.1 Introduction

To fully appraise the performance of the wave absorption system a comprehensive test program was conducted. Both regular and random waves were used. The methods of analysis for the various wave trains have already been discussed. (Chapter 3). Wherever possible the tests were all repeated for both absorption 'out' and 'in'. In some cases it was not possible to repeat a particular test with wave absorption 'out' due to the wave instability under resonant conditions. The causes of this were discussed in chapter 3 and will be dealt with later. High and low degrees of reflection from the spending beach end of the channel were used with wavescreens constructed for this purpose (see below). Graphical output similar to that presented in chapter 5 for regular waves was used for interpretation. The random wave analysis used the Frequency Response Function analysis for determining incident and reflected wave spectra from a composite wave train recorded at two or more locations in the channel, as described in chapter 3.

7.2 Wavescreens

To enable the tests to be performed with different amounts of wave reflection, provision was made for mounting a screen of vertical timber slats across the channel near the toe of the spending beach 13.94m away from the paddle mean position. The base of the slats located into an aluminium channel section and the tops were bolted to a frame running horizontally above the channel (Plates 7.1 and 7.2). This arrangement allows for convenient changes of wavescreen slat combination with no need to drain the channel. More importantly, the vertical slat arrangement is independent of water depth or wave height as an influence over the reflection coefficient.

Various slat combinations were tested, and at the outset of testing the various combinations were arbitrarily given the numbers listed in Table 7.1 to distinguish them from each other.

PLATE 7.1 PARTIAL WAVESCREEN

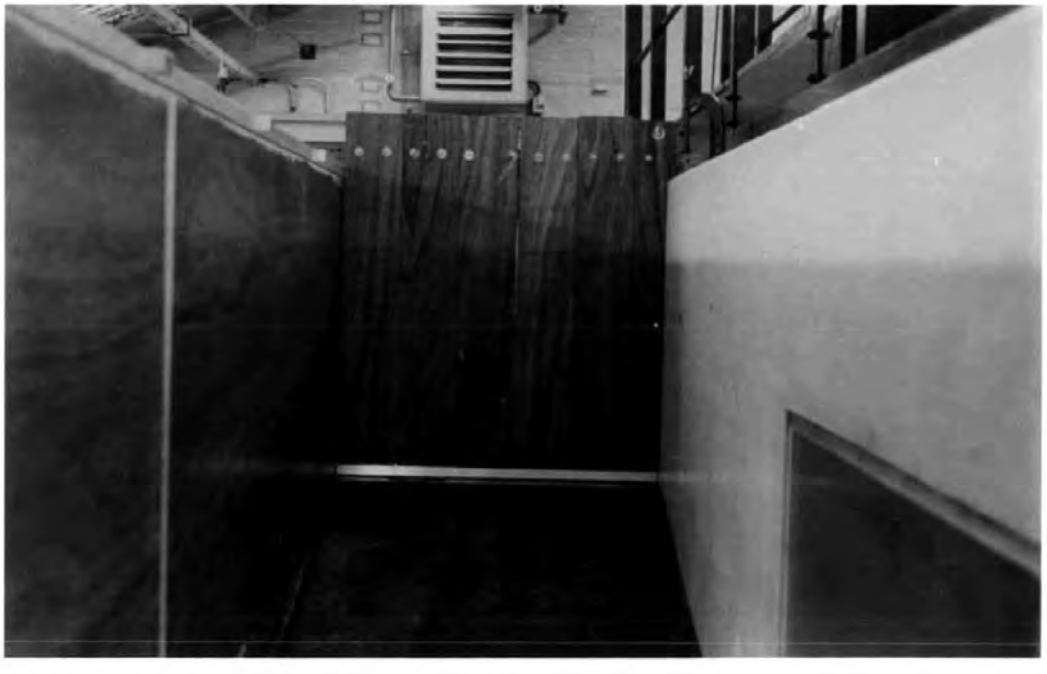

PL[illegible] 7.2 [illegible]

Wavescreen Number	Slat Arrangement
0	No screen
1	Full screen 150mm slats
2	150mm slats, 2 and 5 missing
3	150mm slats, 3, 4 and 6 missing
4	150mm slats 2 and 5 only in place
5	75mm slats, alternate with gaps, 1 in place.

Table 7.1 Wavescreen Combinations

The 150mm slats were numbered 1 to 6 across the channel with 1 on the left hand side of the channel facing in the direction of wave propagation.

With a full (i.e. No. 1) wavescreen there was still wave transmission through the gaps between the slats and the reflection coefficient of this 'full' wavescreen was typically in the region 60-70%. If the maximum level of reflection had been increased to 100% many more of the regular wave tests would have had to be abandoned when wave absorption was 'out'.

Only the results obtained with the tests with either none or a 'full' wavescreen are presented here since all the other wavescreen combinations led to results in between these two 'extremes'.

The formation of nodes and antinodes in a closed channel was discussed in Chapter 3. An antinode must always be formed at the 'full' wavescreeen. In both sets of tests (regular and random), frequencies were chosen to introduce the effect of both nodes and antinodes at the paddle front. (In the random tests the frequency was chosen to be the peak spectral frequency).

7.3 Regular Wave Tests

7.3.1 Introduction

The regular wave tests were conducted in the same fashion as described in Chapter 5 for the optimisation and calibration of the paddle. In this case the tests were repeated for both wave absorption 'in' and 'out' and with high and low degrees of reflection. The wave envelope program (Chapter 4) was used for analysis.

In addition to the basic series of tests additional frequencies other than 0.1 Hz increments from 0.1 Hz, were calculated to introduce the effect of nodes or antinodes at the paddle front. A third wave gauge, in a fixed location 2.3m from the paddle mid-stroke position, was also used. The gauge was connected to the HP spectrum analyser to provide information about the 'cleanness' of the waves produced. The regular wave spectra obtained from the wave gauge connected to the spectrum analyser have been plotted in two ways. The first plot shows the spectrum at a suitable scale to include the variance density associated with spectral peaks without truncation, the second is the spectrum plotted at the largest scale available on the spectrum analyser (40mV full scale voltage). The second type of graph, whilst not showing the peaks clearly, give a much better impression of any high frequency noise in the signal.

In addition to the wave gauge measurements the paddle actuator stroke length was measured for each test. This allowed the relationships between paddle movement and wave amplitide to be determined.

As in the previous tests (Chapter 5) all quantities are, where applicable, amplitudes rather than crest-trough heights.

7.3.2 Results

Figure 7.1 illustrates the effect of wave absorption on the transfer function of the ratio of Wave Amplitude/Input Voltage against Frequency described in Chapter 5. It can be seen that with the small levels of reflections from the spending beach the absorption circuit has little effect on the waves generated.

FREQUENCY vs WAVE AMPLITUDE/INPUT VOLTAGE

1.00 m NO WAVESCREEN

ABSN : OUT ———— ABSN : IN — — —

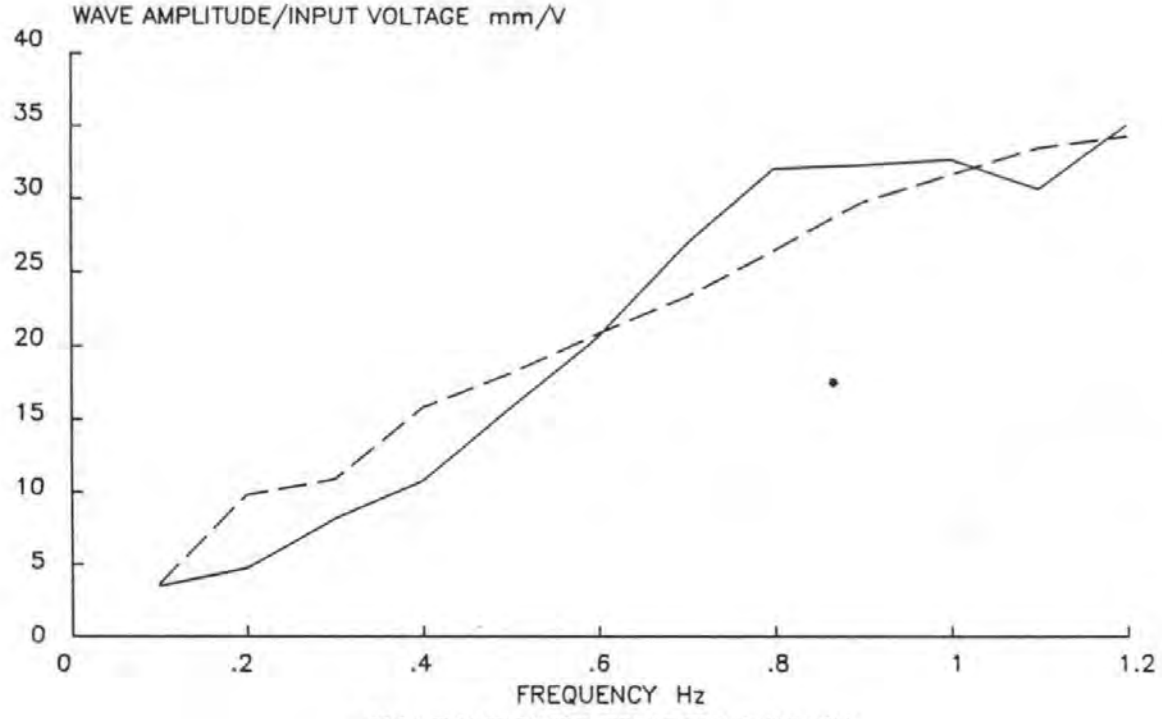

FIG 7.1 TRANSFER FUNCTION WITH AND WITHOUT ABSORPTION

FREQUENCY vs REFLECTION COEFFICIENT

1.00 m NO WAVESCREEN

ABSN : OUT ———— ABSN : IN — — —

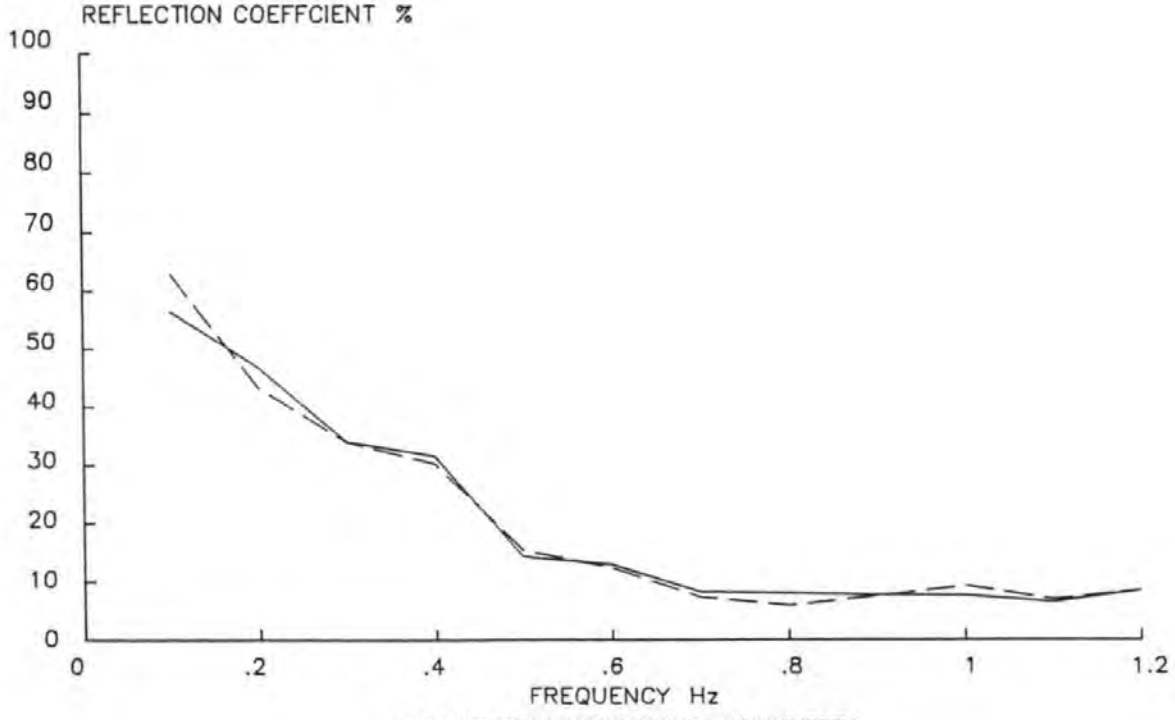

FIG 7.2 REFLECTION CHARACTERISTICS – NO WAVESCREEN

FREQUENCY vs WAVE AMPLITUDE/INPUT VOLTAGE

1.00 m FULL WAVESCREEN

ABSN : OUT ———— ABSN : IN ----------

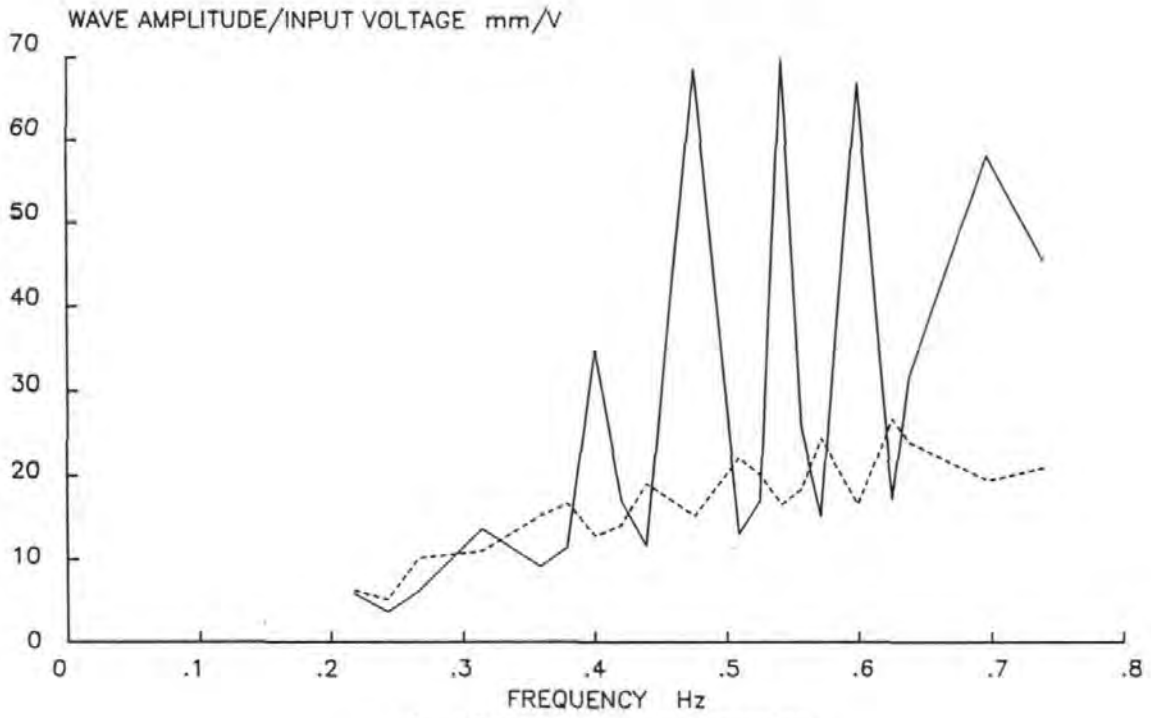

FIG 7.3 TRANSFER FUNCTION – FULL WAVESCREEN

FREQUENCY vs WAVE AMPLITUDE/INPUT VOLTAGE

1.00 m FULL WAVESCREEN

ABSN:IN–N/I

ABSN: IN – N

ABSN: IN–A

ABSN:OUT N/I

ABSN:OUT–N

ABSN: OUT–A

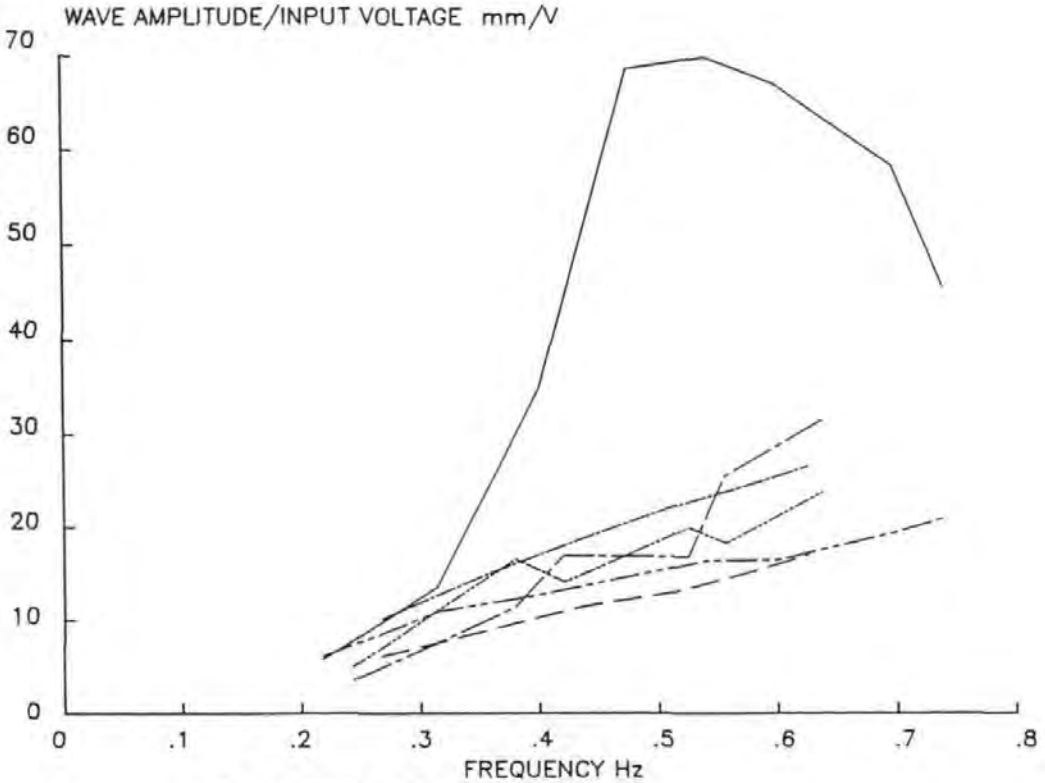

FIG 7.4 TRANSFER FUNCTION – FULL WAVESCREEN

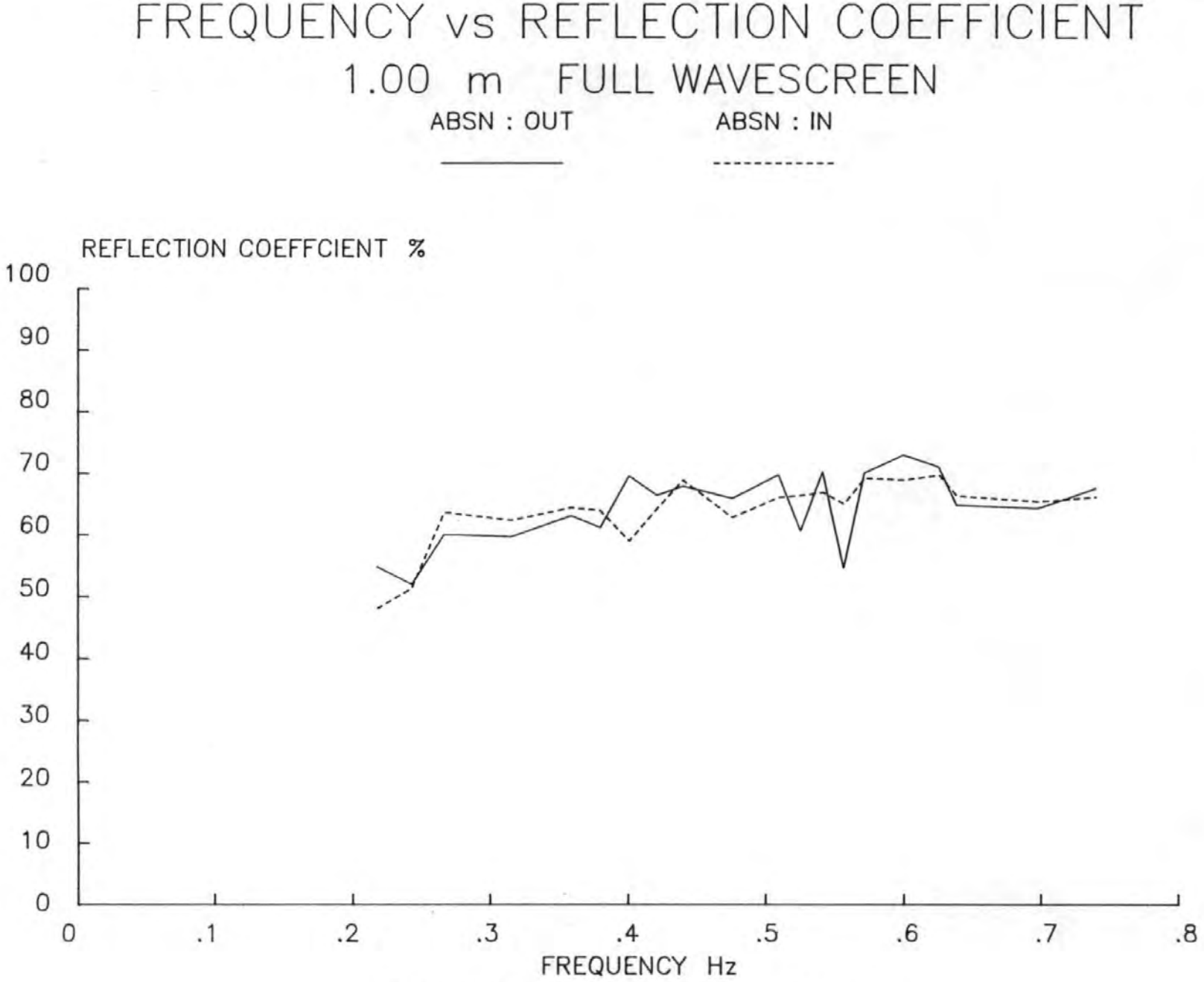

FIG 7.5 REFLECTION CHARACTERISTICS – FULL WAVESCREEN

The difference in the two curves can be explained by reference to Figure 6.3. Here it is seen that at 0.6 Hz the loop gain is unity and in Figure 7.1 the 'in' and 'out' curves are coincident, below 0.6 Hz the loop gain is less than unity and the waves with absorption 'in' are greater than with absorption 'out'. The opposite is true above the loop gain is greater than unity. Figure 7.2 illustrates that the reflection characteristics are very similar whether wave absorption is active or not.

The problem of resonance is highlighted in Figure 7.3 in which the parameters are the same as those in Figure 7.1 but with the incident waves largely reflected by the full screen rather than absorbed by the spending beach. The high peaks in the absorption 'out' curve occur where the distance between the screen and paddle was an integer multiple of half wave lengths for the given frequency. In these circumstances the partial standing wave has anti-nodes at both the wavescreen and the paddle. The low points in the absorption 'out' curves correspond to situations where there was an anti-node at the wavescreen (as must always be the case) but a node at the paddle.

The differences are highlighted in Figure 7.4 which shows all the various node/anti-node combinations plotted separately. Figure 7.4 can be better understood with reference to Table 7.2.

N	-	Node, node formed at paddle
A	-	Anti-node, anti-node formed at paddle
N/I	-	Non-Integer, Intermediate position between node or antinode at paddle.

Table 7.2 Notation used on Figure 7.4

The reflection characteristics for absorption 'in' or 'out' illustrated in Figure 7.5 remain broadly similar with reflection coefficients beween 50% and 70%.

The general form of Figure 7.3 can be explained with recourse to linear wave theory, water particle motion and the actuator stroke length measurements. At a node, where to a first approximation, the water surface has no vertical motion, the particle motion is primarily horizontal, whereas at an anti-node the particle motion is primarily vertical. Thus, in circumstances where an anti-node should form at the paddle, the paddle should have little or no horizontal motion once the required waves have been established. If the paddle continues to have a significant horizontal motion, an additional unwanted motion will be imposed on the water and the incident waves will continue to grow until sufficient energy is dissipated either by breaking or by some other means. In the present tests energy was dissipated both by leakage through the screen and on the spending beach. This enabled the resonance peaks of the absorption 'out' curve to be defined for low-amplitude control signals.

In circumstances where a node should form at the paddle, the horizontal motion of the paddle should increase to match the increased excursion of the water particles once the standing wave has formed. If the paddle's motion does not increase, the reflection (or more precisely the re-reflection) will effectively reduce the height of the incident waves. Hence the low points in the absorption 'out' curve. With the absorption system 'in' the paddle was able to make automatic adjustments of the type described above. Figure 7.6 gives an indication of how much the motion of the paddle had been altered once steady-state conditions were reached in the tests with a full wavescreen. Thus, by comparison with its motion without absorption, the stroke of the paddle was changed by around 70% at those frequencies which caused nodes or anti-nodes to form at the paddle. Figure 7.7 shows the three cases of nodes, anti-nodes or intermediate points at the paddle separately to illustrate the different paddle motions. This is as would be expected with an approximately linear system given the level of reflection from the wavescreen.

FREQUENCY vs PADDLE STROKE VARIATION
1.00 m FULL WAVESCREEN

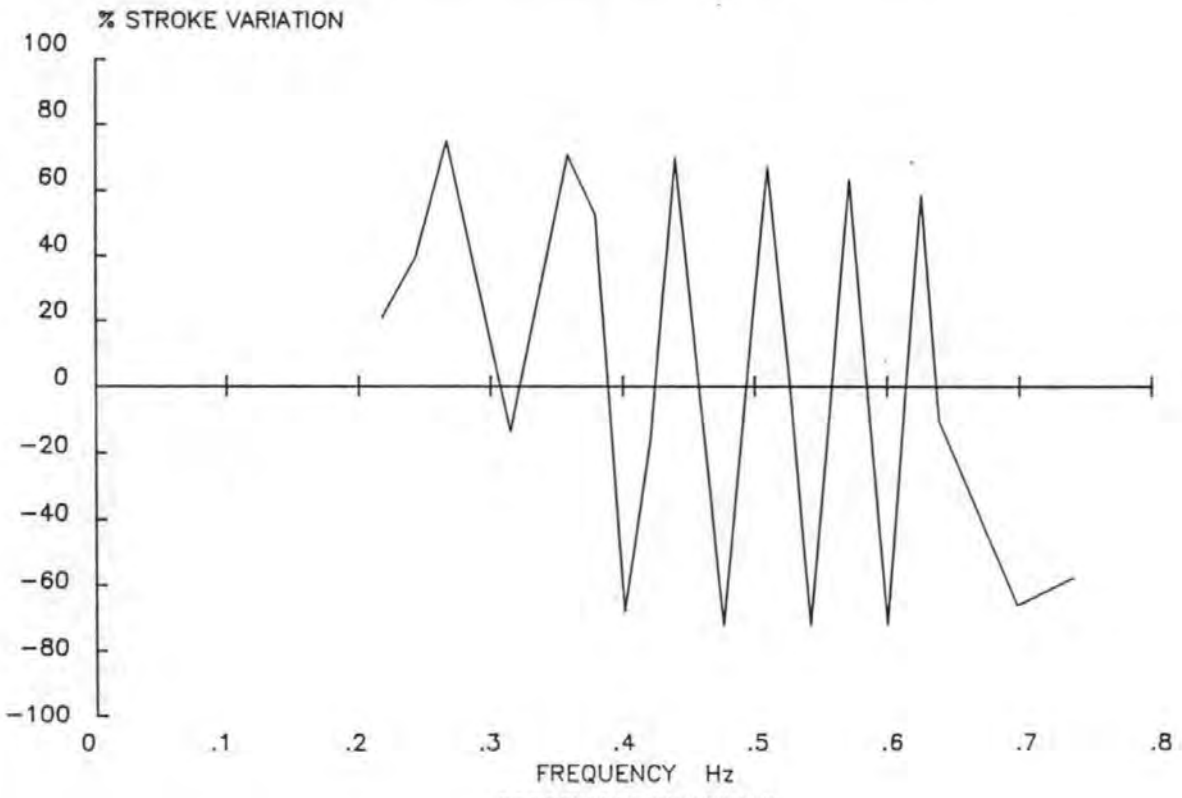

FIG 7.6 PADDLE STROKE VARIATION

FREQUENCY vs PADDLE STROKE VARIATION
1.00 m FULL WAVESCREEN

ANTINODE ——— NODE — — — INTERMEDIATE .....

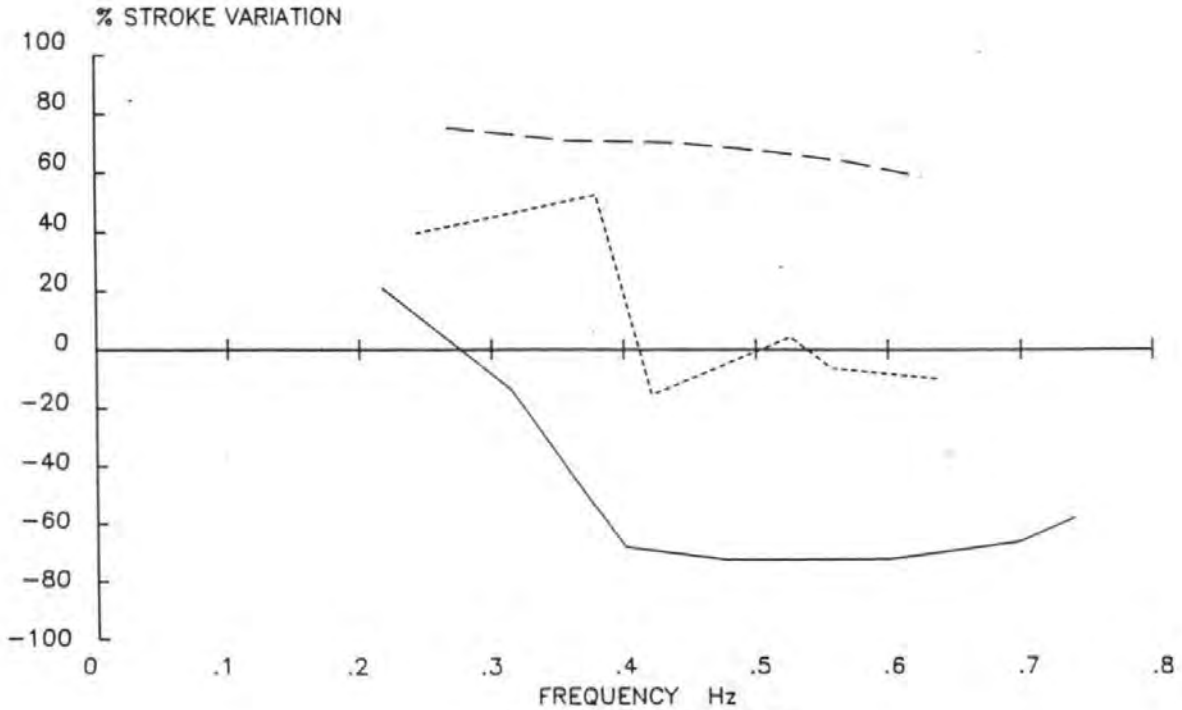

FIG 7.7 PADDLE STROKE VARIATION

A plot of Wave Amplitude/Paddle Stroke Amplitude vs frequency, Figure 7.8 further illustrates the point made above. It is also interesting to compare the two curves for wave absorption 'in' and 'out'. When wave absorption is 'out' the paddle stroke is a constant determined by the amplitude of the control signal. The high and low points in the curve are due to the effects of resonance and the formation of anti-nodes or nodes at the paddle as discussed above. When absorption is 'in' both the wave amplitude and paddle stroke can vary depending on the water particle motion discussed above. The two curves are very similar which suggests the system is essentially linear.

Examples of regular wave spectra for each of the three conditions of node, anti-node, or intermediate point at the paddle are given in Figures 7.9 - 7.20 for the full wave-screen. In each set it can be clearly seen how the wave absorption system, whilst retaining the same spectral peak amplitude, greatly reduces the level of high frequency noise in the signal. This reduction could be readily detected by visual observations of the tests.

The limitations of the present system are highlighted in Figure 7.3 where the absorption 'in' curve can be seen to exhibit a systematic oscillation that is generally out of phase with the absorption 'out' curve. A good smoothed fit to the absorption 'in' curve is provided by the corresponding curve in Figure 7.2.

7.4 Random Wave Tests

7.4.1 Introduction

The random wave test results were analysed by means of the Frequency Response Function method of analysis which was described in Chapter 3. In a similar fashion to the regular waves the effect of half-integer wavelengths in the channel was investigated The wavelength was based on the spectral peak frequency. All tests were carried out using full length sequences (see chapter 2) for a range of wave spectra with different significant wave heights and peak frequencies (see above). Wavescreens were used as before to provide various degrees of reflection and all tests were repeated with the absorption system both 'in' and 'out'. Table 7.3 lists some of the

FREQUENCY vs WAVE AMPLITUDE/PADDLE STROKE

1.00 m FULL WAVESCREEN

ABSN : OUT ABSN : IN

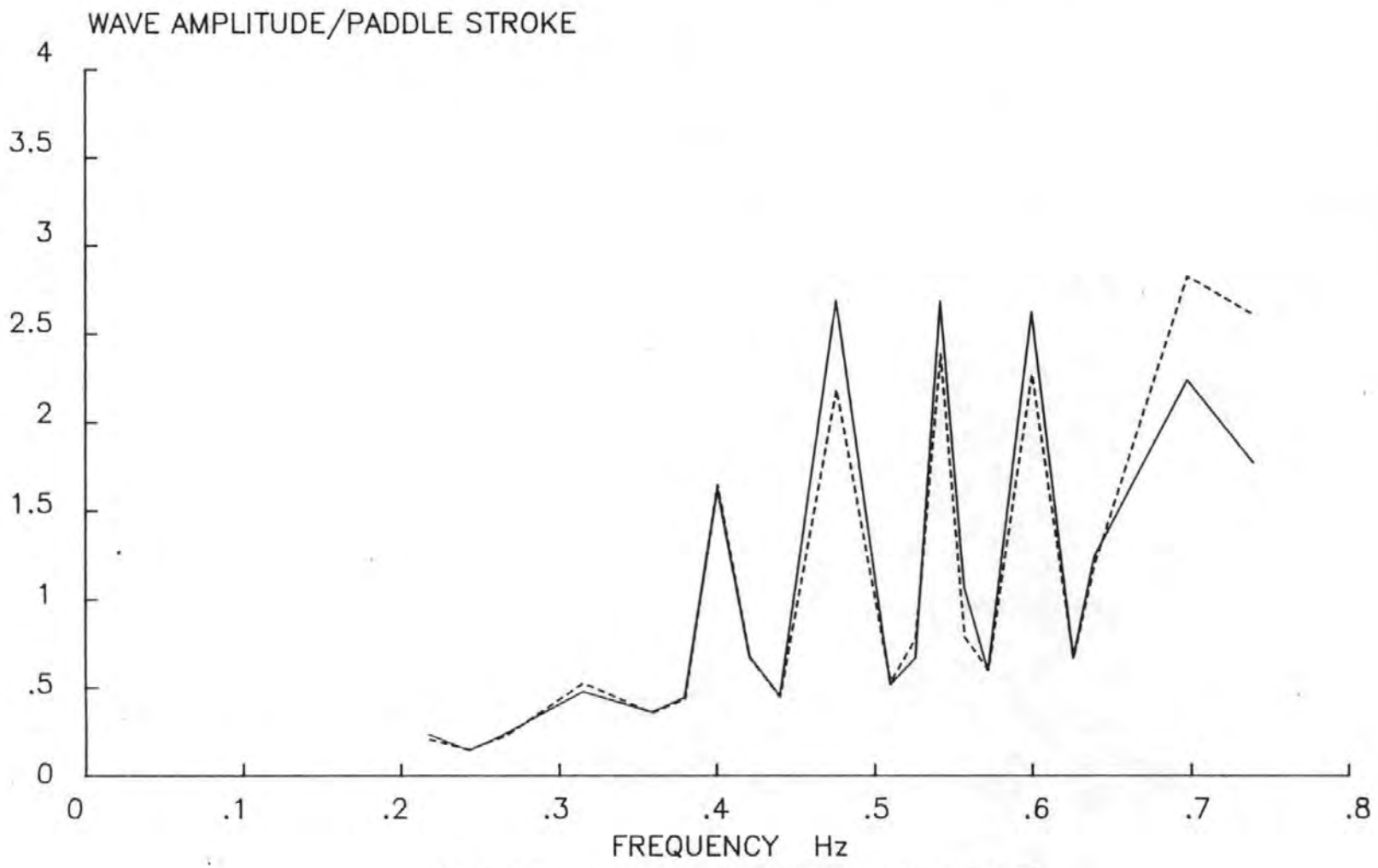

FIG 7.8 WAVE AMPLITUDE/PADDLE STROKE TRANSFER FUNCTION

REGULAR WAVE SPECTRUM

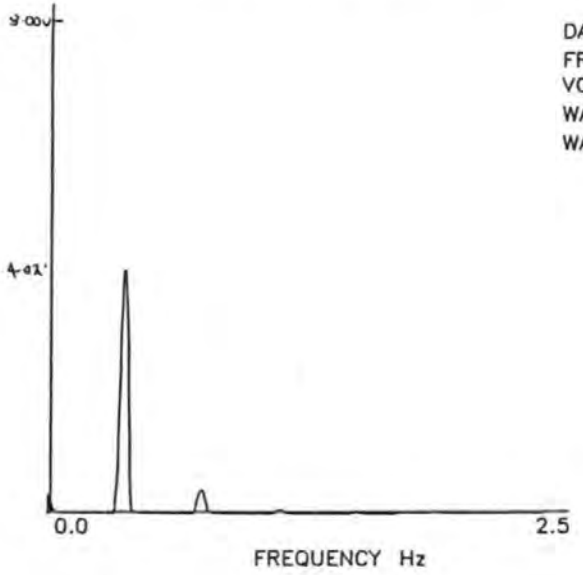

DATE : 18-12-85
FREQUENCY OF SINEWAVE 0.401
VOLTAGE GAIN : 4.00
WAVE ABSORBTION (IN) OUT
WAVESCREEN : FULL

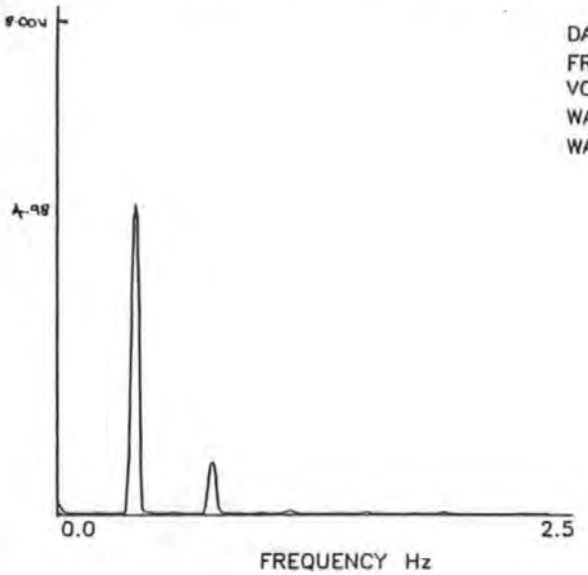

DATE : 18-12-85
FREQUENCY OF SINEWAVE 0.401
VOLTAGE GAIN : 1.49
WAVE ABSORBTION IN (OUT)
WAVESCREEN : FULL

REGULAR WAVE SPECTRUM

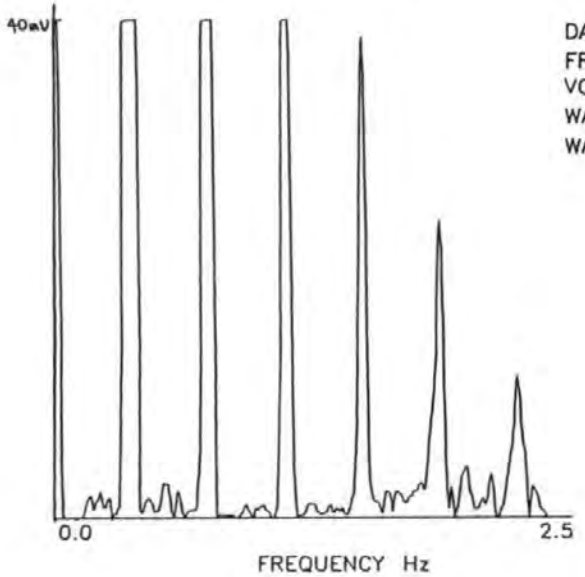

DATE : 18-12-85
FREQUENCY OF SINEWAVE 0.401
VOLTAGE GAIN : 4.00
WAVE ABSORBTION (IN) OUT
WAVESCREEN : FULL

REGULAR WAVE SPECTRUM

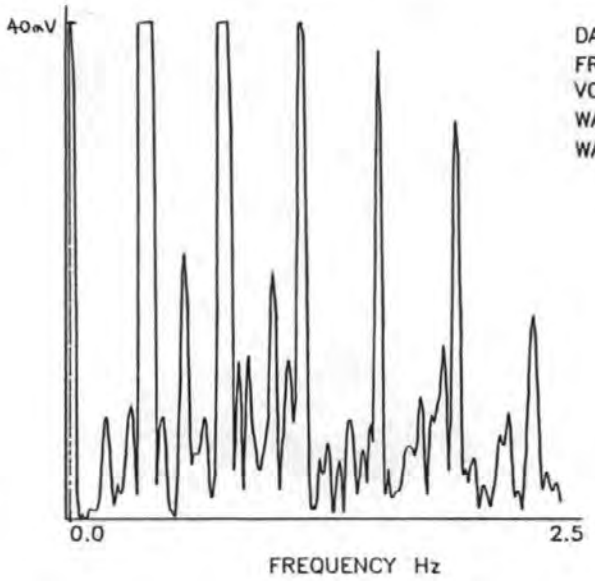

DATE : 18-12-85
FREQUENCY OF SINEWAVE 0.401
VOLTAGE GAIN : 1.49
WAVE ABSORBTION IN (OUT)
WAVESCREEN : FULL

REGULAR WAVE SPECTRUM

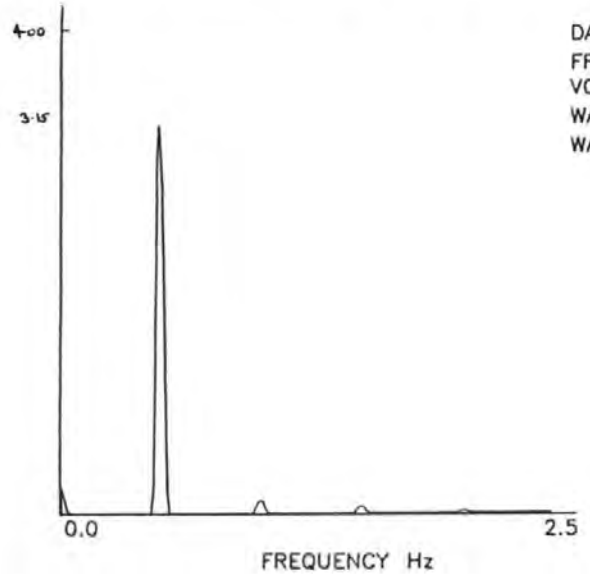

DATE : 17-1-86
FREQUENCY OF SINEWAVE 0·526
VOLTAGE GAIN : 2·00
WAVE ABSORBTION (IN) OUT
WAVESCREEN : FULL

REGULAR WAVE SPECTRUM

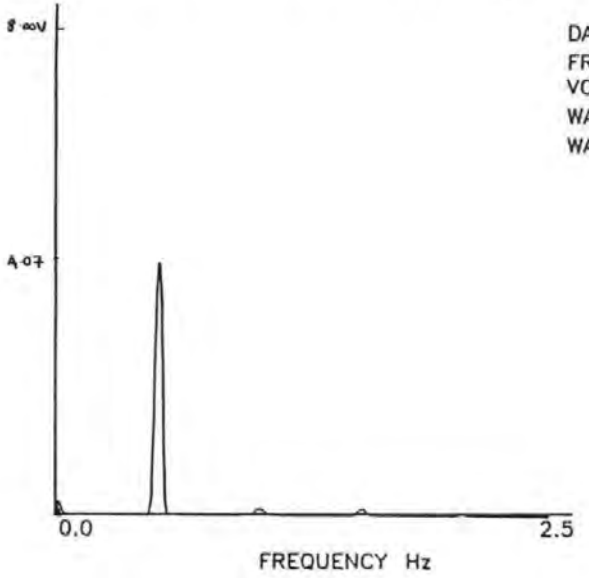

DATE : 17-1-86
FREQUENCY OF SINEWAVE 0·526
VOLTAGE GAIN : 2·00
WAVE ABSORBTION IN (OUT)
WAVESCREEN : FULL

REGULAR WAVE SPECTRUM

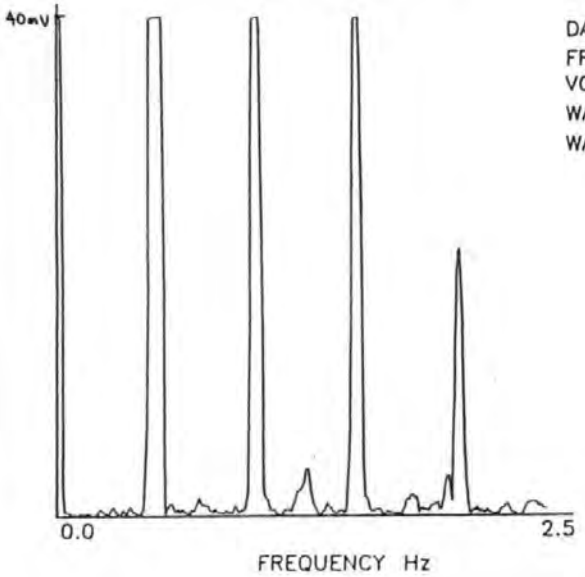

DATE : 17-1-86
FREQUENCY OF SINEWAVE 0·526
VOLTAGE GAIN : 2·00
WAVE ABSORBTION (IN) OUT
WAVESCREEN : FULL

REGULAR WAVE SPECTRUM

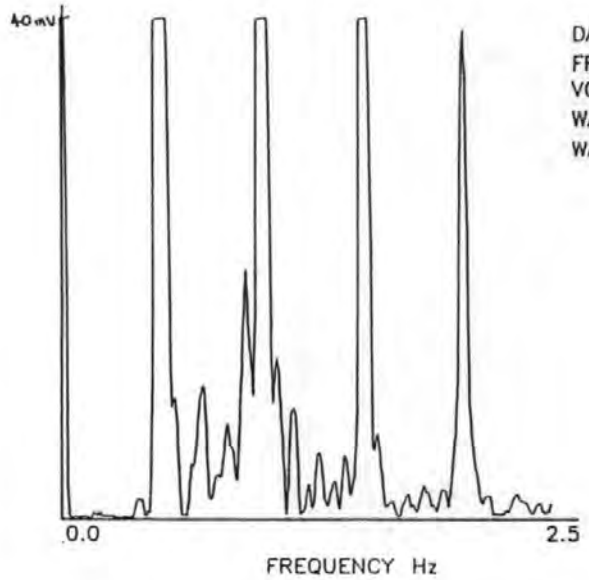

DATE : 17-1-86
FREQUENCY OF SINEWAVE 0·526
VOLTAGE GAIN : 2·00
WAVE ABSORBTION IN (OUT)
WAVESCREEN : FULL

REGULAR WAVE SPECTRUM

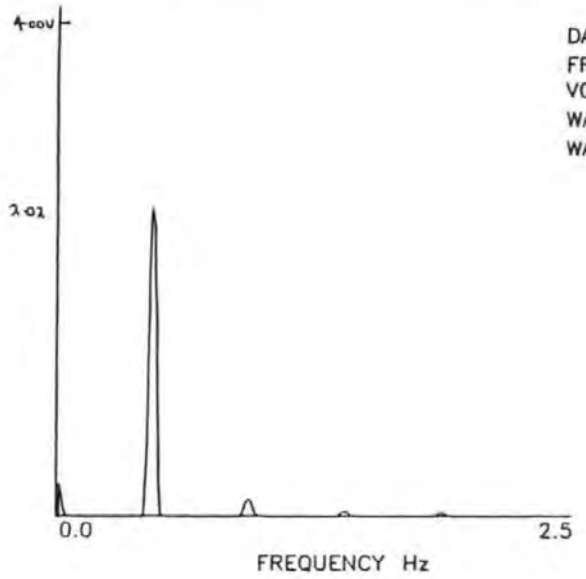

DATE : 18-12-85
FREQUENCY OF SINEWAVE 0.5
VOLTAGE GAIN : 2.00
WAVE ABSORBTION IN (OUT)
WAVESCREEN : FULL

REGULAR WAVE SPECTRUM

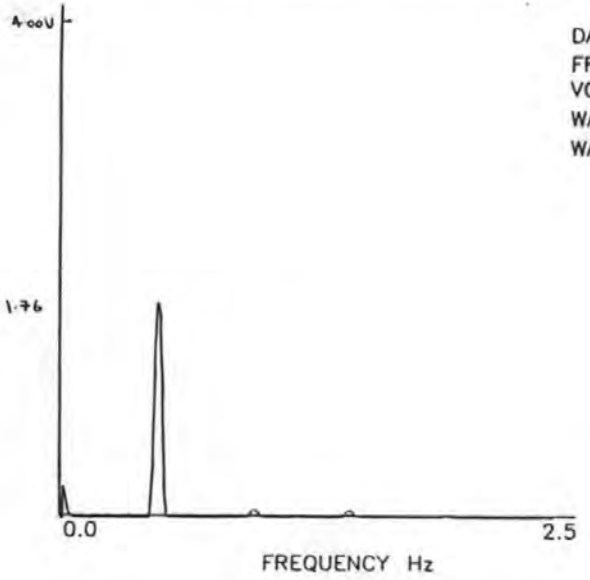

DATE : 18-12-85
FREQUENCY OF SINEWAVE 0.5
VOLTAGE GAIN : 1.37
WAVE ABSORBTION IN (OUT)
WAVESCREEN : FULL

100

REGULAR WAVE SPECTRUM

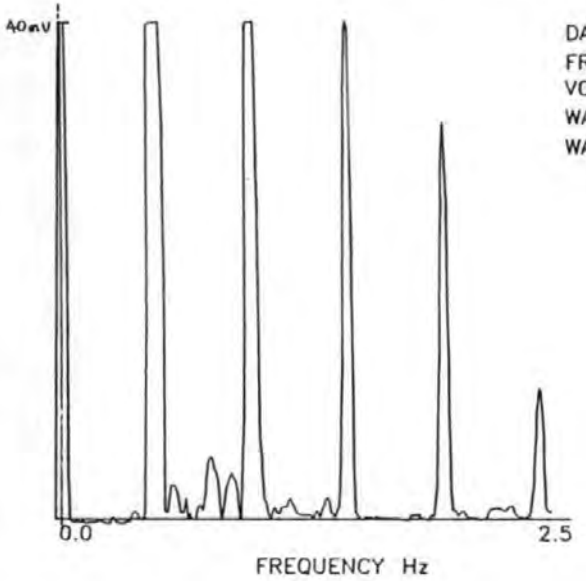

DATE : 18-12-85
FREQUENCY OF SINEWAVE 0.5
VOLTAGE GAIN : 2.00
WAVE ABSORBTION IN (OUT)
WAVESCREEN : FULL

REGULAR WAVE SPECTRUM

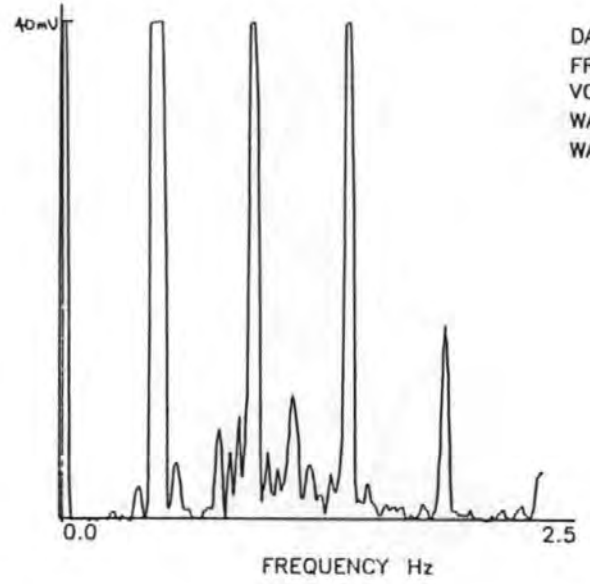

DATE : 18-12-85
FREQUENCY OF SINEWAVE 0.5
VOLTAGE GAIN : 1.37
WAVE ABSORBTION IN (OUT)
WAVESCREEN : FULL

parameters used. On all examples of incident spectra the 'theoretical spectrum' has been plotted. The 'theoretical spectrum' is calculated by the Hydraulics Research wave generation program NEWSYN (see chapter 2).

The nomenclature in use for wave spectra at present is very confusing with spectra derived from single or multiple wave gauge meausrements. In the subsequent discussion the following nomenclature is used to try and keep super and subscripts to an acceptable level.

- S_{ii} - Incident Spectrum calculated from estimates made by the three pairs of gauges 1-2, 2-3, 1-3.
- S_{rr} - Reflected Spectrum calculated from estimates made by the three pairs of gauges 1-2, 2-3, 1-3.
- S_{11} - 'Point' Spectrum measured at gauge 1.
- S_{22} - 'Point' Spectrum measured at gauge 2.
- S_{33} - 'Point' Spectrum measured at gauge 3.
- S_{12} - Incident Spectrum estimated from measurements from gauges 1 and 2.
- S_{23} - Incident Spectrum estimated from measurements from gauges 2 and 3.
- S_{13} - Incident Spectrum estimated from measurements from gauges 1 and 3.

Random Wave File name	$\bar{H}_s$m	$\bar{T}_z$2s	HRL Gain setting volts	Separation of Gauges 1-2 m	2-3 m	1-3m
RAN.97	.970	1.71	5.27	1.729	5.580	7.309
RAN.185	.185	1.79	5.99	2.032	5.277	7.309
RAN.1	.100	1.86	6.75	2.024	5.285	7.309
RAN.25	.250	2.08	9.42	2.539	4.770	7.309

Table 7.3 Random Wave Parameters

7.4.2 Analysis Procedure

Three wave gauges, spaced as shown above, were included in the data acquisition scheme outlined in Chapter 2. The test length was determined to include a full length sequence (Chapter 2). The results of the tests were first analysed with the conventional software for single gauges. The results from the single gauge analyses were used in verifying the new Frequency Response Function software as well as highlighting the problems which arise from just using single gauge analysis. A twenty second segment of the time history was also plotted as a check on the correct operation of the wave gauges. (Any attenuation due to water contamination would be apparent in the time history).

The results from each pair of gauges (i.e. 1-2, 2-3, 1-3) were then used in conjunction with the Frequency Response Function analysis program to obtain estimates of incident and reflected spectra. Each complete analysis took approximately 25 minutes.

The tests were repeated for each of the four cases (i.e. no wavescreen/full wavescreen for wave absorption 'in' and 'out').

7.4.3 Random Wave Results

Table 7.4 summarises the results from the single gauge analysis. Figures 7.21-7.22 are examples of the spectra produced from a composite wave train for each of the four situations mentioned above. Figure 7.23 is a 20 second example of the wave time history. From all the single gauge analysis it is clear how impossible the task of appraising the wave absorption system would be. No real information can be gained from the various spectra except that the wave absorption facility changes the situation!

The Frequency Response Function analysis is all the more powerful and beneficial in quantifying what is actually happening in the channel. A typical set of results from the tests are presented in Figures 7.24 - 7.30. The four permutations of test are each shown in Figures 7.24 - 7.27 with the incident spectra, S_{ii} from the Frequency Response Function analysis compared to a single point spectrum - S_{11}. With no wavescreen the two spectra (S_{ii} and S_{11}) compare well, as would be

expected with such small degrees of reflection. When the full wavescreen is present however, the effect of the formation of partial nodes and anti-nodes is cearly visible as peaks and troughs in the graphs.

The most revealing of the graphs however, are the incident and reflected spectra shown in Figures 7.28 - 7.30. The effectiveness of the absorption system is clearly illustrated by the similarity of the two absorption 'in' incident wave spectra (the two lowest curves in Figure 7.28 and shown at a greater scale in Figure 7.29). This despite the fact that the corresponding reflected wave spectra are quite different. Indeed, the absorption 'in', with no wavescreen curve can hardly be distinguished from the frequency axis of Figure 7.30, whereas the absorption 'in' and full wavescreen curve is the second highest.

The advantages of an absorption system are highlighted by the lack of similarity in both magnitude and shape of the two absorption 'out' curves compared to the similarity of the two absorption 'in' curves (Figure 7.28). Due to the presence of strong multiple reflections and re-reflections, the highest level of variance density for both incident and reflected waves were achieved when the 'full' wavescreen was in use. This is as would be expected and it might be thought possible to counteract this effect by simply reducing the primary input from a non-absorbing wavemaker. However, in practice the required correction would be far from simple due to the changes in spectral shape.

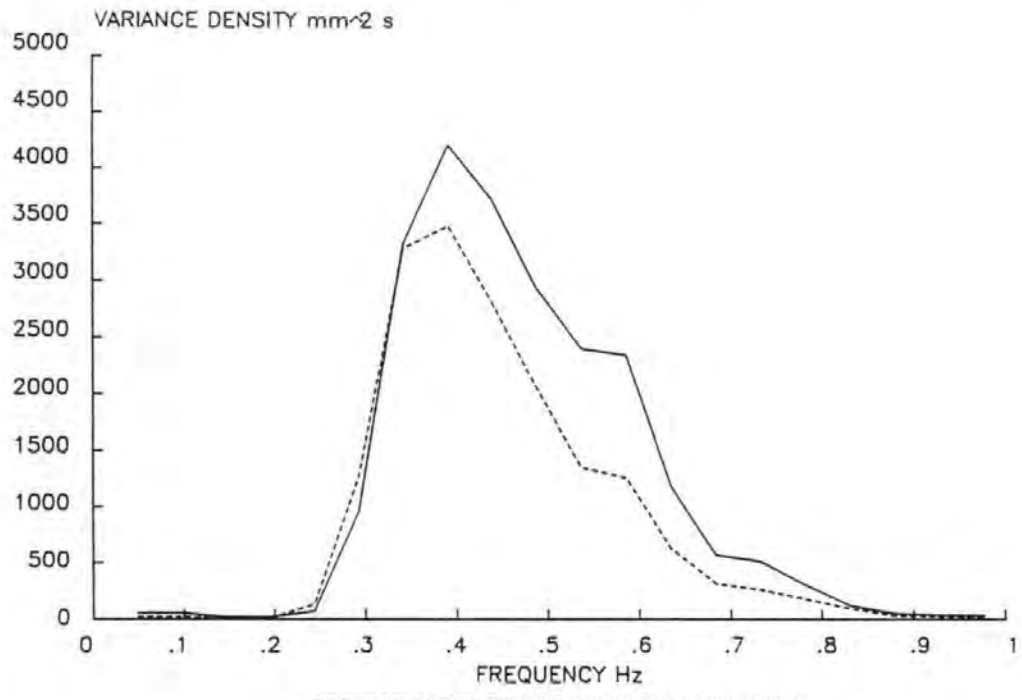

FIG 7.21 COMPARISION OF 'POINT' SPECTRA WITH NO WAVESCREEN

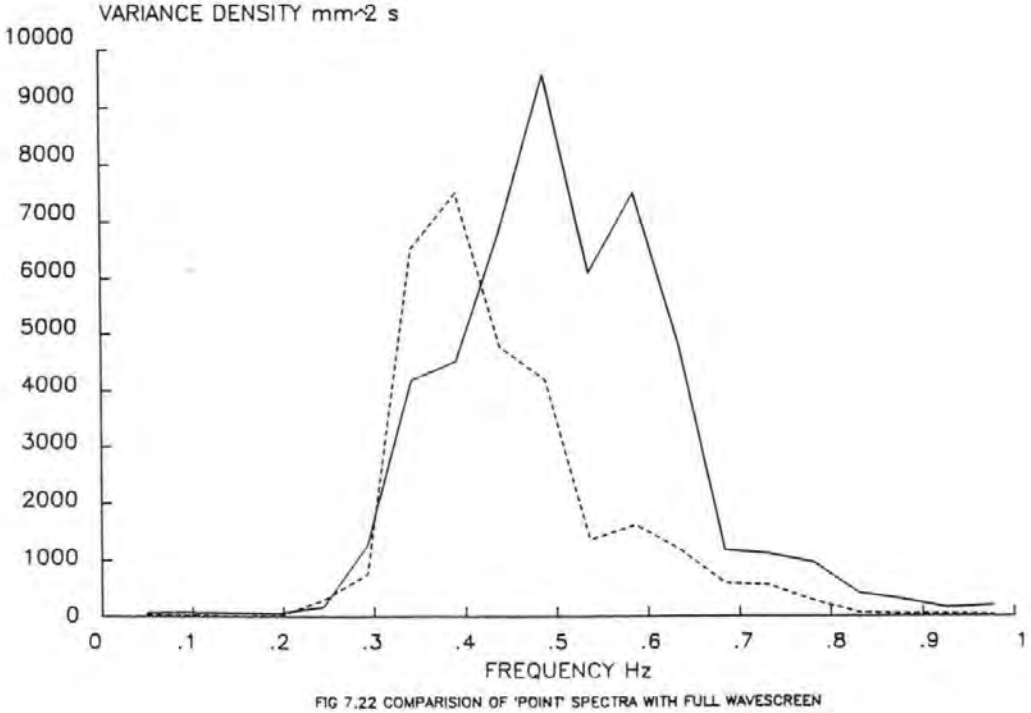

FIG 7.22 COMPARISION OF 'POINT' SPECTRA WITH FULL WAVESCREEN

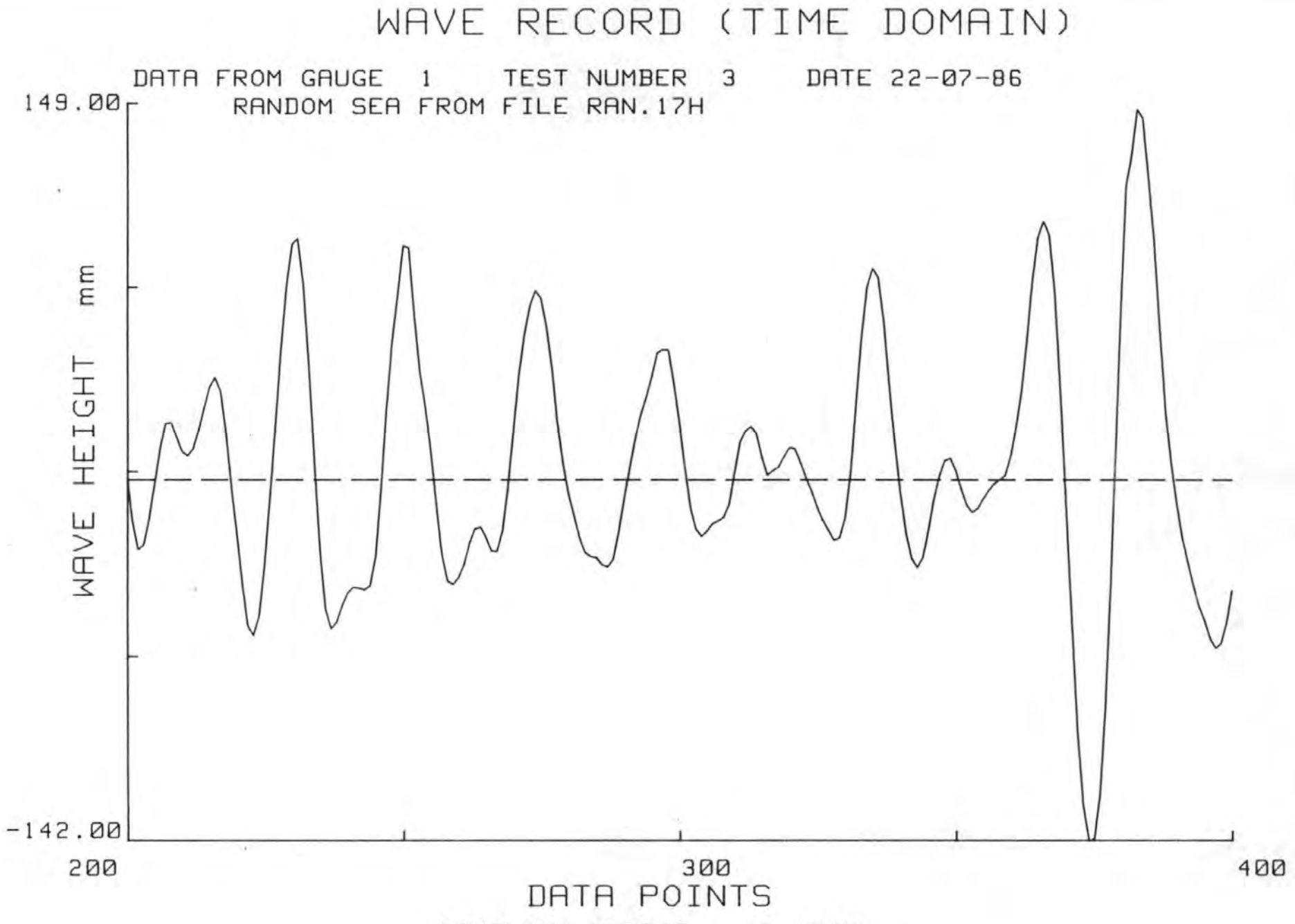

FIG 7.23 20 SECOND WAVE RECORD FROM AN ABSORPTION TEST

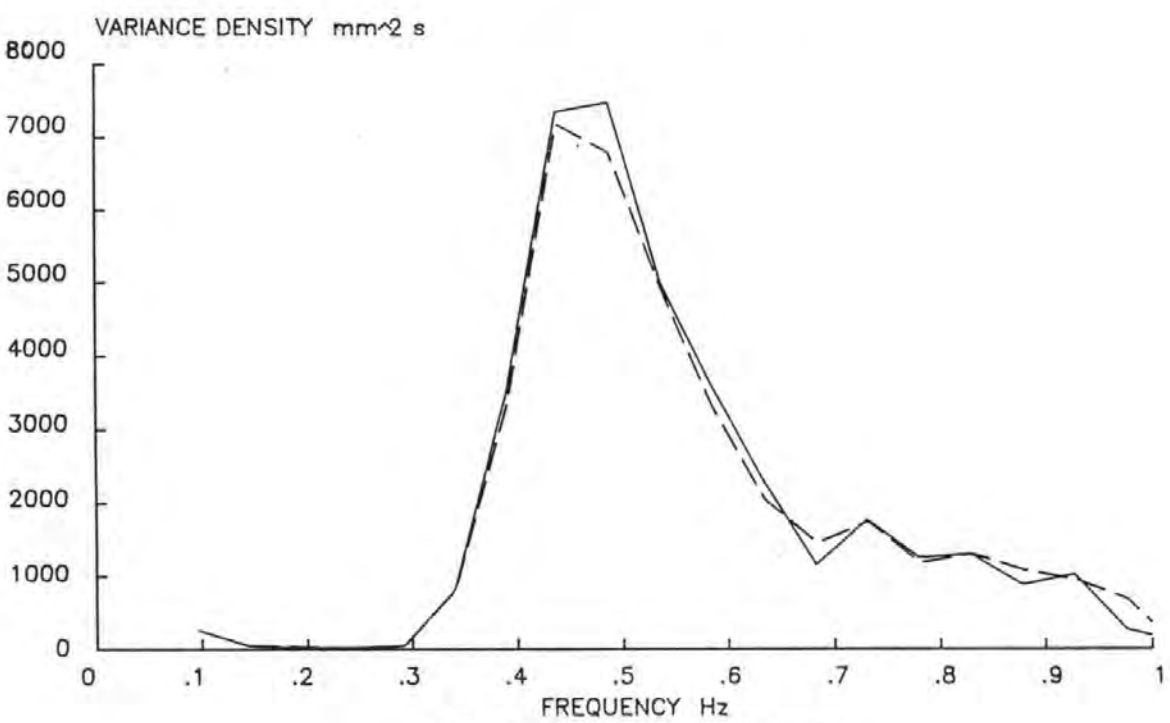

FIG 7.24 FREQUENCY RESPONSE FUNCTION OUTPUT

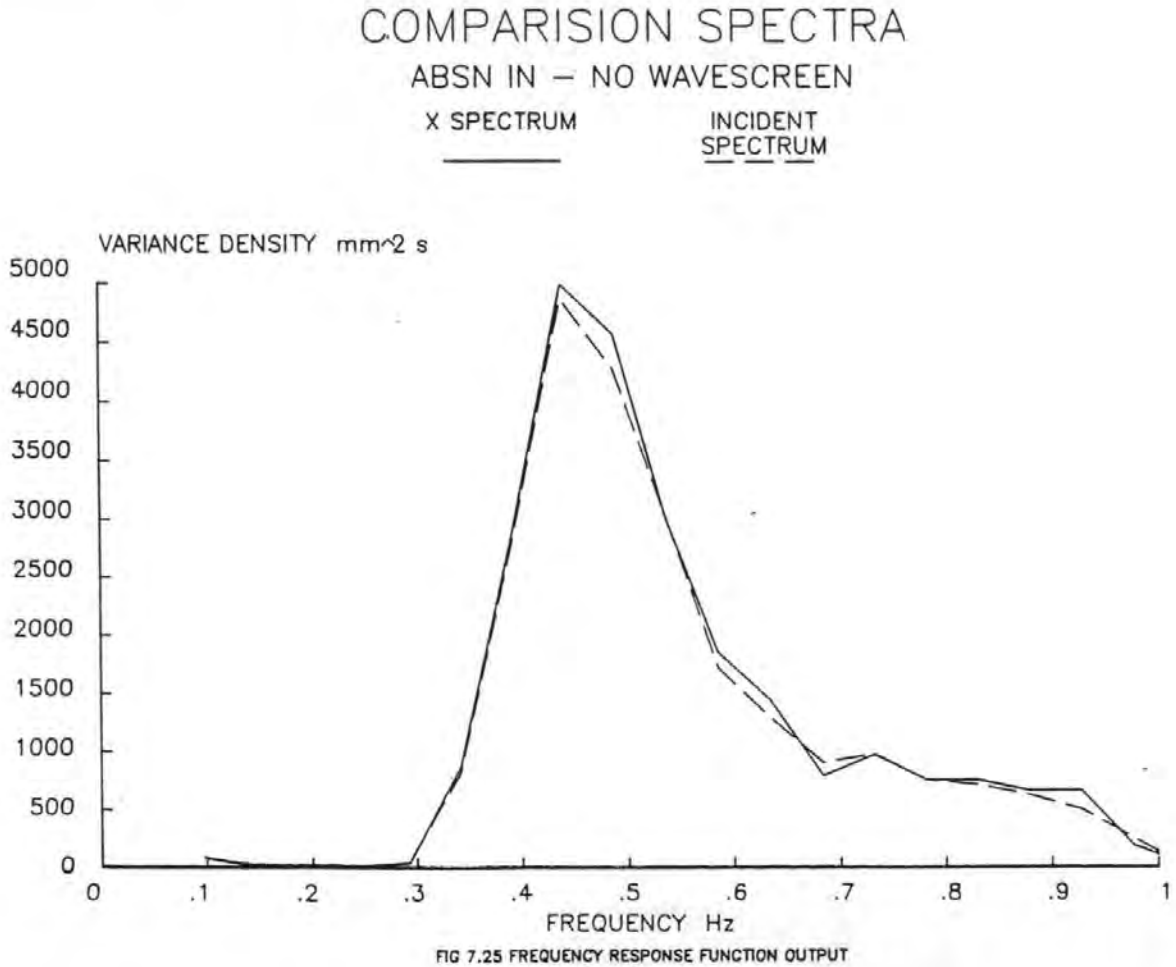

FIG 7.25 FREQUENCY RESPONSE FUNCTION OUTPUT

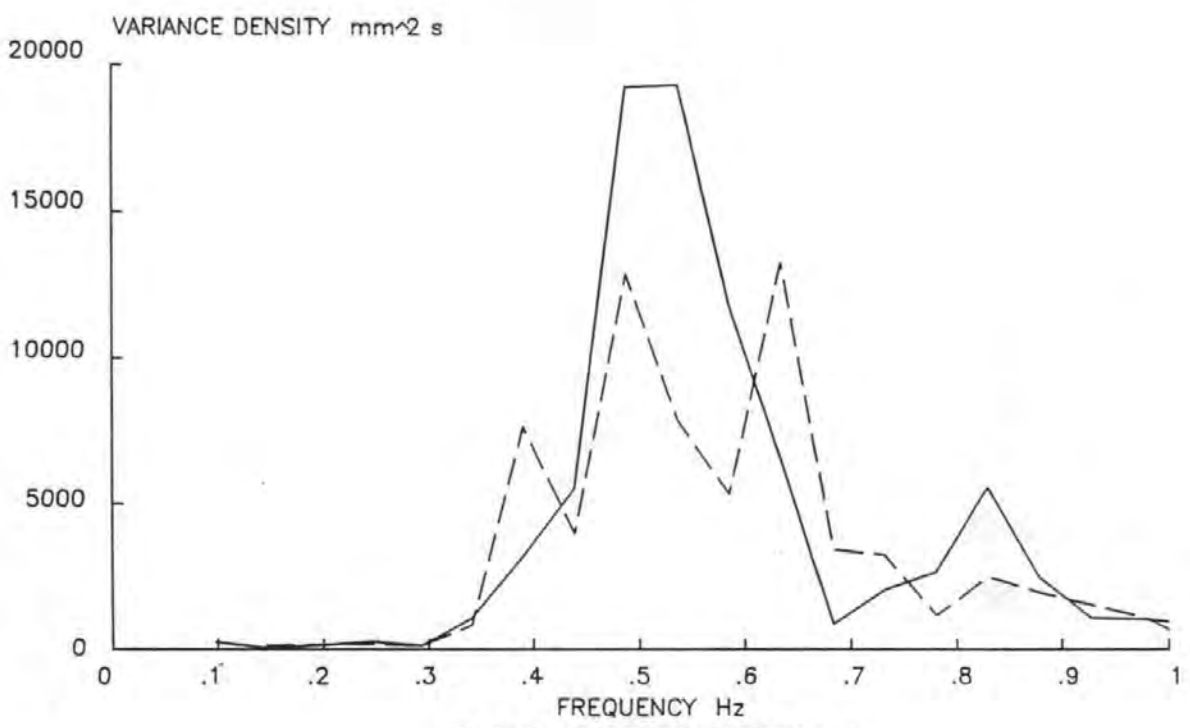

FIG 7.26 FREQUENCY RESPONSE FUNCTION OUTPUT

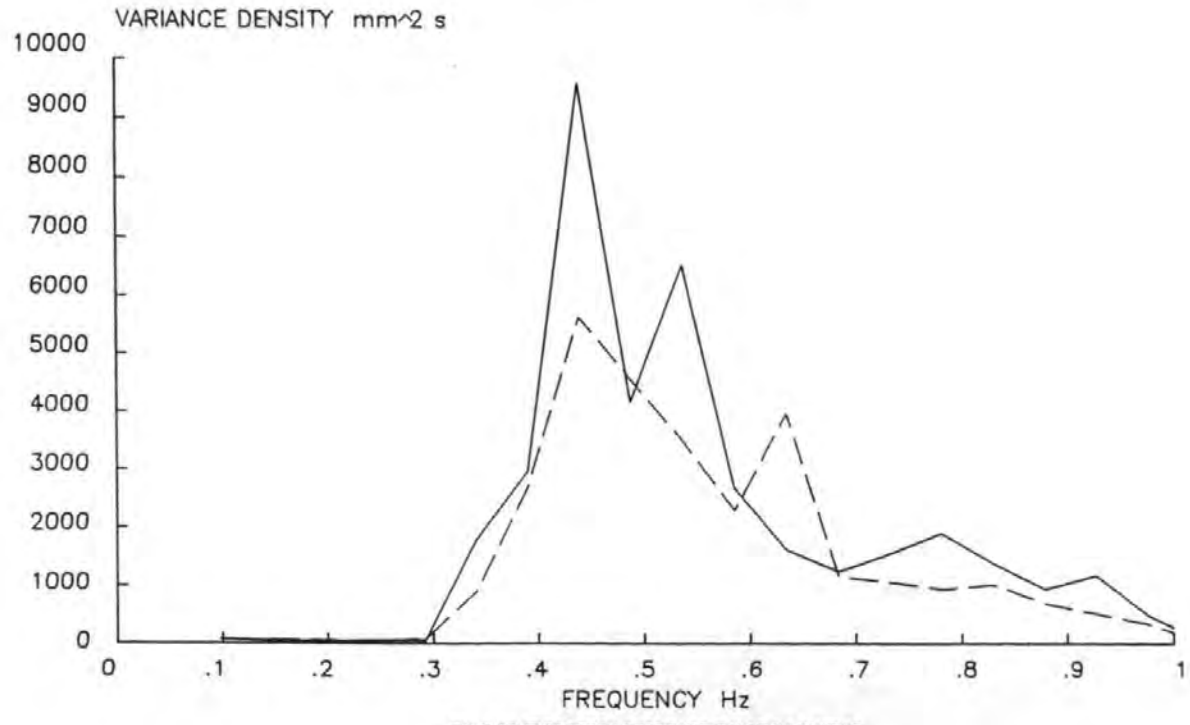

FIG 7.27 FREQUENCY RESPONSE FUNCTION OUTPUT

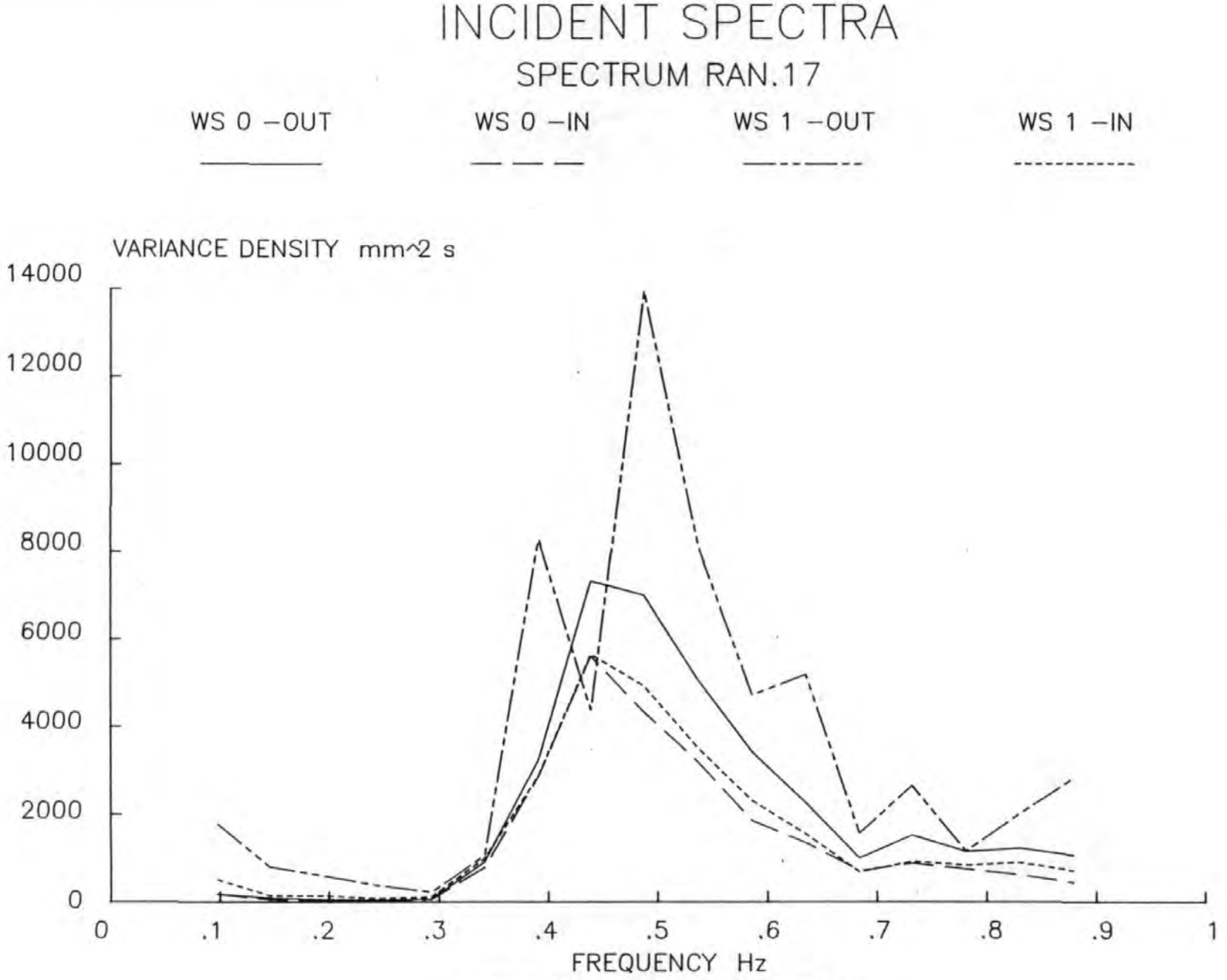

FIG 7.28 A COMPARISION OF THE INCIDENT SPECTRA

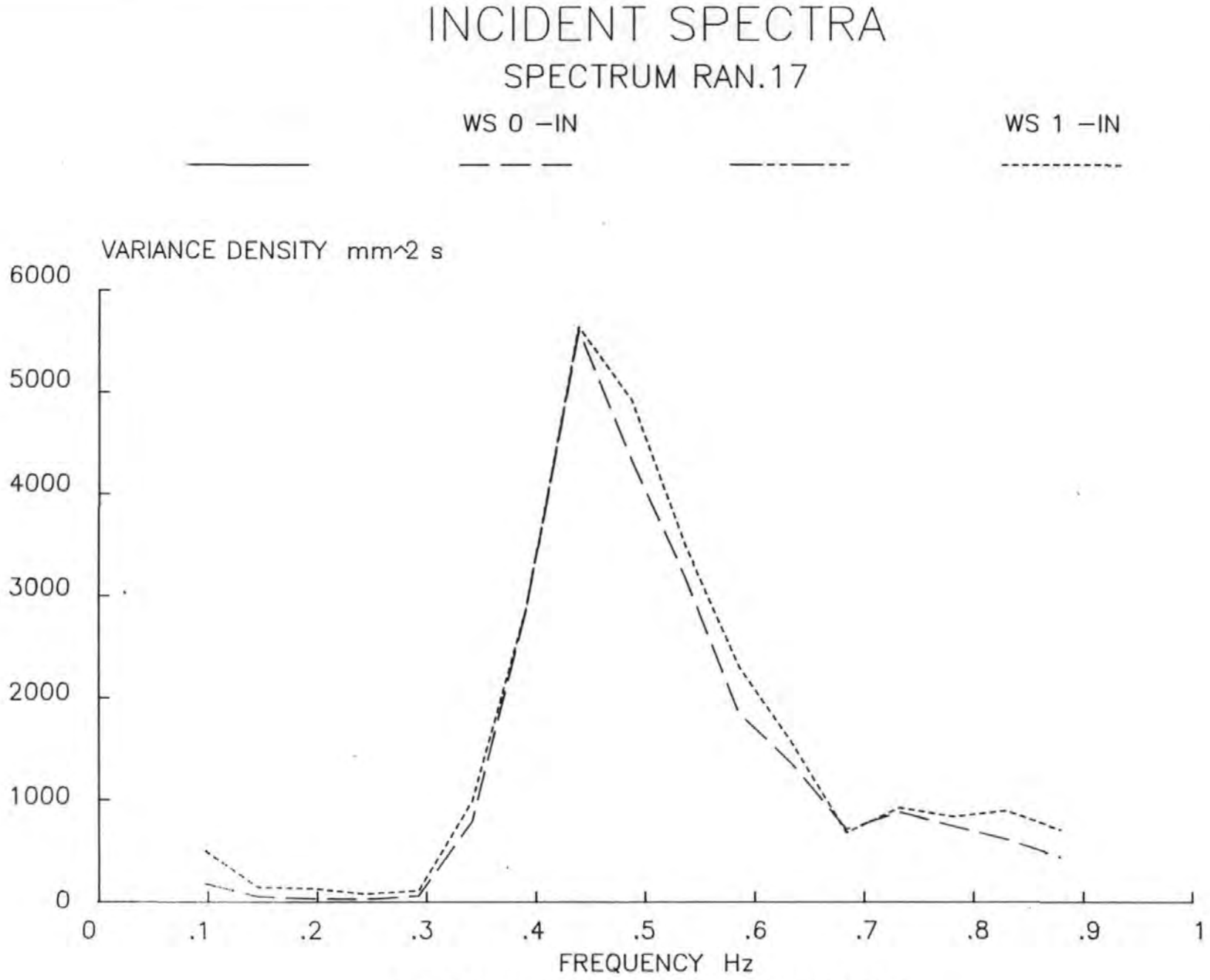

FIG 7.29 A COMPARISION OF INCIDENT SPECTRA WITH ABSN 'IN'

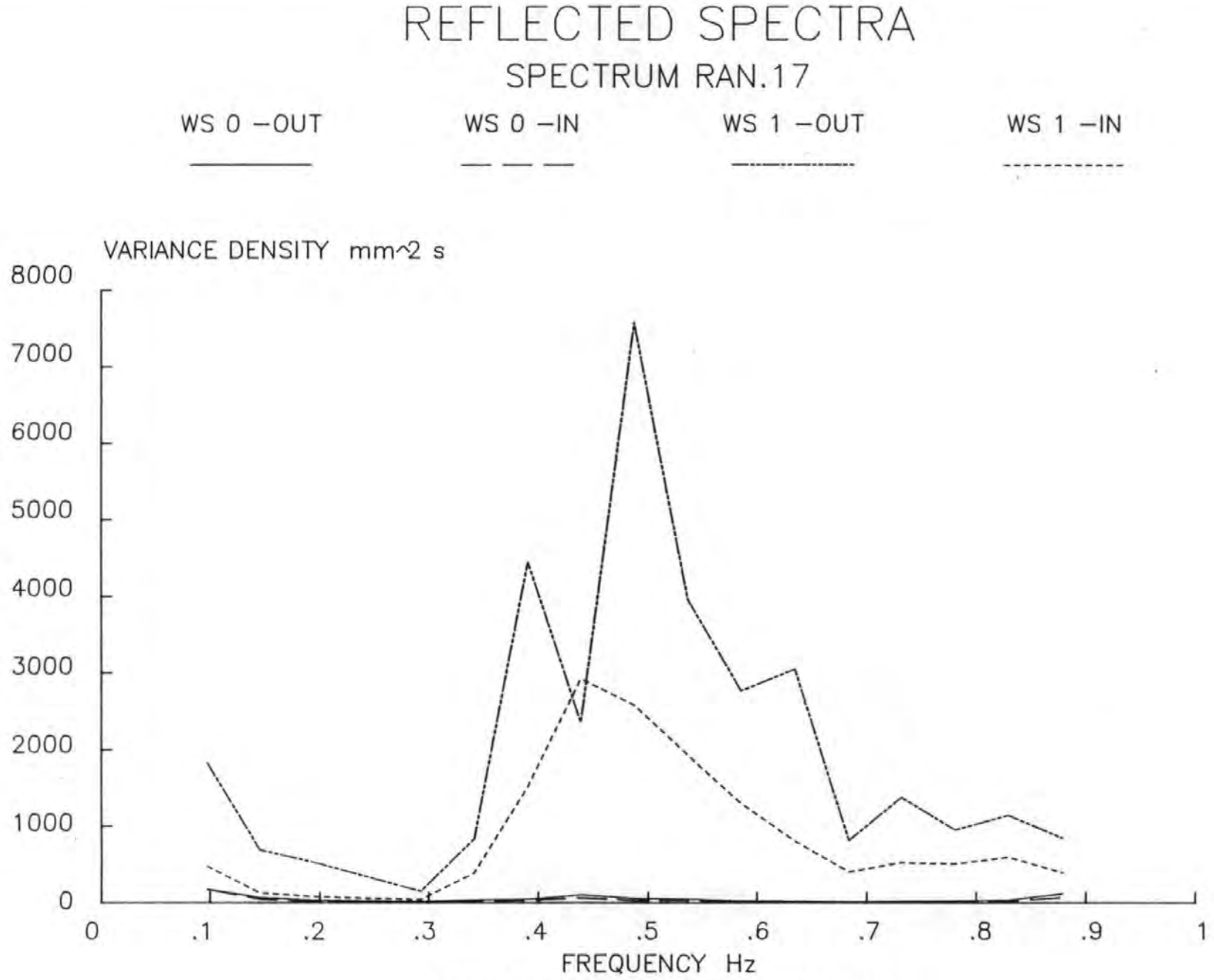

FIG 7.30 A COMPARISION OF THE REFLECTED SPECTRA

Test No.	Gauge No.	$\bar{H}_s$mm	$\bar{T}_z$s	fp Hz	Absn?	WAVESCREEN	Sea
1	1	95.02	1.832	.439	OUT	0	RAN.09
	2	100.56	1.811	.439			
	3	101.82	1.886	.439			
2	1	78.64	1.897	.439	IN	0	RAN.09
	2	79.08	1.898	.439			
	3	80.65	1.899	.439			
3	1	115.18	1.918	.391	OUT	0	RAN.1
	2	112.01	1.918	.391			
	3	114.23	1.959	.391			
4	1	90.97	2.041	.391	IN	0	RAN.1
	2	90.02	2.038	.391			
	3	93.64	2.052	.391			
5	1	95.54	1.807	.439	OUT	5	RAN.09
	2	95.11	1.834	.439			
	3	104.55	1.888	.439			
6	1	75.43	1.773	.439	IN	5	RAN.09
	2	77.89	1.844	.439			
	3	78.05	1.814	.439			
7	1	115.08	1.899	.391	OUT	5	RAN.1
	2	116.75	1.945	.391			
	3	116.82	1.915	.391			
8	1	90.26	2.016	.391	IN	5	RAN.1
	2	90.61	2.073	.391			
	3	83.10	2.013	.391			
9	1	159.84	1.654	.537	OUT	1	RAN.09
	2	161.61	1.716	.391			
	3	151.87	1.685	.537			
10	1	98.90	1.869	.439	IN	1	RAN.09
	2	103.11	1.872	.488			
	3	94.05	1.770	.537			
11	1	183.11	1.738	.439	OUT	1	RAN.1
	2	169.00	1.891	.391			
	3	165.04	1.869	.537			
12	1	113.85	2.022	.391	IN	1	RAN.1
	2	102.57	1.933	.439			
	3	108.00	2.094	.391			

Table 7.4 Results from Single Gauge Analysis

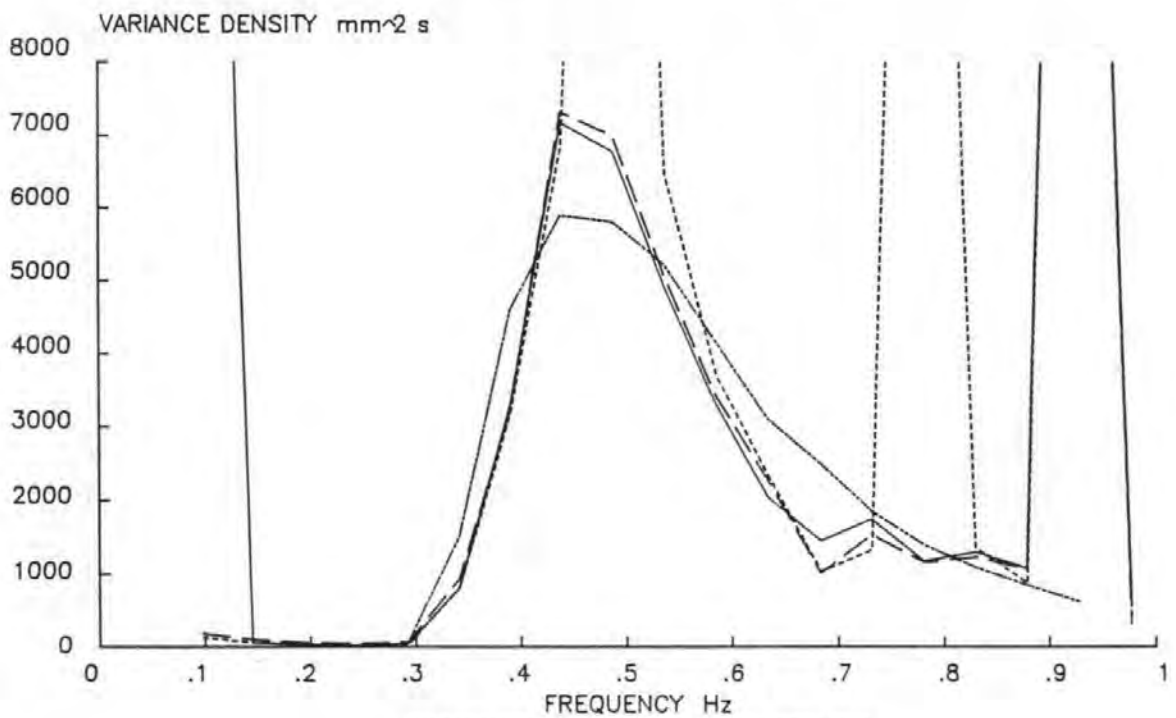

FIG 7.31 INCIDENT SPECTRA FROM A THREE GAUGE ARRAY

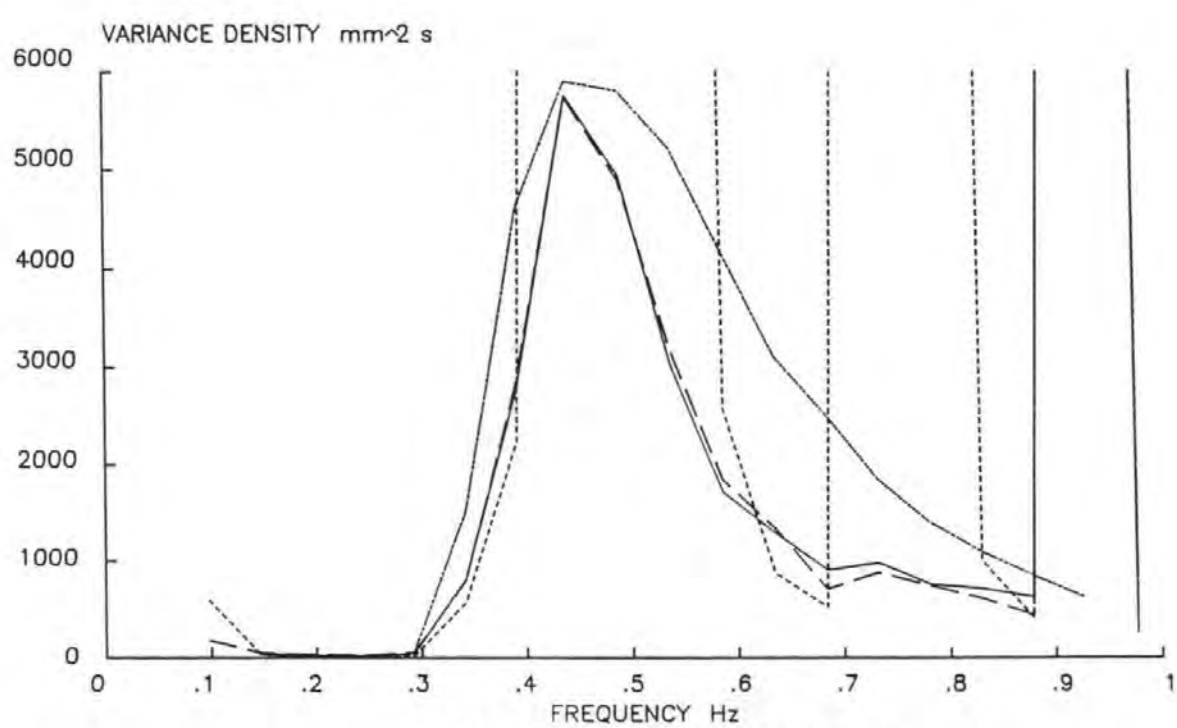

FIG 7.32 INCIDENT SPECTRA FROM A THREE GAUGE ARRAY

INCIDENT SPECTRA TEST 3

ABSN OUT – FULL WAVESCREEN

GAUGES 1–2 S= 1.736 m
GAUGES 2–3 S= 0.874 m
GAUGES 1–3 S= 2.610 m
THEORETICAL

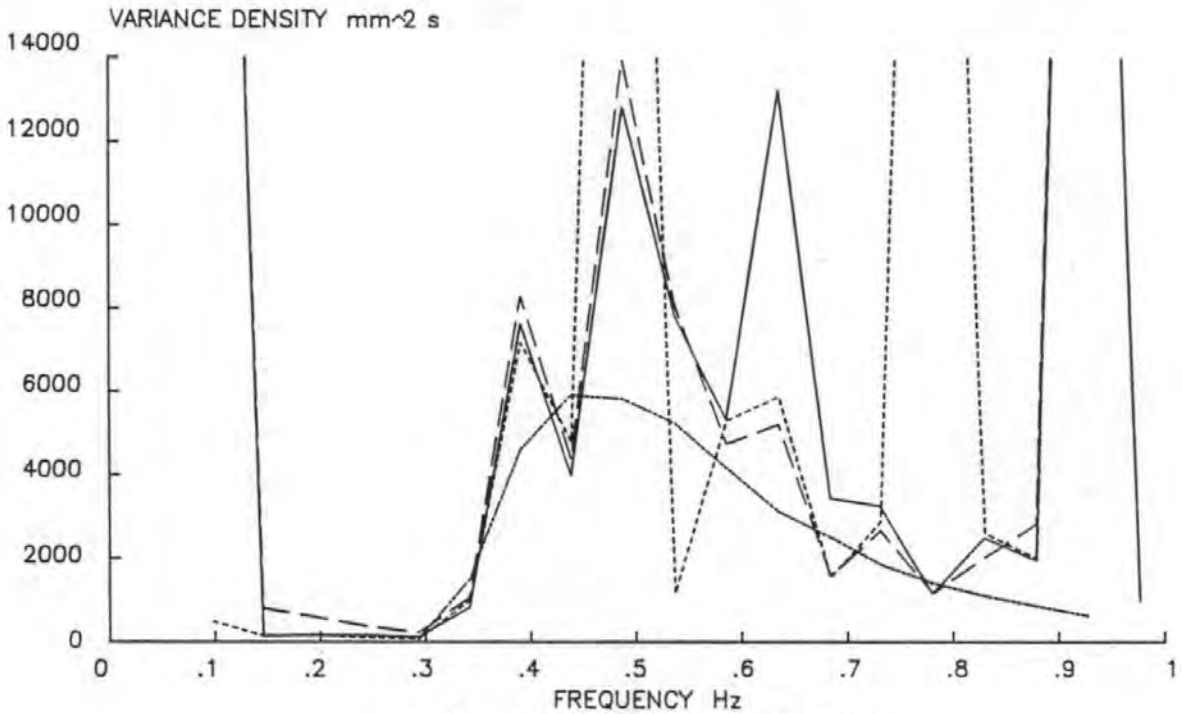

FIG 7.33 INCIDENT SPECTRA FROM A THREE GAUGE ARRAY

INCIDENT SPECTRA TEST 4

ABSN IN – FULL WAVESCREEN

GAUGES 1–2 S=1.736
GAUGES 2–3 S=0.874
GAUGES 1–3 S=2.610
THEORETICAL

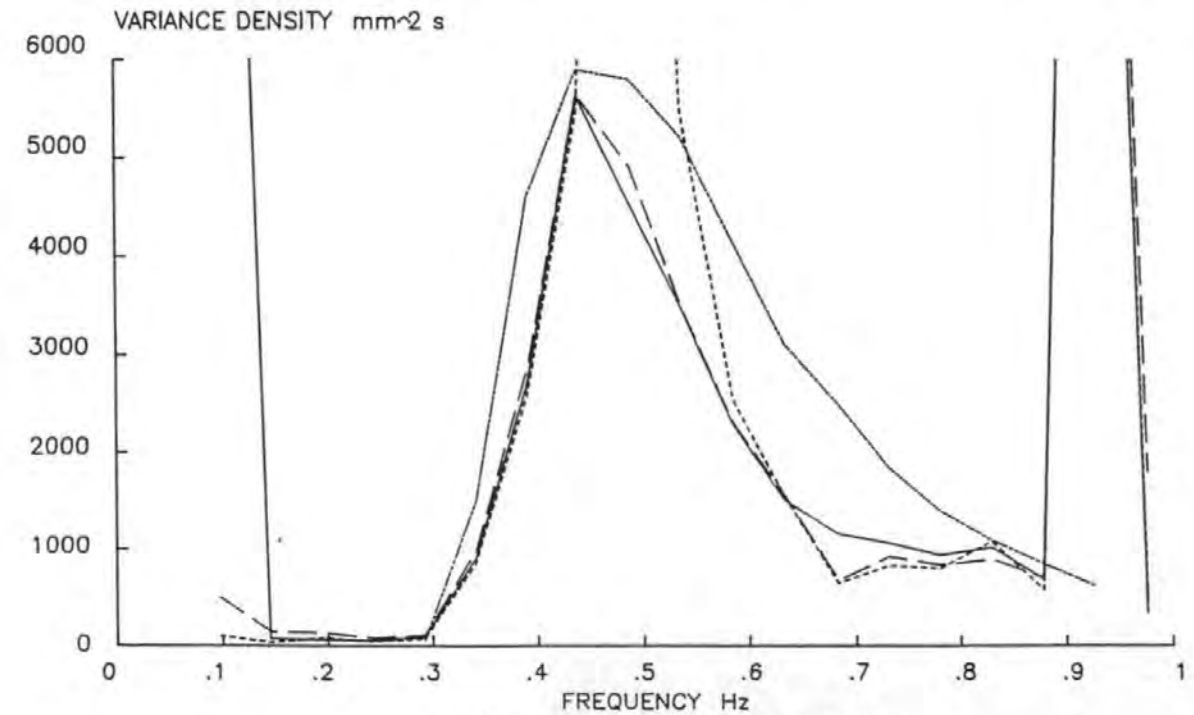

FIG 7.34 INCIDENT SPECTRA FROM A THREE GAUGE ARRAY

Test Number	Incident fp/Hz	Incident H_{si}/m	Reflected fp/Hz	Reflected H_{sr}/m	Composite fp/Hz	Composite H_s/m	Theoretical fp/Hz	Theoretical H_{si}/m	Wave Absn?
1	.439	.100	.391	.025	.439	.098	.475	.097	OUT
2	.439	.081	.439	.021	.439	.079	.475	.097	IN
3	.391	.115	.391	.038	.391	.114	.439	.100	OUT
4	.391	.093	.391	.031	.391	.091	.439	.100	IN
5	.439	.098	.439	.025	.439	.095	.475	.097	OUT
6	.488	.084	.488	.054	.439	.077	.475	.097	IN
7	.391	.117	.391	.036	.391	.116	.439	.100	OUT
8	.391	.097	.391	.041	.391	.090	.439	.100	IN
9	.439	.131	.439	.096	.537	.161	.475	.097	OUT
10	.439	.089	.439	.063	.488	.101	.475	.097	IN
11	.439	.139	.439	.101	.391	.176	.439	.100	OUT
12	.391	.093	.391	.066	.391	.108	.439	.100	IN

Table 7.5 Random Wave Test Results

7.4.4 Effects of the Gauge Spacing

As discussed earlier the Frequency Response Function method of analysis is not valid if sin(ks)=0. (Chapter 3 and Appendix C). The method of obtaining maximum resolution with 3 gauges was also discussed. Figures 7.31 - 7.34 show the three estimates of incident spectrum, S_{12}, S_{23} and S_{13} for a particular test. The graphs cover the permutation of test configuraiton as mentioned earlier. A theoretical spectrum is overlain in each case.

It can be readily seen that in the areas where each pair of gauges provides a valid analysis the 3 curves are very similar. Thus an estimate of variance density from any pair of gauges at a particular frequency is 'correct' By use of all 3 curves it is possible to obtain variance density estimates at all frequencies in the range of interest (0-1 Hz) which enables estimates of spectral moments to be made and hence a value for the significant incident wave height $\bar{H}_{si}$ can be obtained from $\bar{H}_{si} = 4\sqrt{m_o}$ (Chapter 3).

The estimations of variance density also compares well to the theoretical when little reflection is present or wave absorption is 'in'.

7.5 Conclusions

The test results show that the wave absorption system installed in the control loop of the paddle is very successful in eliminating the presence of re-reflections in the channel. Also it has been shown that good absorption characteristics can be achieved with a less than perfect filter design. If required, even better results could be obtained by use of a more complex filter.

The wave channel facility with wave absorption 'in' is in effect 'semi-infinite' in length i.e. the location of the paddle (or channel length) is not a factor in the test results obtained from a reflective structure. This fact will be exploited to investigate overtopping with a higher degree of operational control and accuracy than has been previously possible.

7.6 Recommendations to Improve Wave Absorption System

Apart from the less than perfect filter design discussed in Chapter 6 the other main area for potential improvement lies in the calibration of the system.

A recommendation for a future absorption system would be to incorporate the tuning potentiometer (INVERT/NORMAL) on the front panel of the hydraulic system controls and show the output level of the potentiometer with a meter similar to the Error/Position meter used for hydraulic control After an initial calibration, the meter could be scaled in terms of absorption efficiency. At the start of a test the potentiometer could be adjusted as necessary. A calibration by meter would be much more convenient as the paddle wave gauge is relatively inaccessible, and adjustments made from the wave gauge calibration require a degree of subjectivity which a meter could eliminate quickly and effectively.

The design of the paddle wave gauge could also be improved with a more solid chassis which would eliminate some of the vibration problems which occur with small paddle movements at low frequencies. It would also be possible to allow for the vertical paddle movements in the design of the filter and thus, the wave gauge could be rigidly fixed to the paddle front.

CHAPTER 8

WAVE OVERTOPPING

8.1 Introduction

Accurately estimating the amount of water which will wash over a coastal structure can be vital to design engineers. Building seawalls or breakwaters high enough to completely prevent overtopping is often unacceptable because of aesthetics and costs.

In practice it is very difficult to prevent perfectly wave overtopping. Therefore, a breakwater must be designed based on the concept of allowable wave overtopping, on the premise of a cost/aesthetic trade-off with 'unacceptable' conditions to the lee of a breakwater.

What is 'unacceptable' will depend upon the use for which the structure is intended. Clearly more overtopping will be acceptable for a breakwater, such as the one in Plymouth Sound, the function of which is to protect large vessels at anchor than for a breakwater to protect small crafts in a marina. Another important consideration is the provision of calm water for the berthing of ships.

A number of previous studies of wave overtopping were reviewed in Chapter 1. As recently as 1984 Douglass concluded that "Better data is sorely needed" in his review of irregular wave overtopping rates.

The tests performed here are intended to compliment the existing data and in particular a comparison to Owen (1980) is presented. The test parameters (see Section 8.2) were chosen to provide data on 'low' structures beyond the regions previously examined ('low' refers to the crest elevation above still water level s.w.l.).

The data collected would also provide an appraisal of the wave absorption system installed in the wave maker equipment and described earlier. By use of the wave absorption system a much better control of the sea state was possible than it had been previously. Thus, it was much easier to 'target' the tests to areas of interest rather than run a series of tests and investigate what physical situations arose due to the re-reflections from a conventional paddle.

8.2 Factors influencing the Overtopping Discharge

Wave overtopping is an extremely complex coastal phenomenon. (Douglass 1984). Variables include structure characteristics (shape, height, slope, roughness, porosity, berm width, offshore slope etc); wave characteristics (height, period, direction, statistical description); water depth; wind speed and direction; air and water densities and viscosities etc.

A number of the above parameters cannot be easily varied in a laboratory channel (densities, wind effects etc) and for the purpose of this investigation they are regarded as constant.

Time has also prevented an investigation into some of the other parameters (such as the effect of a berm on the seaward slope of a breakwater, which is known to decrease the overtopping (Owen 1980) if all the other parameters remain constant).

A typical breakwater may have the shape shown below:

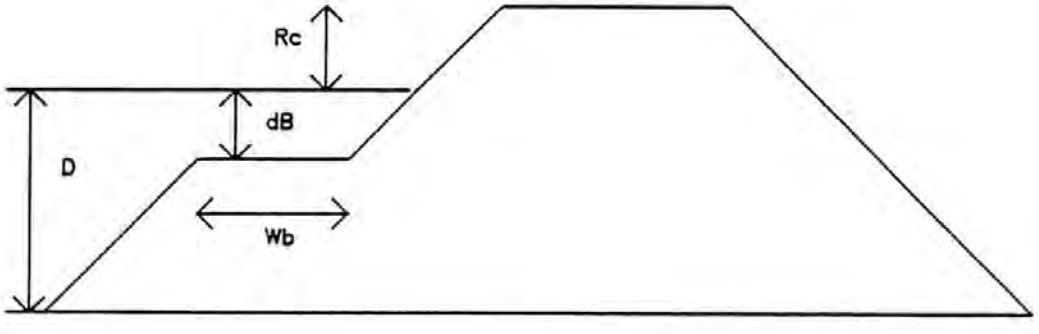

Figure 8.1 A Typical Breakwater Profile

where R_C = Crest elevation above s.w.l.

d_B = Berm Elevation

d_s = Water depth

M = Breakwater slope

W_b = Berm width

Due to limitations of time or space (or both) various physical and structural parameters have not been investigated. Some of the parameters are listed below with a brief description of their influence on overtopping discharge.

i. Seaward slope off the toe of the breakwater. A steeper slope will increase the overtopping discharge.

ii. Berm breakwaters. A submerged berm will decrease the overtopping discharge.

iii. Angle of wave attack. Owen (1980) found that maximum overtopping discharge occurred with waves at 15° to the normal.

iv. The roughness of breakwater slopes. The Shore Protection Manual (1984) states that a rip-rap slope will only have 40% of the run-up for a given wave compared to a smooth slope. Hence the overtopping discharge would be decreased.

v. Slope permeability, A porous slope will give lower overtopping rates (Weggel 1978).

The simplified breakwater profiles used in the overtopping tests had seaward slopes of 1:1 and 1:2, a smooth slope and horizontal crest (Figure 8.2). A range of test parameters is given in the next chapter.

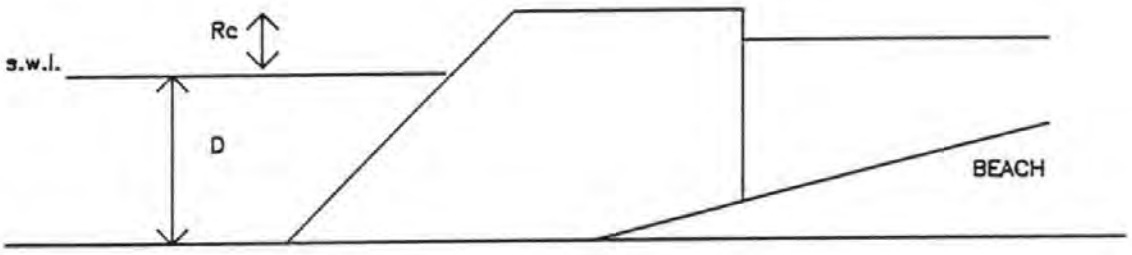

Figure 8.2 Test Breakwater Profile

The construction of the breakwater is discussed in Section 8.4.

The wave characteristics which influence the overtopping discharge have been defined in earlier chapters. For the sake of convenience the relevant parameters are listed below:

i) Significant Wave Height ($\bar{H}_s$).

ii) Mean zero-crossing period (T_z)

iii) Shape of an Incident Spectrum.

Also needed for comparison (Section 8.5) will be a count of the total number of waves in a record. The significant wave height used for analysis and interpretation was where appropriate the incident significant wave height given by $\bar{H}_{si} = 4\sqrt{m_o}$ where m_o is calculated from the estimate of incident spectrum using the 3 gauge array. (Chapter 3).

8.3 Maximum Overtopping Discharge

In order to be able to design equipment to measure the wave overtopping discharge an estimate of the maximum discharge expected was needed. The equipment could then be designed to cope with discharges up to the expected maximum.

Some of the more recent work (Owen 1980) has suggested that the overtopping discharge over a breakwater can be calculated from dimensionless coefficients derived from the results of hydraulic model tests. The published coefficients were used to calculate the maximum overtopping discharge expected. The calculation is shown below.

Test Parameters

Slope 1:1
Crest Elevation 0.05m
Significant Wave Height 0.20m
Mean zero-crossing period 2.0s

The dimensionless freeboard R^* is defined as:

$$R^* = \frac{R_c}{T_z \sqrt{gH_s}} \tag{8.1}$$

The dimensionless discharge Q^* is defined as:

$$Q^* = \frac{Q}{(T_z g \bar{H}_s)} \tag{8.2}$$

Coefficients A and B are found from Figures 8.3 and 8.4 respectively (Owen 1980) such that:

$$A = 0.0076$$

and

$$B = 20.1$$

OVERTOPPING COEFFICIENT A

NORMAL WAVE ATTACK – NO BERM

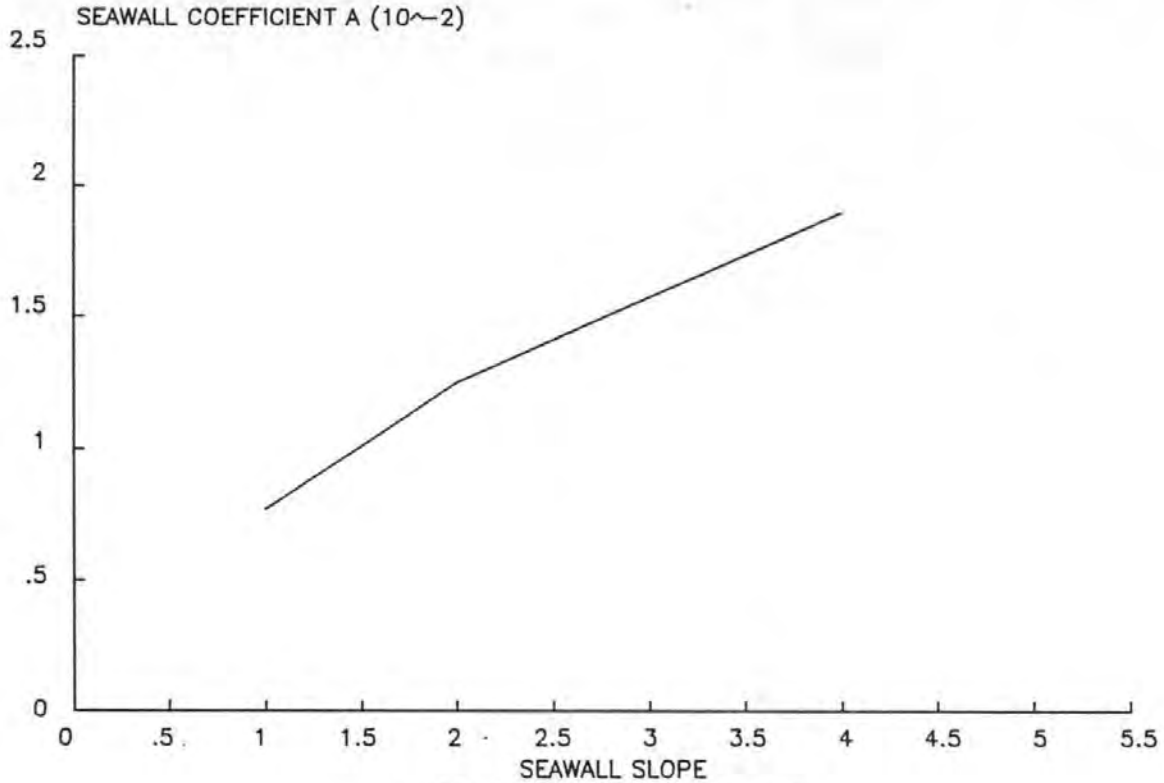

FIG 8.3 COEFFICIENT 'A' FOR SIMPLE SEA WALLS

OVERTOPPING COEFFICIENT B

NORMAL WAVE ATTACK – NO BERM

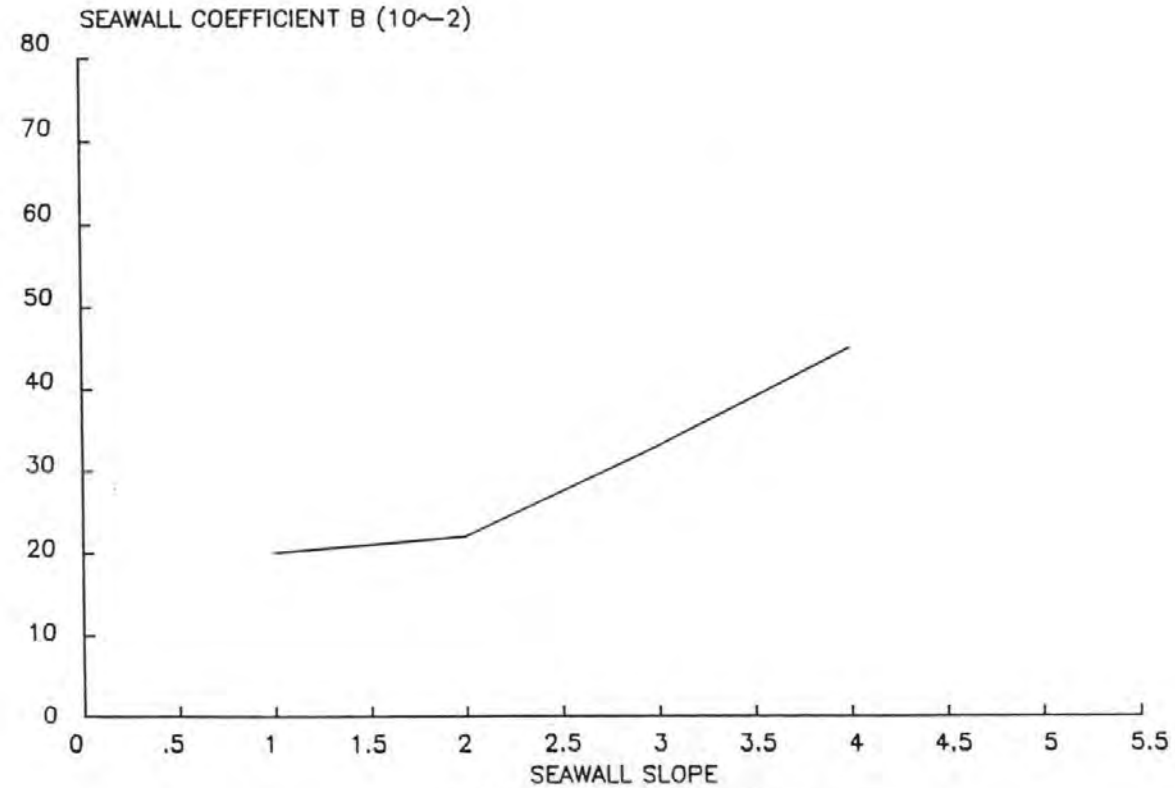

FIG 8.4 COEFFICIENT 'B' FOR SIMPLE SEAWALLS

The dimensionless discharge, Q^*, is thus defined as:

$$Q^* = Ae^{-BR^*} \tag{8.3}$$

From (8.3) we obtain:

$$Q^* = 5.309 \times 10^{-3}$$

rewriting equation (8.2) we obtain;

$$Q = Q^* T_z g \bar{H}_s \tag{8.4}$$

From equation (8.4)

$$Q = 0.021 m^3/s/m \text{ run}$$
$$= 21 \text{ litres/second/m of breakwater crest.}$$

The design of the overtopping equipment outlined below was based on a maximum expected overtopping discharge of 21 litres/second.

8.4 Design of Breakwater and Overtopping Measurement Equipment

8.4.1 Breakwater

As mentioned above, a simplified breakwater was used in the tests. The seaward slope was smooth and two slopes of 1:1 and 1:2 were used. The breakwater was constructed from ¼" marine ply. In order to locate the breakwater securely within the channel it was constructed to lie between two side panels (Plate 8.1). The side panels were then clamped to the channel sides. The above technique avoided the problem of having to drill holes into the channel sides. Throughout the overtopping tests no movement of the breakwater was detected.

The basic shape shown in Plate 8.1 has a seaward slope of 1:1. The 1:2 slope fitted onto the existing structure. (Plate 8.2).

In order to try and prevent the side panels having an effect on the wave climate they were tapered facing the direction of wave propagation (Figure 8.5). The two side panels occupied less than 1.5% of the channel width. During the overtopping tests no effects due to the side panels could be detected visually.

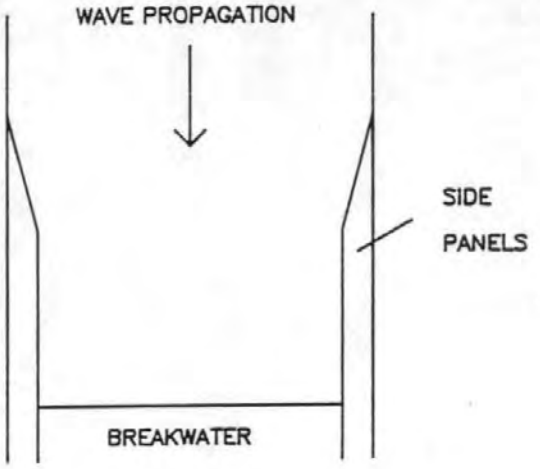

Figure 8.5 Side Panels

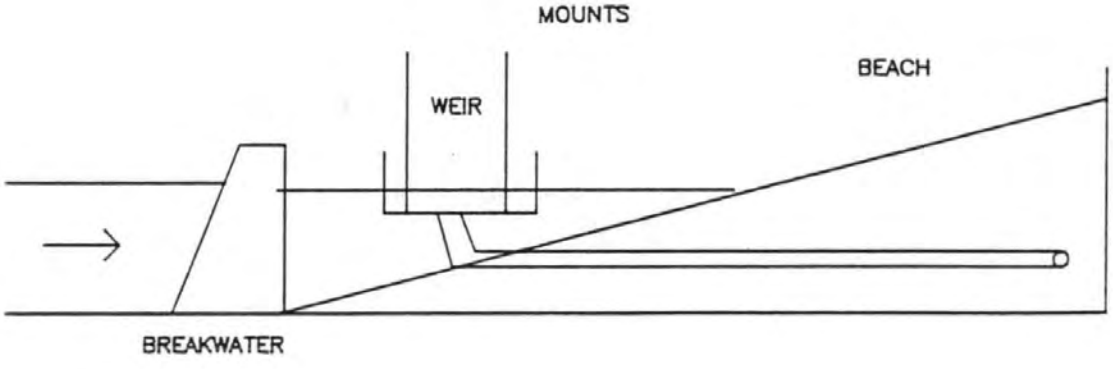

Figure 8.6 Breakwater Construction Details (Not to Scale)

The breakwater was located at the foot of the 'spending' beach.

8.4.2 Measurement of the Overtopping Discharge

In the area directly behind the breakwater a pond was formed bounded by the breakwater, the 'spending' beach and the end of the channel. Any waves which 'overtopped' flowed into this area. To accurately measure the overtopping discharge the pond had to be 100% watertight. To ensure this the pond was lined with plastic sheet fixed around the borders of the channel.

To measure the overtopping discharge an overflow weir system designed to cope with a maximum discharge (as calculated in 8.3) was constructed.

Within the watertight pond behind the breakwater a weir with two, parallel, one metre crests was located (Plate 8.3). The two crests were perpendicular to the breakwater crest. The flow over the weir went down a 4" pipe which ran through a hole in the waterproof liner and the 'spending' beach and out of the channel area to a collection sump (see below).

To try and prevent reflections within the stilling area behind the breakwater which would possibly prevent accurate measurements of the overtopping discharge, the weir was profiled. Two tapered ends, (Figure 8.7, Plate 8.3) helped the flow of water around the ends of the weir. The calmer the water the less the risk of water returning over the breakwater. Observations of the tests showed that the profiled weir was successful in preventing any water being returned to the main area of the channel.

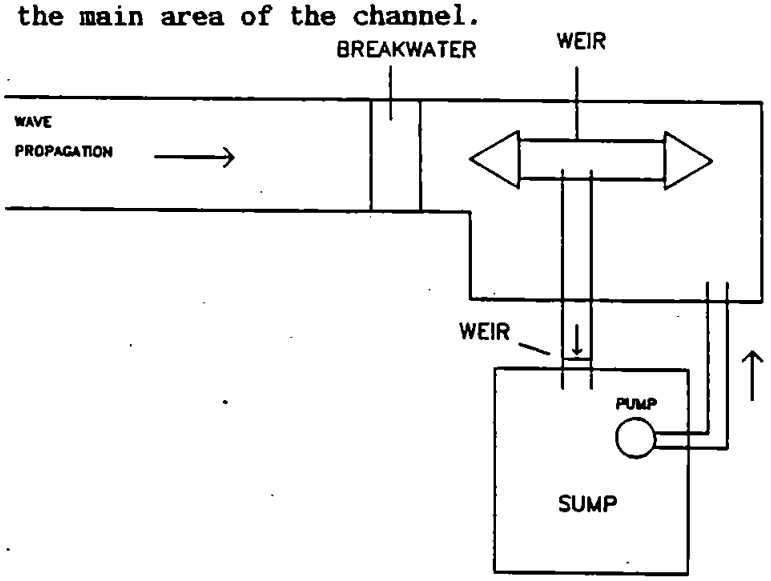

Figure 8.7 Profiled Discharge Weir

As mentioned above, the water flows over the weir and into a pipe system. The pipe system exits from the channel and discharges the water into a rectangular channel set into the floor of the hydraulics laboratory. At the end of the channel was a sharp-crested rectangular weir (Plate 8.4). On the downstream side of the weir was a sump, 1m deep, 2m long, 0.75m wide.

The water flowed over the weir and into the sump. A submersible pump in the sump returned the water to the wave channel to try and keep the water level in the channel constant.

A wave gauge monitored the flow over the weir (Plate 8.4). The wave gauge was included in the data acquisition system of Wave Monitor-Microlink-HP computer.

The computer program DISCHARGE was written to analyse the data collected from the wave gauge associated with the weir. The program used the standard weir equation (Herschy 1985) to calculate a mean overtopping discharge as well as the total test discharge. The instantaneous discharge at each sampling interval was calculated and the mean discharge found from all the instantaneous values.

8.5 A Count of the Overtopping Waves

Allsop (1978) and Owen (1980) published graphs of the percentage of waves overtopping (% of total waves in record) against the dimensionless freeboard (see 8.3). In order to make the same comparison here a computer program, OVERTOP, was written to calculate the number of waves which overtop during a test. A wave gauge mounted on the breakwater crest was included in the data acquisition system to facilitate this.

The overtopping waves were detected in the digital record in the following manner. The program counted a separate wave as a block of numbers starting and finishing with zeros. For example a part of the digital record may look something like that shown below:

0 0 721 890 650 221 15 0 0 0 100 90 17 0 0

PLATE 8.1 1:1 [illegible]

PLATE 3.2 1:2 BREAKWATER

PLATE 8.3 OVERTOPPING WEIR

PLATE 8.4 CALIBRATED WEIR AND COLLECTION SUMP

The program OVERTOP interprets the above piece of digital record as containing two waves. One wave begins at 721 and ends at 15, the second wave starts at 100 and ends at 17.

The program was checked against visual observations and found to be accurate.

8.6 Incident and Reflected Spectra

By making use of the Frequency Response Function analysis described in Chapter 3, the incident wave conditions were calculated for each test and hence the sea state defined more rigorously than was previously possible.

An array of three gauges spaced according to the criteria set out in Chapter 3 was used to obtain information over the whole frequency range of interest (0-1Hz). One of the three gauges was positioned directly over the toe of the breakwater. A check on mean water level could then be made.

The three gauges were located and spaced as shown below:

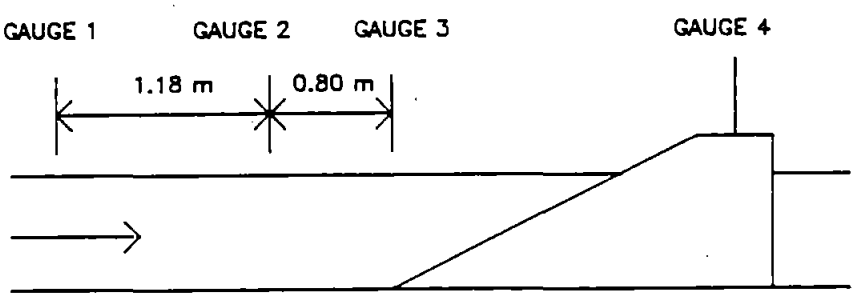

Figure 8.6 Wave Gauge Locations

where S_1 is chosen to have maximum resolution at the spectral peak frequency and S_2 is chosen to have maximum resolution at the frequency at which the analysis with S_1 is not valid. (See Chapter 3 and Appendix C).

The determination of incident and reflected spectra allowed a comparison of the measured reflection coefficient with the reflection coefficient calculated from the surf similarity parameter (Shore Protection Manual 1984). The method of determining reflection coefficient values from a surf similarity parameter is explained in the next chapter.

8.7 Wave Spectrum Generation

The Hydraulics Research Ltd software for random wave generation was used to produce the random wave spectra for the overtopping tests. Spectra were chosen to test the absorption system when nodes, antinodes or partial nodes were formed at the paddle front (see Chapters 3 and 7) and the effect these situations had on wave overtopping.

The wave spectrum generation program USERN was modified to provide the user with a choice of possible feedback connections for a given sequence length. (Sequence lengths and feedback connections were described in Chapter 2). Table 8.1 details some of the possible feedback connections available for various sequence lengths.

By a change in feedback connections, different complete or 'full' (i.e. all possible shift register positions) spectra can be generated with the same statistical properties, up to 4 for each sequence length was possible. The overtopping tests were carried out with different 'full' length spectra to investigate whether wave overtopping was influenced by the precise wave train, or statistically stable for a 'random' sea. The results of this are discussed in the next chapter.

Sequence length	Feedback from stages			
	set one	set two	set three	set four
2	ONLY ONE CONNECTION PATTERN POSSIBLE (1,2)			
3	(1,3)	(2,3)	(1,3)	(2,3)
4	(1,4)	(3,4)	(1.4)	(3,4)
5	(2,5)	(3,5)	(1,2,3,5)	(2,3,4,5)
6	(1,6)	(5,6)	(1,2,5,6)	(1,4,5,6)
7	(3,7)	(1,7)	(6,7)	(4,7)
8	(2,3,4,8)	(1,2,7,8)	(1,6,7,8)	(1,3,5,8)
9	(3,4,6,9)	(4,9)	(5,9)	(3,5,6,9)
10	(3,10)	(7,10)	(2,3,8,10)	(2,8,9,10)
11	(2,11)	(2,5,8,11)	(1,3,7,11)	(2,3,5,11)

Table 8.1 Feedback Connections for 'Full-Length' Spectra

8.8 Tests on Wave Absorption System

Throughout the wave overtopping tests a continual monitoring and appraisal of the wave absorption facilty was undertaken. It was hoped that any, as yet undiscovered, anomalies in the system would be highlighted during the course of a comprehensive series of tests. In the event, no problems were encountered, other than the need to maintain a close scrutiny over the calibration of the paddle wave gauge (see Chapter 5).

As mentioned in 8.7, spectra were chosen to produce nodes, antinodes or partial nodes at the paddle front to test fully the system.

The majority of the overtopping tests were conducted with wave absorption 'in', however, a small number of tests were performed with absorption 'out' for a comparison. The effect of no wave absorption is discussed in the next chapter.

8.9 Test Procedure

For each single overtopping test a random sea was generated in the channel. A 2k (i.e. 2048) data sample was collected for storage and analysis from the following five wave gauges:-

3 in the channel for Frequency Response Function Analysis and the calculation of wave statistics.

1 on the breakwater crest to count the number of waves overtopping.

1 at the sharp-crested weir to measure head to calculate the overtopping discharge.

The sampling interval for each test was chosen in order to create a test length equal to the repeat length of a given spectrum. This ensures statistical stability in the analysis.

For example:

If the repeat time for a given spectrum was 4 mins 57 secs, = 297 secs, the sampling period, Δt, was

$$\Delta t = \frac{297}{2048} = 0.145 \text{ secs}$$

The results from the overtopping tests are tabulated and illustrated graphically in the next chapter.

CHAPTER 9

WAVE OVERTOPPING TEST RESULTS

9.1 Introduction

Presented here are the results of over 100 wave overtopping tests carried out on two breakwater profiles with various crest elevations above still water level. The crest elevations used were all 'low'. ('Low' in this instance is used to signify close to or at mean water level). Previous model tests on such structures have not considered the combination of parameters used here.

Space precludes the full presentation of more than a few tests. The results are, however, fully tabulated. Unless otherwise stated, all the results shown are for a Pierson-Moskowitz spectrum with the wave absorption system 'in', Figure 9.1. A number of tests with the wave absorption 'out' and a different spectrum were performed for comparison and they will be discussed where appropriate.

9.2 Breakwaters

The two breakwater profiles used in the overtopping tests had a 1:1 seaward slope and a 1:2 seaward slope. Both breakwaters had a crest 0.90m above the channel bed, which was horizontal. No berms were considered. Crest elevations above still water level varied from 0.10m to 0.04m. The lower limit on crest elevation was the lowest possible crest elevation for which the weir and pump arrangement could cope with the overtopping discharge which resulted under the test conditions.

No attempt was made to test with a breakwater at anything but perpendicular wave attack. Owen (1982) suggested that the maximum overtopping discharge occurred with a wave attack of 15° to the perpendicular.

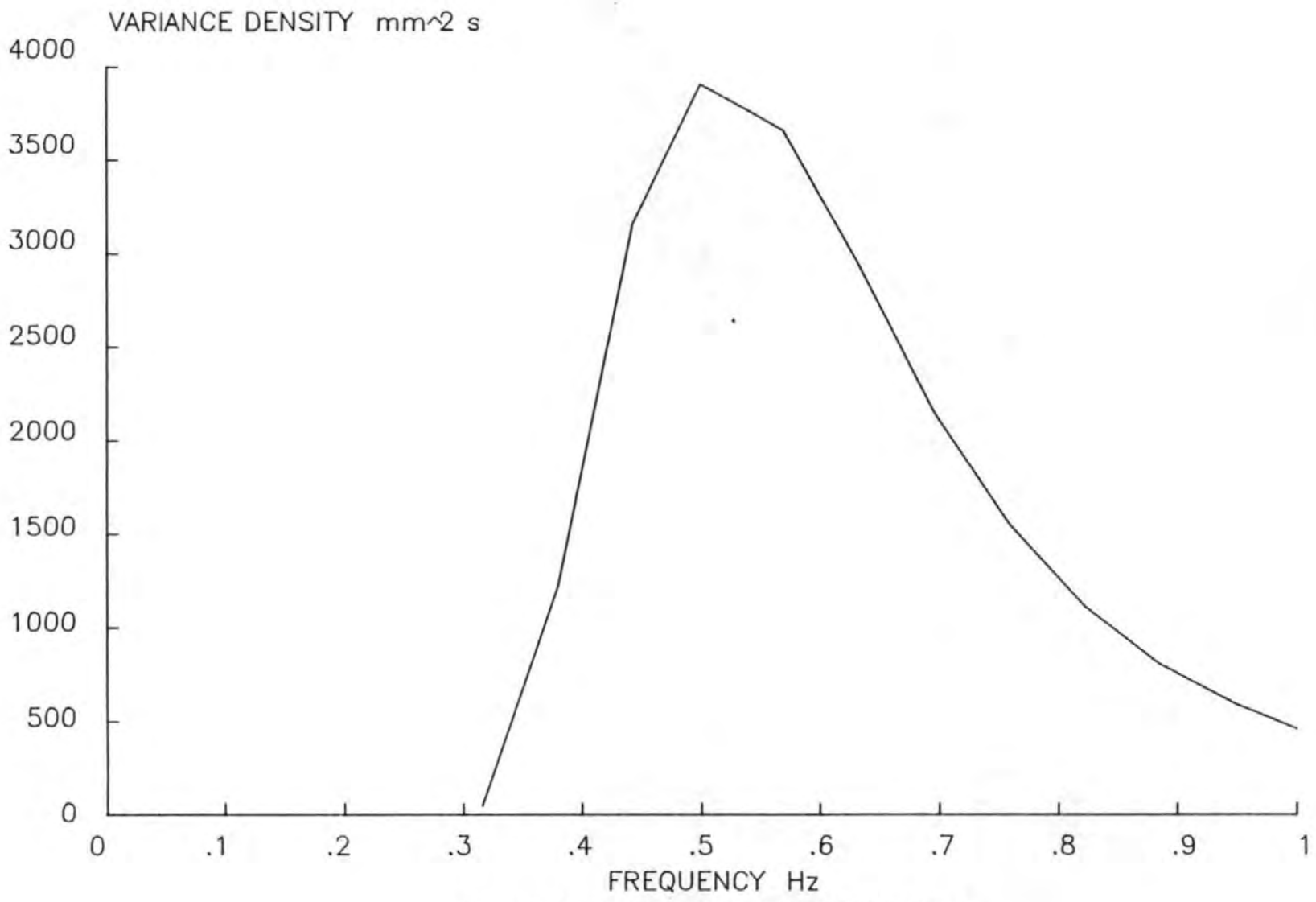

FIG 9.1 P–M SPECTRUM USED FOR OVERTOPPING TESTS

9.3 Results

9.3.1 Wave Spectra

Shown here are examples of the incident and reflected spectra calculated for each test (with the three gauge array) derived using the Frequency Response Function method described in Chapter 3. (Figures 9.2 - 9.5). Figures 9.2 and 9.3 are with the 1:1 slope and Figures 9.4 and 9.5 are the 1:2 slope.

A comparison of all the spectra calculated in a single test overlain is given in Figure 9.6. The X-Spectrum and Y-Spectrum on Figure 9.6 are the so called 'point' spectra measured at the two discrete locations in the channel. Figure 9.6 indicates that the peak frequency of the incident spectrum is higher than that of any of the 'point' spectra. This may be due to the effects of the reflected waves on the 'point' spectra and the possibility that the gauges may be located at nodes or antinodes from the reflection patterns.

Figure 9.7 is a plot of the Incident Spectra from both the 1:1 and 1:2 slopes together with the theoretical spectrum. It can be seen that the 1:2 slope result especially gives an incident spectrum very similar to the theoretical. The result from the 1:1 slope is not as good but the similarity is clear. The difference in peak energy is of the order of 10% for the 1:1 slope and 5% for the 1:2 slope. The peak frequency shift noted above is also evident here. A slight loss of high frequency components is also noticeable. The loss may be due to either the resolution of the Frequency Response Method, or the inability of the wave paddle and/or absorption system to react as accurately in the higher frequency range. A decrease in the performance of the wave gauges is another source of potential variation.

Figure 9.8 shows the increase in reflected energy with the 1:1 slope breakwater (see next section). The implication of similar incident spectra with different degrees of reflection will be discussed in Section 9.4.

INCIDENT SPECTRUM
15/4/87 TEST 4

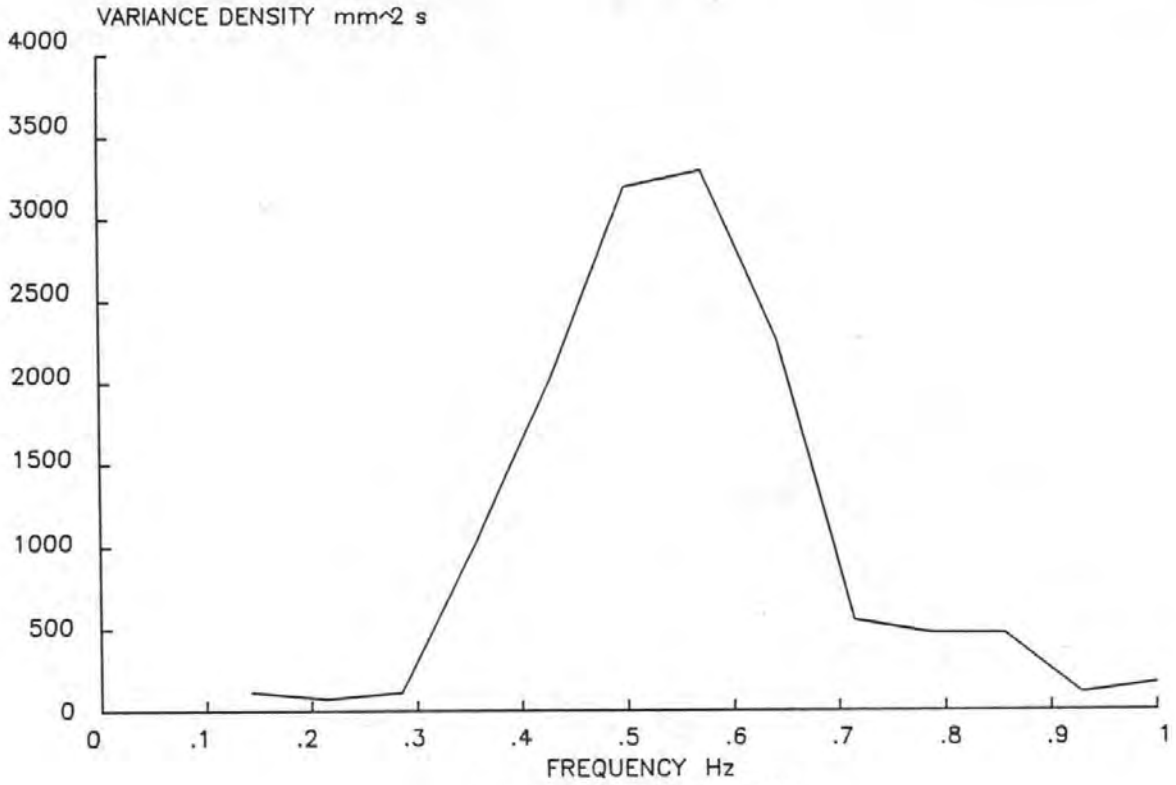

FIG 9.2 INCIDENT SPECTRUM 1:1 SLOPE

REFLECTED SPECTRUM
15/4/87 TEST 4

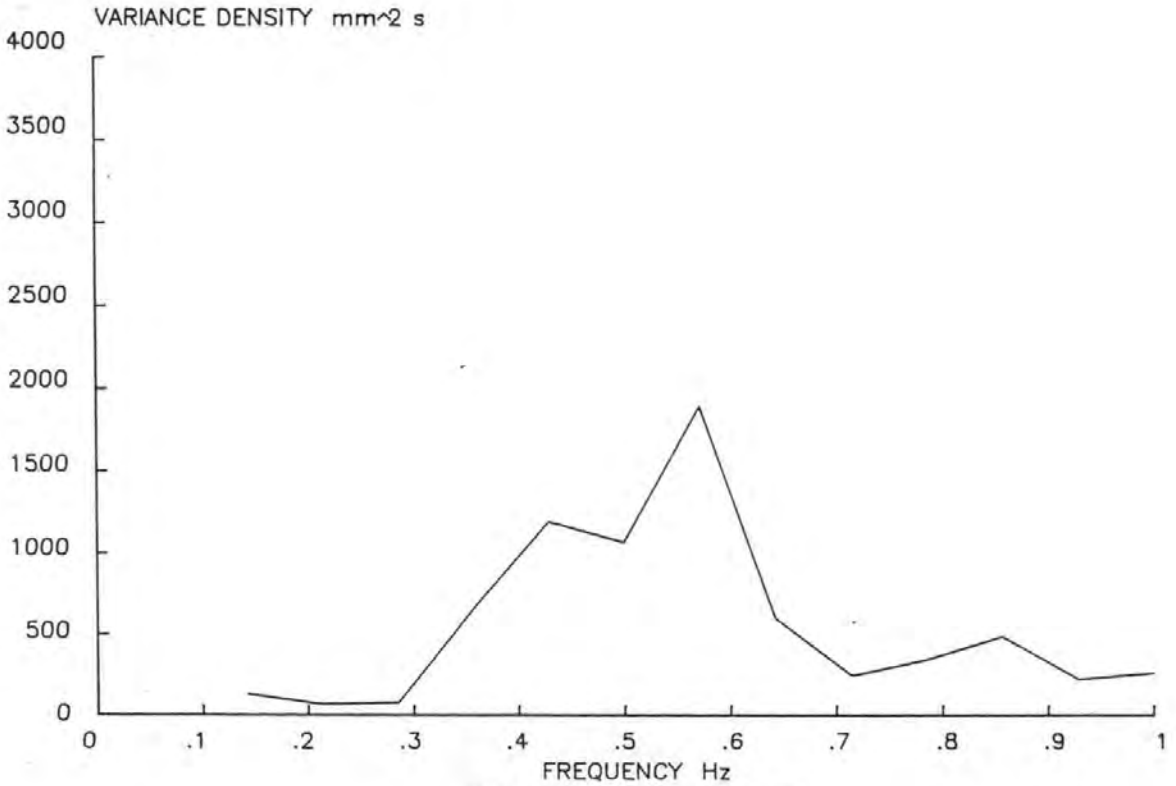

FIG 9.3 REFLECTED SPECTRUM 1:1 SLOPE

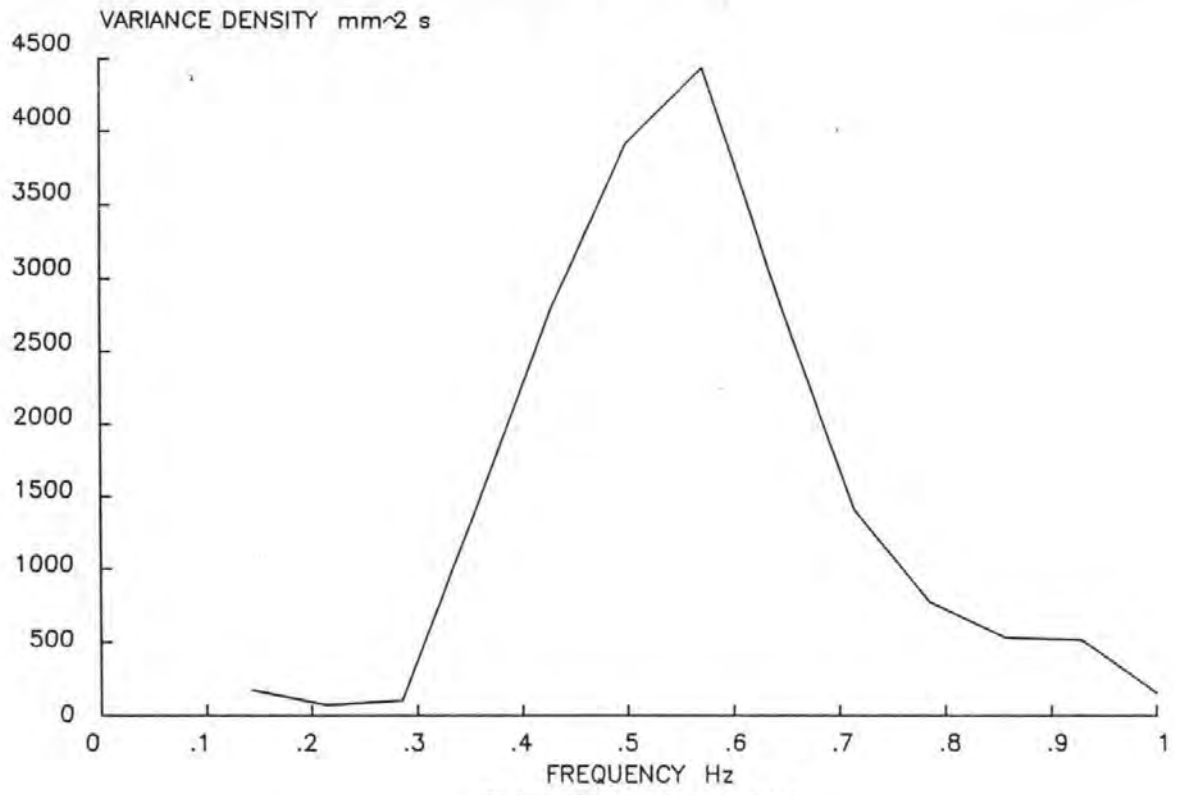

FIG 9.4 INCIDENT SPECTRUM 1:2 SLOPE

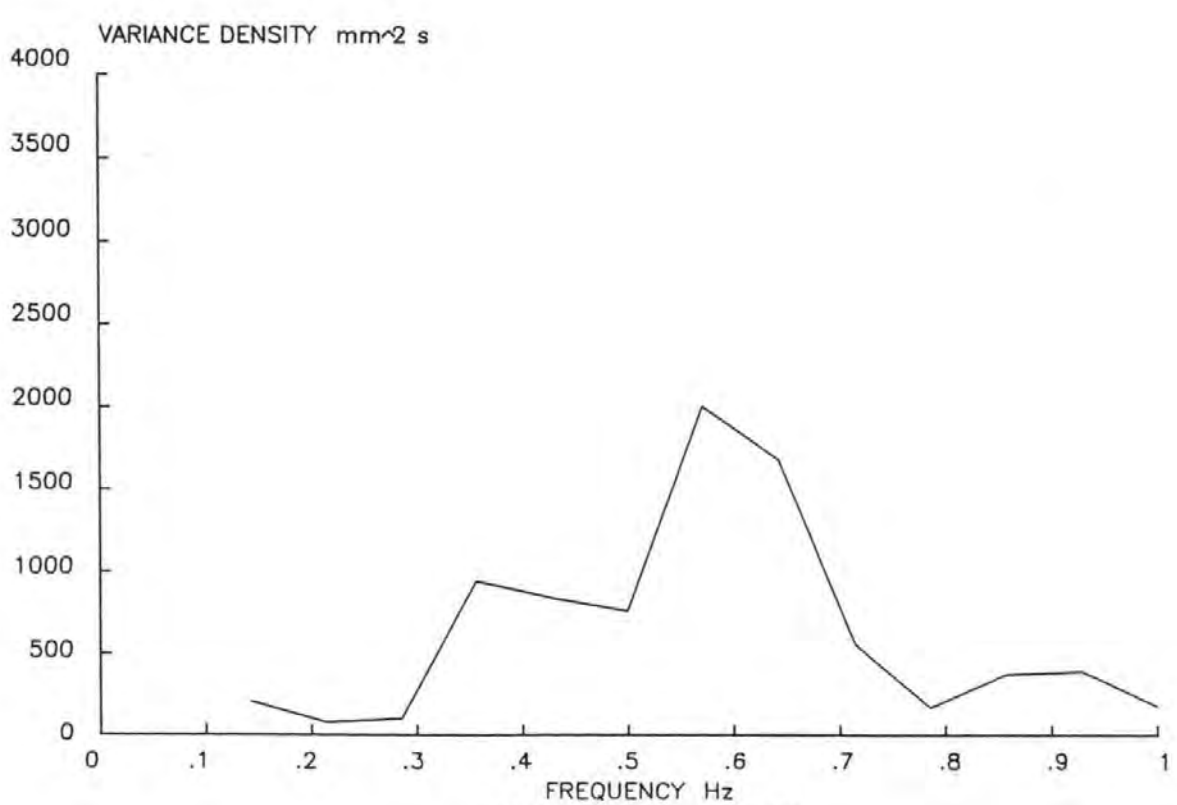

FIG 9.5 REFLECTED SPECTRA 1:2 SLOPE

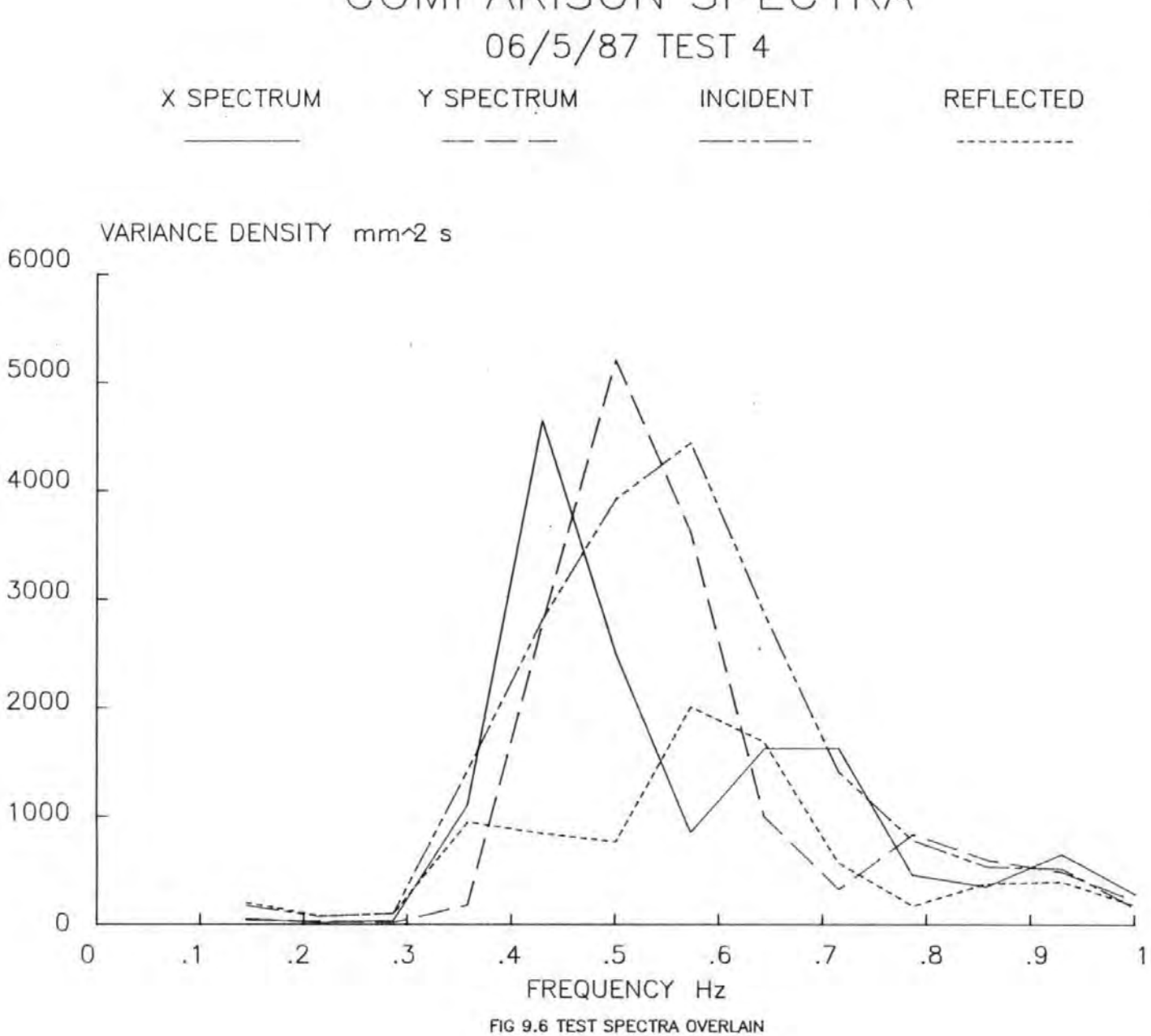

FIG 9.6 TEST SPECTRA OVERLAIN

INCIDENT SPECTRA

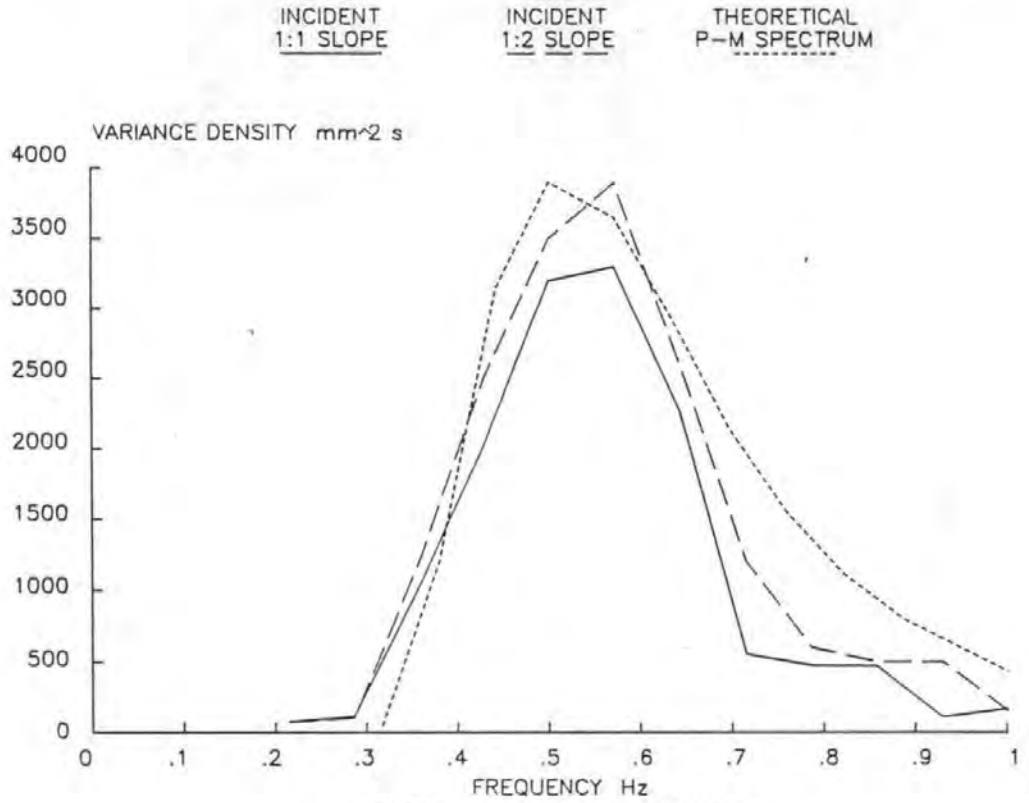

FIG 9.7 A COMPARISON OF THE INCIDENT SPECTRA

REFLECTED SPECTRA

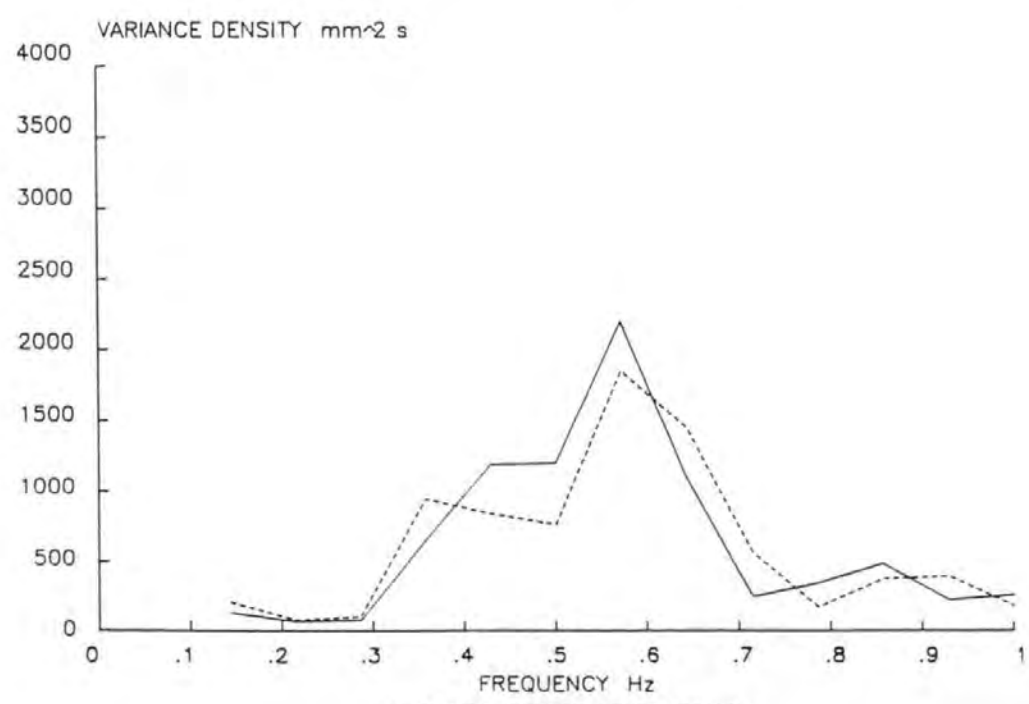

FIG 9.8 A COMPARISON OF REFLECTED SPECTRA

To investigate the influence of the spectral shape on the overtopping discharge a small number of tests were performed with a Newman spectrum with the same signifiant wave height as the Pierson-Moskowitz spectrum shown in Figure 9.1. The peak energy level of the Newman spectrum was 30% greater than the Pierson-Moskowitz spectrum. The incident and reflected spectra from such a test are illustrated in Figure 9.9 and 9.10 respectively.

The Newman spectrum compared to the theoretical Newman is given in Figure 9.11. Again the shape and scale are very similar, with again a similar loss of the higher frequency energy to the Pierson-Moskowitz spectra.

The effect of the different spectral shape on the overtopping discharge is discussed in Section 9.3.4.

9.3.2 Wave Reflections

From the data obtained on the incident and reflected spectra calculated above, it is possible to determine the reflection coefficient, ρ, defined as:

$$\rho^2(f) = S_{rr}/S_{ii} \qquad (9.1)$$

where S_{ii} and S_{rr} are the incident and reflected spectral estimates at frequency f respectively.

The Shore Protection Manual gives estimates of wave reflections from breakwaters defined in terms of a surf similarity parameter, Σ, given as:

$$\Sigma = \frac{1}{\text{Cot } \theta \sqrt{H_{si}/L_o}} \qquad (9.2)$$

where θ is the slope of the breakwater structure under consideration, H_{si} is the incident significant wave height and L_o the deep water wavelength defined as:

$$L_o = gT^2/2\pi \qquad (9.3)$$

INCIDENT SPECTRUM
13/5/87 TEST 1

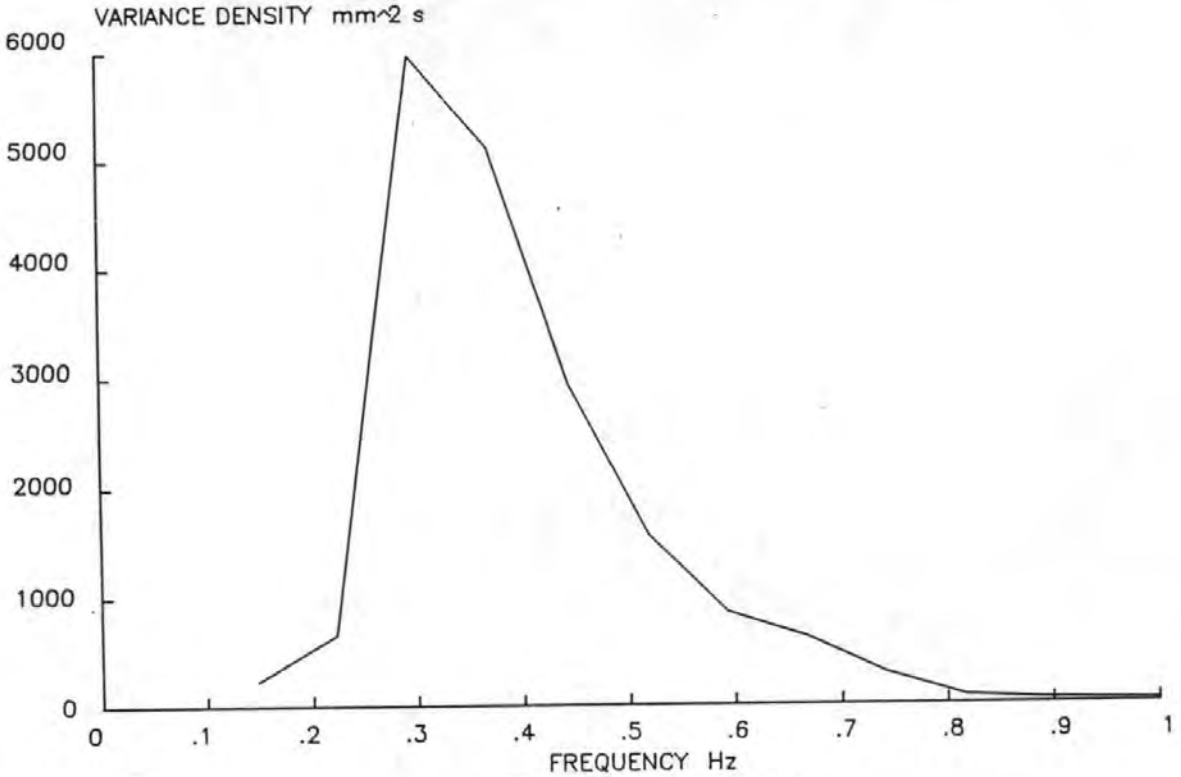

FIG 9.9 INCIDENT NEWMAN SPECTRUM

REFLECTED SPECTRUM
13/5/87 TEST 1

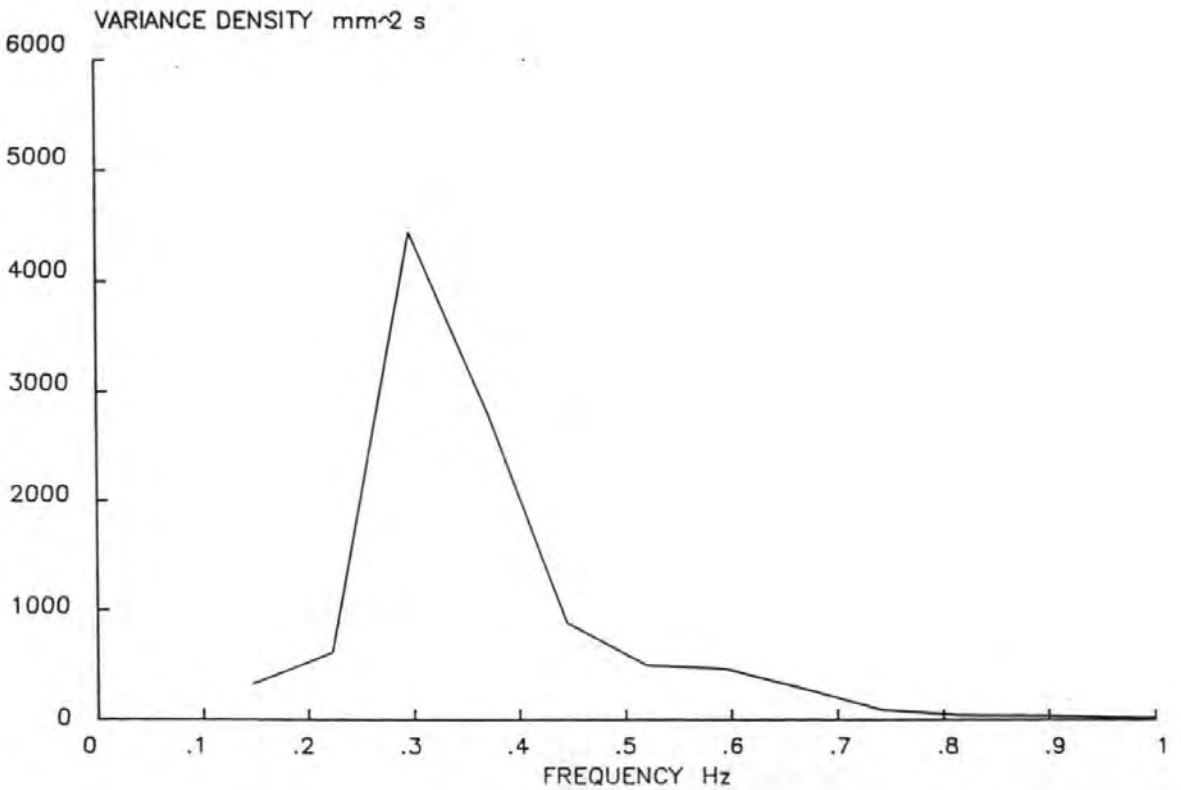

FIG 9.10 REFLECTED NEWMAN SPECTRUM

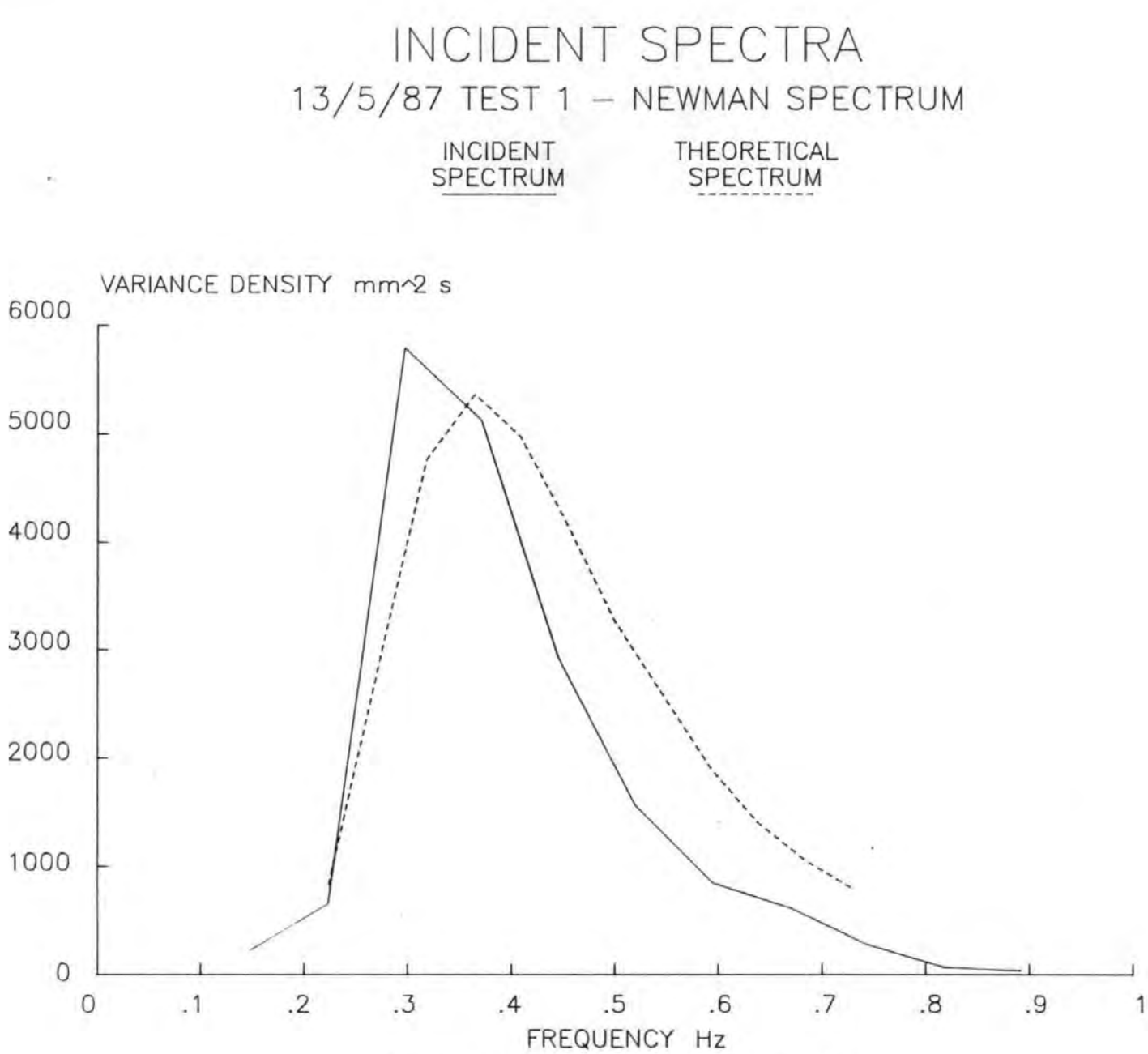

FIG 9.11 A COMPARISON OF NEWMAN SPECTRA 1:2 SLOPE

For each test the reflection coefficient has been calculated with the two methods described above (i.e. surf similarity and Incident/Reflected) at the peak frequency and a comparison shown in Tables 9.1 and 9.2.

The results agree very well in all cases, with approximately 85% reflection from the 1:1 slope and 60% from the 1:2 slope.

The results from the Frequency Response analysis were also used to plot Frequency vs Reflection Coefficient graphs over the whole frequency range of interest.

Examples of these graphs are shown in Figures 9.12 and 9.13. It can be seen that in both cases (1:1 and 1:2 slope) the reflection coefficient varies over the frequency range of interest (0-1Hz). The minimum reflection being at around 0.6Hz. Towards either end of the scale the reflection increases. At the low frequency shown there is very little difference in the degrees of reflection from either breakwater slope (approx 90%).

The shape of the reflection coefficient graphs obtained compared well with the results obtained earlier during the optimisation of the wave absorption system (Chapter 7).

When wave absorption is 'out' the degree of reflection and the calculation of reflection coefficient is complicated by the presence of re-reflected (and higher order) waves. In most of these cases the values of reflection coefficient calculated from the Frequency Response Method do not correspond well to the values predicted by the Shore Protection Manual. (The tests with wave absorption 'out' are marked * in tables 9.1 and 9.2).

This inaccuracy is probably due to the H_{si} not being a correct incident significant wave height with wave absorption 'out' due to the presence of re-reflections in the direction of wave propagation. H_{si} in each case is calculated from Equation 3.15.

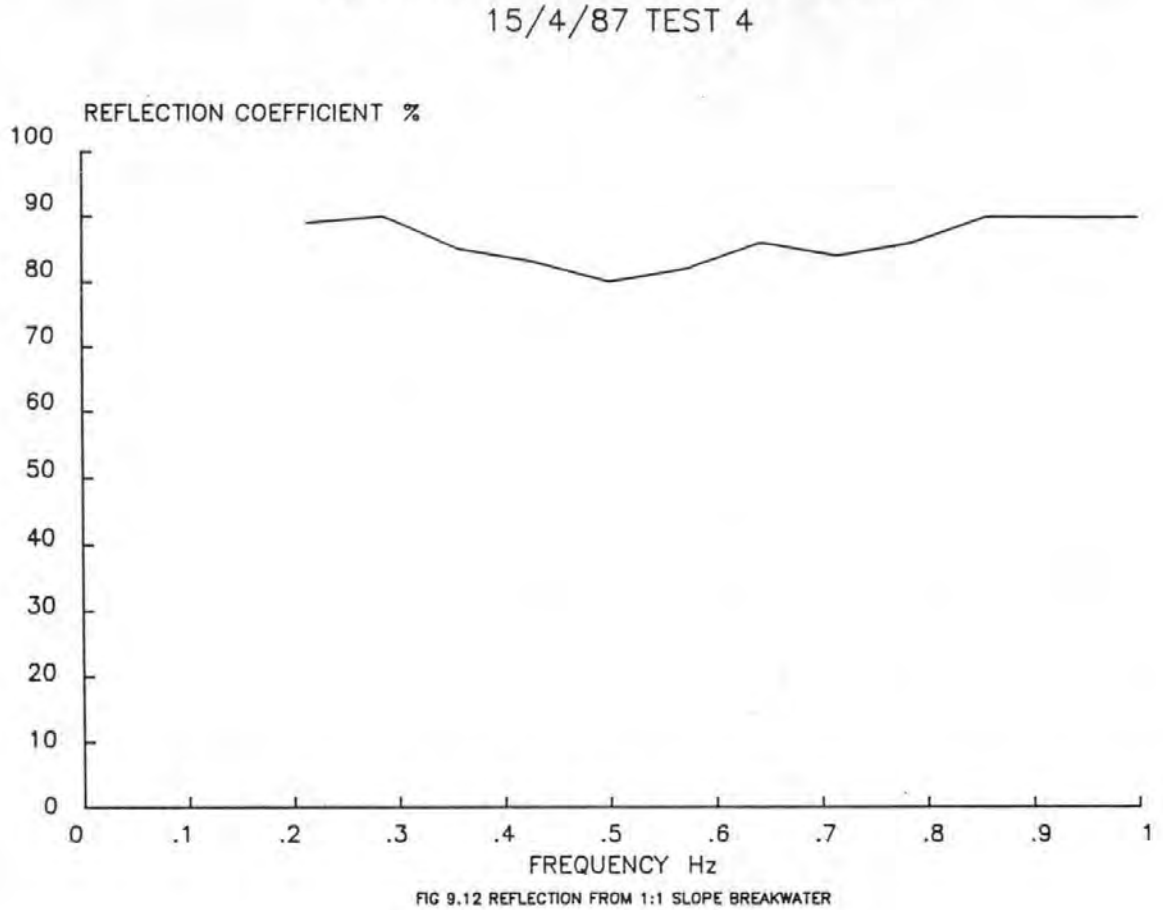

FIG 9.12 REFLECTION FROM 1:1 SLOPE BREAKWATER

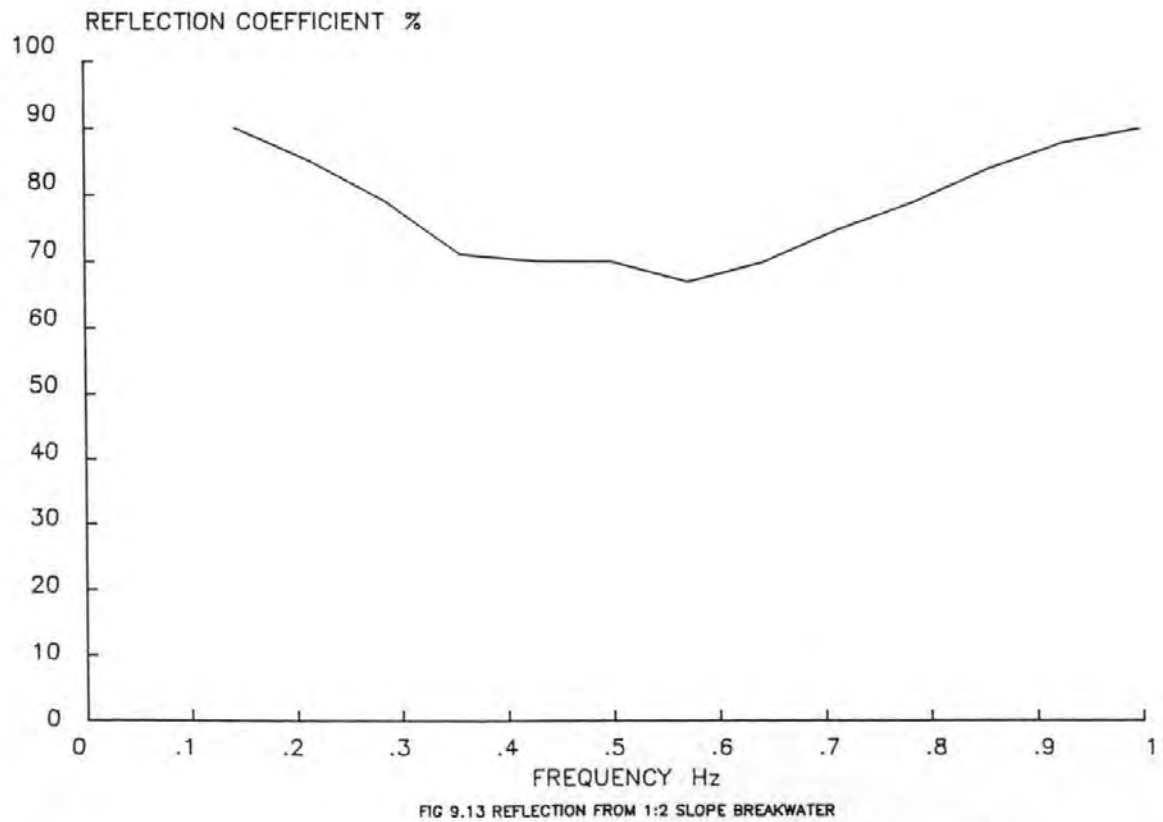

FIG 9.13 REFLECTION FROM 1:2 SLOPE BREAKWATER

In every case of wave absorption 'out' the Shore Protection Manual method with the surf Similarity parameter under-estimates the degree of reflection compared to the values calculated from the Frequency Response Analysis.

The values of the reflection coefficients from the surf similarity parameter in the tables below are calculated from the graph published in the Shore Protection Manual

Test No.	$\bar{H}_{si}$	T_z	L_o	ξ	ρ (graph) %	ρ (Frequency Response) %
1	.184	1.34	2.80	4.64	80	81
2	.150	1.37	2.90	4.42	79	81
3	.150	1.47	3.37	4.74	81	80
4	.170	1.36	2.89	4.12	76	92
5	.160	1.30	2.64	4.86	75	85
6	.090	1.38	2.97	5.74	88	85
7	.090	1.36	2.89	5.67	86	82
8	.090	1.50	3.51	6.24	89	91
9	.100	1.32	2.72	5.22	85	87
10	.100	1.44	3.24	5.69	86	88
11	.100	1.33	2.76	5.25	85	88
12	.100	1.41	3.10	5.57	86	87
13	.090	1.34	2.80	5.58	86	87
14	.100	1.37	2.93	5.41	85	88
15	.090	1.39	3.02	5.79	87	90
16	.090	1.36	2.89	5.67	86	93
17	.100	1.35	2.85	5.34	85	88
18	.100	1.41	3.10	5.57	83	85
19	.099	1.34	2.80	5.32	82	84
20	.096	1.38	2.97	5.56	81	85
21	.098	1.33	2.76	5.47	81	85
22	.099	1.38	2.97	5.48	82	85
23	.098	1.38	2.97	5.51	83	85
24	.098	1.38	2.97	5.51	83	85
25	.099	1.33	2.76	5.28	80	84
26	.104	1.44	3.24	5.58	86	81
27	.099	1.31	2.68	5.20	85	80
28	.103	1.43	3.19	5.57	86	81
29	.099	1.34	2.80	5.32	85	84
30	.099	1.34	2.80	5.32	85	84
31	.099	1.37	2.93	5.44	85	83
32	.097	1.36	2.89	5.46	85	83
33	.096	1.34	2.80	5.40	85	81
34	.061	1.40	3.06	2.25	47	65
35	.099	1.46	3.33	1.83	35	70
36	.123	1.16	2.10	4.13	75	44
37	.120	1.22	2.32	4.40	78	56
38	.088	1.12	1.96	4.72	80	46
39	.142	1.23	2.36	4.08	75	43
40	.104	1.99	6.18	7.71	90	80
41	.070	1.99	6.18	9.34	95	74

Table 9.1 Reflection Coefficient values for 1:1 Slope

Test No.	$\bar{H}_{si}$	T_z	L_o	Σ	ρ (graph) %	ρ (Frequency Response) %
1	.140	1.72	4.62	2.80	60	69
2	.130	1.64	4.20	2.77	58	68
3	.128	1.75	4.78	2.98	65	66
4	.128	1.67	4.35	2.84	59	58
5	.120	1.56	3.80	2.74	57	64
6	.123	1.62	4.10	2.82	61	67
7	.073	1.53	3.65	3.45	70	63
8	.049	1.34	2.80	3.69	72	75
9	.138	1.65	4.27	2.71	58	62
10	.140	1.67	4.36	2.72	58	66
11	.136	1.60	4.61	2.65	57	63
12	.134	1.65	4.27	2.75	59	65
13	.138	1.70	4.51	2.79	60	62
14	.136	1.64	4.20	2.71	58	65
15	.070	1.50	3.51	3.45	71	70
16	.055	1.39	3.02	3.61	72	73
17	.137	1.72	4.62	2.83	59	68
18	.135	1.66	4.30	2.75	59	66
19	.134	1.56	3.80	2.60	55	58
20	.134	1.64	4.20	2.73	58	59
21	.133	2.73	4.67	2.89	62	58
22	.141	1.60	4.00	2.60	55	60
23	.086	1.59	3.95	3.31	68	69
24	.055	1.40	3.06	3.64	70	72
25*	.123	1.30	2.64	2.26	45	53
26*	.123	1.35	2.85	2.35	48	61
27*	.073	1.22	2.32	2.75	58	69
28*	.066	1.30	2.64	3.08	64	72
29	.105	1.99	6.18	3.74	74	71
30	.014	1.99	6.18	3.74	74	72
31*	.124	2.08	6.75	3.60	71	64
32	.130	2.11	6.95	3.57	71	75

Table 9.2 Reflection Coefficient Values for 1:2 Slope

9.3.3 Wave Records

Included here are some examples of the wave records measured during the overtopping tests (Figures 9.15 to 9.18). A comparison of the trace collected from the gauge placed over the toe of the breakwater (gauge 3) with the traces from the two gauges placed offshore shows how localised the effects of overtopping and reflections are, on the composite wave train.

Tables 9.3 and 9.4 detail a comparison of some of the relevant parameters calculated at each gauge location. Figure 9.14 shows the location of the wave gauges in the channel for the P-M spectrum and the 1:2 breakwater slope.

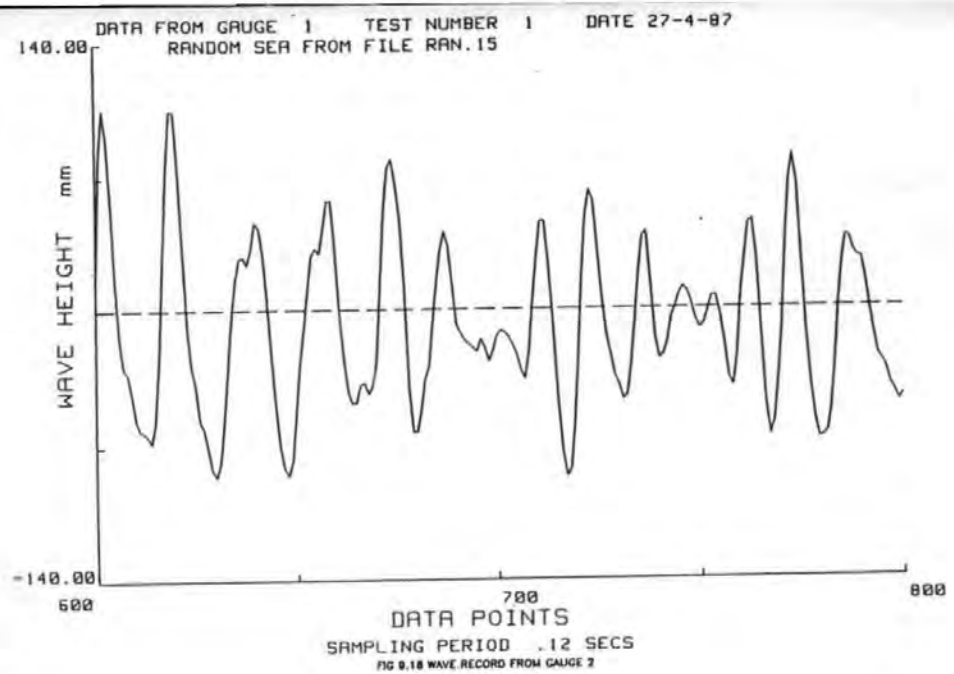

FIG 9.16 WAVE RECORD FROM GAUGE 2

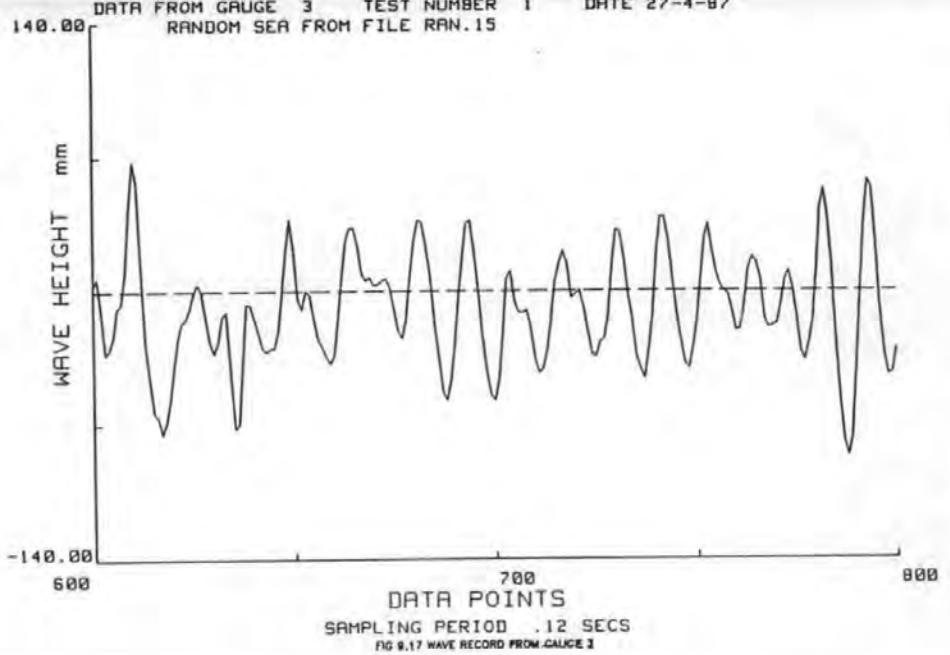

FIG 9.17 WAVE RECORD FROM GAUGE 3

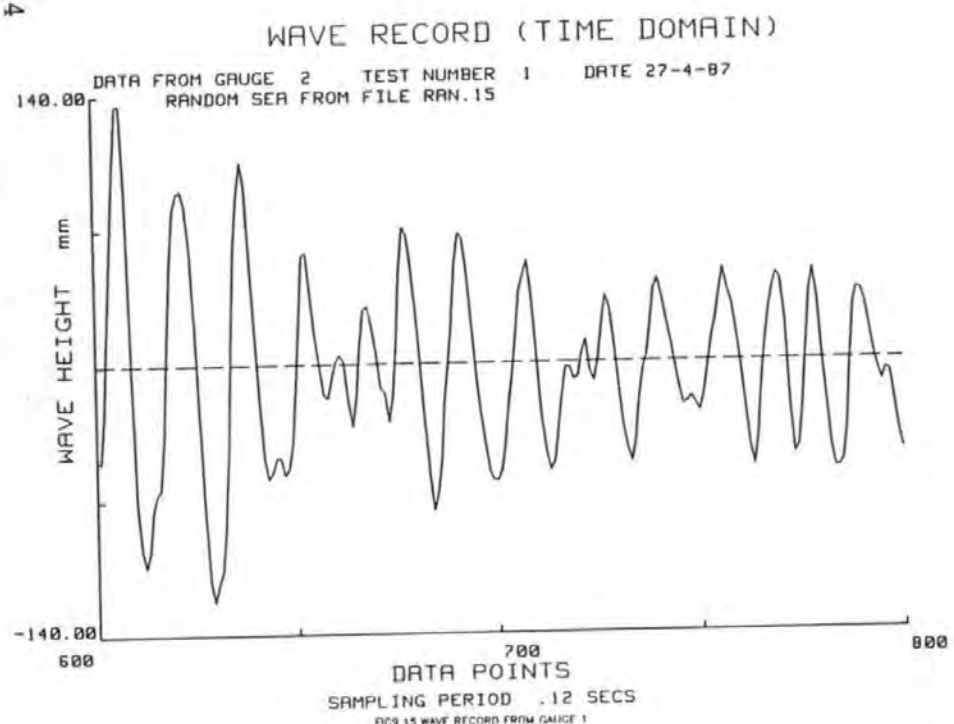

FIG 9.15 WAVE RECORD FROM GAUGE 1

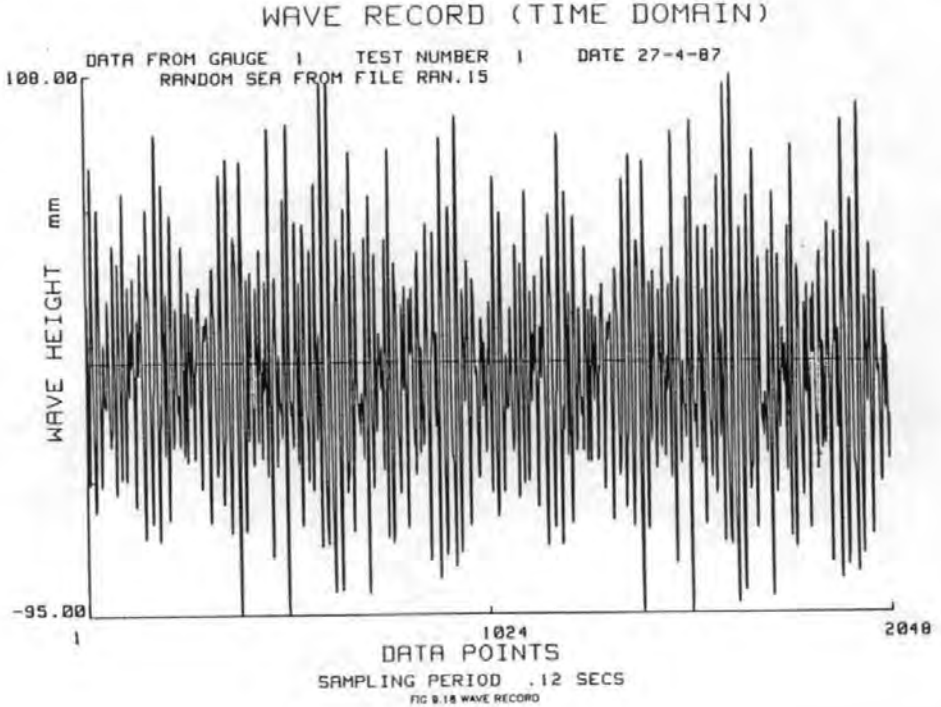

FIG 9.18 WAVE RECORD

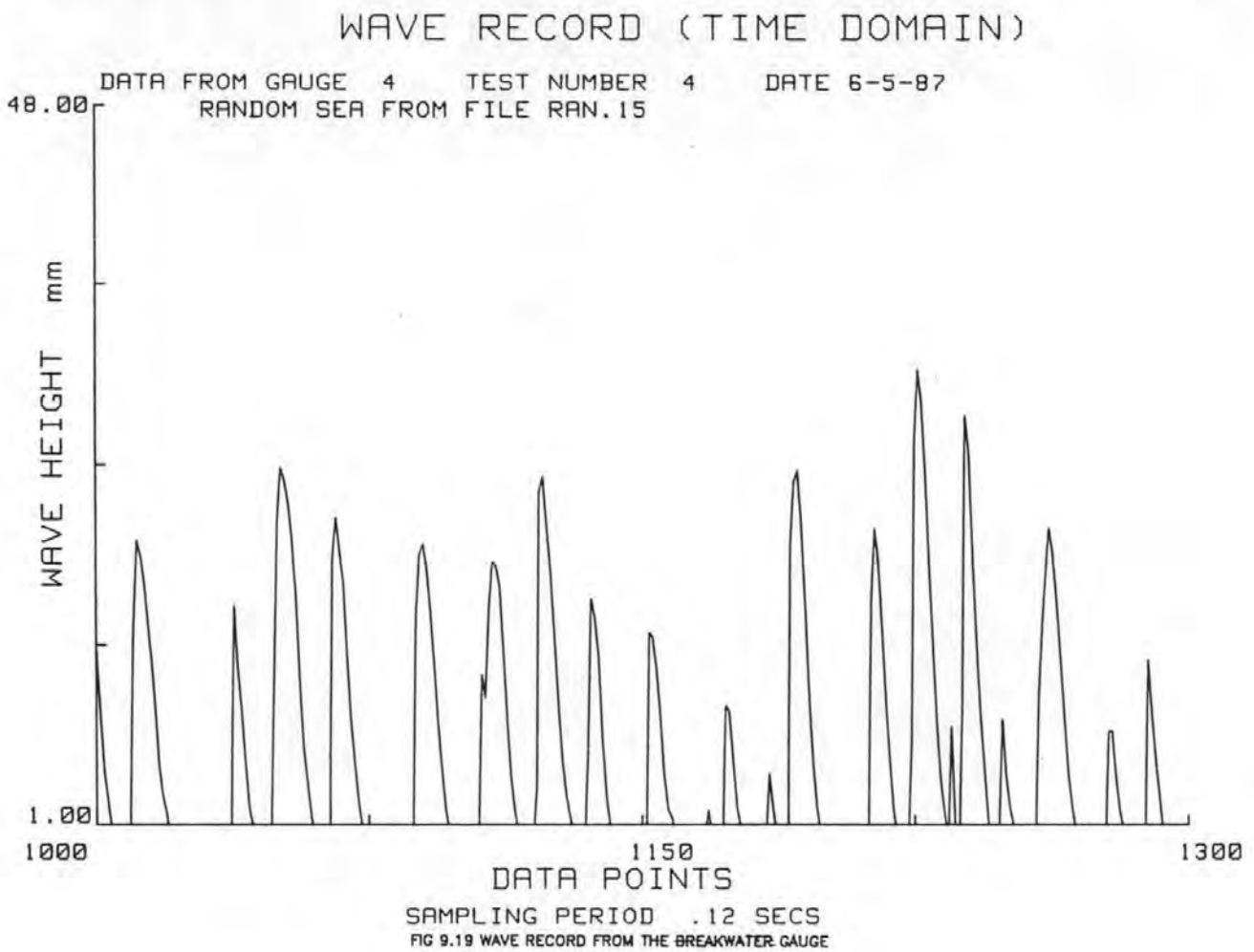

FIG 9.19 WAVE RECORD FROM THE BREAKWATER GAUGE

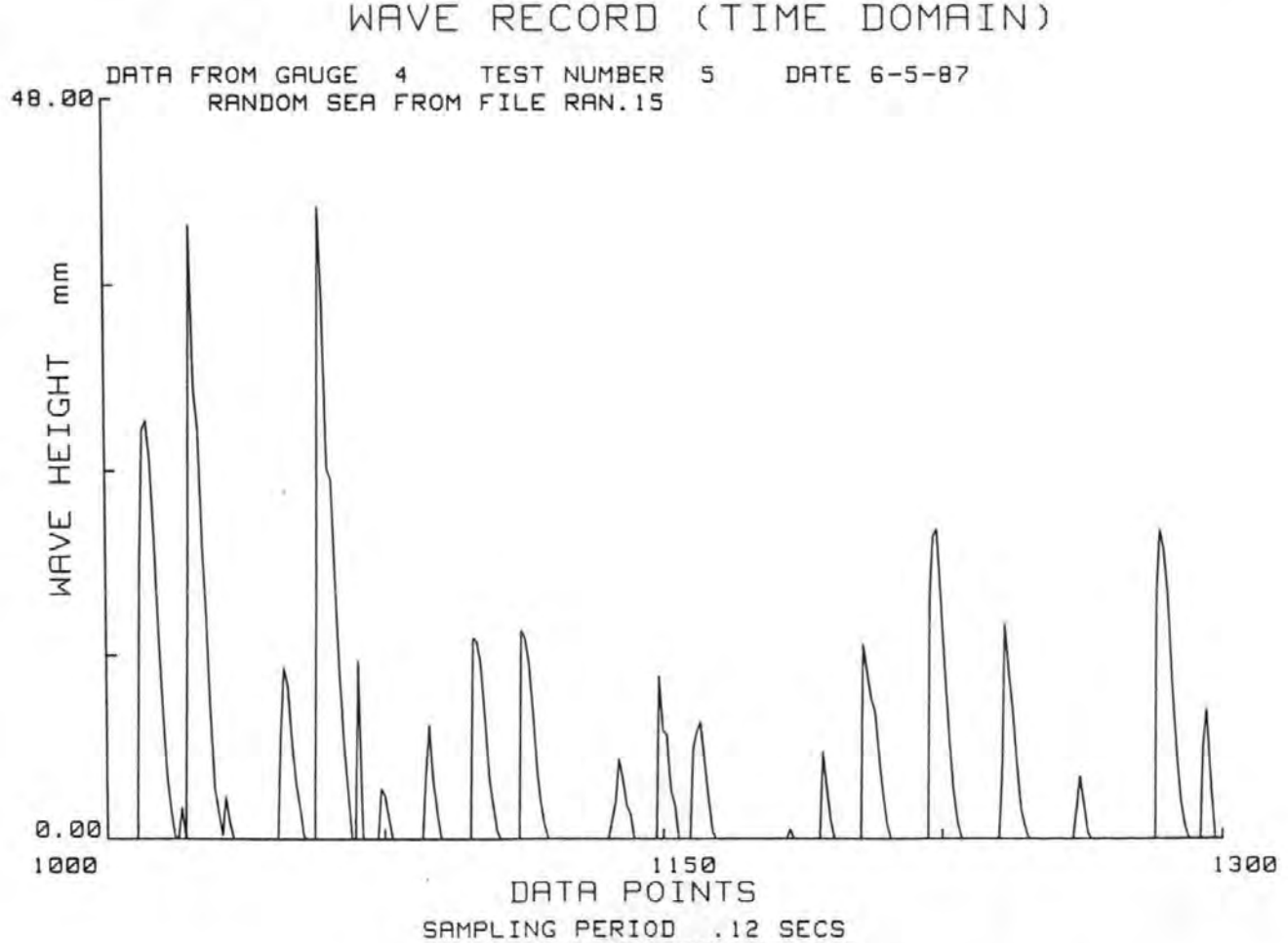

FIG 9.20 WAVE RECORD FROM THE BREAKWATER GAUGE

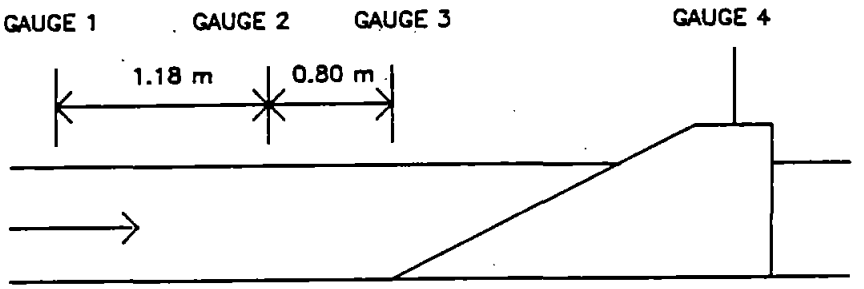

Figure 9.14 Location of Wave Gauges

On the 1:1 slope breakwater, table 9.3 shows that the significant wave height, $\bar{H}_s$, measured in the time domain, over the toe of the breakwater is considerably less than the significant wave height offshore. The zero-crossing period decreases as the waves approach the breakwater. It is likely that this phenomenon is due to the pattern of nodes and anti-nodes formed by reflection from the breakwater. The same large decrease is not apparent in the tabulated results from the 1:2 slope probably due to the decrease in reflection from this shallower slope.

The calculation of $\bar{H}_s$ from spectral moments (Chapter 3) also exhibited this phenomenon.

The results from table 9.3 (1:1 slope) illustrate the problems involved in evaluating all the relevant parameters with confidence and consistency between workers. Owen (1980), for example, makes no mention of where the wave statistics were measured (or how). Thus a plot of the percentage of waves in a test overtopping could vary by as much as 20% depending upon whether the total number of waves in the test was measured offshore or at the breakwater toe. The dimensionless parameters, R^* and Q^* can be up to 25% different when using the results from either gauge 1 or gauge 3 (see table 9.5) (section 9.3.4).

All the calculations performed for the tests presented herein used the zero-crossing period measured over the breakwater toe. The other statistics such as significant wave height were derived from the estimates of incident and reflected spectra from the 3 gauge array.

In all the tests a time domain 'wave by wave' analysis of the wave records agrees within ± 2mm to the spectral estimate of significant wave height via a FFT and the use of spectral moments (see Chapter 3).

	Gauge 1			Gauge 2			Gauge 3		
Test No	$\bar{H}_s m$	$T_z s$	N	$\bar{H}_s m$	$T_z s$	N	$\bar{H}_s m$	$T_z s$	N
1	.129	1.605	155	.133	1.520	164	.093	1.376	181
2	.121	1.502	165	.136	1.669	149	.089	1.335	184
3	.116	1.664	149	.116	1.517	164	.089	1.502	166
4	.133	1.510	164	.132	1.590	155	.098	1.503	188
5	.132	1.562	159	.129	1.565	159	.098	1.443	173
6	.119	1.717	144	.131	1.462	169	.097	1.328	188
7	.136	1.668	149	.130	1.465	170	.098	1.411	176
8	.132	1.619	154	.125	1.500	166	.094	1.336	187
9	.132	1.634	152	.126	1.475	169	.096	1.365	182
10	.128	1.617	153	.126	1.486	168	.093	1.348	180
11	.134	1.672	148	.129	1.516	164	.093	1.361	183
12	.128	1.590	156	.124	1.499	166	.097	1.348	185
13*	.193	1.601	154	.201	1.559	160	.133	1.338	186
14*	.194	1.713	145	.203	1.531	162	.149	1.465	181
15*	.195	1.677	148	.202	1.488	167	.149	1.465	170
16*	.192	1.543	162	.200	1.411	177	.166	1.363	182
17*	.210	1.709	145	.219	1.661	150	.158	1.298	192

Table 9.3 Wave Statistics from 3 Wave Gauges, 1:1 Slope.

	Gauge 1			Gauge 2			Gauge 3		
Test No	$\bar{H}_s m$	$T_z s$	N	$\bar{H}_s m$	$T_z s$	N	$\bar{H}_s m$	$T_z s$	N
1	.146	1.717	144	.099	1.392	178	.140	1.717	145
2	.116	1.555	160	.122	1.696	146	.130	1.642	152
3	.115	1.583	157	.109	1.650	151	.128	1.753	142
4	.113	1.599	156	.126	1.800	138	.128	1.669	149
5	.112	1.517	162	.124	1.628	151	.120	1.557	159
6	.118	1.478	167	.122	1.665	148	.122	1.615	154
7	.074	1.477	168	.075	1.598	155	.073	1.527	163
8	.048	1.350	184	.051	1.480	168	.049	1.340	184
9	.133	1.570	159	.138	1.758	141	.138	1.654	151
10	.134	1.565	159	.130	1.722	144	.141	1.671	148
11	.140	1.488	167	.132	1.684	147	.136	1.602	154
12	.134	1.601	155	.132	1.695	147	.134	1.651	151
13	.131	1.502	165	.135	1.660	150	.138	1.704	146
14	.130	1.546	160	.133	1.615	154	.136	1.644	151
15	.081	1.417	170	.074	1.534	162	.070	1.499	166
16	.056	1.358	184	.056	1.445	172	.055	1.387	178

Table 9.4 Wave Statistics from 3 Wave Gauges, 1:2 slope

Test No	Gauge 1			Gauge 3		
	R^*	$Q^* \times 10^{-4}$	N%	R^*	$Q^* \times 10^{-4}$	N%
1	.01720	3.861	71.5	.02423	5.932	59.1
2	.01657	3.245	49.7	.02285	5.220	39.6
3	.01732	3.161	31.8	.02535	5.598	26.9
4	.01716	3.425	43.5	.02352	5.343	37.2
5	.01716	3.205	40.1	.02333	5.526	33.9
6	.07134	3.068	45.1	.02497	5.349	37.7
7	.01665	2.795	35.1	.02387	4.639	28.1

Table 9.5 A Comparison of the Dimensionless Parameters Calculated at the Breakwater Toe and 1.98m Offshore

In the tables above (9.3-9.5) the following notation was used:

H_s - significant wave height

T_z - zero up-crossing period

N - number of waves in record

N% - percentage of waves in record overtopping breakwater

* - test with wave absorption 'out'

ρ - reflection coefficient

9.3.4 Overtopping Discharge

For each test the overtopping discharge was measured with the sharp-crested weir as described in the previous chapter. The results from the tests are shown in Tables 9.6 and 9.7.

The relationship between overtopping discharge and breakwater crest elevation above still water has been plotted on Figures 9.21 - 9.22. The plots are of dimensionless discharge, Q^*, vs dimensionless freeboard, R^*, as defined in Chapter 7 and given again below for the sake of convenience:

$$R^* = \frac{R_c}{\bar{H}_s} \sqrt{\frac{S}{2\pi}} \qquad (9.4)$$

$$Q^* = \frac{Q}{\sqrt{g\bar{H}_s^3}} \sqrt{\frac{S}{2\pi}} \qquad (9.5)$$

DIMENSIONLESS OVERTOPPING

A COMPARISON WITH OWEN 1980

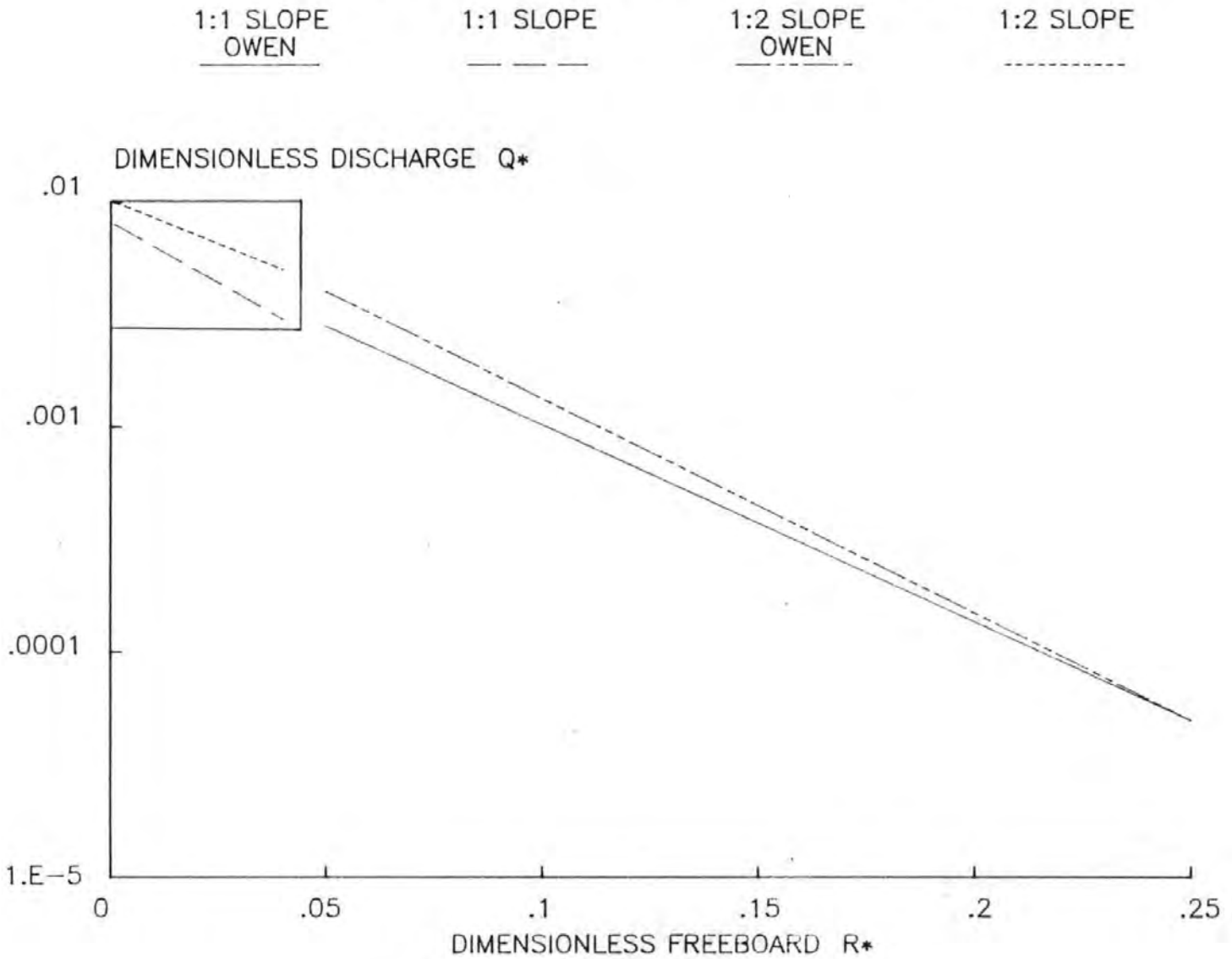

FIG 9.21 DIMENSIONLESS OVERTOPPING DISCHARGE

DIMENSIONLESS OVERTOPPING

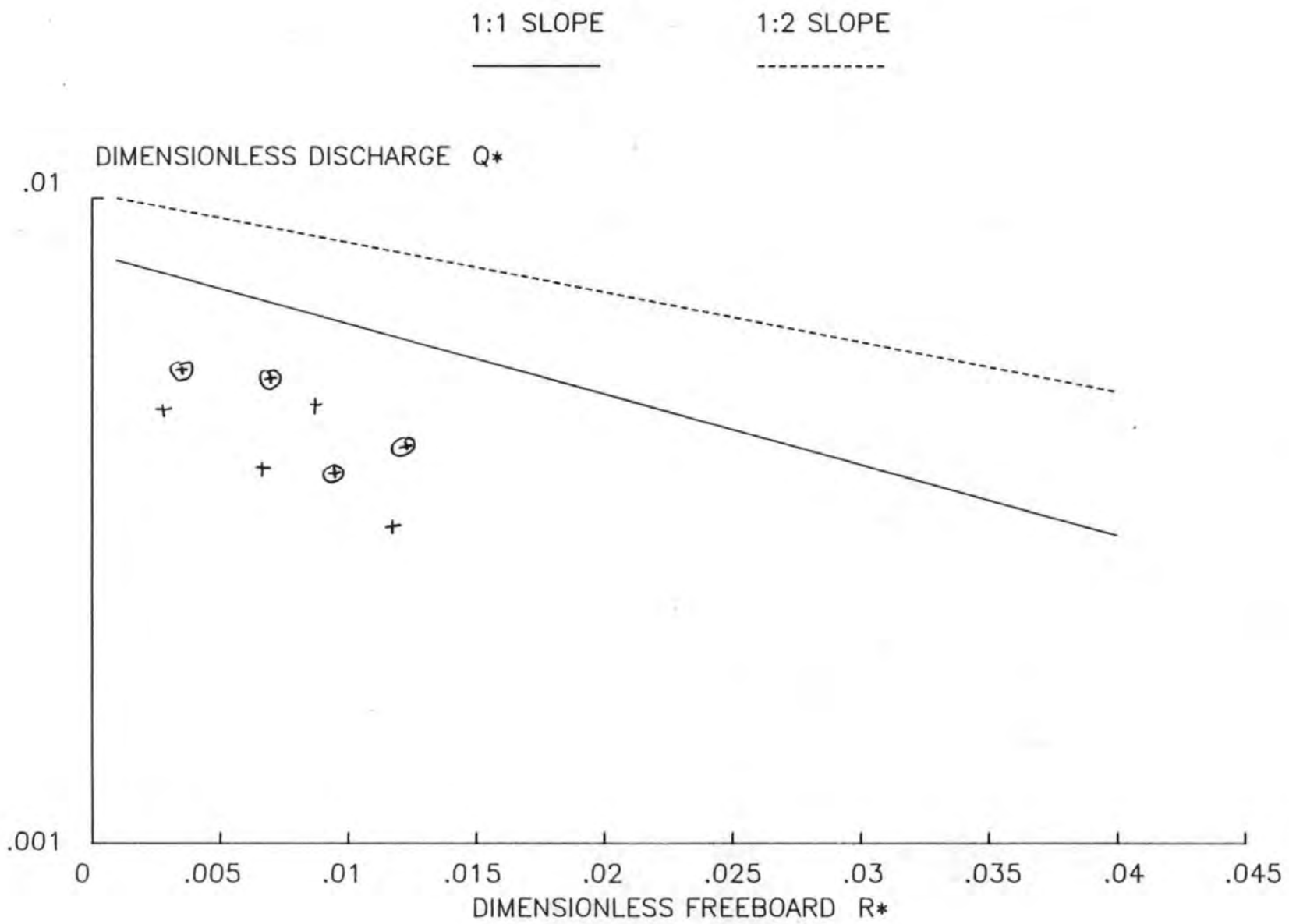

FIG 9.22 DIMENSIONLESS OVERTOPPING

where R_c is the crest elevation above still water level

$\bar{H}_s$ is the significant wave height

S is the wave steepness given by:

$$S = H_s/L_o \tag{9.6}$$

for $$L_o = gT_z^2/2\pi \tag{9.7}$$

The results show that provided the wave record is a 'full' spectrum rather than a part of a long sequence ('full' spectra and sequence lengths were fully described in an earlier chapter) the overtopping discharge measured, is the same, no matter what the wave pattern is. The above result holds true for both the 1:1 and 1:2 slope breakwaters, at all the crest elevations above still water level tested.

Examination of the results from a test where the sequence length was 'long' compared to the test length highlights the problem of defining accurately the test parameters. The calculated overtopping discharges from many tests with different portions of the same long sequence (also statistically the same spectra as when a full sequence was used) are quite variable. Thus, as would be expected, different parts of the sequence give different discharges. The results do, however, lie on the same, albeit in different parts, line.

This emphasises the importance of accurately defining the test parameters. To obtain 'statistically correct' results you should use full length sequences from the chosen spectrum.

Figures 9.19 and 9.20 are plots of the wave record measured with gauge 4, placed on the breakwater crest. The record shows the time and magnitude of the overtopping waves.

An estimation of the overtopping discharge, Q, was also made by calculating the flow over the crest volumetrically. Figure 9.20 shows a part of the wave overtopping record and a computer program was written to calculate the area of water contained within the record.

This was converted to a volume by assuming the wave crest was perpendicular to the breakwater over the whole width of breakwater. A comparision of the two methods of calculating the overtopping discharge for some of the tests is given in Table 9.8. The results agree favourably.

The volumetric method may be a possible technique for the measurement of full-scale overtopping discharges. The main assumption to be made is that the waves are strictly one-dimensional, thus the profile must be assumed to extend uniformly over the whole width of the breakwater. In a full-scale environment an array of wave gauges would be needed to more accurately measure the wave profile over the breakwater crest.

Test No.	Full or Partial Sequence (F/P)	$\bar{H}_s$ m	Q $m^3/s/m$	$Q^* \times 10^{-4}$	R^*
1	F	.130	.00401	9.166	.01958
2	F	.150	.00456	9.105	.01809
3	F	.150	.00431	8.029	.01689
4	F	.170	.00471	8.495	.01723
5	F	.160	.00556	11.003	.01350
6	F	.090	.00109	3.428	.02266
7	F	.090	.00964	3.240	.02359
8	F	.090	.0004	1.521	.02157
9	F	.100	.00015	2.566	.02312
10	F	.100	.00049	1.408	.02114
11	F	.100	.00148	4.286	.01431
12	F	.099	.00257	7.925	.01517
13	F	.096	.00289	8.875	.01491
14	F	.098	.00262	8.171	.01526
15	F	.099	.00287	8.550	.01467
16	F	.098	.00287	8.624	.01475
17	F	.098	.00293	8.830	.01478
18	F	.099	.00306	8.452	.01523
19	F	.104	.01550	42.031	.01096
20	F	.099	.02160	67.939	.01240
21	F	.013	.02460	68.159	.01114
22	F	.099	.02440	74.742	.01208
23	F	.099	.02610	79.890	.01207
24	F	.099	.02570	76.890	.01179
25	F	.097	.02560	79.033	.01205
26	F	.096	.02430	76.762	.01226
27	P	.061	.00249	11.857	.01842
28	P	.099	.00326	9.081	.01379
29	F	.123	.00651	18.558	.01565
30	F	.120	.00439	12.162	.01503
31	P	.088	.00597	24.818	.01924
32	P	.142	.00795	18.558	.01377

Table 9.6 Overtopping Discharge from 1:1 Slope Breakwater

Test No.	Full or Partial Sequence (F/P)	$\bar{H}_s$ m	Q $m^3/s/m$	$Q^* \times 10^{-4}$	R^*
1	F	.140	.00190	0.323	.01586
2	F	.130	.00092	1.156	.01721
3	F	.128	.00157	2.848	.01625
4	F	.128	.00120	2.290	.01706
5	F	.120	.00142	3.099	.01889
6	F	.123	.00143	2.921	.01799
7	P	.073	.00037	1.335	.02470
8	P	.049	.00002	.142	.03435
9	F	.138	.00158	2.822	.01037
10	F	.141	.00321	5.546	.01015
11	F	.136	.00334	6.240	.01078
12	F	.134	.00343	6.301	.01054
13	F	.138	.00342	5.908	.01006
14	F	.136	.00329	5.982	.01050
15	P	.070	.00078	3.027	.01606
16	P	.055	.00017	.879	.01958
17	F	.137	.00601	10.036	.00799
18	F	.135	.0520	9.418	.00834
19	F	.134	.00477	9.258	.00890
20	F	.134	.00481	8.901	.00849
21	F	.133	.00477	8.432	.00808
22	F	.141	.00472	8.491	.00846
23	P	.086	.00163	4.845	.01093
24	P	.055	.00042	2.271	.01551
25	F	.123	.00190	4.829	.01396
26	F	.123	.00177	4.324	.01344
27	P	.073	.00012	.5156	.01929
28	P	.066	.00002	.1044	.01908

Table 9.7 Overtopping Discharge from 1:2 Slope Breakwater

Q (weir) $m^3/s/m$	Q (volumetric) $m^3/s/m$
.006010	.006439
.005196	.007077
.004771	.005566
.004810	.004907
.004765	.004574
.004722	.004242
.00163	.001270
.000420	.000358
.00190	.00180
.001767	.002775
.000121	.000361
.000200	.000369
.005966	.005966
.004365	.004643

Table 9.8 A Comparison of Overtopping Discharge Measured over a Sharp-Crested Weir and Volumetrically over the Breakwater.

Figure 9.21 shows how the results compare with previous test data (Owen 1980). The inset box contains the results of the present study. The tests results inside the box are shown in full on Figure 9.22.

The results presented here compare well with Owen's test results and extend the validity of his discharge curves much closer to a crest elevation approaching still water level. The scatter of results from the present study is shown on Figure 9.22.

The results from the 1:2 slope breakwater are less scattered, perhaps due to the lower levels of reflections present.

As mentioned earlier, a number of tests were performed with a Newman spectrum with the same significant wave height as the Pierson-Moskowitz spectrum used for the majority of the tests.

Table 9.9 compares the overtopping discharge measured from the two different spectra at the same crest elevation.

Q (P-M) $m^3/s/m$	Q (Newman) $m^3/s/m$
0.00334	0.00436
0.00343	0.00597

Table 9.9 A Comparison of Overtopping Discharge from two different spectra

The Newman Spectrum produced approximately 30% greater overtopping discharge than the P-M spectrum. If the two spectra are compared (Figure 9.23) it is seen that the peak energy level of the Newman Spectrum is approximately 30% higher than the peak energy level of the P-M Spectrum, even though the significant wave heights are very similar.

From the limited tests performed with different spectra it could, perhaps, be suggested that the overtopping discharge is more accurately related to peak wave energy, rather than significant wave height. More tests would have to be conducted to verify this theory.

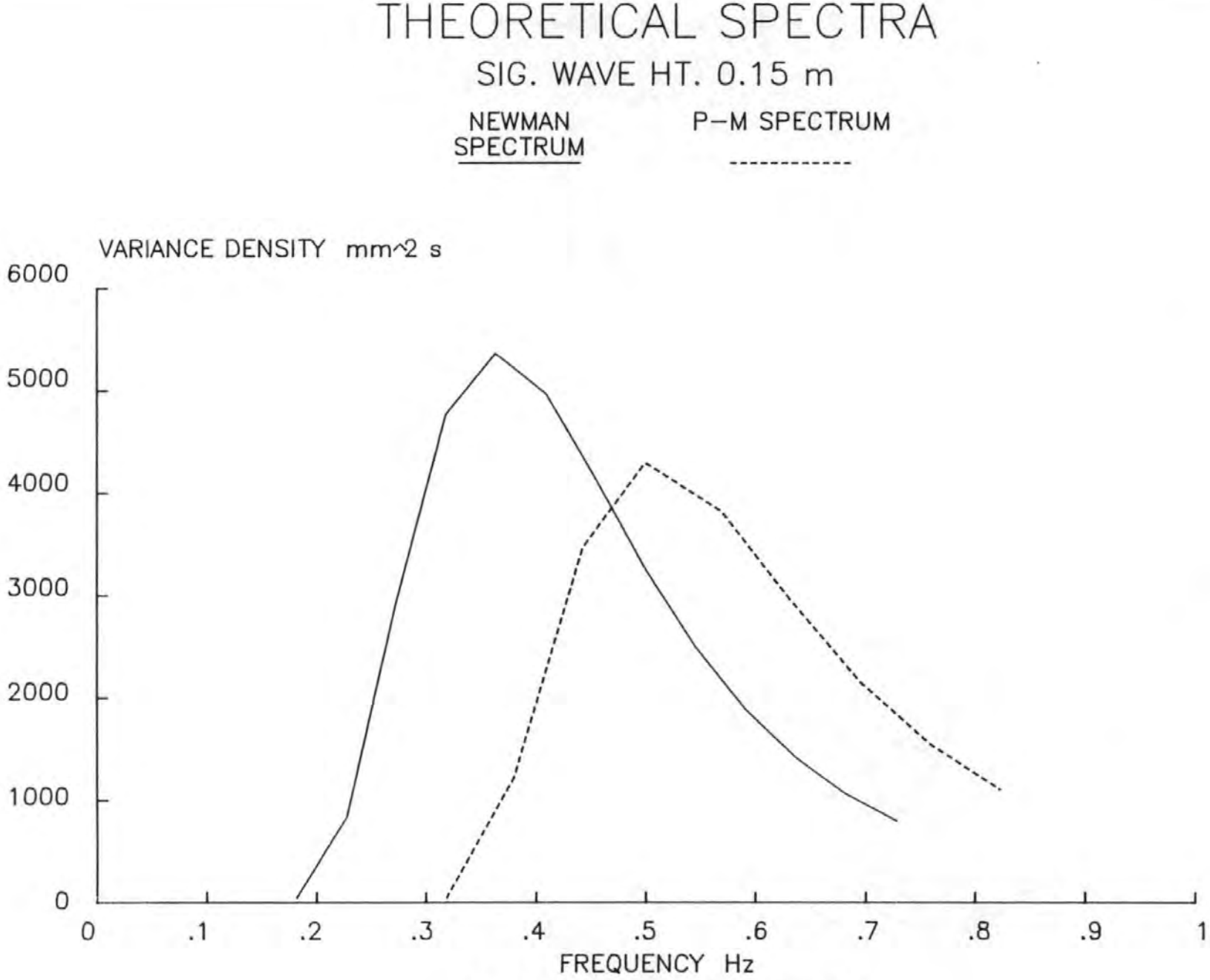

FIG 9.23 P–M SPECTRUM AND NEWMAN SPECTRUM

PERCENTAGE WAVES OVERTOPPING

A COMPARISON WITH OWEN 1980

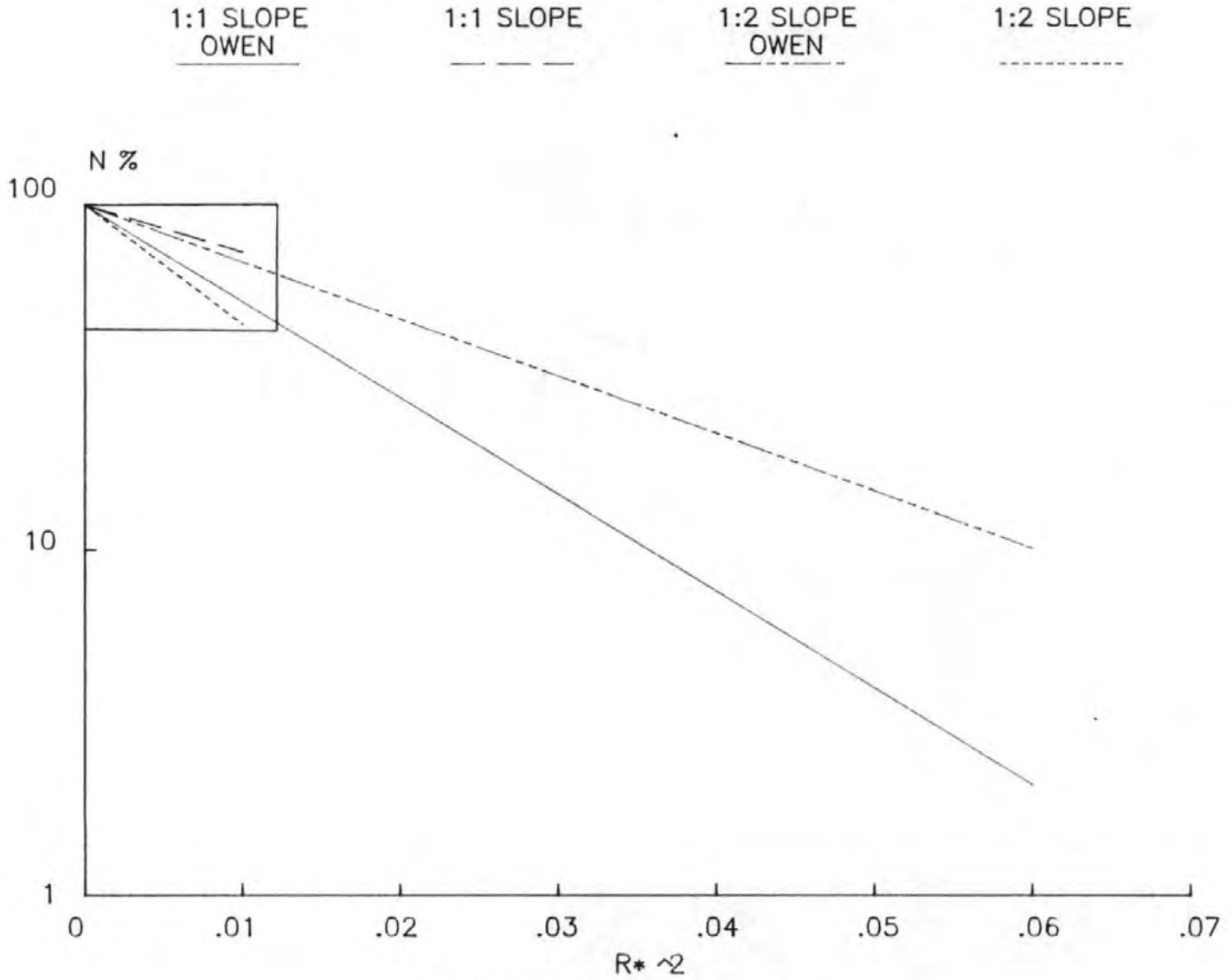

FIG 9.24 PERCENTAGE WAVES OVERTOPPING

PERCENTAGE WAVES OVERTOPPING

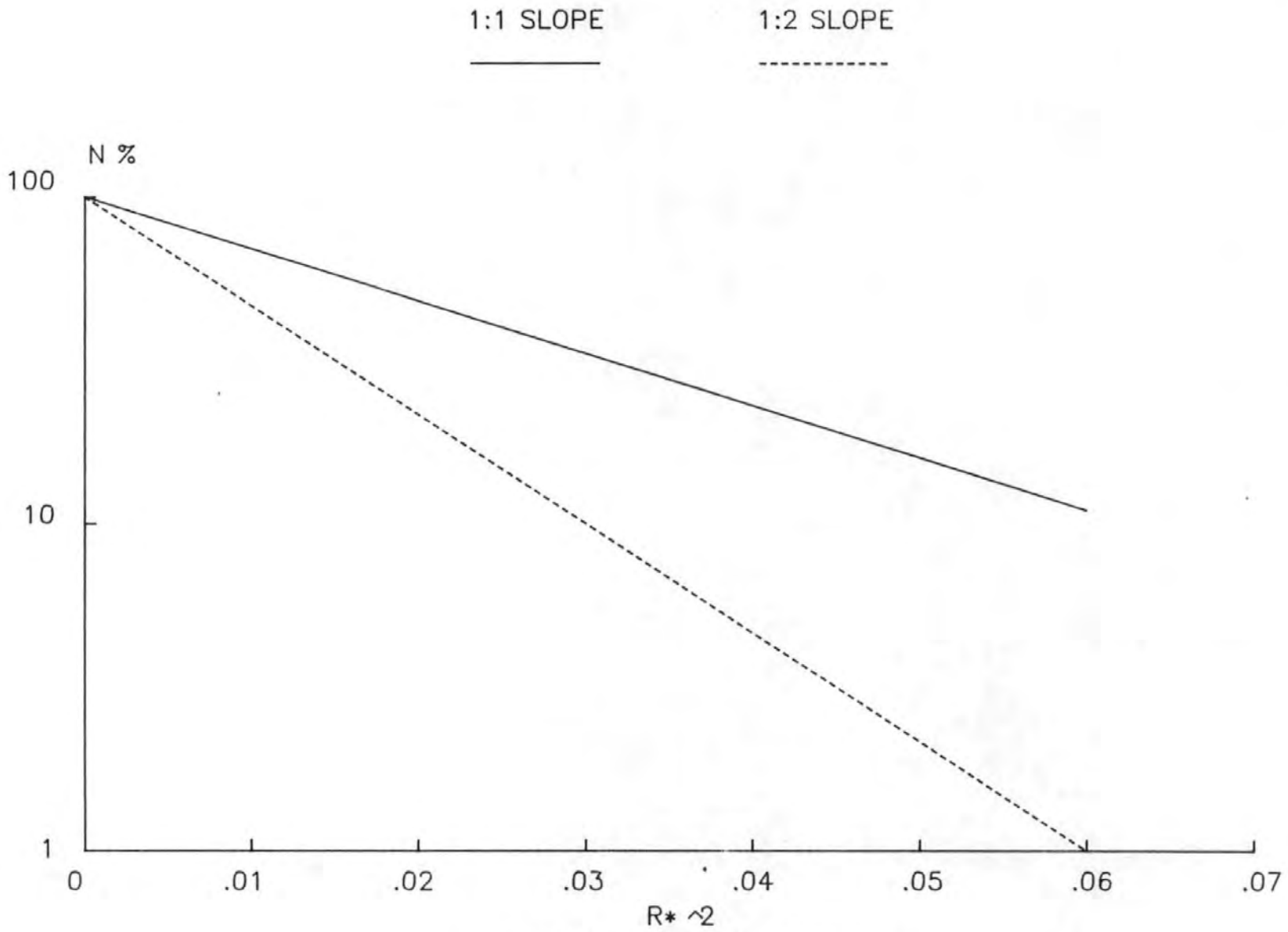

FIG 9.25 PERCENTAGE WAVES OVERTOPPING

The percentage of waves overtopping has also been plotted. Figure 9.24 compares the results from the present study with Owen (1980). Figure 9.25 is an expanded view of the results presented here. Again the agreement with previous tests is good.

The Newman spectrum results are not included on Figures 9.24 and 9.25 since the calculations for discharge do not agree.

9.3.5 Regular Wave Tests

Included in the test program was a small number of regular wave tests. A 0.5Hz sinewave was used. The overtopping discharge from the regular wave tests are shown on Figure 9.22 as + and + for the 1:1 and 1:2 slopes respectively. The regular wave results do not seem to fit well with the irregular wave test results at all. Insufficient regular wave tests have been carried out to thoroughly investigate this phenomena, it does not, however, seem unreasonable when the choice of parameters is considered.

The wave height used in equations (9.4) and (9.5) to calculate the dismensionless parameters R^* and Q^* for the regular wave tests is the total peak-trough wave height. It is not correct to assume that this is equivalent to the significant wave height for irregular waves.

The results of the regular wave tests are summarised in Table 9.10. A comparison to discharge values for regular wave tests given in the Shore Protection Manual is given in Table 9.10.

Slope	H_sm	T_zs	R^*	Q $m^3/s/m$	$Q^* \times 10^{-3}$	Wave Absn	Q(SPM)
1:1	.104	1.99	.00995	.01316	2.59	IN	.0220
1:1	.070	1.99	.01212	.00473	1.38	OUT	.0041
1:2	.105	1.99	.00990	.00083	16.108	IN	.0012
1:2	.104	1.99	.00995	.00121	23.934	OUT	.0010

Table 9.10 Summary of Regular Wave Test Results

In the table above it is interesting to note that the two results of overtopping discharge which most closely agree with the overtopping discharges calculated by the method described in the Shore Protection Manual are those for which wave absorption was not used. Since the Shore Protection Method is based on a very limited number of model tests which need interpolation to match the test conditions, no great significance should be attached to the result.

The percentage number of waves overtopping in the regular wave tests is naturally 100% and thus the results of regular wave tests cannot be related to any results on Figure 9.25.

9.4 Wave Absorption

The beneficial effects of the wave absorption system have already been seen in Figures 9.7 and 9.11 where it was seen that the Incident Wave Spectrum remains close to the theoretical spectrum for different degrees of reflection. The closer correlation to the Shore Protection Manual estimates of reflection coefficient with wave absorption 'in' was also discussed in Section 9.3.2. Thus the wave absorption system enables a more accurate model of the full-scale situation to be created.

Figures 9.26 and 9.27 illustrate the difference made to the incident spectra with wave absorption 'in'. The incident spectrum with wave absorption 'in' is smaller than for absorption 'out' due to the elimination of re-reflections (and higher orders). The loss of high frequency components with wave absorption 'in', as noted earlier is also seen again. The high frequency loss suggests that the wave absorption system may not be as responsive or accurate at the higher frequencies - this may be a mechanical problem with the wave paddle or a software problem in the wave absorption circuit board. This agrees with the regular wave tests on the absorption system in Chapter 7 where a loss is noticed in the higher frequencies (Figure 7.1). This is also consistent with the loop gain of the system discussed in Chapter 6. An alteration of the filter on the circuit board may help to solve the problem (see Chapter 6).

A comparison of Figures 9.28 and 9.29 shows the effect the wave absorption system has on the wave spectra measured at discrete locations within the channel.

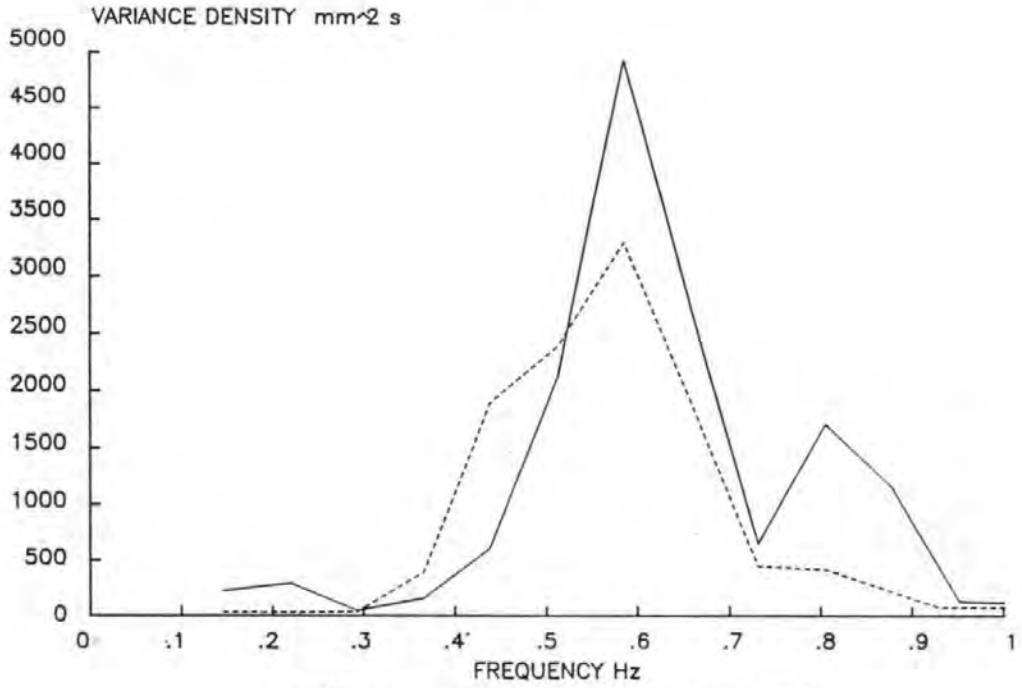

FIG 9.26 A COMPARISON OF THE EFFECT OF THE ABSORPTION CIRCUIT

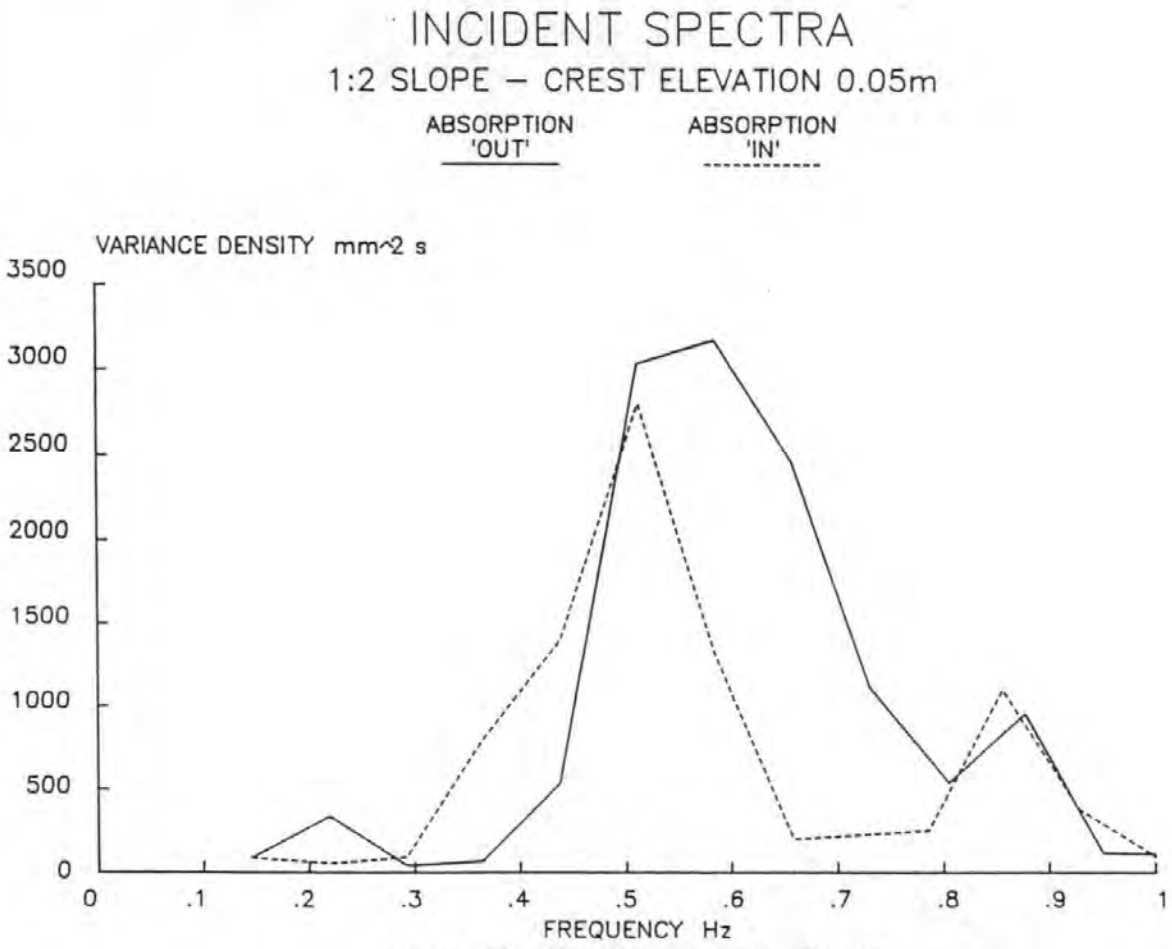

FIG 9.27 INCIDENT SPECTRA WITH AND WITHOUT ABSORPTION

'POINT' SPECTRA – ABSN 'OUT'

1:2 SLOPE P–M SPECTRUM

SPECTRUM AT GAUGE 1 — SPECTRUM AT GAUGE 2 — SPECTRUM AT GAUGE 3

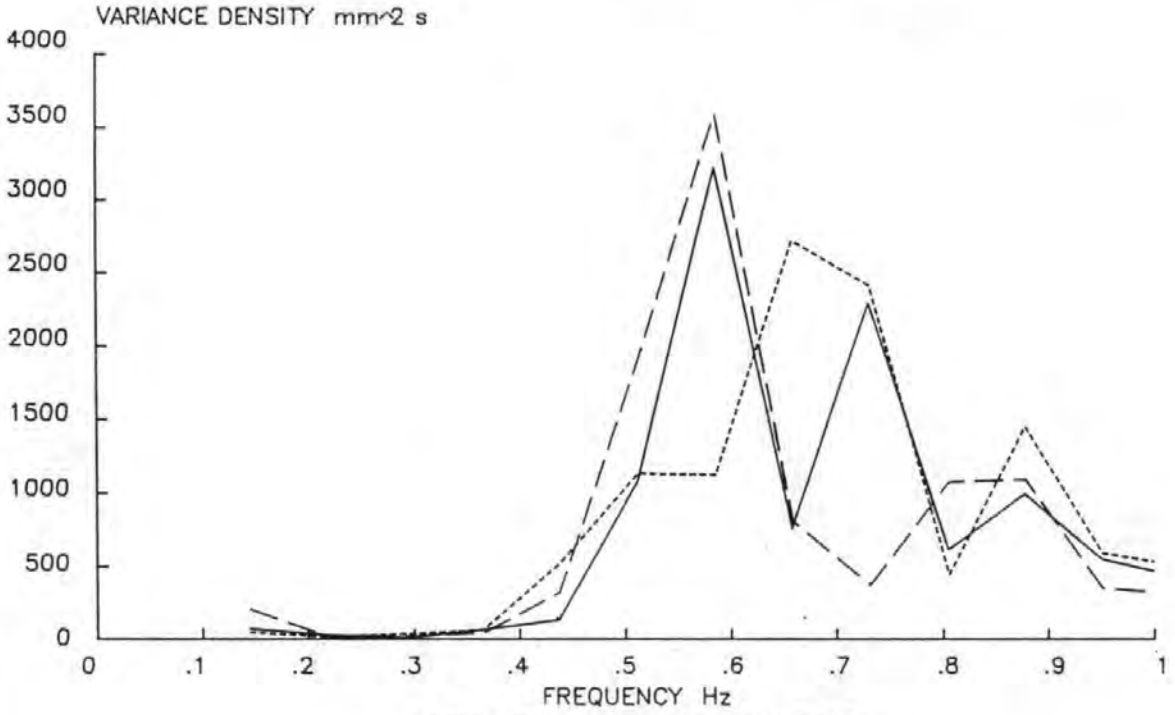

FIG 9.28 'POINT' SPECTRA WITH WAVE ABSORPTION 'OUT'

'POINT' SPECTRA –ABSN 'IN'

1:2 SLOPE – P–M SPECTRUM

SPECTRUM AT GAUGE 1 — SPECTRUM AT GAUGE 2 — SPECTRUM AT GAUGE 3

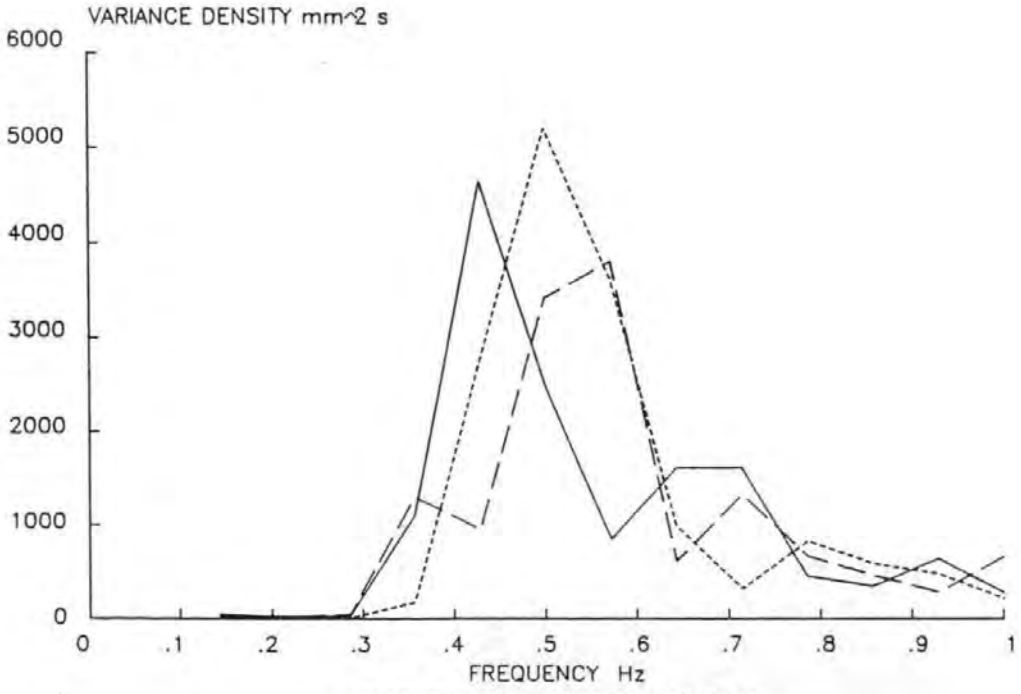

FIG 9.29 'POINT' SPECTRA WITH WAVE ABSORPTION 'IN'

Tables 9.11 and 9.12 compares results for discharge with and without the wave absorption system.

Wave Absn?	H_s m	Q $m^3/s/m$	Q^* x 10^{-4}	R^*
IN	.100	.00289	8.8747	.01491
IN	.099	.00257	7.9250	.01517
OUT	.123	.00651	18.558	.01365
OUT	.120	.00439	12.162	.01503

Table 9.11 The Effect of Wave Absorption on Overtopping Discharge 1:1 Slope.

Wave Absn?	H_s m	Q $m^3/s/m$	Q^* x 10^{-4}	R^*
IN	.141	.00321	5.546	.01015
IN	.136	.00334	6.239	.01078
OUT	.123	.00177	4.324	.01344
OUT	.123	.00190	4.829	.01396

Table 9.12 The Effect of Wave Absorption on Overtopping Discharge 1:2 Slope.

The effect of wave absorption on overtopping discharge does, in reality, come down to the fact that with no wave absorption the incident spectrum is ill-defined and very spiked. Thus any direct comparison of discharges is not appropriate due to the large differences in incident sea states.

The one point that is clear from a comparison is the importance of physical measurements in all tests. If the generated spectrum was assumed 'correct' then the results would be highly misleading.

9.5 Summary and Conclusions

A large number of overtopping tests have been carried out on two breakwater profiles 1:1 and 1:2 seaward slopes for crest elevations close to still water level.

The results from the overtopping tests with a P.M. spectrum, agree well with previous test results (Owen 1980) although the test range has been extended to include crest elevations not previously considered. The results are plotted in dimensionless form. Thus the validity of Owens method of estimating the overtopping discharge over the breakwaters considered in the present study has been shown to extend into a new area not previously considered.

Different 'full length' spectra with the same spectral properties were used in the test and no discernable difference in overtopping discharge was found, provided the spectral properties were the same. Tests with parts of a very long sequence were found to give varying results. The results from part sequences agree with the full sequence results when plotted, the required spectrum, however, is not created in the channel. Thus the test is a different test to that defined by the input parameters.

The analysis software and in particular the Frequency Response analysis all works effectively. From the three wave gauge array it is possible to determine fully the Incident and Reflected wave characteristics produced in the channel. An analysis of this form enables the relevant parameters to be calculated with more confidence, since three separate estimates of the incident and reflected spectra are obtained (Gauges 1-2, 2-3, 1-3).

The wave absorption system is effective in removing the presence of re-reflected waves from the channel. An incident spectrum much closer in form to the theoretical spectrum, as output from the BBC, microcomputer is produced. The incident spectrum is repeatable and good stability of the waves (i.e. no resonance) is achieved. The results of tests with wave absorption 'in' also agree much better with empirical reflection data published in the Shore Protection Manual.

The main advantage found with the wave absorption system was the confidence with which tests could be carried out. There was no need to worry about resonance or standing wave patterns being formed. The tests were also much more accurately targetted beforehand i.e. when a choice of tests parameters were chosen you could be confident the conditions generated in the channel would be close to those required.

CHAPTER 10

NUMERICAL OVERTOPPING MODEL

10.1 Introduction

In order to evaluate overtopping discharges mathematically a numerical model of the overtopping process was developed. The model is written in IEM FORTRAN 77 on the HP 9816S computer which was used for the laboratory work.

The purpose of the model was to predict the water surface elevation and horizontal water particle velocities on a breakwater slope and over a horizontal crest to obtain results for comparison with the laboratory work. No previous examples of overtopping models could be found, although the closely related run-up problem has been modelled on a number of occasions. A review of numerical models of run-up is included in Chapter 1.

Since the type of breakwater structure used in the physical studies had a fairly steep slope, up to 1:1, the commonly used (for run-up) characteristic equations cannot be applied here since the vertical accelerations are significant. The approach adopted was to allow for the vertical accelerations without including them in the integration The effectiveness of the method will be discussed in the next chapter.

The solution of the modified momentum equation and the 1-D continuity equation formed the basis of the solution to the overtopping problem. Although the equations are one dimensional in respect to all variables, the second, vertical, dimension has been taken into account and the equations can be regarded as quasi 2-D.

The method of solution of the 2 equations is with a finite element mesh in the space domain and a finite-difference time step.

In all the following algebraic development the x, y and z directions are taken to follow standard cartesian conventions with z in the vertical plane.

10.2 Governing Equations

The run-up and overtopping process is governed by a coupled set of equations. The continuity and momentum equations

$$\text{Continuity} \quad \frac{\partial \eta}{\partial t} + \frac{\partial}{\partial x}\left[U(h+\eta)\right] = 0 \qquad (10.1)$$

$$\text{Momentum} \quad \frac{\partial U}{\partial t} + U\frac{\partial U}{\partial x} = -\frac{g\partial \eta}{\partial x} + F_x \qquad (10.2)$$

where F_x is the term introduced to account for vertical accelerations. F_x is derived in full in Appendix E.

The application of the above two equations is made with the following assumptions.

The flow in the region under consideration is assumed to be inviscid and incompressible. The density of the water and the atmospheric pressure remains constant. The effect of wind, percolation, coriolis and tide generating forces are neglected. Currents are not present and the incoming wave is assumed to enter still water.

For a 1-D (in space) model there is no change in any quantity in the y-direction i.e. the direction perpendicular to the x-axis in the horizontal plane. This means refraction and diffraction are not involved.

The bottom is smooth and frictional forces are ignored.

10.3 The Finite Element Method

10.3.1 Introduction

The finite element method of solution is now a widely used and accepted method of analysis. The technique is well documented and the intention here is only to deal with the salient points pertinent to the solution of the above equations.

There are many advantages to a finite element solution some of which include:

i. Complex geometry is simply included
ii. A moving boundary is easily coped with
iii. With non linear shape functions high accuracy can be achieved with few nodes and elements
iv. Changes of the forcing function wave are easily dealt with.

10.3.2 Galerkin Finite Element Method

Briefly the Galerkin method is a method of weighted residuals (Zienkiewicz 1977). The method includes taking a weighted error or residual, integrating the residual over the domain of interest and setting the result equal to zero. Thus, with the continuity and momentum equations approximated by a finite sum, the velocity, U, and water surface devation, η, are expressed as follows:-

$$\bar{U}(x,t) = \sum_{i=1}^{P} N_i(x)\, U_i(t) \qquad (10.3)$$

$$\bar{\eta}(x,t) = \sum_{i=1}^{P} N_i(x)\, \eta_i(t) \qquad (10.4)$$

where the bar ($\bar{U}$, $\bar{\eta}$) signifies an approximation, P is the number of degrees of freedom, N_i are the Galerkin trial functions and U_i and η_i are discrete values of the variables at points.

Let the governing differential equation be of the form:

$$L\,\Phi - f = 0 \qquad (10.5)$$

where L is a differential operator, Φ a variable and f a known function
Let $\bar{\Phi}$ be an approximation to Φ such that:

$$\bar{\Phi} = \sum_{i=1}^{P} N_i\, \Phi_i \qquad (10.6)$$

Equation (10.5) can then be written as:

$$L\,\bar{\Phi} - f = \bar{R} \qquad (10.7)$$

where $\bar{R}$ is the weighted residual due to the approximation. Hence from the principal of orthogonality. (If $\bar{\Phi} = \Phi$ then $L\Phi - f$ must be orthogonal to N_i).

$$\int_D N_i \, (L\bar{\Phi} - f) = 0 \qquad i = 1, \ldots\ldots P \tag{10.8}$$

or

$$\int_D N_i \, \bar{R} = 0 \qquad i = 1, \ldots\ldots P \tag{10.9}$$

where D is the domain of interest.

Briefly it is seen that the technique reduces to a set of algebraic equations. An example is given below:

$$\text{Let } \frac{\partial U}{\partial x} = ax \quad x_1 \leqslant x \leqslant x_2 \tag{10.10}$$

where U is a variable and a a constant.

The approximation is:

$$U = \sum_{i=1}^{2} N_i \, U_i \tag{10.11}$$

$$\text{i.e.} \quad U = N_1 U_1 + N_2 U_2 \tag{10.12}$$

where N_1 and N_2 are functions of x.
Since U_1 and U_2 are discrete values of x they do not depend on x, thus:

$$\frac{\partial U}{\partial x} = \frac{\partial N_1}{\partial x} U_1 + \frac{\partial N_2}{\partial x} U_2 \tag{10.13}$$

If we write $\frac{\partial N_i}{\partial x}$ as N_i^1

$$(N_1^1 \, U_1 + N_2^1 \, U_2) - ax = 0 \tag{10.14}$$

from the principal of orthogonality

$$\int_{x_1}^{x_2} N_1 \left[(N_1^1 \, U_1 + N_2^1 \, U_2) - ax \right] dx = 0 \tag{10.15}$$

$$\int_{x_1}^{x_2} N_2 \left[(N_1^1 U_1 + N_2^1 U_2) - ax \right] dx = 0 \qquad (10.16)$$

equations (10.15) and (10.16) can be written in matrix form as:

$$\begin{bmatrix} \int_{x_1}^{x_2} N_1^1 N_1^1 dx & \int_{x_1}^{x_2} N_1^1 N_2^1 dx \\ \int_{x_1}^{x_1} N_2^1 N_1^1 dx & \int_{x_1}^{x_2} N_2^1 N_2^1 dx \end{bmatrix} \begin{bmatrix} U_1 \\ U_1 \end{bmatrix} = \begin{bmatrix} \int_{x_1}^{x_2} (N_1 ax) dx \\ \int_{x_1}^{x_2} (N_2 ax) dx \end{bmatrix} \qquad (10.17)$$

As N_1 and N_2 are known the integrations can be carried out quite easily. Solution of (10.17) yields U_1 and U_2 and hence U from (10.12).

Application of the finite element method to the above solution involves splitting the problem domain into small portions or elements (discretisation). The smaller the elements the smaller the residual or error will be. The values at distinct points (nodes) are calculated for the whole problem domain. The approximation is introduced through the shape (trial) functions.

A simple example with linear shape functions is given below.

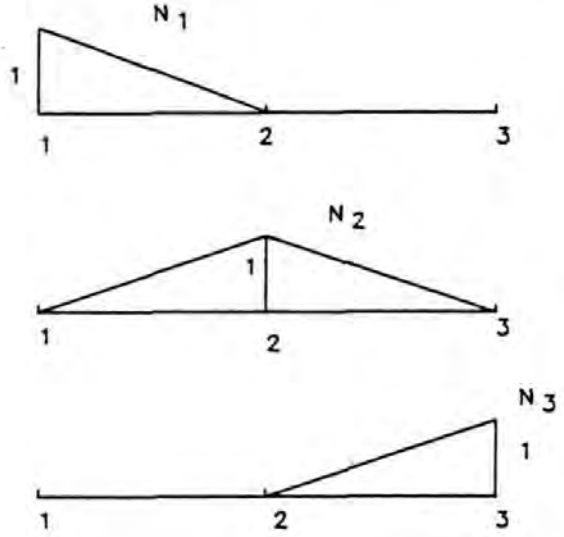

Figure 10.1 Linear Shape Functions

1-2 represents a one-dimensional element of length l, and U_1 and U_2 are the values of U at the nodes. If we assume U varies linearly within the element

$$U = \left[1 - x/l\right] U_1 + \left[\frac{x}{L}\right] U_2 \qquad (10.18)$$

$$U = N_1 U_1 + N_2 U_2 \qquad (10.19)$$

where $N_1 = 1 - \frac{x}{l}$ and

$$N_2 = \frac{x}{l}$$

It is seen that these are linear shape functions and there are two degrees of freedom per element. (Owen and Hinton 1980).

In the case of water surface elevation we do not have linear variation between nodes. There are two possible solutions. One is to make the elements small so that the variation becomes approximately linear. A large number of elements would then be needed, increasing the computational time. The second solution is to use non-linear shape functions since we require that the gradient of the shape functions are continuous over the nodes (i.e. C^1 continuity). Non-linear shape functions are used in the solution to this problem. Continuity of gradient means the solution is less dependent upon element size. (Hinton 1980).

The shape functions used in the model are limbs of a Hermitian cubic interpolation function. We also need to use the gradient of the variable at the nodes in addition to the variable itself. i.e. four degrees of freedom per element. (Wang et al 1972)(Strang and Fix 1973).

The variable is given by:

$$U = N_1 U_1 + N_2 U_1^1 + N_3 U_2 + N_4 U_2^1 \qquad (10.20)$$

N_1 to N_4 are as follows:-

$$\left.\begin{aligned} N_1 &= 1-3\left[\frac{x}{l}\right]^2 + 2\left[\frac{x}{l}\right]^3 \\ N_2 &= x+1\left[\left[\frac{x}{l}\right]^3 - 2\left[\frac{x}{l}\right]^2\right] \\ N_3 &= 3\left[\frac{x}{l}\right]^2 - 2\left[\frac{x}{l}\right] \\ N_4 &= 1\left[\left[\frac{x}{l}\right]^3 - \left[\frac{x}{l}\right]^2\right] \end{aligned}\right\} \qquad (10.21)$$

It can be seen that for non-linear shape functions there will be four integral relationships per element.

10.3.3 Element Assembly

In order to arrive at a solution for the whole problem, the element matrices must be assembed correctly. The assembled matrix is called the global matrix and it is the solution of the global matrix which yields the solution.

In the problems under consideration here we are only working in one space dimension (the time dimension will be dealt with later) and thus we can use line elements.

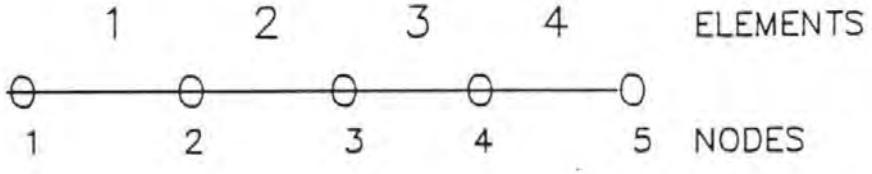

Figure 10.2 Assembly of line elements

From Figure 10.2 it can be seen that the value at a node is shared by two elements.

As stated above each element matrix will be 4x4 and the value and its derivative will be continuous over the node i.e.

$$U_2^1 = U_1^2 \quad \text{where} \tag{10.22}$$

U_1^2 is the value of U at node 2 in element 1 and U_1^2 is the value of U at node 1 in element 2.

Using the above fact the two elements are assembled as follows:

$$\begin{bmatrix} C_{11} & C_{12} & C_{13} & C_{14} & 0 & 0 \\ C_{21} & C_{22} & C_{23} & C_{24} & 0 & 0 \\ C_{31} & C_{32} & C_{33}+R_{11} & C_{34}+R_{12} & R_{13} & R_{14} \\ C_{41} & C_{42} & C_{43}+R_{21} & C_{44}+R_{22} & R_{23} & R_{24} \\ 0 & 0 & R_{31} & R_{32} & R_{33} & R_{34} \\ 0 & 0 & R_{41} & R_{42} & R_{43} & R_{44} \end{bmatrix} \begin{Bmatrix} \dot{U}_1 \\ \dot{U}_1^1 \\ \dot{U}_2 \\ \dot{U}_2^1 \\ \dot{U}_3 \\ \dot{U}_3^1 \end{Bmatrix} = \begin{Bmatrix} B_1 \\ B_2 \\ B_3+F_1 \\ B_4+F_2 \\ F_3 \\ F_4 \end{Bmatrix} \tag{10.23}$$

where C_{ij} are the values from element matrix 1
R_{ij} are the values from element matrix 2

the values of B_i and F_i came from the RHS of equation (10.17).

In general if we have N elements the global matrix will be of size m x m where m = 2(N) + 2.

Assembly for all the elements and solving by a method such as direct Gaussian elimination yields all the values of U and U^1.

10.4 Problem Domain

The run-up/overtopping problem investigated here is concerned with flow up to and over a breakwater crest.

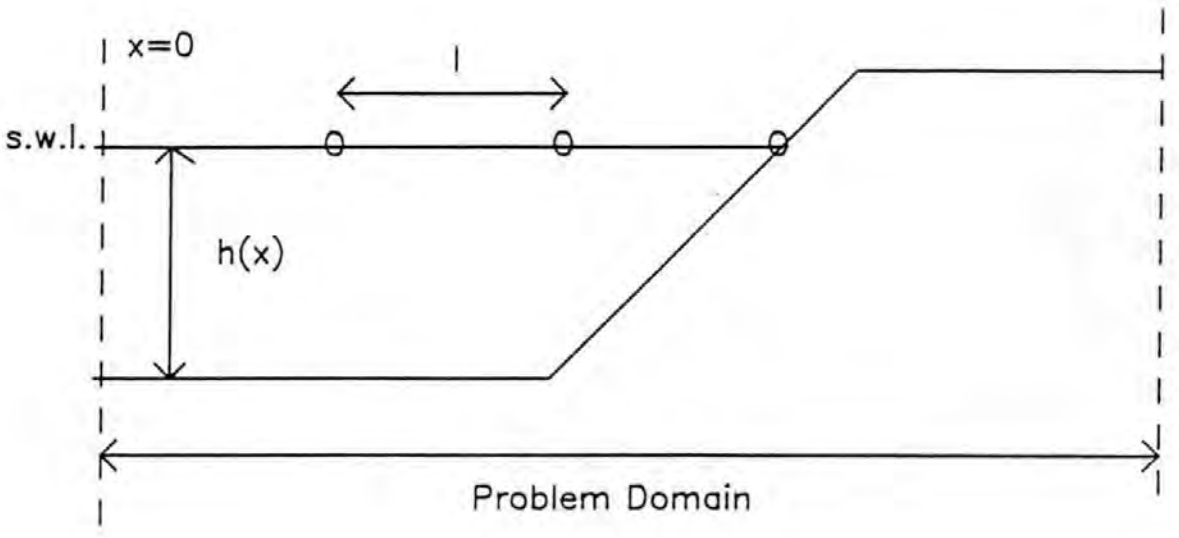

Figure 10.3 Spatial Discretisation

The model has two limits. X=0 is the upstream boundary, it is at this point that the incoming wave is introduced. The upstream boundary remains fixed. At the downstream end the situation is more complicated. Initially the downstream boundary is at the point where the free surface makes contact with the breakwater. As the wave runs up the breakwater the point of contact will move up and over the breakwater. Additional elements will have to be introduced to permit this (see Section 10.9). A node will always be at the tip of the moving water surface At an arbitrary point x=X the water is assumed to have 'overtopped' as an additional approximation is needed to calculate the overtopping discharge at this point. This is discussed in Section 10.10.

The discretisation as shown in Figure 10.3 requires that there be a node at x=0. The value of η at this node can be calculated as the wave is introduced here. The choice of forcing function i.e. a regular or random wave will be discussed in Section 10.7. The problem is started with still water conditions i.e. η=0 at all nodes.

10.5 Solution System-Space Domain

The run-up/overtopping problem is defined by the coupled continuity and momentum equations (10.1), (10.2). The Galerkin technique is applied to both equations in each element and the resultant element matrices are assembled to give global continuity and global momentum matrices. The solution of the two matrices yields the time derivatives of η and U. The time derivatives are then stepped up in time to give the values of η and U.

The solution may be represented as:

$$U = N_1 U_1 + N_2 U'_1 + N_3 U_2 + N_4 U'_2 \qquad (10.24)$$

$$\eta = N_1 \eta_1 + N_2 \eta'_1 + N_3 \eta_2 + N_4 \eta'_2 \qquad (10.25)$$

10.5.1 Element Matrix-Continuity Equation

On application of the Galerkin technique to equation (10.1) over a single element the following integral relationship results:

rewriting the equation with the time dependent terms on the LHS

$$\frac{\partial \eta}{\partial t} = - \frac{\partial}{\partial x} \left[U(h+\eta) \right]$$

$$= - \left[U \frac{\partial}{\partial x} (h+\eta) + (h+\eta) \frac{\partial U}{\partial x} \right] \qquad (10.26)$$

Taking N_1 as the weighting function

$$\int_0^i N_1 \left[\frac{\partial \eta}{\partial t} \right] dx = - \int_0^i N_1 \left[U \frac{\partial}{\partial x} (h+\eta) + (h+\eta) \frac{\partial U}{\partial x} \right] dx \qquad (10.27)$$

Substituting for the values of U and Π from equations (10.24) and (10.25)

$$\int_0^i N_1 \left[N_1 \dot{\Pi}_1 + N_2 \dot{\Pi}_1 + N_3 \dot{\Pi}_2 + N_4 \dot{\Pi}_2^1 \right] dx =$$

$$\int N_1 \Big[(N_1 U_1 + N_2 U_1^1 + N_3 U_2 + N_2 U_2^1)\left(\frac{\partial h}{\partial x} + N_1^1 \Pi_1 + N_2^1 \Pi_1^1 + N_3^1 \Pi_2 + N_4 \Pi_2^1\right)$$

$$+ (h + N_1\Pi_1 + N_2\Pi_1^1 + N_3\Pi_2 + N_4\Pi_2^1)\ (N_1^1 U_1 + N_2^1 U_1^1 + N_3^1 U_2 + N_4^1 U_2^1) \Big] dx \qquad (10.28)$$

Similar relationships are obtained if N_2, N_3 and N_4 are used as the weighting functions. Where the dot notation implies a time derivative

The LHS of equation (10.28) is written in matrix form as

$$[C_{11}.\ C_{12},\ C_{13},\ C_{14}] \qquad \begin{Bmatrix} \dot{\Pi}_1 \\ \dot{\Pi}_1^1 \\ \dot{\Pi}_2 \\ \dot{\Pi}_2^1 \end{Bmatrix}$$

where

$$C_1 j = \int_0^L N_1 N_j \, dx$$

$$j = 1 \ldots\ldots 4$$

Using B_1 to denote the RHS of equation (10.28)

$$(C_{11},\ C_{12},\ C_{13},\ C_{14}) \begin{Bmatrix} \dot{\Pi}_1 \\ \dot{\Pi}_1^1 \\ \dot{\Pi}_2 \\ \dot{\Pi}_2^1 \end{Bmatrix} = \left[B_1 \right]$$

From the 3 other relationships obtained using N_2, N_3 and N_4 as weighting functions the element matrix becomes

$$\begin{bmatrix} C_{11} & C_{12} & C_{13} & C_{14} \\ C_{21} & C_{22} & C_{23} & C_{24} \end{bmatrix} \begin{Bmatrix} \dot{\Pi}_1 \\ \dot{\Pi}_1^1 \end{Bmatrix} = \begin{Bmatrix} B_1 \\ B_2 \end{Bmatrix} \qquad (10.30)$$

$$\begin{bmatrix} C_{31} & C_{32} & C_{33} & C_{34} \\ C_{41} & C_{42} & C_{43} & C44 \end{bmatrix} \begin{Bmatrix} \eta_2 \\ \dot{\eta}_2^1 \end{Bmatrix} \quad \begin{Bmatrix} B_3 \\ B_4 \end{Bmatrix}$$

The continuity element matrix will be symmetric since

$$C_{ij} = \int_0^L N_i N_j \, dx \qquad (10.31)$$

The other element matrices are calculated in the same way and the global continuity matrix assembled as shown in equation (10.23) remembering that at each node the value and its gradient are single valued, i.e. $\dot{\eta}_2^1 = \dot{\eta}_1^2$

10.5.2 Element Matrix - Momentum Equation

The momentum equation (10.2) is operated upon in exactly the same way. In this case there are a number of terms for the Fx value included to account for vertical accelerations. The derivation of the vertical acceleration term is given in Appendix E.

Ignoring terms smaller than 3rd order the momentum equation (10.2) can be re-written as:

$$\frac{\partial U}{\partial t} + U\frac{\partial U}{\partial x} = -\frac{h+\eta}{2}\left[\frac{\partial^2}{\partial x \partial t}\left(-U\frac{\partial h}{\partial x}\right) + \frac{\partial}{\partial x}\left[U\frac{\partial}{\partial x}\left(-U\frac{\partial h}{\partial x}\right)\right]\right]$$

$$-\frac{\partial \eta}{\partial x}\left[\frac{\partial}{\partial x}\left(-U\frac{\partial h}{\partial x}\right) + U\frac{\partial}{\partial x}\left(-U\frac{\partial h}{\partial x}\right) + g\right] \qquad (10.32)$$

In the same way as for the continuity equation we apply the Galerkin technique over a single element to equation (10.32) we obtain

$$\int_0^1 N_1\left(\frac{\partial U}{\partial t} + U\frac{\partial U}{\partial x}\right)\partial x = -\int_0^1 N_1\left[\frac{h+\eta}{2}\left[\frac{\partial^2}{\partial x \partial t}\left(-U\frac{\partial h}{\partial x}\right) + \frac{\partial}{\partial x}\left(U\frac{\partial}{\partial x}\left(-U\frac{\partial h}{\partial x}\right)\right)\right]\right.$$

$$\left.\frac{\partial \eta}{\partial x}\left[\frac{\partial}{\partial t}\left(-U\frac{\partial h}{\partial x}\right) + U\frac{\partial}{\partial x}\left(-U\frac{\partial h}{\partial x}\right) + g\right]\right] dx \qquad (10.33)$$

Similar relationships are obtained with N_2, N_3, and N_4 as the weighting functions. Collecting the time dependent terms of U on the LHS and the space dependent terms on the RHS we have

$$\int_0^1 N_1\left[\dot{U} + \frac{h+\eta}{2}\frac{\partial}{\partial x}\left(-\dot{U}\frac{\partial h}{\partial x}\right) + \frac{\partial \eta}{\partial x}\left(-\dot{U}\frac{\partial h}{\partial x}\right)\right] dx =$$

$$\int_0^1 N_1 \left[U\frac{\partial U}{\partial x} - \frac{h+\eta}{2}\left[\frac{\partial}{\partial x}\left[U\frac{\partial}{\partial x}\left[-U\frac{\partial h}{\partial x}\right]\right]\right] - \frac{\partial \eta}{\partial x}\left[U\frac{\partial}{\partial x}\left[-U\frac{\partial h}{\partial x}\right]+g\right]\right] dx \quad (10.34)$$

On substitution of U and η from equations (10.24) and (10.25) we have on the LHS

$$\int_0^1 N_1 \Bigg\{ (N_1\dot{U}_1 + N_2\dot{U}_1^{\frac{1}{2}} + N_3\dot{U}_2 + N_4\dot{U}_2^{\frac{1}{2}}) - \left[\frac{h}{2} + (N_1\eta_1 + N_2\eta_1^{\frac{1}{2}} + N_3\eta_2 + N_1\eta_2^{\frac{1}{2}})/2\right]$$

$$\left[(N_1^{\frac{1}{2}}\dot{U}_1 + N_2^{\frac{1}{2}}\dot{U}_1^{\frac{1}{2}} + N_3^{\frac{1}{2}}\dot{U}_2 + N_4^{\frac{1}{2}}\dot{U}_2^{\frac{1}{2}})\frac{}{} + (N_1\dot{U}_1 + N_2\dot{U}_1^{\frac{1}{2}} + N_3\dot{U}_2 + N_4\dot{U}_2^{\frac{1}{2}})\frac{\partial^2 h}{\partial x^2}\right]$$

$$- \left[(N_1^{\frac{1}{2}}\eta_1 + N_2^{\frac{1}{2}}\eta_1^{\frac{1}{2}} + N_3^{\frac{1}{2}}\eta_2 + N_4^{\frac{1}{2}}\eta_2^{\frac{1}{2}})\ (N_1\dot{U}_1 + N_2\dot{U}_1^{\frac{1}{2}} + N_3\dot{U}_2 + N_4\dot{U}_2^{\frac{1}{2}})\frac{\partial h}{\partial x}\right]\Bigg\} dx \quad (10.35)$$

In matrix form (10.35) becomes

$$\begin{bmatrix} C_{11} & C_{12} & C_{13} & C_{14} \end{bmatrix} \begin{Bmatrix} \dot{U}_1 \\ \dot{U}_1^{\frac{1}{2}} \\ \dot{U}_2 \\ \dot{U}_2^{\frac{1}{2}} \end{Bmatrix} \quad (10.36)$$

where $C_{ij} = \int_0^L N_i \left[N_j \left(\frac{h}{2} + (N_1\eta_1 + N_2\eta_1^{\frac{1}{2}} + N_3\eta_2 + N_4\eta_2^{\frac{1}{2}})/2 \right.\right.$

$$\left.\left.(N_j\frac{\partial h}{\partial x} + N_j\frac{\partial^2 h}{\partial x^2}) - (N_1^{\frac{1}{2}}\eta_1^{\frac{1}{2}} + N_2^{\frac{1}{2}}\eta_1^{\frac{1}{2}} + N_4^{\frac{1}{2}}\eta^{1}{}_2)\ N_j\right] dx \quad (10.37)$$

In a similar fashion to the continuity element matrix, with N_2, N_3 and N_4 as weighting functions we have an element matrix as

$$\begin{bmatrix} C_{11} & C_{12} & C_{13} & C_{14} \\ C_{21} & C_{22} & C_{23} & C_{24} \\ C_{31} & C_{32} & C_{33} & C_{34} \\ C_{41} & C_{42} & C_{43} & C_{44} \end{bmatrix} \begin{Bmatrix} \dot{U}_1 \\ \dot{U}_1^{\frac{1}{2}} \\ \dot{U}_2 \\ \dot{U}_2^{\frac{1}{2}} \end{Bmatrix} = \begin{Bmatrix} B_1 \\ B_2 \\ B_3 \\ B_4 \end{Bmatrix} \quad (10.38)$$

It is clear from equation (10.37) that the element momentum matrix will not be symmetric.

10.5.3 Continuity RHS Vector

From the RHS of equation (10.28) we can obtain a result for the values of B_i in equation (10.30).

$$B_i = \int_0^1 N_i \Big[(N_1U_1 + N_2U_1^1 + N_3U_2 + N_4U_2^1)\left(\frac{\partial h}{\partial x} + N_1^1\Pi_1 + N_2^1\Pi_1^1 + N_3^1\Pi_2 + N_4\Pi_2^1\right)$$

$$+ (h + N_1\Pi_1 + N_2\Pi_1^1 + N_3\Pi_2 + N_4\Pi_2^1)(N_1^1U_1 + N_2^1U_1^1 + N_3^1U_2 + N_4^1U_2^1)\Big] \; dx$$

$$i = 1 \ldots . 4 \qquad (10.39)$$

10.5.4 Momentum RHS Vector

On substitution of U and Π into the RHS of equation (10.34) we have

$$B_i = \int_0^1 N_i \Big[(N_1U_1 + N_2U_1^1 + N_3U_2 + N_4U_2^1)(N^1{}_1U_1 + N_2^1U_1^1 + N_3U_2 + N_2U^1{}_2)2\frac{\partial h}{\partial x}$$

$$+ \left(\frac{h}{2} + (N_1R_1 + N_2N_1^1 + N_3\Pi_2 + N_4\Pi_2^1)/2\right)\Big[(N_1U_1 + N_2U_1^1 + N_3U_2 + N_2U_2^1)2\frac{\partial h}{\partial x}$$

$$+ 3(N_1U_1 + N_2^1U_1^1 + N_3^1U_2 + N_4^1U_2^1)\frac{\partial^2 h}{\partial x^2} + (N_1^1U_1 + N_2^1U_1^1 + N_3^1U2 + N_4^1U_2^1)2\frac{\partial h}{\partial x}$$

$$+ (N_1U_1 + N_2U_1^1 + N_3U_2 + N_4U_2^1)\ (N^1{}_1^1U_1 + N^1{}_2^1U_1^1 + N^1{}_3^1U_2 + N^1{}_4^1U_2^1)\frac{\partial h}{\partial x}\Big]$$

$$+ (N_1\Pi_1 + N_2\Pi_1^1 + N_3\Pi_2 + N_4\Pi_2^1)\Big[(N_1U_1 + N_2U_1^1 + N_3U2 + N_4U_2^1)2\partial h/\partial x$$

$$+ (N_1U_1 + N_2U_1^1 + N_3U_2 + N_4U_2^1)(N_1^1U_1 + N_2^1U_1^1 + N_3^1U_2 + N_4^1U_2^1)\frac{\partial h}{} + g\Big]\Big] \; dx$$

$$i = 1 \ldots\ldots . 4 \qquad (10.40)$$

10.5.5 Assembly

The element matrices and vectors are assembled for all the elements and direct Gaussian elimination used to solve the resultant sets of simultaneous equations. The solution of the two matrices yields the time derivatives $\dot{U}$ and $\dot{\Pi}$. The problem can be solved subject to the imposition of the boundary conditions on U and Π which are discussed later.

10.6 Time Integration

In order to avoid any error due to the use of constant rates of change of U and η within the time step, an iterative procedure is necessary. The iteration is introduced in the steps of time integration via the predictor-corrector technique (McCalla, 1967). A predictor-corrector method moves back and forth between time steps to ensure that the error introduced by a purely forward marching scheme is reduced by successive iterations to less than a specified tolerance. This ensures that due consideration is given to the simultaneous and non-linear change in U and η. A higher order method was not considered since the increase in computational time was not considered to merit the possible increase in accurary.

10.6.1 Euler Predictor-Corrector Method

Let the velocity at a given node be U(t) at time t. From the above Finite Element step we obtain the time rate of change of U at time t ie $\dot{U}(t)$.

With the value of $\dot{U}(t)$ the value of U at $(t+\Delta t)$ is predicted as

$$U^P\ (t+\Delta t) = U(t) + \dot{U}(t).\Delta t \qquad (10.41)$$

also

$$\eta^P\ (t+\Delta t) = \eta(t) + \dot{\eta}(t).\Delta t \qquad (10.42)$$

Using these values of U and η for the instant $(t+\Delta t)$ the time rates of change of U and η, $\dot{U}(t+\Delta t)$ and $\dot{\eta}(t+\Delta t)$ can be calculated within the Finite Element step. Corrected values of U and η at $(t+\Delta t)$ are now arrived at using the mean of the time rates of change at t and $(t+\Delta t)$.

$$U^C\ (t+\Delta t) = U(t) + [(\dot{U}(t) + \dot{U}(t+\Delta t))/2]\ \Delta t \qquad (10.43)$$

$$\eta^C\ (\ (t+\Delta t) = \eta(t) + [(\dot{\eta}(t) + \dot{\eta}(t+\Delta t))/2]\ \Delta t \qquad (10.44)$$

The process is repeated until two successive corrected values differ by less than a pre-set tolerance. Figure 10.4 shows the logic for successive iterations.

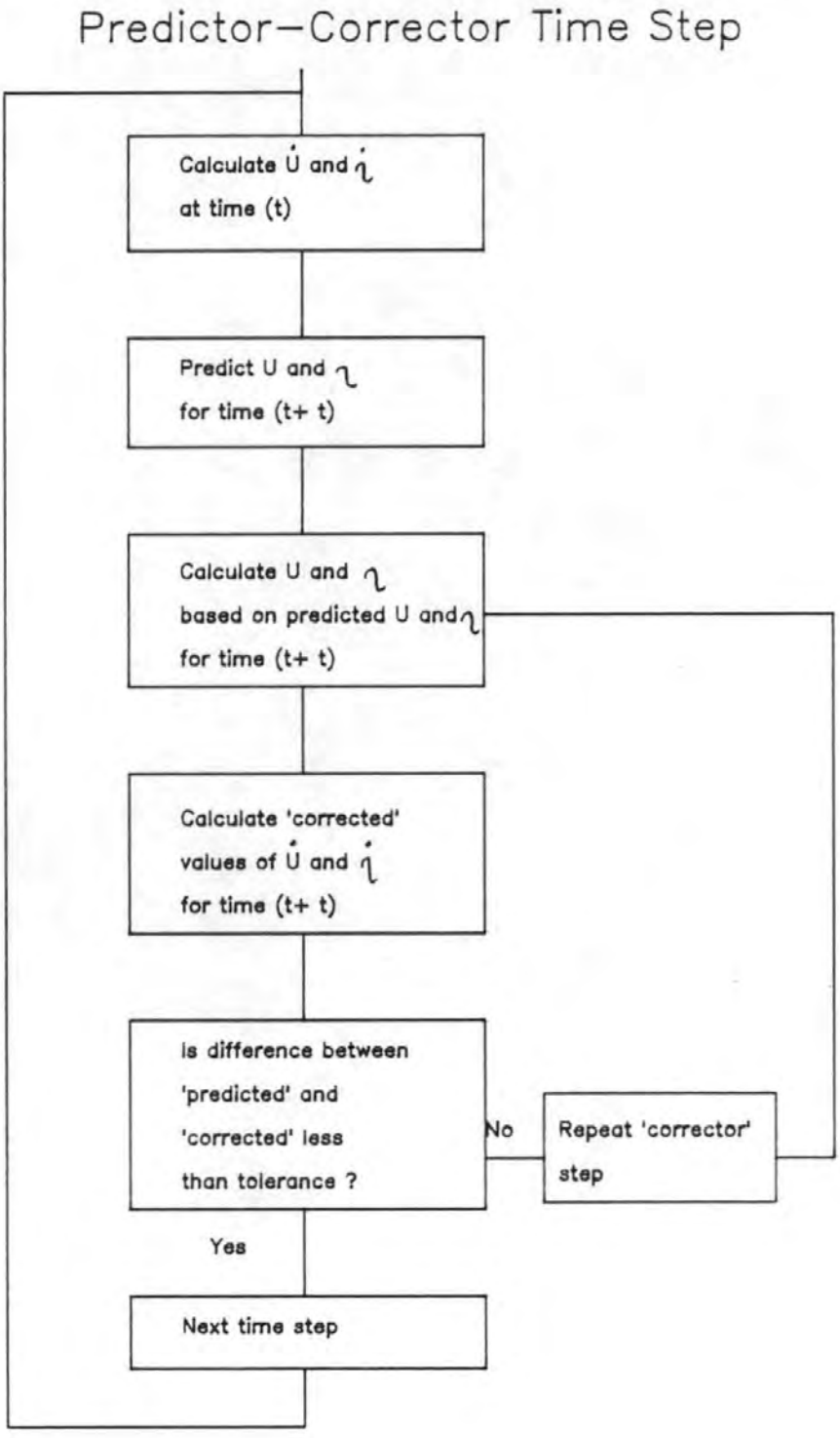

FIG 10.4 PREDICTOR–CORRECTOR SCHEME

10.7 The Forcing Function

The effect of an incoming wave to the breakwater is introduced through the upstream boundary condition at x=0.

Initially in the development of the model a sinewave forcing function was used as this was simple to implement and code.

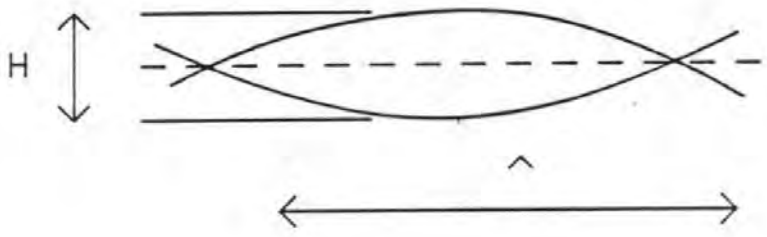

Figure 10.5 Sinusoidal Wave

Wave heights h, wave length L and wave period, T are specified. The water level profile at x=0 and the constant is given by

$$\eta(o,t) = \frac{h}{2} \sin\left\{\frac{2\pi t}{T}\right\} \qquad (10.45)$$

It would be a simple coding exercise to allow the model to run random waves. A real digital data set could be read at the correct time intervals. In this manner the model could run random waves.

10.8 Boundary Conditions

The solution requires the determination of two unknowns, namely U and η and hence we need two boundary conditions. One on U and one on η. The boundary conditon on η is supplied from a value of $\dot{\eta}$ calculated at x=0 from the forcing function value as given above. The boundary condition on U is given by a value of $\dot{U}$ at the downstream end i.e. the tip of the water body. Once the water body has reached the point at which overtopping is assumed to occur a different calculation of $\dot{U}$ is performed. The two different boundary calculations are described in the appropriate sections on element splitting and the weir function.

10.9 Element Splitting

In a run-up/overtopping problem the downstream boundary will change with time as the wave propagates up the breakwater slope. As the wave moves along the crest a new problem arises. At an arbitrary point we must decide that the wave has 'overtopped'. The technique for dealing with this will be explained in the next section.

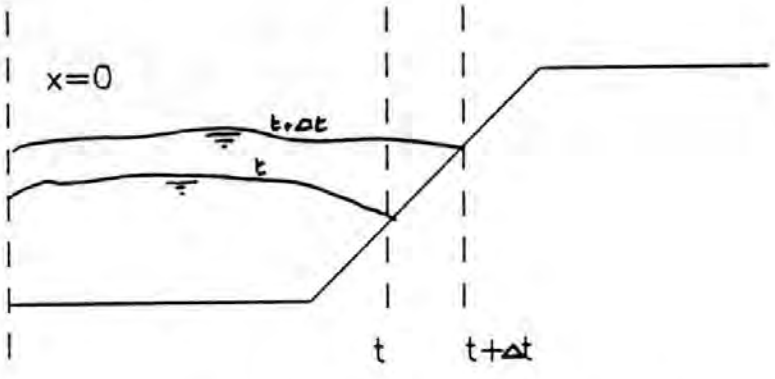

Figure 10.6 Moving Downstream Boundary

The upstream section will remain unchanged in time at x=0. Moving boundary problems such as this are classified as Stefan problems. (Varogli and Liam Finn 1977). The common characteristic of Stefan problems is that the position of the moving boundary at the next time step is to be obtained by solving the governing equations, but the equations cannot be applied until the position of the boundary is known. This 'vicious' circle is usually overcome by adopting an iterative technique.

The error normally associated with fixed grid schemes can be eliminated by use of a mobile node at the water tip and letting this node move with the water during run-up. Figures 10.7 and 10.8 demonstrate.

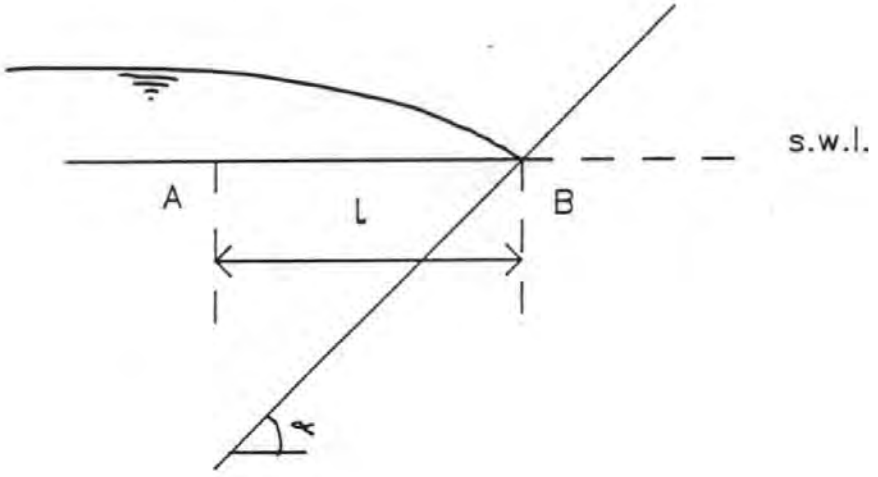

Figure 10.7 Water Profile and End-Element at Time t

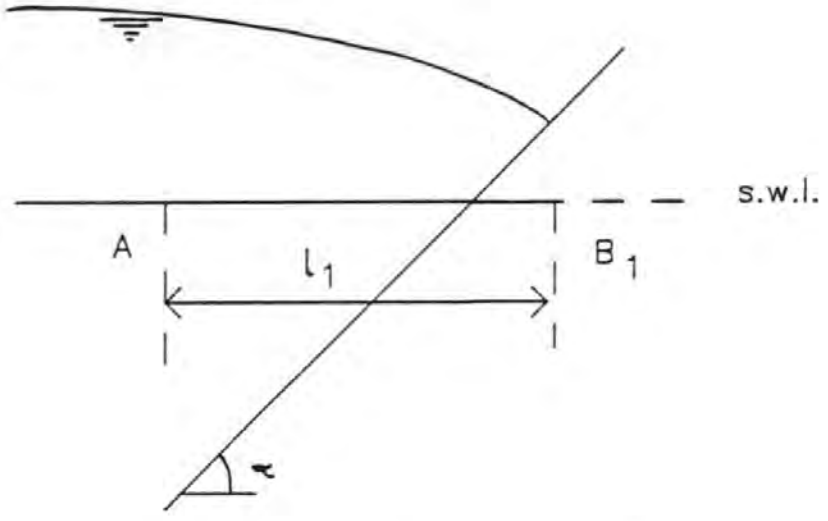

Figure 10.8 Water Profile and End-Element at time t+Δt

If at time t the wave has reached the shoreline and is about to climb up the breakwater slope as in Figure 10.7. The last element (end-element)(AB) has a length l which will be the same as the length of all the other elements. At time (t+Δt) the tip of water has moved up (Figure 10.8). We let the last node move with the tip and take up the position B_1 at (t+Δt). The end element now has a length of l_1.

If the above process was allowed to repeat the end-element would become considerably longer than the other non-moving elements and the solution would become unstable. In order to prevent this we split the end element into two new elements when l_1 exceeds a pre-determined length such as 25% greater than l.

A new node is thus introduced between the existing two nodes. The values at the new node are easily calculated as the following.

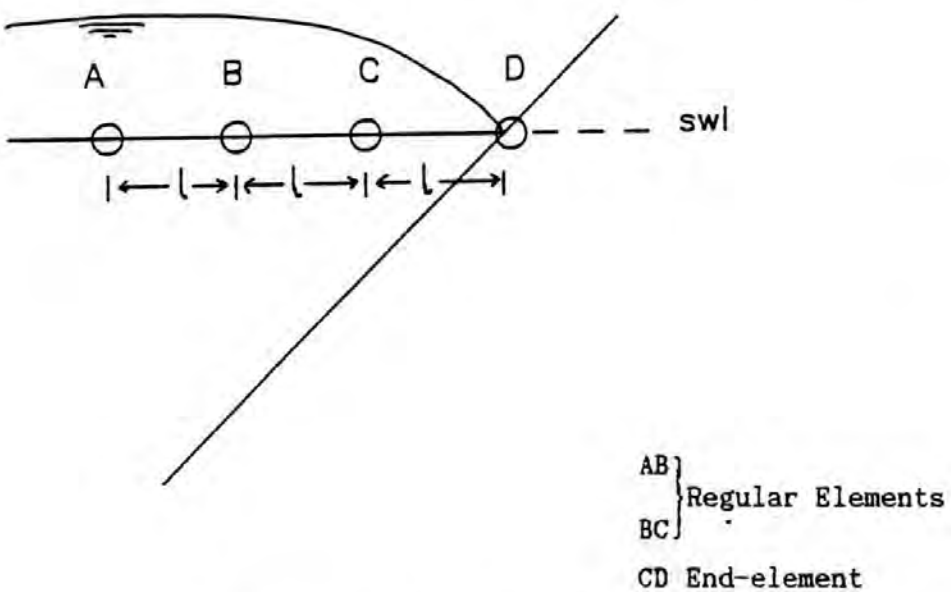

Figure 10.9 Position at time t

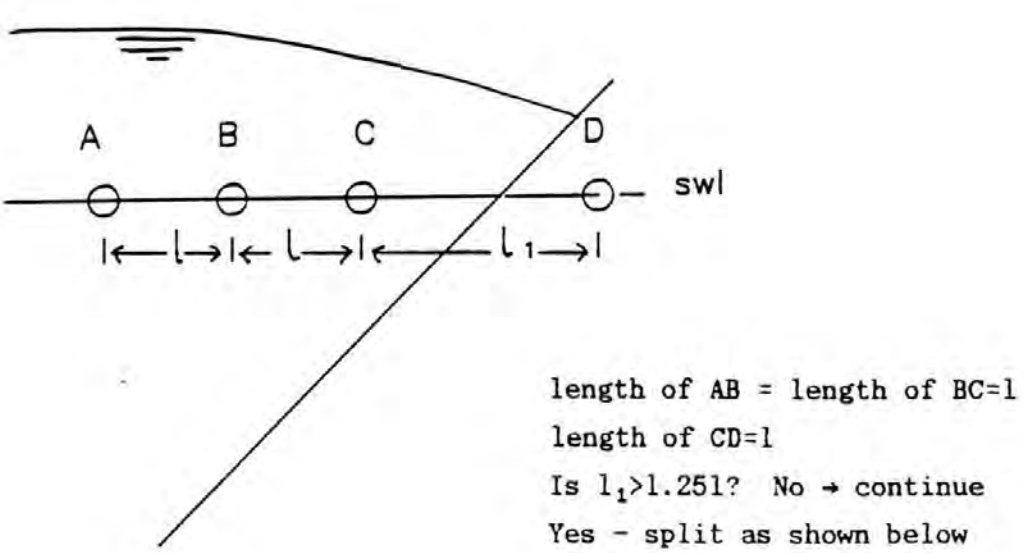

Figure 10.10 Position at time (t+Δt)

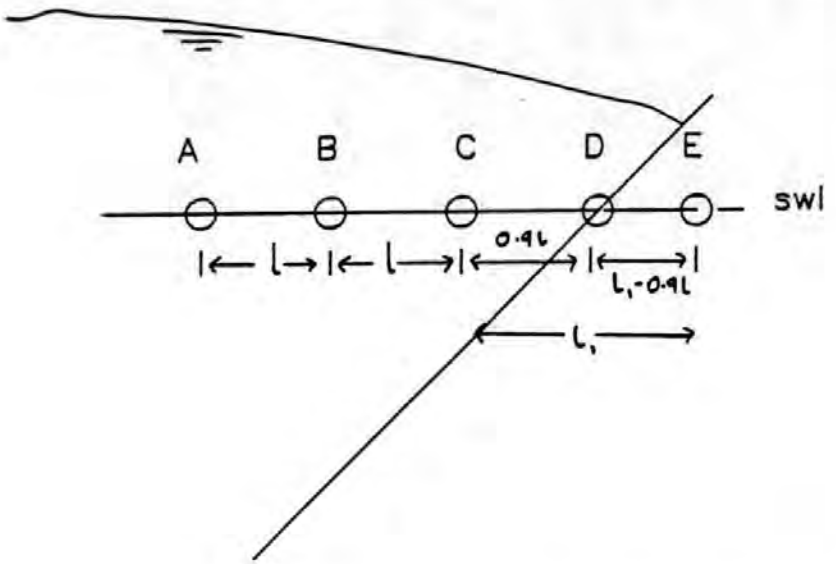

Figure 10.11 Element splitting at time (t+Δt)

The new values at D are given by

$$\left.\begin{aligned} U_D &= U_C N_1 + U_C^i N_2 + U_E N_3 + U_E^i N_4 \\ U_D^i &= U_C N_1^i + U_C^i N_2^i + U_E N_3^i + U_E^i N_4^i \\ \eta_D &= \eta_C N_1 + \eta_C^i N_2 + \eta_E N_3 + \eta_E^i N_4 \\ \eta_D^i &= \eta_C N_1^i + \eta_C^i N_2^i + \eta_E N_3^i + \eta_E^i N_4^i \end{aligned}\right\} \qquad (10.46)$$

where the value of x in the expressions $N_1 - N_4$ and $N_1^i - N_4^i$ is equal to 1, the nodal values at E are, however, the values calculated for the node D in Figure 10.10.

After the split, the element CD remains constant and DE become the end-element as the program continues.

As mentioned earlier an iterative technique is needed to determine the values at the downstream tip. The procedure for this is described below. Let the velocity at the tip be given by U_e and the water level be η_e.

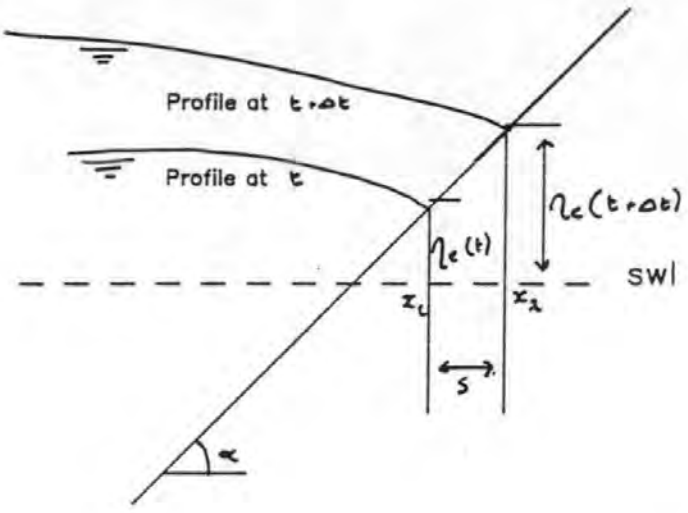

Figure 10.12 Downstream Conditions at time t and (t+Δt)

The horizontal distance travelled by the tip in the interval Δt is S. The mean velocity in Δt is

$$U_m = [U_e\ (t) + U_e\ (t+\Delta t)]/2 \qquad (10.47)$$

where U_e is the velocity at the end node.
Hence

$$S = U_m\ \Delta t \qquad (10.48)$$

It follows that

$$\eta_e\ (t+\Delta t) = \eta(t) + S\ \tan\ \alpha \qquad (10.49)$$

However, to calculate $\eta_e(t+\Delta t)$ we need to know $U_e(t+\Delta t)$ and $U_e(t+\Delta t)$ is unknown until all the quantities at $(t+\Delta t)$ have been computed. This difficulty is overcome within the application of the time step as described in section 10.6.

The value of the velocity $U_e\ (t+\Delta t)$ can be predicted by considering the Lagrangian acceleration of the tip (a_T).

Then

$$U_e\ (t+\Delta t) = U_e(t) + a_T\ (t).\Delta t \qquad (10.50)$$

a_T is also a function of time and within the time-step the mean of the total accelerations $a_T(t)$, and $a_T(t+\Delta t)$ are taken.

The following steps are made within the predictor-corrector steps.

Iteration No 1

$$a_T(t) = \frac{\partial U_e(t)}{\partial t} + U_e(t)\ \frac{\partial U_e(t)}{\partial x} \qquad (10.51)$$

$$U_e(t+\Delta t) = U_e(t) + a_T(t).\Delta t \qquad (10.52)$$

$$U_m = [U_e(t) + U_e\ (t+\Delta t)]/2 \qquad (10.53)$$

$$S = U_m.\Delta t \qquad (10.54)$$

$$n_e(t+\Delta t) = n_e(t) + S \tan \alpha \qquad (10.55)$$

With the value of $U_e(t+\Delta t)$ in (10.52) used as the downstream boundary condition all the values at $(t+\Delta t)$ are computed.

Iteration No. 2

$$a_T\ (t+\Delta t) = \frac{\partial U_e\ (t+\Delta t)}{\partial t} + U_e\ (t+\Delta t)\ \frac{\partial U_e\ (t+\Delta t)}{dx} \qquad (10.56)$$

Mean acceleration at the tip is, therefore,

$$a_m = [a_T(t) + a_T(t+\Delta t)]/2 \qquad (10.57)$$

Hence, the corrected velocity of the tip at $(t+\Delta t)$ is

$$U_e\ (t+\Delta t) = U_e\ (t) + a_m\Delta t \qquad (10.58)$$

$$U_m = [U_e(t) + U_e\ (t+\Delta t)]/2 \qquad (10.59)$$

$$S = U_m\Delta t \qquad (10.60)$$

Therefore the corrected level of the tip at $(t+\Delta t)$ is

$$\eta_e(t+\Delta t) = \eta_e(t) + S \tan \alpha \qquad (10.61)$$

The iterations are continued until two successive values of $U_e(t+\Delta t)$ differ by less than a pre-set tolerance.

10.10 Weir Function

The elements are allowed to split and the downstream tip move until a specified number of elements has been reached. The actual number depends upon the breakwater geometry chosen (see next chapter). Once the pre-set number of elements is reached the wave is considered to have 'overtopped' and an approximation must be made to evaluate the quantity of water which has overtopped. The approximation must also supply the downstream boundary condition in a similar fashion to the technique outlined above.

To calculate the overtopping discharge the crest of the breakwater at an arbitrary point is considered to be a broad-crested weir. By use of the broad-crested weir equation at each time-step a series of instantaneous discharges can be calculated. From instantaneous values a mean overtopping discharge can be calculated.

10.11 Programming Considerations

The numerical overtopping program, OVERTOP, is written as a series of complimentary subroutines called as required from a main control segment. As mentioned earlier the model is written in Fortran 77 and runs on the HP9816S. The use of a microcomputer for a complex program did not present any noticeable problems and quite satisfactory run-times were achieved (see later). Each subroutine performed a seperate operation in the process and some subroutines were used more than once in a single iterative step. A flow diagram for the program is given in Figure 10.13 and a list, together with a brief description of each subroutine is given below (Table 10.1).

To help speed execution time, user input is kept to a minimum, with only the date, test number and number of time steps input each time, to distinguish test results. Other parameters which may wish to be varied, such as water depth, crest elevation etc. are at present altered by 'editing' the program. It would be a relatively straightforward operation to add an 'edit' subroutine to vary the various modelling parameters if required. For development this was not considered due to the speed at which it was possible to 'edit' and recompile the program. One advantage of a microcomputer.

During the debugging and optimisation of the program it was found that the most useful parameter to be able to vary was the number of time-steps since on occasions the program would 'crash' before any data was obtained. All input/output data being printed after all the computations were complete and the results written to disc. This was to maximise the computational capability of the computer. By suitable choice of the number of time-steps, calculations could be stopped just before a 'crash' and the results examined to try and ascertain why the program failed at a particular stage. Most problems with the program were caused by ill-conditioned matrices. The effect and causes of this will be discussed in the next chapter.

One disadvantage of using a microcomputer is that disc access time is relatively slow. Originally the program was written in the conventional manner for Finite Element programs with the element matrices and vectors calculated and written to disc sequentially then read back during the global assembly process. Since the disc access time was slow the program was changed so that each element matrix and vector was written to an internal file within the computer's memory for subsequent assembly. The use of internal files sped up execution time by a factor of four. A typical run of 20 time-steps would take approximately 3½ minutes.

Subroutine		Function
MAIN	-	Controls calling order of subroutines
INIT	-	Initialises all variables and arrays
DATA	-	Contains all relevent input data such as element lengths, water depths etc.
SHAPES	-	Calculates shape functions and their first two derivatives for use in element calcuations, (equations 10.21)
SORTER	-	Decides which value to use depending on iteration number i.e. 'old' or 'predicted'.
CONTIN	-	Calculates continuity element matrix (10.28).
MOMENT	-	Calculates momentum element matrix (10.35).
CONVEC	-	Calculates continuity element RHS vector (10.39)
MOMVEC	-	Calculates momentum element RHS vector (10.40).
GEOMET	-	Calculates slope and gradients for defined breakwater geometry.
ASSEMB	-	Assembles global matrices.
VECASS	-	Assembles global vectors.
SOLUTION	-	Controls the solving of the global equations
BOUNDY	-	Applies boundary conditions.
SINE	-	Forcing function input (or RANDOM for random waves).
GAUSS	-	Gauss elimination to solve global equations.
TIMEST	-	Euler predictor-corrector time step (10.41-10.44)
SPLITER	-	Decides if another element is needed at downstream boundary.
WEIRF	-	Calculates discharge (10.10)
STEPUP	-	Steps model up in time.
RESULTS	-	Prints all input/output and table of η and U values in addition to the overtopping discharge.

Table 10.1 Numerical Model Subroutines.

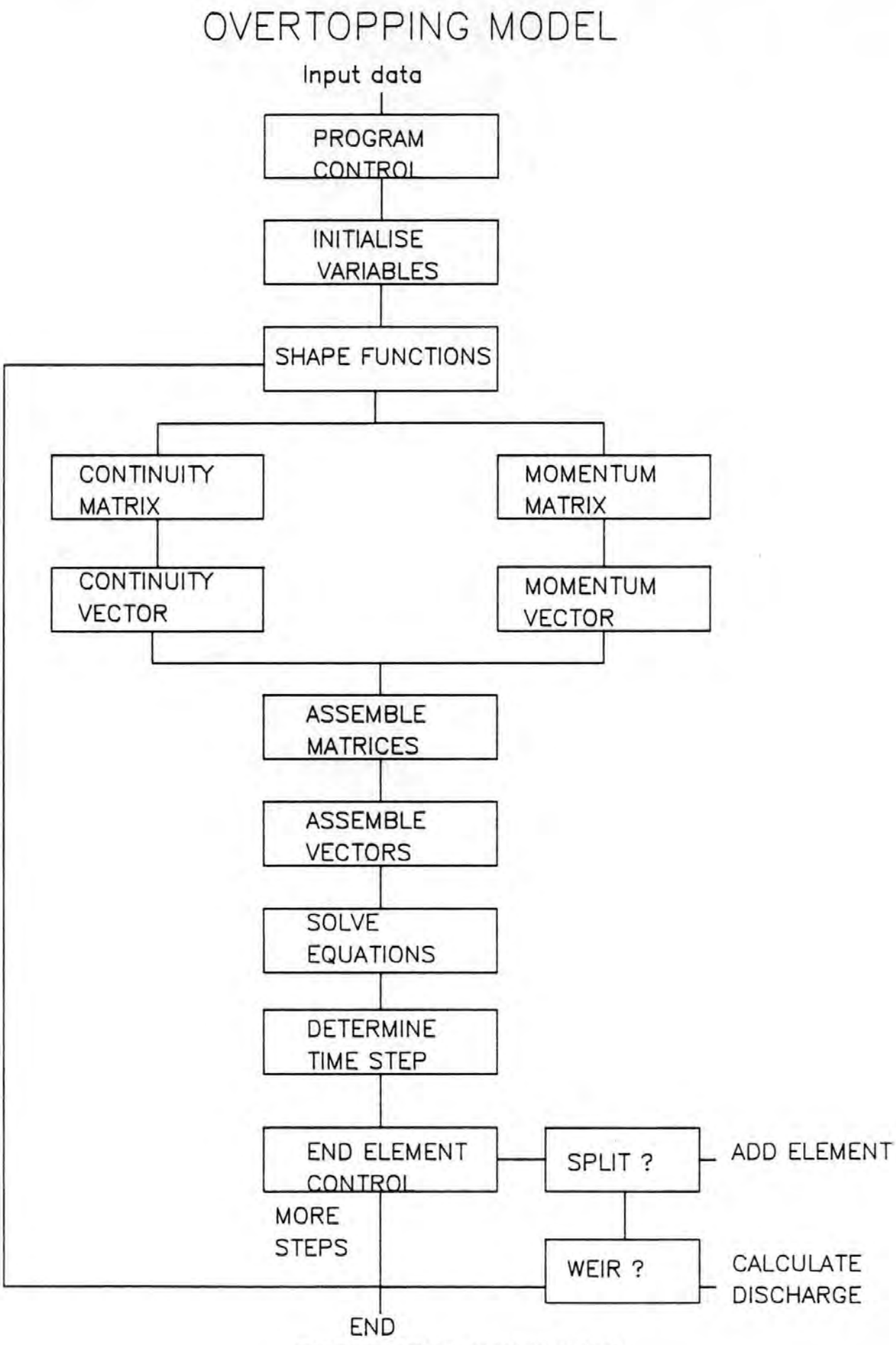

FIG 10.13 NUMERICAL MODEL FLOWCHART

CHAPTER 11

NUMERICAL OVERTOPPING RESULTS

11.1 Introduction

Presented here are the results from the numerical model the theory for which was described in the previous chapter. The majority of the tests were, for simplicity, conducted with the monochromatic sine wave as a forcing function. The results of overtopping discharge for the monochromatic waves were compared to the laboratory wave tests and the overtopping data published in the Shore Protection Manual (1978).

Many of the numerical model tests were conducted with identical physical parameters (i.e. $\bar{H}_s$, T_z) but with different numeric parameters, such as element length or time step. Comparisons of similar physical, but different numeric test parameters are given below. The comparison of numerical parameters allows an analysis of the stabiltiy of the model to be undertaken.

Unfortunately, it was not possible to obtain any meaningful results from a breakwater with a 1:1 seaward slope. The most likely reason for this is that as a breakwater slope steepens, the vertical accelerations become more significant. To obtain reliable results from a 1:1 slope it is suggested that a 2-D model would be needed to take vertical accelerations fully into account. The results presented here are for "simple" breakwater slopes of 1:2 and 1:10. The full range of test parameters is given in Table (11.1).

Slope 1:	H_s m	T_z s	R_c m	M.W.L. m
2	2.0	12.0	1.0	4.0
2	0.4	1.0	0.5	4.0
2	0.4	2.0	0.5	4.0
2	0.4	2.0	0.5	5.0
2	0.25	2.5	0.5	5.0
2	2.0	2.0	1.0	4.0
2	0.4	2.0	0.4	4.0
2	1.0	2.0	1.0	8.0
10	2.0	12.0	1.0	4.0
10	0.4	1.0	0.5	4.0
10	0.2	12.0	0.5	4.0
10	0.5	12.0	1.0	4.0
10	0.4	10.0	0.5	4.0

Table 11.1 Range of Regular Wave Tests for Numerical Model

11.2 Regular Wave Tests

11.2.1 Introduction

The forcing function of the regular wave tests was a sine wave (see section 10.7). The incident wave height at each time step was calculated and used as the upstream boundary condition (section 10.8). Results are presented for the overtopping discharges calculated over a cycle of full wave lengths. The mean discharge Q is given. Also presented are illustrations of the run-up and overtopping of a breakwater shown as time-step increments from a typical computer analysis. The effect of introducing extra elements as the run-up progresses can also be seen (section 10.9).

11.2.2 Overtopping Discharge

Table (11.2) compares the values of overtopping discharge obtained numerically to the physical tests and data in the Shore Protection Manual.

$\bar{H}_s$	Q_{PHYS}	Q_{MATH}	Q_{SPM}
m	m^3/s	m^3/s	m^3/s
0.25	0.022	0.011	0.029
0.40	0.0012	0.035	0.0188
0.50	0.009	0.023	0.013
1.0	0.041	0.005	0.048
2.0	0.500	0.120	0.419

Table 11.2 Comparison of Discharge for a 1:2 Slope

From the above table and Figures 11.1 and 11.2 it can be readily seen that agreement between physical tests and the Shore Protection Manual is good whilst the numerical model results compare less well. Various reasons for this will be discussed later. Figures 11.1 and 11.2 are plots of dimensionless freeboard vs dimensionless discharge, the definitions for which were given in Chapter 9.

As will be discussed later a variation of the numeric parameters (i.e. element length) as opposed to the physical parameters (i.e. wave length etc) also had an effect on the result of the overtopping discharge. The numerical results above are a selection of test results where the combination of numerical parameters appeared to give good stability (see later).

11.2.3 Run-up Profiles

Figures 11.3-11.6 are examples of the run-up on the breakwater prior to wave overtopping. The stage up to the commencement of overtopping is shown. The profiles emphasise the importance of introducing elements at the downstream or landward boundary as run-up progresses. The difference in the size of the problem domain is clearly seen. Also illustrated is the point at which the wave is considered to have 'overtopped'. It is at this location that an estimate of the overtopping discharge is made by use of the weir approximation set out in the previous chapter. Wave overtopping was approximated as flow over a weir by Takada (1974).

The run-up profiles show that whilst the estimate of overtopping may not be accurate the model is at least progressing with time in the expected fashion. This is perhaps best illustrated in Figure 11.7 which is a superimposition of successive time steps.

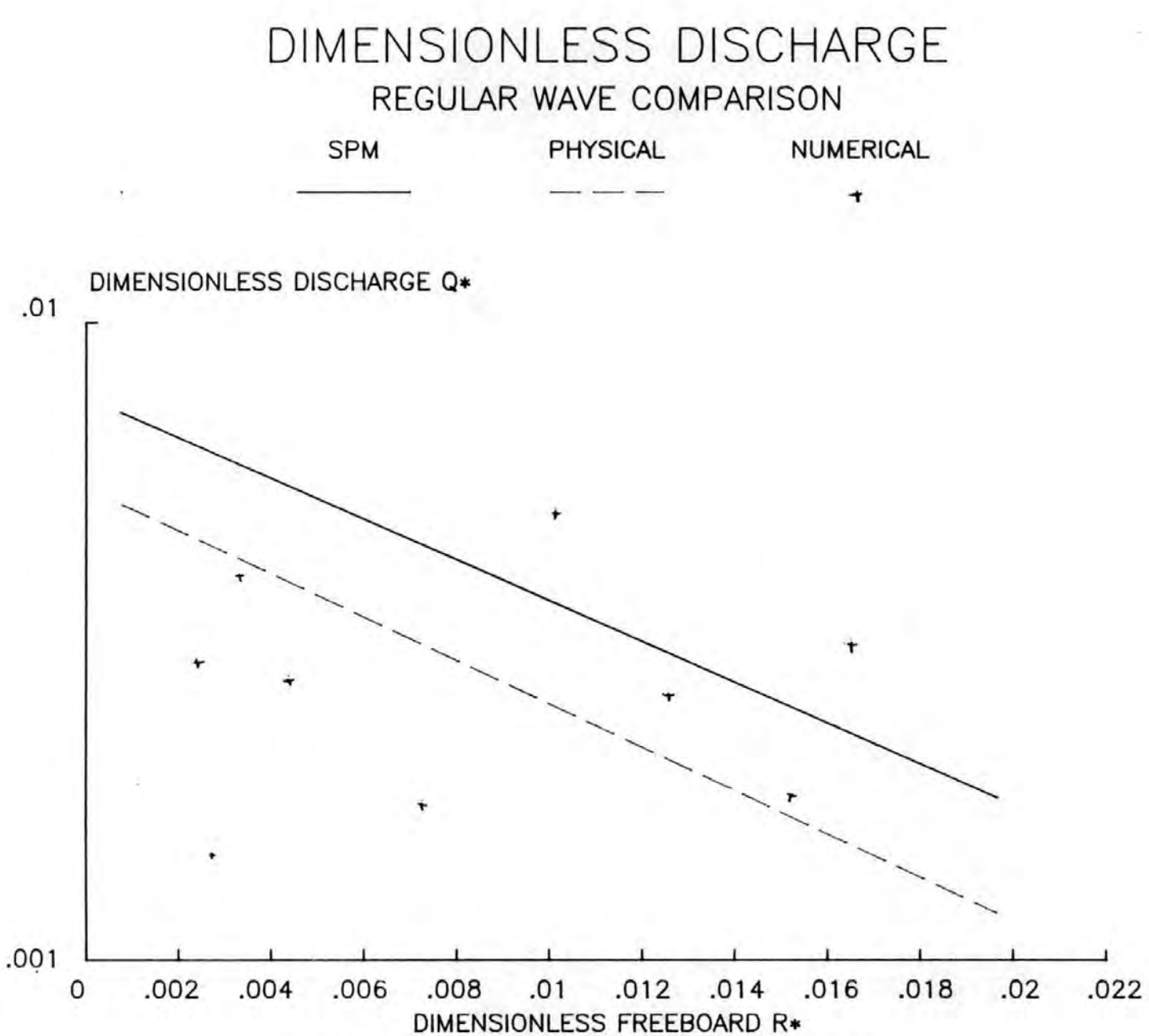

FIG 11.1 DIMENSIONLESS DISCHARGE COMPARISON ON 1:2 SLOPE

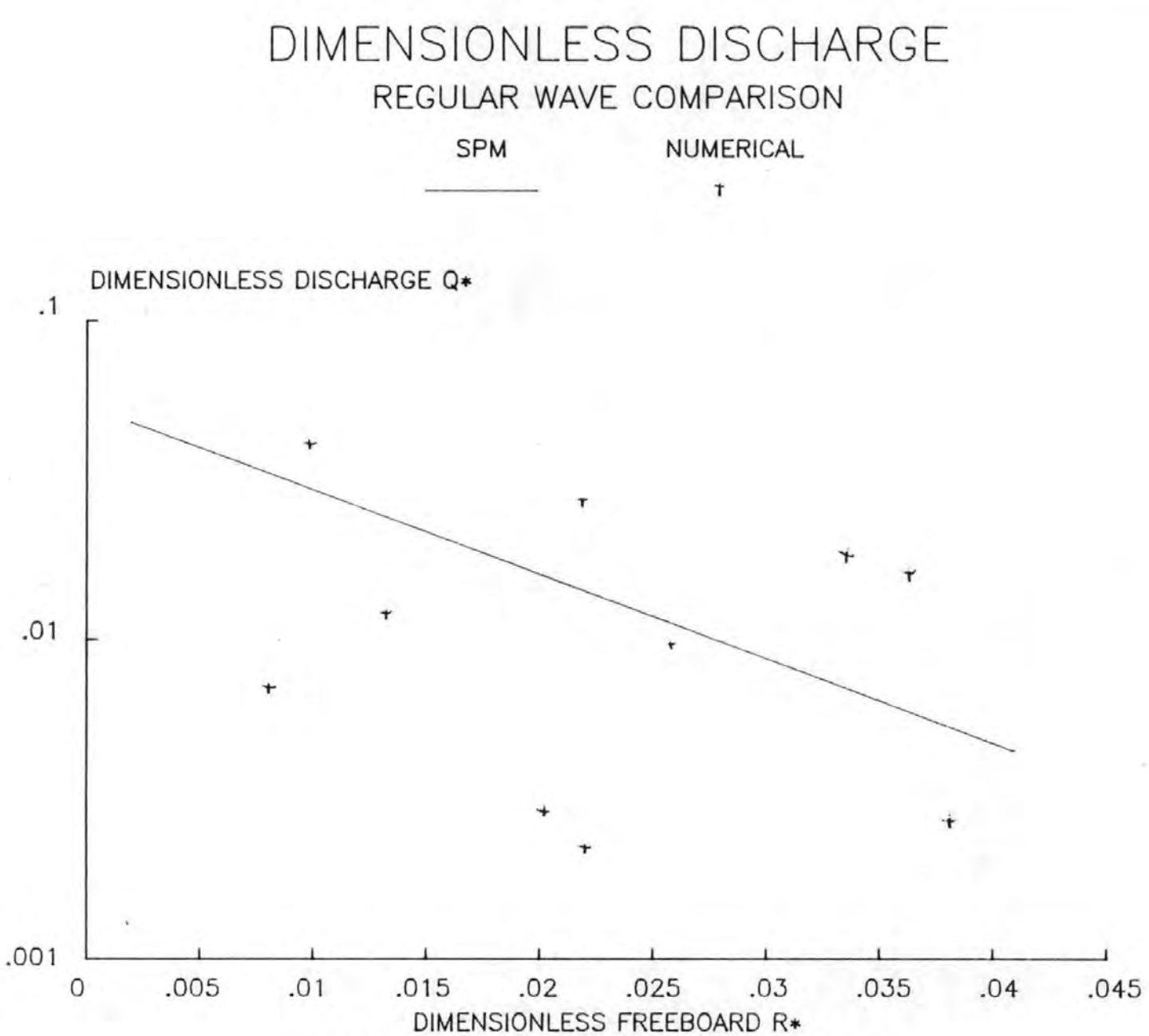

FIG 11.2 DIMENSIONLESS DISCHARGE COMPARISON ON 1:10 SLOPE

NUMERICAL OVERTOPPING MODEL

Slope 1:2
Water depth 4.0 m
Crest elevation : 1.0m
Wave height : 0.40m
Zero-crossing period : 2.0s
Time step : 0.1s
Sine wave
Element length : 1.2m

Date : 30-05-87
Test No 4
Time step(s) shown
4

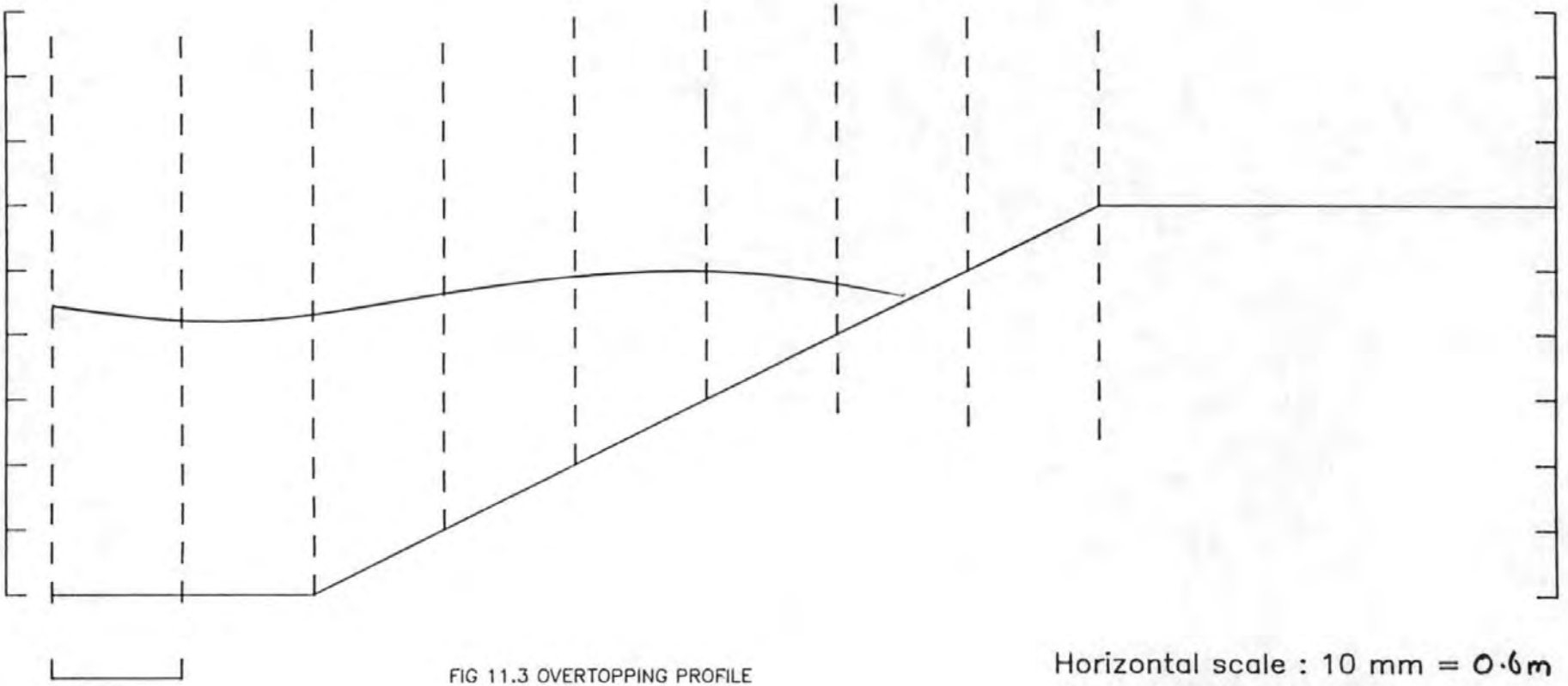

FIG 11.3 OVERTOPPING PROFILE

Horizontal scale : 10 mm = 0.6m
Vertical scale : 10 mm = 0.4m

NUMERICAL OVERTOPPING MODEL

Slope 1:2
Water depth 4.0 m
Crest elevation : 1.0m
Wave height : 0.40m
Zero–crossing period : 2.0s
Time step : 0.1 s
Sine wave
Element length : 1.2m

Date : 30-05-87
Test No. 4
Time step(s) shown
5

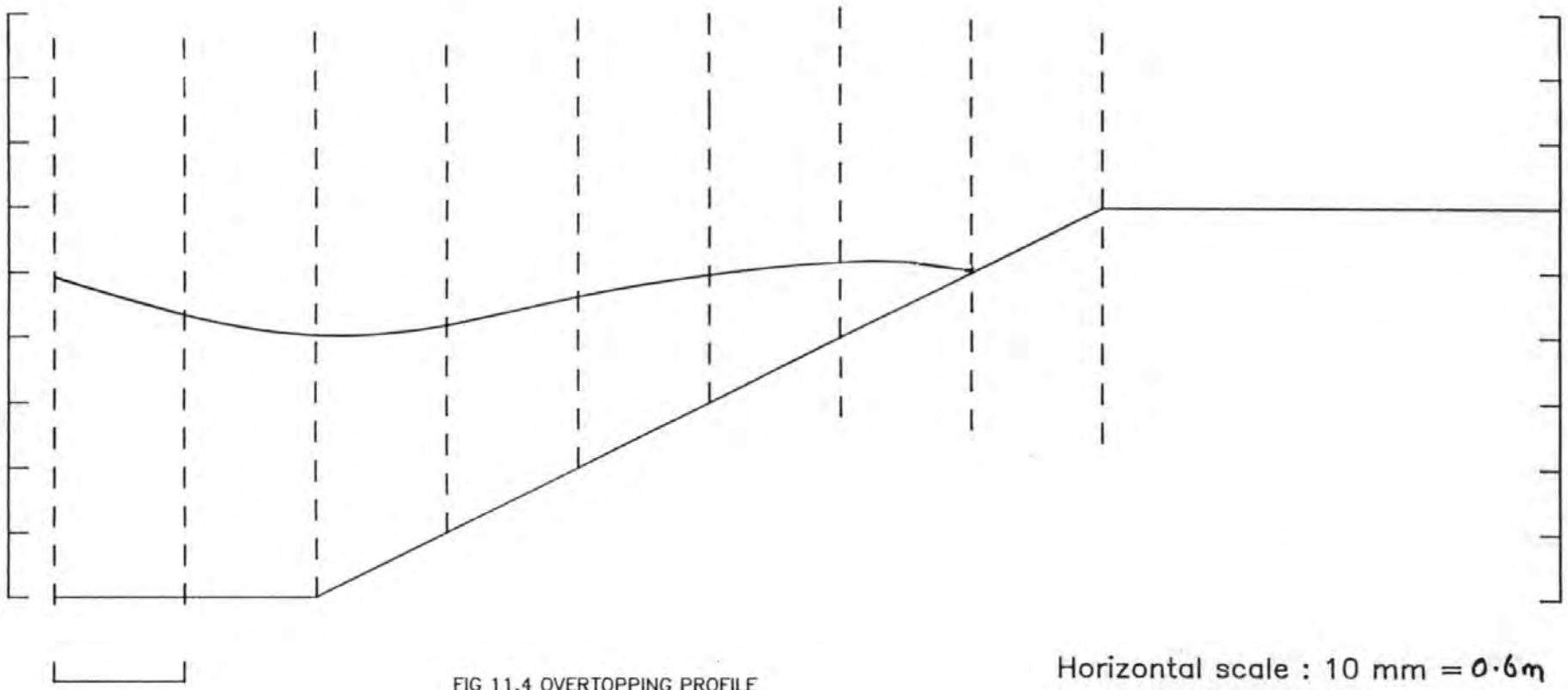

FIG 11.4 OVERTOPPING PROFILE

Horizontal scale : 10 mm = 0.6m
Vertical scale : 10 mm = 0.4m

NUMERICAL OVERTOPPING MODEL

Slope 1:2
Water depth 4.0 m
Crest elevation : 1.0m
Wave height : 0.40m
Zero–crossing period : 2.0s
Time step : 0.1s
Sine wave
Element length : 1.2m

Date : 30-05-87
Test No. 4
Time step(s) shown
6

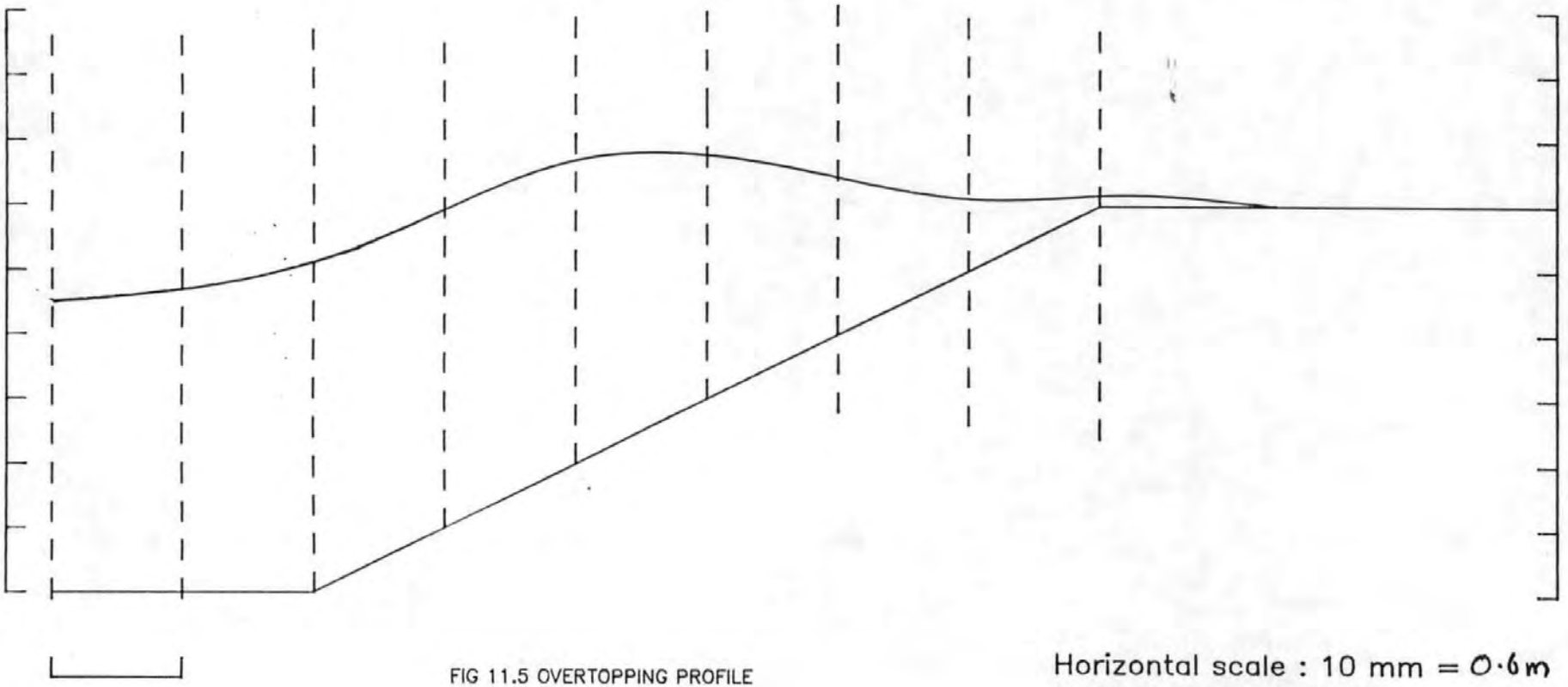

FIG 11.5 OVERTOPPING PROFILE

Horizontal scale : 10 mm = 0.6m
Vertical scale : 10 mm = 0.4m

NUMERICAL OVERTOPPING MODEL

Slope 1:2
Water depth 4.0 m
Crest elevation : 1.0m
Wave height : 0.40m
Zero-crossing period : 2.0s
Time step : 0.1s
Sine wave
Element length : 1.2m

Date : 30-05-87
Test No. 4
Time step(s) shown
7

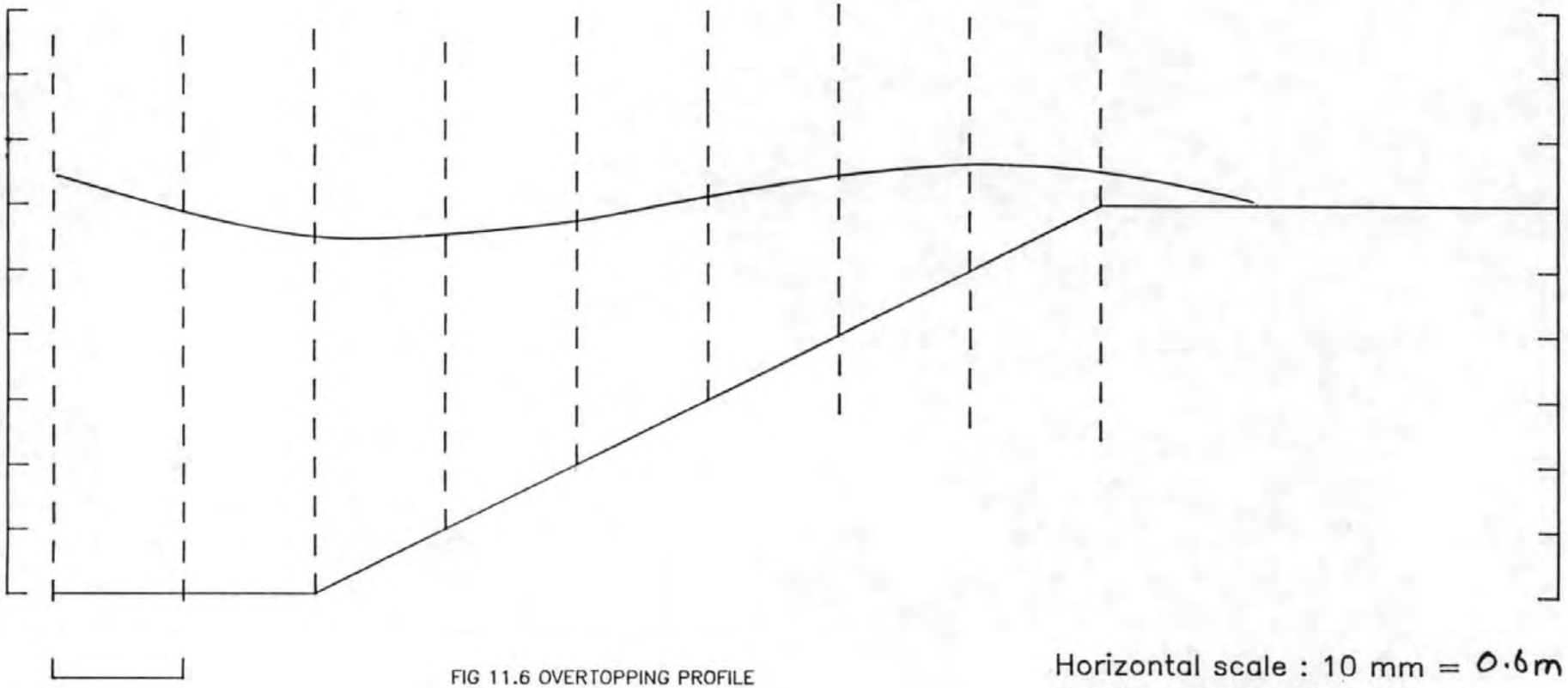

FIG 11.6 OVERTOPPING PROFILE

Horizontal scale : 10 mm = 0.6m
Vertical scale : 10 mm = 0.4m

NUMERICAL OVERTOPPING MODEL

Slope 1:2
Water depth 4.0 m
Crest elevation : 1.0m
Wave height : 0.40m
Zero-crossing period : 2.0s
Time step : 0.1s
Sine wave
Element length : 1.2m

Date : 30-05-87
Test No. 4
Time step(s) shown
4, 5, 6, 7

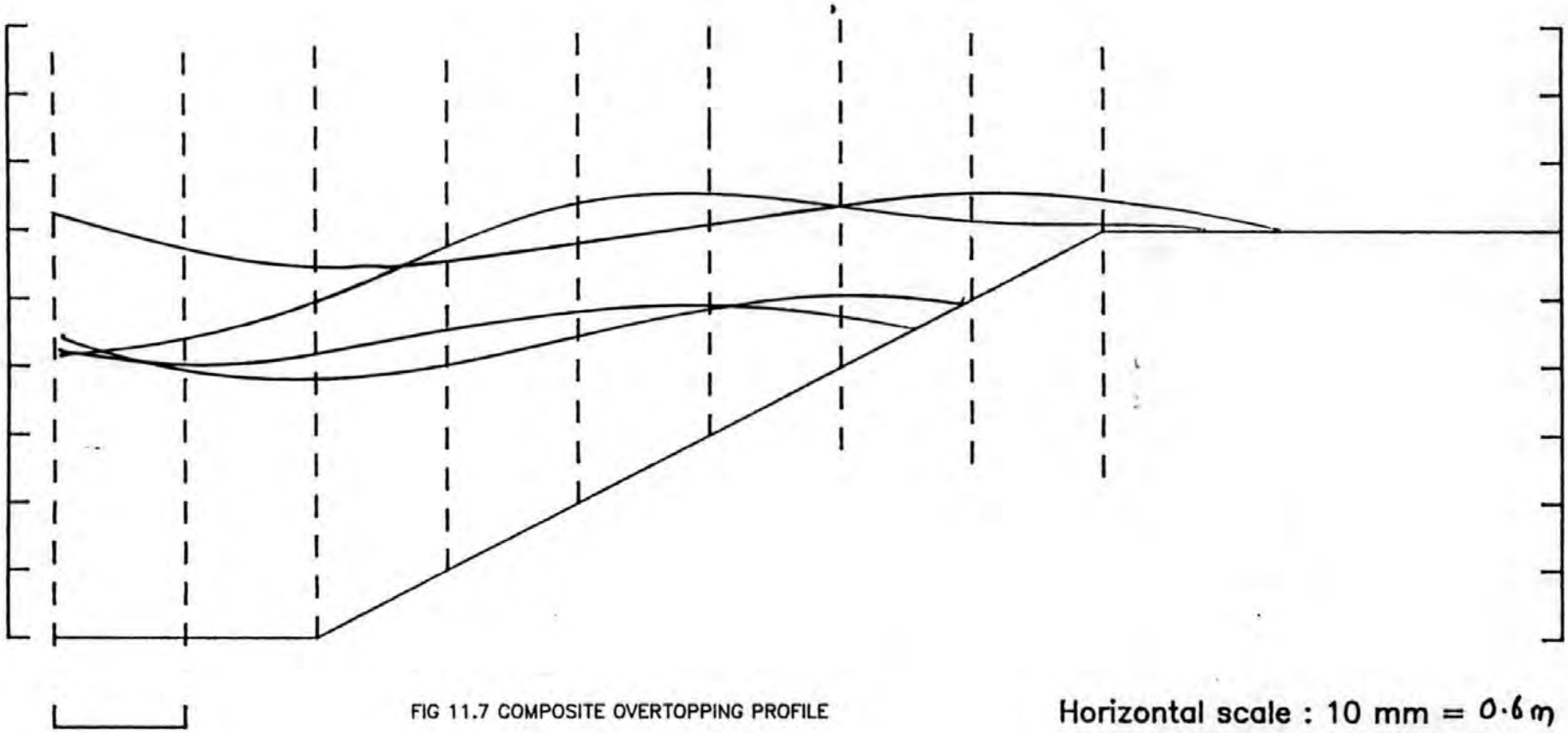

FIG 11.7 COMPOSITE OVERTOPPING PROFILE

Horizontal scale : 10 mm = 0.6 m
Vertical scale : 10 mm = 0.4m

The profiles also illustrate how the model deals with the wave once it has 'overtopped'. It would be quite a complex problem to numerically estimate the quantity of water which returns down the seaward slope of the breakwater. This downrush is known to effect the uprush of the next wave and here is one of the inherent inaccuracies in a model of this type. The problem of reflection will be dealt with later in the chapter.

The 'overtopped' wave is used to provide the downstream boundary condition for the next time step interation as discussed in the previous chapter.

The run-up profiles agree reasonably with physical run-up results (Jensen and Sorensen 1982) as well as other numerical run-up investigations (Stephens et al 1988).

11.2.4 Velocity Results

Since the model was a coupled solution of the momentum and continuity equations, in addition to a solution for water surface elevation, which is more readily interpreted, an estimate of velocity at each time step was obtained. Table 11.3 is an example of the velocities calculated at each node during part of an analysis.

Time	Node								
secs	1	2	3	4	5	6	7	8	9
.2	.0760	.0027	.0004	.0001	-	-	-	-	-
.4	.1715	.0020	.003	.0009	.0004	.0002	.0001	-	-
.6	.0201	.0308	.0115	.0043	.0019	.0008	.0003	.0001	-
.8	.1563	.1732	.0132	.0036	.0018	.0009	.0005	.0002	.0001
1.0	.1275	.1541	.1423	.0433	.0202	.0084	.0037	.0011	.0005
1.2	.1147	.1321	.1500	.1300	.0601	.0231	.0091	.0025	.0021
1.4	.0923	.1212	.1323	.1500	.1365	.0462	.016	.0051	.0072
1.6	.0751	.1001	.1751	.1921	.2100	.2083	.0392	.0661	.0469

Table 11.3 Example Velocity Results

Table 11.3 gives velocities for a 1Hz sinewave with an element length of 2m and stillwater level of 4.00m.

11.3 Reflections

Techniques for dealing with reflections within numerical models were described in Chapter 1. All the various methods are fairly sophisticated and their possible inclusion in the 1-D model was not

justified given the approximate nature of the model (with regard to vertical accelerations). The simplest way to cope with reflection is the same as a possible solution used in physical modelling. That is to make the upstream boundary distant from the structure under test. In a numerical model of the type used here that would involve the addition of many more nodes and element and hence a decrease in the speed of calculation.

With the regular waves used in the numerical tests the overtopping will also be regular and repeatable for each cycle. Thus the model need not be too large to obtain an estimate of the mean wave overtopping discharge.

The presence of reflections may help to explain some of the irregularities which developed after a number of iterations, other possible causes will be discussed later.

11.4 The effect of choice of numerical parameters on the overtopping results

11.4.1 Introduction

In a 'perfect' numerical model of a physical process a change of the numerical parameters used in that model would not affect the physical results. In practice a 'perfect' numerical model is invariably impossible to achieve. By definition a numerical model is always an 'approximation' to the physical system it is intended to simulate. During the development of the overtopping model various different combinations of time-step, element length etc were explored to try and achieve as good an approximation as possible. The following section deals with the numerical optimisation.

11.4.2 Time-step

The need for a small time-step increment must be balanced with the need for efficient computation. Time-steps from 0.01 - 2 seconds were used, with varying degrees of success. If the change was too small (as in the 0.01s case) the residual error in the calculations as a percentage of the change in elevation and velocity became too large. The results from this small time-step were thus extremely unreliable.

In the region 0.05-0.1 seconds very little difference in results was found. Above about 0.5 seconds the time-step increment appeared to become too large for reliable computation from the previous time-step.

The results from various time-steps in the range described above are given in Table 11.4.

Surface elevation at node 4 (metres)

Time	time-step			
Seconds	.01	.06	.10	.50
.01	0			
. 1	0	.0885	.0924	
. 2	.0003	-.4434	-.4076	
. 3	.0012	-.8946	-.8076	
. 4	-.0014	.0090	.0076	
. 5	-.0085	.3328	.3924	-.0014
1.0	-.0261	.5187	.6924	.0127

Table 11.4 Comparison of Surface Elevations for Various Time-steps

In the above table, values between exact time-steps were computed by linear interpolation.

11.4.3 Number of Elements and Element Length

More elements in the same problem domain should lead to a more accurate representation. There is also the trade-off of the need for increased memory requirements and a subsequent increase in execution time. Naturally an increase in the number of elements leads to a decrease in the element length. Since the Finite Element method calculates values at each node (at both ends of each element) the smaller the element length the more accurate the solution should be.

Tests with a discretisation of five and six elements showed no discernable difference in the result for the overtopping discharge Q. Fig. 11.7 shows the run-up of a sinewave computed with five and six elements in the same problem domain discretisation.

11.5 Ill-Conditioning

The effect of ill-conditioning has been mentioned at various earlier stages as a cause of computational problems. The presence of large and small elements in a matrix results in very large and very small

eigen values for the global matrix. Due to finite machine precision, the resulting accumulation of round-off errors causes loss of significant figures. The most frequent result is a divide by zero error with the Gaussian elimination stage of the solution of the global matrices (Burnett 1987).

One solution to the ill-conditioning problem is to solve the various parts of the global problem in smaller refined meshes. The stability of the model can be improved by the use of more sophisticated pivoting to solve the simultaneous equations (Johnson and Reiss 1982).

Ill-conditioning was a major source of problems with the development of the numerical models and it was only by careful selection of numerical and physical parameters that the results were obtained. Even in some of the more successful runs of the model the total desired number of time-steps was not achieved due to a 'divide by zero' error. In general in these cases the results appeared to be valid up to two time-steps before the error occurred. Table 11.5 shows the results of water surface elevation just prior to a program failure.

time-step	Node				
	1	2	3	4	5
23	.0941	.2817	.8195	.8946	.0603
24	.0901	-.3391	1.6761	-4.9290	7.7948
25	.0851	-3.6831	6.1533	-5.3328	23.1568

Table 11.5 Results up to Run-time error 'divide by zero'.

11.6 Validation, Calibration and Accuracy of the Numerical Model

The numerical model was as much as possible calibrated against the results from the physical overtopping tests. During the initial trials of the model certain diagnostic output was written to the line printer (such as values of boundary conditions, errors in iterative steps etc). and these values were, where possible, checked against hand calculations.

The results of run-up profiles shown of the previous pages indicate that the solution of the 1-D momentum and continuity equations was giving a realistic approximation to wave run-up and overtopping. The numerical results as tabulated are less reliable and the model is not particularly accurate. Possible reasons for the inaccuracy include

the effects of the vertical accelerations on the fairly steep sloped breakwater (i.e. the 1-D approximation of the model) and the neglect of any allowance for frictional effects. Possible improvements are discussed in section 11.7.

11.7 Possible Improvements to Model

11.7.1 Numerical Improvements

An improvement which could be made to the existing model in order to solve the instability problem would be a more complex routine for the solution of the global matrices. At present standard gaussian elimination is used to solve these equations. More sophisticated options include full or partial pivoting in the gaussian elimination process or a relaxation technique (Johnson and Reiss 1982).

Another area in which it may be possible to obtain a more accurate solution include the weir approximation to calculate the overtopping discharge.

Whilst the improvements mentioned above would improve the accuracy and applicability of the present 1-D model the results for the 1:1 slope model suggest that an altogether more complex model is required to solve this problem (see below).

11.7.2 Physical Improvements

As discussed above the developed model was a simple 1-D interpretation of an extremely complex 3-D phenomena and many possible refinements could be added if required.

The Shore Protection Manual (1984) suggests that a wind correction factor of 1.4 is applied to all overtopping calculations. The wind correction factor is empirically derived and would equally need to be applied to the physical test results. As mentioned above frictional losses were also not considered.

The limitation of a 1-D model became apparent during the development of the model and thus is reflected in the often poor results obtained.

It is suggested that to obtain a significant improvement in accuracy a 2-D model is developed. The 2-D model would have the major advantage of including the vertical accelerations within the solution system instead of making an allowance for them in the momentum equation as is done here.

The 2-D model would have the great advantage that complex geometries (e.g. bermed breakwaters, sloping beds) could be easily included in the solution.

A 1 or 2-D model could also have the roughness of armour units included.

A major feature which may be of interest would be to superimpose a tidal cycle into the program. The variation of mean water level would then become an additional variable in the problem. This may be of use to the design engineer who wishes to obtain estimates of overtopping discharge over a tide cycle. If he is only interested in the maximum overtopping discharge then a tide cycle would be of no significant interest.

11.8 Conclusions

A 1-D finite element model developed and implemented on a microcomputer has been designed to approximate wave overtopping.

The 1-D model as developed gives a reasonable representation of run-up on the 1:2 breakwater slope, but it was not possible to obtain results for a 1:1 slope breakwater. The estimates of overtopping of discharge does not compare favourably with the results of the physical model tests and results published in the Shore Protection Manual. The results do, however, show that a finite element solution to the 1-D momentum and continuity equations is a satisfactory approximation to the complex and varied problem of wave run-up and overtopping.

Results from various combinations of physical and numerical parameters have shown the dependance, or otherwise, of the solution on these parameters.

CHAPTER 12

SUMMARY AND CONCLUSIONS

12.1 Conclusions

A wavemaker facility which consists of twin wedge paddles has been developed. The paddles operate under an electro-hydraulic system. The motion of the paddle is controlled by a BBC microcomputer. The computer runs digital software to generate a regular or pseudo-random wave as required. The use of a microcomputer and digital to analogue converter proved highly effective in operating a paddle of this type.

The random wave generation is achieved with a software implementation of a binary feedback register. The software implementation proves a simple and effective way of producing a pseudo-random signal. The output is also easily tailored to the users specific requirements.

A comprehensive data acquisition system has been created. Based upon twin wire resistance wave gauges the analogue voltage is converted to a twelve bit digital signal for collection, storage and analysis. The data acquisition system can simultaneously collect up to 4k of data from up to eight wave gauges. The data is calibrated to wave height by a least squares regression analysis which also provides a check on the linearity of the wave gauges. Provided the gauges are kept clean, good linearity is achieved. Examples of contaminated gauges are given in the text.

The software to control data acquisition has been written to be sufficiently flexible in its uses as well as being easy to use. To compliment the data acquisition programs a menu-driven analysis suite has been written.

The analysis programs all use the digital wave records in the same form as they are stored by the acquisition software, thus data processing is kept to a minimum. Various statistical and graphical routines are available, all of which have been thoroughly verified, to produce results suitable for interpretation of wave data.

The most important analysis procedure is the Frequency Response Function method of analysis. This procedure is a method to determine incident and reflected spectra from a composite wave train. Simultaneous measurements of the composite wave train at two or more known points in the channel are needed for the analysis.

The Frequency Reponse Function method has been shown to allow a more accurate representation of the wave climate present in the channel. The incident spectrum is a much more representative standard to adopt for comparision and interpretation. Reflection data is also obtained. Use of the Frequency Response Function software was particularly applicable to the testing, and appraisal of the absorption system designed for the wave maker.

It is also shown that an accurate representation of the incident spectrum over a wide frequency range can be derived with the use of only three wave gauges provided the spacing of the gauges is calculated correctly.

The ease of use of the data acquisition and analysis software suite together with its speed and portability has demonstrated the particular advantages of a system based around a powerful microcomputer. The excellent graphical output was made use of to aid interpretation and presentation of test results. The laboratory wave generation facility is now supported by a wide ranging, user-friendly, menu-driven software suite able to cope with most of the anticipated situations for which the wave facility was designed. Manuals describing the software have been written to help the inexperienced user.

The paddles were commissioned at the start of the project and the dynamic response of the paddles over a wide range of sinewaves, from 0.1Hz up to the limit imposed by wave breaking, determined.

A transfer function of input signal voltage to resultant incident wave height was found.

The incident wave height was determined with an analysis procedure based on a wave record from a traverse of a length of the channel under steady-state conditions. The spending beach at the opposite end of the channel to the paddle was found to produce approximately 5-10% reflection in the frequency range tested.

A paddle transfer function was determined for three water depth, 0.6m, 0.8m and 1.0m. The transfer functions at 1.0m and 0.8m were almost identical, the 0.6m transfer function was, however, much lower. This difference is most probably due to the front face of the paddle being less immersed in water with a depth of 0.6m. Although the 0.8m water depth also results in less paddle face immersion the depth may be sufficient for a further increase to have no effect. If the depth of immersion is greater than half a wavelength then the particle orbital motion will have reduced to zero.

The transfer functions were compared to a theoretical transfer function for a wedge paddle. The comparison is shown graphically in chapter 5. The theoretical transfer function shows a slightly higher incident wave height for a given signal voltage up to 1Hz where the two lines coincide. This is much as would be expected since the theoretical transfer function makes no allowances for losses in the system due to friction or water moving between the sides of the paddle and the channel walls.

The results of the optimisation of the paddle and the transfer functions were presented to Hydraulics Research Ltd. to be incorporated in the design of a wave absorption circuit board for the paddles.

The absorption circuit was designed on feedback principles and essentially involves incorporating an extra loop in the paddle control signal. Reflections from a structure at the opposite end of the channel to the paddle are detected at the paddle front by means of a paddle mounted wave gauge. The paddle wave gauge consists of two twin wire resistance gauges wired in series to average any variation in water surface elevation across the width of the channel.

The voltage signal from the paddle mounted wave gauge is fed back into the paddle control loop and compared to the original input signal. The difference in the desired and the actual signals is used to drive the paddle. Thus any re-reflections are prevented from being generated at the paddle. Essentially the paddle makes waves equal and opposite to any reflected waves as well as still generating the desired input signal.

The advantages of an absorption system based around a paddle mounted wave gauge working under feedback principles is the ease with which it can be incorporated into an existing facility. With relatively inexpensive modifications any traditional wave facility can benefit from the techniques described.

The absorption system has been comprehensively tested under a variety of regular and random wave conditions. The initial regular wave tests with the spending beach in place demonstrated that the addition of an absorption feedback loop made no significant difference to the dynamic characteristics of the paddle.

To test wave absorption under a more demanding environment a system of wavescreens was built. Varying degrees of reflection could be chosen up to a 'full' screen which gave approximately 80% wave reflection. Higher degrees of reflection could have been used but it would have become impossible to obtain any results with absorption 'out' for comparison purposes.

The results from the regular wave tests were obtained with the wave envelope procedure mentioned above in the original calibration of the paddle. The data acquisition software written, together with a specially written program to perform the envelope analysis, made the processing of results a much less laborious task. The testing program was thus much speeded up.

By suitable choice of frequency for the input signal it was possible to reproduce the condition of forming a node or antinode at the paddle front (an antinode must always be formed at a vertical impermeable barrier such as the 'full' wavescreen). With no absorption system the conditions mentioned above lead to resonance and eventually the water will wash over the sides of the channel.

With the wave absorption system active the resonant condition does not occur. After a suitable period (the time for waves to propagate to the wavescreen and return to the paddle), a steady state is achieved.

When the frequency is chosen to reproduce an antinode at the paddle front the paddle motion reduces to negligible levels. That is there is maximum vertical water excursion and minimum paddle horizontal movement. The opposite is true when a node is formed at the paddle.

The transfer function for a 'full' wavescreen of input control voltage to wave height is smoothed out by the absorption system and the conditions of resonance are prevented.

Use of a Spectrum Analyser also showed how much 'cleaner' with wave absorption the signal was. Nearly all the high frequency noise on the signal was removed by the wave absorption system. The effect was visually noticeable in the laboratory and the Spectrum Analyser confirmed the result.

Subsequent to the regular wave tests on the absorption system a series of tests with random waves was conducted. Here the data acquisition and analysis system was invaluable. The Frequency Response Function method of analysis was used to determine incident and reflected spectra from the composite wave train.

All the results showed that when the absorption system was switched 'in' the incident spectra (from the same spectrum input signal) were very similar or the same, no matter what the degree of reflection was. Thus a test with a 'full' wavescreen had the same incident spectrum as a test with up to 80% less reflection.

The varying degres of reflection was demonstrated by the difference in the estimates of reflected spectrum. Spectra were chosen with peak frequencies to cause the resonant conditions mentioned above and no deterioration in performance was detected.

When the incident spectra were compared to the theoretical spectra used as an input signal the correlation was very good. There was a slight loss of the higher frequency components of the spectrum. This may be due to the inability of the paddle to respond quite as efficiently at the higher frequencies or due to the not ideal filter design described in Chapter 6.

With the wave absorption system operative re-reflections are removed from the channel and a highly stable incident wave train produced. It is thus possible to generate the same incident wave conditions irrespective of the degree of reflection within the channel. The channel is then, in effect, 'semi-infinite' in that the length of the channel is not a variable to be considered in the test.

Wave absorption allows much closer operational control on tests and test conditions. The repeatability of tests and tests upon different structures with the same incident wave conditions is both easier to arrange but is also more accurate.

A wave absorption system based on feedback principles has been derived and implemented, the results obtained being very encouraging.

Laboratory equipment has been designed to measure wave overtopping over simplified breakwaters. The equipment was designed to be able to cope with the maximum amount of wave overtopping expected based on previous, similar, model tests. A system of an interconnecting overflow weir and a calibrated sharp-crested weir was used to measure the overtopping quantities. Once the water had been measured it was returned to the channel to try and keep the mean water level as constant as possible during a test.

The breakwaters constructed were of a simplified type, in that no attempt was made to model slope roughness or porosity. Seaward slopes of 1:1 and 1:2 were used.

The results of the tests were analysed with the data acquisition and analysis system set up earlier. Wave absorption was used in the majority of the tests so that the tests could be more closely controlled. The use of wave absorption would provide a further appraisal of that system and would also highlight any deficiencies in

the system not already observed. After more than 100 wave overtopping tests no shortcomings or faults (other than those previously mentioned) were found. The absorption system allowed the tests to be much more accurately 'targetted' and controlled. The benefit of a wave absorption system was apparent throughout the test programme and use of a similar system in all future breakwater tests is highly recommended.

The wave overtopping tests were intended to compliment, rather than duplicate, tests which had already been undertaken. With this in mind, all the tests were performed on low-crest breakwaters, that is breakwaters with their crests at or just above mean water level. Most tests were undertaken using random waves. The results of the tests were compared to existing results, in particular those of Owen (1980) and the Shore Protection Manual (1984).

The comparison of results was made with the results of tests conducted with a test length equal to the repeat length of the random sea spectrum used and tests where the spectral repeat length was much greater than the test time.

The software used to generate the random spectra was modified to allow alternative selections of feedback connections to produce different random wave trains with identical statistical properties.

A quantative comparison of the results from various 'full-length' spectra with identical physical conditions indicated that, within the general scatter of results expected from laboratory experiments, there was no difference in the total overtopping discharge measured. This result implies that wave groups do not have a significant effect on the total discharge for the given sea conditions, although it is known that the overtopping 'potential' of a single wave is affected by the preceding wave. The results suggest that wave overtopping should be quantified against wave spectra, rather than wave height although for individual waves this is, of course, not practical.

The tests conducted with segments of 'long' spectra not unsurprisingly gave unpredictable results although they were consistent with the presentation of the results in a dimensionless form (see below).

Owen (1980) presented his wave overtopping results in terms of two dimensionless parameters; the dimensionless freeboard

$$R^* = \frac{R_c}{H_s}\sqrt{\frac{S}{2\pi}}$$

and the dimensionless discharge $Q^* = Q/(T_z g H_s)$

where S is wave steepness = H_o/L_o
R_c is crest elevation above mean water level
Q is measured overtopping discharge.

The results obtained here were presented in the same way to allow comparison to Owen's work, although there is very little overlap in areas tested the results of the 'low' breakwater tests do correlate very well with an extrapolation of Owens work. The freeboard/discharge curves for both the 1:1 and 1:2 seaward breakwater slope give good agreement.

Wave reflection measurements made from the estimates of incident and reflected spectra compare very well with estimates of reflection published in the Shore Protection Manual (1984). The comparison is not as good for tests conducted with wave absorption 'out'.

Two measurements of the overtopping discharge were made, the main measurement was made from a wave gauge measuring the flow over the calibrated sharp-crested weir. The gauge was included in the data collection system and a programme was written to calculate the total discharge during a test. A further wave gauge was mounted on the crest of the breakwater to note and count, the occurrences of overtopping waves.

It was found that if this gauge was calibrated then a good estimate of the discharge could be obtained by calculating the volume of the wave as it passed the gauge. It is suggested that this may be a way of making full-scale wave overtopping measurements. In all but the simplest 1-D situations an array of gauges would be needed but even with a limited number of gauges (or pressure transducers) a reasonable estimate of wave overtopping could be made.

The number of waves overtopping (as a % of total of waves in the record) was also plotted and compared to existing results. The results compared favourably, but did highlight a recurrent problem with coastal wave tests and analysis, that of accurately defining the measurements and test conditions.

In many previous reports on wave run-up and overtopping various parameters such as: number of waves in a record, or locations (inshore or offshore) where measurements were taken are not given. This makes comparison of results extremely difficult.

Accurate wave overtopping measurements have been made within a laboratory environment regarded conventionally as unsuitable for such measurements. The inclusion of a wave absorption system into the paddle control loop has created a facility eminantly suitable for such a purpose. The on-line micro-computer based data acquisition and analysis system also proved to be an ideal tool within the laboratory environment.

A numerical model of the wave overtopping process has been developed. The model is a 1-D space/time solution of the momentum and continuity equations. The space domain is handled with non-linear 1-D Finite Elements whilst the time incrementation is achieved with a predictor-corrector Finite Difference iteration. The Finite Element solution of the continuity and momentum equations yields the time derivatives of water surface elevation and water particle velocities. The predictor-corrector step gives the values of water surface elevation and water particle velocity.

To prevent the model becoming too complicated, assumptions were made concerning the flow, such as the assumption of an inviscid and incompressible fluid. Bed friction was also neglected.

The fairly steep breakwater slopes under consideration meant that the vertical water particle accelerations would be significant. In order to compensate for this, whilst still retaining a 1-D model the 1-D momentum equation was modified to include a term for the vertical accelerations whilst not including them in the integration. The success of this assumption was dependent upon the slope (see later).

The model was implemented on the micro-comupter used in the laboratory work and this highlights the versitility of such a machine in the complete cycle of events from data collection through to numerical simulation.

The model was set-up to introduce a sine wave at the upstream limit of the model, into still water. Additional elements were introduced at the downstream boundary as the water moved up the seaward slope of the breakwater. At a predetermined location on the breakwater crest the wave was assumed to have 'overtopped' and no additional elements introduced. A routine to calculate the discharge at this location, based on an overflow weir approximation, also handled the computation of the downstream boundary condition.

Certain combinations of the numerical parameters, such as element length, time step etc., caused instability within the model and time had to be spent on obtaining a 'balanced' set of numerical parameters to obtain results. In the event it did not prove possible to obtain any meaningful results from the numerical model with the 1:1 slope. It is believed that a slope of that great a steepness needs a two-dimensional model representation since the vertical water particle velocities will have a large significance on the computations. A stable solution to the problem of run-up and overtopping on the 1:2 slope was obtained.

Various comparisons of the results of the 1:2 breakwater slope problem were performed. Results have been presented for comparison both with the physical laboratory tests, previous work and the data presented in the Shore Protection Manual.

The run-up up the breakwater slope was predicted satisfactorily by the model, thus proving that the theoretical basis for the model was well founded, at least when the seaward breakwater slope was not too steep. The limit to which the model is valid was in the region of 1:1½. It appeared that with a slope greater than 1:1½ it was not possible to obtain any results due to numerical instability.

Whilst the run-up profiles modelled the physical situation reasonably, the estimates of overtopping discharge were not as accurate. Reliable results were obtained with a comparison between the various model runs. The good comparison between model runs illustrates that the ultimate choice of numerical parameters is not critical provided that a stable combination of parameters can be found.

If the time step in the model was reduced too much then machine round-off errors became larger than the incremental changes in the main variables and no solution was possible.

In order to obtain a better estimation of overtopping discharge a more accurate method than the broad-crested weir approximation needs to be found. Any improvement is likely to be a much more complex solution than the simple approximation used.

The model gives a good representation of run-up and whilst wave overtopping has been modelled a better solution for the discharge calculation is needed.

12.2 Recomendations for Future Work

12.2.1 Laboratory system

Wave absorption could be improved and made far more 'user-friendly' than the present prototype system by including some means of direct calibration with a sensitivity meter incorporated in the hydraulic system control.

A redesigned paddle wave gauge would also eliminate some of the vibration problems at low frequencies and small movements. (The vertical excursion of the paddle has now been included in the wave absorption filter circuit in a subsequent absorption system).

The graph of loop gain (Chapter 6) illustrates the ability of wave absorption to be highly effective with a less-than-perfect filter design. With a little more analysis is would be possible to design a filter which matches the paddle characteristics much more accurately.

Until a reliable, comprehensive computer model of overtopping becomes available there will always be a need for more physical breakwater studies. Some form of full-scale measurement is also desirable from a calibration point of view.

12.2.2 Numerical Model

It appears that the 1-D solution of the momentum and continuity equations have been taken to their limit of applicability in this study. A 2 or even 3-D model of wave overtopping would be a valuable engineering tool in breakwater and seawall design.

The overtopping process is highly complex and a major effort would be required to produce the 'all-embracing' model required.

APPENDIX A

COMPUTER OUTPUT

A1 Introduction

Appendix A contains examples of computer analysis output for the main data acquisition and analysis programs as well as the Numerical Overtopping program. In addition a list of the statistical routines and data file handling routines is given. An idea of the typical execution times of the more frequently used complex analysis programs will be found at the end of Appenidx A.

A2 Statistical Analysis Routines Available

After a basic statistical analysis of mean, standard deviation, skewness, kurtosis, maxima and minima has been carried out prior to any spectral analysis from the program suite driven by MASTER1 the following routines can be accessed.

Menu Name	Subroutine Name		Action
TRANSFORM	STAT02	-	Transform data to zero mean value
NORMALISE	STAT03	-	Normalises data
STANDARDISE	STAT04	-	Standardises data
WAVE STATS	WAVESTAT	-	Calculates $\bar{H}_s$, T_z and higher percentiles
WAVE PLOT	PLOT	-	Plots any part of time history
DISTRIBUTION	STAT08	-	Calculates distribution of maxima or minima
PROBABILITY	STAT05	-	Calculates probability density functions
SPECTRUM	STAT21	-	Calculates Variance Density Spectrum.

Table A.1 Statistics Menu

A3 Data File Handling Programs

The following programs are used as 'stand-alone' programs as they can be used to supplement the main analysis programs as well as prepare data for this analysis.

Program		Action
READER	-	Prints all or part of data file on the computer screen
PRINTER	-	Prints all or part of data file on line printer
VOLTAGE	-	Converts a digital record to a ±5 volts record
FILECONV	-	Calibrates digital record to mm wave height with M & C values
FILEUNCONV	-	Converts calibrated record back to digital record
FILESORT	-	Copies data files between discs
MREAD	-	Prints the copies of a Masterfile
RANGE	-	Provides constant output from Microlink to check operation of data acquisition system
MASTER	-	Creates a Masterifle for use in analysis programs

Table A.2 Data File Handling Programs

A3 Output Listings

The following are all examples of run-time output from the main data acquisition and analysis. The program from which the output originates is found at the beginning of each listing.

A4 Execution Times

The following list details the approximate times to run the main analysis program. The times are given for a typical analysis of a 4k data set.

Program	Execution Time
Basic Statistics	2 mins
Variance Density Spectrum	5 mins
Wave Plot	4 mins
Frequency Response Function	25 mins*
Wave Envelope Analysis	
Numerical Model (20 time steps)	3½ mins

* The time for the 3 pairs of wave gauges 1-2, 2-3, 1-3.

?ECTRUM : RAN.15

)SKOWITZ SPECTRUM

)DEL PARAMETERS

FREQUENCY	ENERGY	PADDLE T/F
6.331246E-2	0.000000E0	3.600000E-3
1.266249E-1	0.000000E0	4.611747E-3
1.899374E-1	0.000000E0	7.017621E-3
2.532499E-1	9.889429E-10	9.849494E-3
3.165623E-1	4.352817E-5	1.266249E-2
3.798748E-1	1.215831E-3	1.519499E-2
4.431873E-1	3.465465E-3	1.859124E-2
5.064997E-1	4.295787E-3	2.251998E-2
5.698122E-1	3.812750E-3	2.758497E-2
6.331246E-1	2.944435E-3	3.132499E-2
6.964371E-1	2.150420E-3	3.385748E-2
7.597496E-1	1.542486E-3	3.638998E-2
8.230620E-1	1.106089E-3	3.823062E-2
8.863745E-1	7.995374E-4	3.886375E-2
9.496870E-1	5.847655E-4	3.949687E-2
1.012999E0	4.333428E-4	4.000000E-2

.g. wave height =150.6172 mm
ero crossing period=1.6078 secs
)del Water Depth =0.8000 m

PROTOTYPE PARAMETERS

Frequency HZ	Energy M*M*S
6.331246E-2	0.000000E0
1.266249E-1	0.000000E0
1.899374E-1	0.000000E0
2.532499E-1	9.889429E-10
3.165623E-1	4.352817E-5
3.798748E-1	1.215831E-3
4.431873E-1	3.465465E-3
5.064997E-1	4.295787E-3
5.698122E-1	3.812750E-3
6.331246E-1	2.944435E-3
6.964371E-1	2.150420E-3
7.597496E-1	1.542486E-3
8.230620E-1	1.106089E-3
8.863745E-1	7.995374E-4
9.496870E-1	5.847655E-4
1.012999E0	4.333428E-4

.g. wave height =0.1506 m
ero crossing period=1.6078 secs
)ectral width parameter=0.4638
lock frequency =4.0520 Hz
aximum volts =6.8474 v
rest factor =4.3407
ater Depth =0.8000m
ROBE SPACINGS
=1.1970m
=0.5982m

WAVE MONITOR CALIBRATION

DATE 15-4-87 TEST NUMBER 1

SET OUTPUT = 5.0

MODULE NUMBER 1

REGRESSION ANALYSIS (LEAST SQUARES)

GRADIENT= .0701 INTERCEPT=-139.6438

CORRELATION COEFFCIENT=1.0000

MEAN=2064.750

POINT	CORRECTED VALUE FOR S.W.L	THEORETICAL VALUES
1	-30.0094	-30
2	-20.2019	-20
3	-9.6938	-10
4	.0437	0
5	9.7812	10
6	20.2192	20
7	29.8166	30
8	40.0445	40

WAVE MONITOR CALIBRATION

DATE 15-4-87 TEST NUMBER 1

SET OUTPUT = 5.0

MODULE NUMBER 2

REGRESSION ANALYSIS (LEAST SQUARES)

GRADIENT= .0868 INTERCEPT=-173.9247

CORRELATION COEFFCIENT= .9999

MEAN=2060.625

POINT	CORRECTED VALUE FOR S.W.L	THEORETICAL VALUES
1	-30.2205	-30
2	-19.8877	-20
3	-9.7286	-10
4	.2569	0
5	9.7214	10
6	19.7937	20
7	29.7792	30
8	40.2857	40

DATE 15-4-87 TEST NUMBER 1

SET OUTPUT = 5.0

MODULE NUMBER 3

REGRESSION ANALYSIS (LEAST SQUARES)

GRADIENT= .0831 INTERCEPT=-163.3356

CORRELATION COEFFCIENT=1.0000

MEAN=2024.500

POINT	CORRECTED VALUE FOR S.W.L	THEORETICAL VALUES
1	-29.9643	-30
2	-19.9863	-20
3	-9.9253	-10
4	-.0305	0
5	9.6979	10
6	20.0916	20
7	30.1526	30
8	39.9643	40

CALIBRATION FINISHED

```
WAVE DATA ANALYSIS :DEPT. OF CIVIL ENGINEERING
                    PLYMOUTH POLYTECHNIC

    MICROLINK DATA LOGGING PROGRAM
*********RESULTS AND PARAMETERS**********


*****************WARNING*****************
THE DATA COLLECTED CONTAINS THE FOLLOWING

DATA HAS 940 ZEROES IN IT
DATA HAS 0 4095'S IN IT

*****************************************

PARAMETERS USED IN DATA LOGGING

A-D CONVERSION MODULE USED:A-12D

WAVE ABSORPTION: IN
No.OF MODULES= 5
LOGGING RATE= .123 SECS
SEC ADDR 1= 1
SEC ADDR 2= 2
SEC ADDR 3= 3
SEC ADDR 4= 4
SEC ADDR 5= 5
CLOCK UNITS= 3
No. OF CLOCK UNITS= 123
POINTS COLLECTED FROM EACH MODULE= 2048

FILE NAME  1= G187041501

FILE NAME  2= G287041501

FILE NAME  3= G387041501

FILE NAME  4= G487041501

FILE NAME  5= G587041501

MASTERFILE= M187041501


DATA LOGGING PROGRAM COMPLETE
```

WAVE DATA ANALYSIS: DEPT. OF CIVIL ENGINEERING
PLYMOUTH POLYTECHNIC

*********STATISTICAL ANALYSIS RESULTS*********

DATE OF TEST 15-4-87

TEST NUMBER 1

DATA FROM DATA FILE G187041501

WATER DEPTH .95 METRES

RANDOM SEA GENERATED BY FILE :RAN.15

WAVE ABSORPTION: IN

MASTER FILE M187041501

12 BIT CONVERSION FOR DATA

DURATION OF TEST= 4.20 MINS

********** STAT01 - RESULTS *************

GAUGE NUMBER 1

NUMBER OF DATA VALUES 2048

MEAN= -5.346 RMS= 36.664

VAR= 1316.309 STANDARD DEVIATION= 36.281

SKEWNESS= .21921 KURTOSIS= 2.82

MAXIMUM= 110.82 MINIMUM=-100.04

-----STAT01 ENDED-----

****** STAT10 - WAVE STATISTICS *********

NUMBER OF ZERO CROSSINGS 154

RECORD LENGTH 248.5 s

MEAN ZERO UP-CROSSING PERIOD= 1.613 S

NUMBER OF WAVES= 153

MEAN WAVE HEIGHT= 88.306 mm

MEDIAN WAVE HEIGHT= 85.943 mm

SIGNIFICANT WAVE HEIGHT (H1/3)= 135.760 mm

MAXIMUM WAVE HEIGHT= 193.686 mm

MINIMUM WAVE HEIGHT= 10.940 mm

```
MAXIMUM WAVE HEIGHT=  193.686 mm

MINIMUM WAVE HEIGHT=   10.940 mm

AVERAGE HIGHEST 10%=  167.100 mm

INSUFFCIENT WAVES FOR HIGHEST 1%

-------STAT10 ENDED-------
```

.572	644989.43	1.239	30515.74	1.905	9271.95	2.572
[illegible]	[illegible]	[illegible]	[illegible]	[illegible]	[illegible]	[illegible]

WAVE DATA ANALYSIS :DEPT. OF CIVIL ENGINEERING
PLYMOUTH POLYTECHNIC

******OVERTOPPING PROGRAM******
RESULTS

DATE OF TEST 15-4-87

TEST NUMBER 1

MASTERFILE NAME M187041501

DATA FILE NAME G487041501

BREAKWATER NUMBER 1

NUMBER OF WAVES 153

NUMBER OF WAVES OVERTOPPING 106

% WAVES OVERTOPPING 69.28

****

WAVE DATA ANALYSIS :DEPT. OF CIVIL ENGINEERNG
PLYMOUTH POLYTECHNIC

OVERTOPPING DISCHARGE CALCULATION

DATE OF TEST : 15-4-87

TEST NUMBER : 1

WATER DEPTH : .95 m

RANDOM SEA FROM FILE : RAN.15

WAVE ABSORPTION : IN

MASTERFILE : M187041501

DATA FILE : G587041501

SAMPLING RATE .123 secs

TEST LENGTH 4.20 Mins

**********OVERTOPPING DISCHARGES**********

MEAN TEST DISCHARGE : .001480 m^3/s

TOTAL DISCHARGE : .372861 m^3

**********ANALYSIS FINISHED**********

*********STATISTICS FINISHED*********

WAVE DATA ANALYSIS: DEPT. OF CIVIL ENGINEERING
PLYMOUTH POLYTECHNIC

************FREQUENCY RESPONSE FUNCTION************
************REFLECTIONS IN RANDOM WAVES************

RESULTS

DATA HAS A COSINE TAPER APPLIED TO IT

DATE OF TEST 15-4-87

TEST NUMBER 1

WATER DEPTH .95 METRES

NUMBER OF DATA POINTS IN FILE G187041501 :2048

NUMBER OF DATA POINTS IN FILE G287041501 :2048

RANDOM SEA FROM FILE: RAN.15

WAVE ABSORPTION : IN

SEPARATION OF PROBES .150 METRES

SAMPLING RATE .123 SECS

********RESULTS OF ANALYSIS*****************

******* SPECTRUM AT X *******

EFFECTIVE RESOLUTION BANDWIDTH= .0516 Hz

ALL S2(F) ARE THE AVERAGE OF 13 RAW ESTIMATES

NORMALISED STANDARD ERROR= 27.7 %

CUT-OFF FREQUENCY= 2.5 Hz

DIVIDE ALL S2(F) BY 10^ 3

F Hz	S2(F)	F Hz	S2(F)	F Hz	S2(F)	F Hz	S2(F)
0.000	33293.02	.667	2697904.98	1.334	52934.31	2.001	
.048	18998.56	.715	813850.35	1.381	29584.66	2.048	
.095	108982.30	.762	172850.13	1.429	31755.10	2.096	
.143	15744.46	.810	760629.39	1.477	11588.26	2.144	
.191	9516.07	.857	1077455.82	1.524	16518.73	2.191	
.238	11568.47	.905	342079.34	1.572	11379.90	2.239	
.286	35612.08	.953	409886.23	1.620	5987.20	2.287	
.333	286151.44	1.000	863877.91	1.667	15167.45	2.334	
.381	3245297.12	1.048	113948.96	1.715	18160.91	2.382	
.429	4925056.02	1.096	26160.95	1.763	9105.01	2.429	
.476	4396107.00	1.143	38558.73	1.810	5270.83	2.477	
.524	706313.88	1.191	38274.44	1.858	15895.70	2.525	
.572	644989.43	1.239	30515.74	1.905	9271.95	2.572	
.619	2455432.61	1.286	39589.18	1.953	4146.19	2.620	

.476	4396107.00	1.143	38558.73	1.810	5270.85	2.477	
.524	706313.88	1.191	38274.44	1.858	15895.70	2.525	
.572	644989.43	1.239	30515.74	1.905	9271.95	2.572	
.619	2455432.61	1.286	39589.18	1.953	4146.19	2.620	

MOMENTS: M0= 1171.62 M1= 677.43 M2= 448
M3= 350.99 M4= 336.40

SIGNIFICANT WAVE HEIGHT = 136.92 mm

SPECTRAL WIDTH PARAMETER = .699282919239

SPECTRAL PEAKEDNESS PARAMETER Q = 2.48049083313

******* SPECTRUM AT Y *******

EFFECTIVE RESOLUTION BANDWIDTH= .0516 Hz

ALL S2(F) ARE THE AVERAGE OF 13 RAW ESTIMATES

NORMALISED STANDARD ERROR= 27.7 %

CUT-OFF FREQUENCY= 2.5 Hz

DIVIDE ALL S2(F) BY 10^ 3

F Hz	S2(F)	F Hz	S2(F)	F Hz	S2(F)	F Hz	S2(F)
0.000	18266.66	.667	956981.91	1.334	61147.41	2.001	
.048	16377.44	.715	122103.24	1.381	13505.17	2.048	
.095	124350.49	.762	457197.53	1.429	22536.86	2.096	
.143	17609.52	.810	884138.97	1.477	48245.03	2.144	
.191	44910.75	.857	1209200.13	1.524	59621.50	2.191	
.238	11550.48	.905	804346.78	1.572	33771.91	2.239	
.286	17313.91	.953	235365.11	1.620	33941.61	2.287	
.333	23868.54	1.000	199718.64	1.667	33072.62	2.334	
.381	363804.35	1.048	295039.29	1.715	20954.30	2.382	
.429	1841681.11	1.096	103070.13	1.763	7928.52	2.429	
.476	4444608.80	1.143	85607.40	1.810	6815.72	2.477	
.524	5668381.05	1.191	31503.27	1.858	12338.77	2.525	
.572	3720971.29	1.239	57087.35	1.905	4735.71	2.572	
.619	2830205.31	1.286	59630.77	1.953	3519.78	2.620	

MOMENTS: M0= 1193.04 M1= 727.01 M2= 496
M3= 394.85 M4= 384.38

SIGNIFICANT WAVE HEIGHT = 138.16 mm

SPECTRAL WIDTH PARAMETER = .680823038275

SPECTRAL PEAKEDNESS PARAMETER Q = 2.95314162525

0.000	73688.95	.667	73688.95	1.334	196.70	2.001
.048	73688.95	.715	73688.95	1.381	77.93	2.048
.095	73688.95	.762	73688.95	1.429	79.91	2.096
.143	4770.59	.810	73688.95	1.477	91.92	2.144
.191	5575.85	.857	73688.95	1.524	54.74	2.191
.238	2891.02	.905	73688.95	1.572	48.01	2.239
.286	4187.49	.953	2376.78	1.620	28.37	2.287
.333	73688.95	1.000	73688.95	1.667	21.52	2.334
.381	73688.95	1.048	2290.00	1.715	7.92	2.382
.429	73688.95	1.096	179.65	1.763	4.41	2.429
.476	73688.95	1.143	61.39	1.810	7.95	2.477
.524	73688.95	1.191	24.06	1.858	20.00	2.525
.572	73688.95	1.239	67.04	1.905	7.70	2.572
.619	73688.95	1.286	103.34	1.953	3.91	2.620

MOMENTS: M0= 801973.73 M1= 46801.04 M2= 14032
M3= 8259.78 M4= 5727.34

SPECTRAL WIDTH PARAMETER = .978330370038

SPECTRAL PEAKEDNESS PARAMETER Q = .506092396181

LIMIT VALUE OF n*PEAK= 73688.9536815

******* REFLECTED SPECTRUM *******

EFFECTIVE RESOLUTION BANDWIDTH= .0516 Hz

ALL S2(F) ARE THE AVERAGE OF 13 RAW ESTIMATES

NORMALISED STANDARD ERROR= 27.7 %

CUT-OFF FREQUENCY= 2.5 Hz

DIVIDE ALL S2(F) BY 10^ 0

F Hz	S2(F)	F Hz	S2(F)	F Hz	S2(F)	F Hz	S2(F)
0.000	73688.95	.667	73688.95	1.334	300.81	2.001
.048	73688.95	.715	73688.95	1.381	65.00	2.048
.095	73688.95	.762	73688.95	1.429	77.37	2.096
.143	4675.54	.810	73688.95	1.477	89.01	2.144
.191	5663.27	.857	73688.95	1.524	47.93	2.191
.238	2837.55	.905	73688.95	1.572	35.28	2.239
.286	4132.85	.953	2994.50	1.620	28.11	2.287
.333	73688.95	1.000	73688.95	1.667	9.26	2.334
.381	73688.95	1.048	2216.56	1.715	22.17	2.382
.429	73688.95	1.096	179.54	1.763	10.53	2.429
.476	73688.95	1.143	139.08	1.810	10.27	2.477
.524	73688.95	1.191	75.48	1.858	15.42	2.525
.572	73688.95	1.239	147.71	1.905	3.21	2.572
.619	73688.95	1.286	205.20	1.953	3.82	2.620

MOMENTS: M0= 799889.67 M1= 45856.97 M2= 13567
M3= 8044.86 M4= 5650.44

SPECTRAL WIDTH PARAMETER = .979423339273

SPECTRAL PEAKEDNESS PARAMETER Q = .507971641707

LIMIT VALUE OF n*PEAK= 73688.9536815

THESE NOTES ARE DESIGNED TO HELP YOU SET UP THE MICROLINK
THEY SHOULD BE READ IN CONJUNCTION WITH THE BIODATA MANUAL

ONLY ONE A-D CONVERTER MAY BE PRESENT IN THE MICROLINK
AT ANY ONE TIME. THE OTHERS MUST BE REMOVED
AN 8 BIT CONVERTER: A-8D OR A 12 BIT CONVERTER: A-12D
IS AVAILABLE

THE 8 BIT COLLECTS ONE BYTE PER SAMPLE
THE 12 BIT TWO BYTES (ONE WORD) PER SAMPLE

. THE A-D CONVERTER MUST BE TO THE LEFT OF THE ANALOGUE INPUTS

```
                 ¦              ¦              ¦              ¦
   YES           ¦              ¦              ¦              ¦NO
```

THE ANALOGUE INPUT MODULES ALL HAVE SECONDARY ADRRESSES
SEC ADDR
THIS IS PRINTED ON THE LOWER PART OF THE MODULE
IT IS NOT NECESSARY FOR THESE TO BE IN ASCENDING ORDER

ANY MODULE IN THE MICROLINK CAN BE ADDRESSED INDIVIDUALLY
OR AS PART OF A SCAN (MULTIPLEX)
THE MICROLINK WILL SCAN THROUGH THE MODULES FROM LEFT TO RIGHT
REGARDLESS OF SEC ADDR'S

IF A MODULE IS NOT TO BE INCLUDED IN A SCAN IT IS REFERRRED
AS A SKIP MODULE
THE MODULE IMMEDIATELY TO THE RIGHT OF THE LAST ACTIVE MODULE
IS THE 'RETURN' MODULE

```
                 ¦              ¦              ¦              ¦
   YES           ¦              ¦              ¦              ¦NO
```

THE HSC (HIGH SPEED CLOCK) CONTROLS THE MULTIPLEXING
BY SCANNING ALL ACTIVE MODULES SIMULTANEOUSLY

THE DATA IS LOGGED TO A BUFFER FROM WHERE IT IS SORTED
INTO FILES FROM EACH MODULE AND THEN STORED ON THE BDAT FILES

IF A PROTECT CODE IS REQUIRED FOR THE BDAT FILES IT IS
CHOSEN AS FOLLOWS:

AFTER THE PROGRAM HAS COMPLETED
TO PROTECT FILE G185032101
TYPE PROTECT 'G185032101' 'AA'
WHERE AA IS THE REQUIRED PROTECT CODE
NB THE ' IN THE ABOVE LINE SHOULD BE A DOUBLE APOSTROPHE

```
                 |                |                |                |
   YES           |                |                |                |NO
```

TIMING

ANY LOGGING RATE CAN BE CHOSEN BY CORRECT CHOICE OF
THE BASIC RATE OF LOGGING (CLOCK RATE)
AND INTERVAL BETWEEN THE CLOCK RATE (No. OF CLOCK UNITS)
FOR EACH SAMPLE

THE CLOCK RATES AVAILABLE ARE:
100 MICROSECONDS
1 MILLISECOND
10 MILLISECONDS
100 MILLISECONDS
1 SECOND

ANY No. OF CLOCK UNITS FROM 1 TO 255 CAN BE CHOSEN

```
                 |                |                |                |
   YES           |                |                |                |NO
```

THE CALIBRATION IS TO CONVERT THE VALUES COLLECTED OFF
THE MICROLINK AND BE ABLE TO CONVERT THEM TO WAVE HEIGHT
IN mm.
IT MUST **ALWAYS** BE CARRIED OUT IN THE CORRECT ORDER
WHICH IS:
START AT A LOW HOLE (9 or 10) AND MOVE THE PROBE I HOLE
(10mm)***INTO*** WATER FOR EACH SUCCESIVE CALIBRATION

S.W.L. **MUST** BE HOLE 4 FROM THE FIRST ONE SELECTED
i.e.HOLE 6, IF 9 WAS THE STARTING POINT

```
                 |                |                |                |
   YES           |                |                |                |NO
```

APPENDIX B

THE FREQUENCY RESPONSE FUNCTION METHOD

Complete expansion of algebra:

Given: $X = I + HR$ ..... (B.1)

$Y = HI + R$ ..... (B.2)

From theory set out in Chapter 3.

where X,Y,I and R are the Fourier transforms as defined in Chapter 3.

Also $X^*X = S_{xx}$ where X^* is the complex conjugate of X (B.3)

$Y^*X = S_{yy}$ where Y^* is the complex conjugate of X (B.4)

$X^*Y = S_{xy} = c+iq$ (B.5)

and

$I^*I = S_{ii}$ where I^* is the complex conjugate of X

$R^*R = S_{rr}$ where R^* is the complex conjugate of X

where S_{ii} and S_{rr} are the incident and reflected spectra respectively

in B.1 $I = X-HR$

in B.2 $R = Y-HI$

$$\therefore \quad I = X-H(Y-HI)$$
$$= X-HY+H^2I$$
$$I-H^2I = X-HY$$
$$I(1-H^2) = X-HY$$

or $$I = \frac{X-HY}{(1-H^2)} \qquad (B.6)$$

$$I^* = \frac{(X-HY)^*}{(1-H^2)} \qquad (B.7)$$

$$\therefore \quad I^*I = S_{ii} = \frac{(X-HY)^*(X-HY)}{(1-H^2)^*(1-H^2)} \qquad (B.8)$$

Similarly in 2

$$R = Y - HI$$

in B.1 $I = X - HR$

$$\therefore \quad R = Y - H(X - HR)$$

$$= Y - HX + H^2R$$

$$R - H^2R = Y - HX$$

$$R(1 - H^2) = Y - HX$$

$$\therefore \quad R = \frac{Y - HX}{(1 - H^2)} \qquad (B.9)$$

$$\therefore \quad R^* = \frac{(Y - HX)^*}{(1 - H^2)^*}$$

$$\therefore \quad R^*R = S_{rr} = \frac{(Y - HX)^*(Y - HX)}{(1 - H^2)^*(1 - H^2)} \qquad (B.10)$$

Equations B.8 and B.10 are used to find the incident and reflected spectra in terms of spectra at X and Y and the cross spectrum S_{xy}.

To keep the algebra clear the algebraic expansions will be done separately for the numerator and denominator.

1. Expansion of $(1 - H^2)^*(1 - H^2)$

For waves in a laboratory channel $H = e^{-ks}$ where k = wave no.

s = separation of X and Y.

$$e^{-ks} = \cos(ks) - i\sin(ks) \qquad (B.11)$$

$$(1 - H^2)^* = (1 - HH)^* = (1 - H^*H^*) \qquad (B.12)$$

$$(1 - H^*H^*)(1 - HH) = 1 - HH - H^*H^* + H^*H^*\,HH \qquad (B.13)$$

Evaluating the terms separately:

$$HH = (\cos.(ks) - i\sin(ks))(\cos(ks) - i\sin(ks))$$
$$= \cos^2(ks) - 2i\sin(ks)\sin(ks) - \sin^2(ks) \qquad (B.14)$$

$$H^*H^* = (\cos.(ks) - i\sin(ks))(\cos(ks) + i\sin(ks))$$
$$= \cos^2(ks) + 2i\sin(ks)\cos(ks) - \sin^2(ks) \qquad (B.15)$$

$$H^*H^*HH = (\cos^2(ks) + 2i\cos(ks)\sin(ks) - \sin^2(ks))\times$$
$$(\cos^2(ks) - 2i\cos(ks)\sin(ks) - \sin(ks))$$
$$= \cos^4(ks) - 2i\sin(ks).\cos^3(ks) - \cos^2(ks)\sin^2(ks)$$
$$+ 2i\sin(ks)\cos^3(ks) + 4\sin^2(ks)\cos^2(ks)$$
$$-2i\sin^3(ks).\cos(ks) - \sin^2(ks).\cos^2(ks) + 2i\sin^3(ks)\cos(ks)$$
$$+ \sin^4(ks)$$

$$= \underline{\cos^4(ks) + 2\sin^2(ks)\cos^2(ks) + \sin^4(ks)} \qquad (B.16)$$

In B.13

$$B.13 = 1 - (B.14) - (B.15) + (B.16)$$

$$\therefore (B.13) = 1 - (\cos^2(ks) - 2i\cos(ks)\sin(ks) - \sin^2(ks) - (\cos^2(ks) + 2i\sin(ks)$$
$$\cos(ks) - \sin^2(ks))$$
$$+ (\cos^4(ks) + 2\sin^2(ks)\cos^2(ks) + \sin^4(ks)) \qquad (B.17)$$

since $\cos^2(ks) + \sin^2(ks) = 1$

$$\cos^2(ks) = 1 - \sin^2(ks)$$

$$(B.13) = 1 - \cos^2(ks) + 2i\cos(ks)\sin(ks) + \sin^2(ks) - \cos^2(ks) - 2i\cos(ks)$$
$$\sin(ks) + \sin^2(ks)$$
$$+ \cos^4(ks) + 2\sin^2(ks)\cos^2(ks) + \sin^4(ks)$$

$$= 1-2\cos^2(ks) + \cos^4(ks) + 2\sin^2(ks)\cos^2(ks) + \sin^4(ks)$$
$$= 1-2(1-\sin^2(ks)) + (\cos^4(ks) + 2\sin^2(ks)\cos^2(ks) + \sin^4(ks)) + 2\sin^2(ks)$$
$$= 1-2 + 2\sin^2(ks) + (\cos^2(ks) + \sin^2(ks))^2 + 2\sin^2(ks)$$
$$= 1-2 + 2\sin^2(ks) + 1 + 2\sin^2(ks)$$
$$= \underline{4\sin^2(ks)} \qquad (B.18)$$

---

2. Expansion of $(X-HY)^*(X-HY)$ for S_{ii}

$$(X-HY)^* = (X^* - H^*Y^*)$$

$$\therefore \quad (X-HY)^*(X-H^*Y^*) = (X^*-H^*Y^*)(X-HY)$$
$$= X^*X - X^*HY - H^*Y^*X + H^*Y^*HY$$
$$= X^*X + H^*HY^*Y - H^*Y^*X - HX^*Y$$

$H^*H = 1$

$X^*X = S_{xx} \therefore \Rightarrow = S_{xx} + S_{yy} - H^*Y^*X - HX^*Y$

$Y^*Y = S_{yy}$

also $S_{xx} = X^*Y = c+iq \quad \therefore (S_{xy})^* = c-iq$

$$\Rightarrow S_{xy} + S_{xy} - H^*(S_{xy}) - H(S_{xy}) \qquad (B.19)$$

in B.19 $-H^*(S_{xy}) = -H^*(c-iq)$

since $H = \cos(ks) - i\sin(ks)$

$$-H^*(S_{xy})^* = -(\cos(ks) + i\sin(ks))(c-iq)$$
$$= -(c\cos(ks) - iq\cos(ks) + ic\sin(ks) + q\sin(ks)) \qquad (B.20)$$

also

in B.19 $-H(S_{xy}) = -H(c+iq)$

$$= -(\cos(ks) - i\sin(ks))(c+iq)$$
$$= -(c\cos(ks) + iq\cos(ks) - ic\sin(ks) + q\sin(ks)) \qquad (B.21)$$

$$(B.20) + (B.21) = -c\cos(ks) - q\sin(ks) - iq\cos(ks) + ic\sin(ks) - c\cos(ks) - q\sin(ks) + iq\cos(ks) - ic\sin(ks)$$

$$= \underline{-2c\cos(ks) - 2q\sin(ks)} \qquad (B.22)$$

combining (B.19) and (B.21)

$\therefore$ equation (B.8) becomes

$$S_{ii} = (S_{xx} + S_{yy} - 2\,c\cos(ks) - 2q\sin(ks))/4\,\sin^2(ks) \qquad (B.23)$$

---

3. Expansion of $(Y-HX)^*(Y-HX)$ for S_{rr}

$$(Y-HX)^* = (Y^* - H^*X^*)$$

$$\therefore \quad (Y-HX)^*(Y-HX) = (Y^* - H^*X^*)(Y-HX)$$

$$= Y^*Y - Y + HX - H^*X^*Y + H^*X^*HX$$

$$= Y^*Y + H^*HX^*X - Y^*HX - H^*X^*Y$$

$H^*H = 1$

$X^*X = S_{xx}$

$Y^*Y = S_{yy} \qquad \Rightarrow = S_{xy} + S_{xx} - Y^*HX - H^*X^*Y$

also $S_{xy} = X^*Y = c+iq \quad (S_{xy})^* = c-iq$

$$= S_{xx} + S_{yy} - H(S_{xy})^* - H^*(S_{xy}) \qquad (B.24)$$

in (B.24) $-H(S_{xy})^* = -H(c-iq)$

since $H = \cos(ks) - i\sin(ks)$

$$H(S_{xy})^* = -(\cos(ks) - i\sin(ks))(c-iq)$$

$$= -(c\cos(ks) - iq\cos(ks) - ic\sin(ks) - q\sin(ks)) \qquad (B.25)$$

also in (B.24) $-H^*(S_{xy}) = -(\cos(ks) + i\sin(ks))(c+iq)$

$$= -(c\cos(ks) + iq\cos(ks) + i\sin(ks) - q\sin(ks)) \qquad (B.26)$$

$$(B.25) + (B.26) = -c\cos(ks) + iq\cos(ks) + ic\sin(ks) + q\sin(ks) - c\cos(ks) - iq\cos(ks) - ic\sin(ks) + q\sin(ks)$$

$$= \underline{-2c\cos(ks) + 2q\sin(ks)} \qquad (B.27)$$

Combining equations (B.18), (B.24), (B.27) equation (B.10) becomes:

$$S_{rr} = (S_{xx} + S_{yy} - 2c\cos(ks) + 2q\sin(ks))/4\sin^2(ks) \qquad (B.28)$$

equations (B.23) and (B.28) are those used to calculate the incident and reflected spectra.

The reflection coefficient $\rho(t)$ is given by

$$\rho^2(f) = S_{rr}/S_{ii} \qquad (B.29)$$

APPENDIX C

WAVE GAUGE SPACING

The pertinent equations in the Frequency Response Function analysis are:

$$S_{ii} = (S_{xx} + S_{yy} - 2c\cos(ks) - 2q\sin(ks))/4\sin^2(ks) \qquad (C.1)$$

$$S_{rr} = (S_{xx} + S_{yy} - 2c\cos(ks) + 2q\sin(ks))/4\sin^2(ks) \qquad (C.2)$$

where (C.1) and (C.2) were described and derived in Chapter 3. From the above equations it is seen that S_{ii} and S_{rr} are undefined if $\sin^2(ks) = 0$.

In order to gain maximum resolution from the technique without the use of many pairs of wave gauges the gauges must be separated to give maxumum resolution around the area of maximum interest (i.e. the peak spectral frequency, f_p).

To ensure maximum resolution about f_p let $\sin^2(ks) = 1$.

In radians $$\sin\left\{\frac{n\pi}{2}\right\} = 1 = ks \qquad (C.3)$$

$\therefore$ for maximum resolution choose a spacing, s, such that:-

$$S_1 = \frac{n\pi}{2k} \qquad (C.4)$$

where S_1 is the spacing between the two gauges 1 and 2 for maximum resolution.

k the wave number is given by $k = 2\pi/L$

where the wavelength L is given by:

$$L = \frac{gT^2}{2\pi}\tanh\left\{\frac{2\pi d}{L}\right\} \qquad (C.5)$$

Equation (C.5) was solved for L by means of an iterative program "WAVELEN" written to store the k values on disc for use by the Frequency Response program "FREQRES".

Since the analysis is undefined when Sin(ks)=0, a third wave gauge is required to give information in the area where S_1 is invalid.

The second spacing, S_2, is calculated to have maximum resolution of the point where S_1 is invalid. S_2 is the spacing between gauges 2 and 3. In this fashion a third spacing, S_3, the sum of S_1 and S_2 can be used to check the validity of the results.

The wave parameter generation program NEWSYN was modified to make the calculation of s_1 and S_2 at the same time as it calculates the spectral densities for wave generation. All the output from the program is sent to a line printer for hard copy output. The revised program was called NEWSYNP (P for printer). Each generated spectrum thus has different spacings S_1 and S_2 and users should be aware of this when performing tests with different spectra.

Example of calculation of spacing, S_1.

Given - Spectrum RAN

Significant wave height	$\bar{H}_s$	= 0.13m
Peak frequency	f_p	= 0.544Hz
Modal period	T_p	= 1.838S

From an iterative solution to (C.5) L = 4.323m

$$\therefore \quad K = \frac{2\pi}{4.324}$$

$$= 1.453$$

hence

$$S_1 = \frac{n\pi}{2k} = 1.08 \qquad n = 1 \text{ is the primary case}$$

Calculation of S_2:

S_1 will be invalid if Sin(ks) = 0

or if $k = 3.14$

The period associated with this wavelength T = 1.36s

Frequency at which S_1 analysis is invalid f = 0.73Hz

$\therefore$ calculate S_2 such that

$$S_2 = \frac{n\pi}{2k} = 1$$

$$S_2 = 0.540m$$

Spacing values used in the absorption system tests and the overtopping tests are given below:

Spectrum type	H_s m	f_p Hz	T_p s	S_1 m	S_2 m
P-M	0.12	0.57	1.75	1.04	0.52
P-M	0.18	0.46	2.17	1.33	0.67
P-M	0.19	0.45	2.22	1.42	0.71
P-M	0.20	0.44	2.27	1.42	0.71
P-M	0.22	0.42	2.35	1.51	0.76

Table C.1 Wave Gauge spacings for Frequency Response Analysis

APPENDIX D

D1 SPECTRAL EQUATIONS

Wave spectra which the Hydraulics Research Software and their defining equations for use in random wave generation are as follows:

D1.1. Moskowitz

$$\text{Peak frequency } fm = \sqrt{\frac{.03849}{H_s}} \qquad (D.1)$$

if the significant wave height $\bar{H}_s$ is defined parameter

or $fm = 0.8212/\bar{T}$

if the zero-crossing period $\bar{T}_z$ is the defined parameter

Spectral ordinates given by: $S(f) = 0.7795 \exp (-1.25 ((fm/f)^4))/2\pi^4 f^5$

where $f = I\ fm/8$ for $I = 1$ to 16

D1.2. Jonswap

Peak frequency $fm = 0.87/\bar{T}$

$$S(f) = \frac{K_g^2}{(2\pi)*f^5} \exp \left[\frac{-5}{4} \left[\frac{fm}{f} \right]^4 \right] \alpha^a$$

where g = acceleration due to gravity

$k = 0.076/X^{0.22}$

where $X = gL_f U_w$

where L_f = effective fetch length

U_w = wind speed 10m above the sea surface

$fm = 3.5g/U_w X^{0.33}$

$\alpha = 3.3$

$w = 0.07$ for $f \leq fm$ or 0.09 for $f > fm$

D1.3. Darbyshire

Peak frequency $fm = 1/(2.703\sqrt{U_w} + 3.55 \times 10_{-6} \times U_w^4)$

Spectral Ordinates $S(f) =$

$$23.9\ mo\ \exp(-\sqrt{(f-fm)^2/(0.0085(f-fm+0.042))}$$

when $f-fm > 0.042$ else $S(f) = 0$

where $mo = 1.083 \times 10^{-5}$

D1.4. Newman

Peak frequency $fm = 1.275/U_w$

Spectral Ordinates $S(f) = \dfrac{2.518 \times 10^{-4}}{f} \exp - \left\{ \dfrac{3fm^2}{f} \right\}$

D1.5. ISSC

Peak frequency $fm = 0.7714/\bar{T}$

Spectral ordinates $S(f) = \dfrac{0.313\bar{H}_s^2 fm^4}{f^5} \exp -(1.25fm^4/f^4)$

In each of the the spectra generated by NEWSYN the first 3 ordinates are set to zero.

In addition there is the option of supplying a spectrum as a set of 16 ordinates, in units of metres-squared seconds; the frequency interval between the ordinates must also be supplied.

The selection of any of the above spectra is achieved by typing the initial letter of the choice then <return>.

D.2 SOME FREQUENCY WINDOWS AND THEIR USE

As mentioned in Chapter 3 the data for wave spectra is tapered by an appropriate taper window, some of the more common windows are given below:

D2.1. Rectangular window

Used to simply truncate data

$$\bar{W}(i/2T-f) = \int_{-T}^{T} \exp\left[-c(i/2T-f)t\right] dt = 2T\sin c(i-2Tf)$$

$w(t) = 1 \quad -T<t<T$

$w(t) = 0 \quad$ elsewhere

D2.2. Bartlett (triangular) window

No longer generally used it is the only window that can be implemented in hardware.

From $w(t) = 1-|t|/T \qquad -T<t<T$

$$\bar{W}(i/2T-f) = T[\text{sinc}(i-Tf)]^2$$

D2.3. Parzen window

From

$w(t) = 1-6t^2/T^2 + 6|t|^3/T^3$ for $t<T/2$

$w(t) = 2(1-|t|)/T^3$ for $T/2 < t < T$

$w(t) = 0$ elsewhere

$$\bar{W}(i/2T-f) = 3/4T\,[\text{sin } c(i-Tf)]^4$$

D2.4. Tukey Window

For $w(t) = \alpha + (1-\alpha) \cos(\pi t/T)$ for $-T < t < T$

$\bar{W}(i/2T-f) = 2\alpha T\,\mathrm{sinc}(i-2Tf) + (1-\alpha)\,T\,[\mathrm{sinc}(i-2Tf+1) + \mathrm{sinc}(i-2Tf+1)]$

If $\alpha = 0.5$ then

$\bar{W}(i/2T-f) = T\,\mathrm{sinc}(i-2Tf)/[1-(i-2Tf)^2]$

This is known as a hanning window.

If $\alpha = 0.54$ then the window is known as a hamming window.

Tukey windows have a simple fourier transform.

D2.5. Cosine Taper

The cosine taper window is the window used in all the analysis routines writen.

For $w(t) = 1$ for $-4/rT < t < 4/5T$

$w(t) = \frac{1}{2} + Y2\cos(s\pi t/t)$ $-T < t$ and $4/5\ T < t < t$

$w(t) = 0$ elsewhere

$\bar{W}(i/2T-f) \simeq T\,\mathrm{sinc}(i-2Tf) + 4/5\ T\mathrm{Sinc}(i-8/5Tf)$

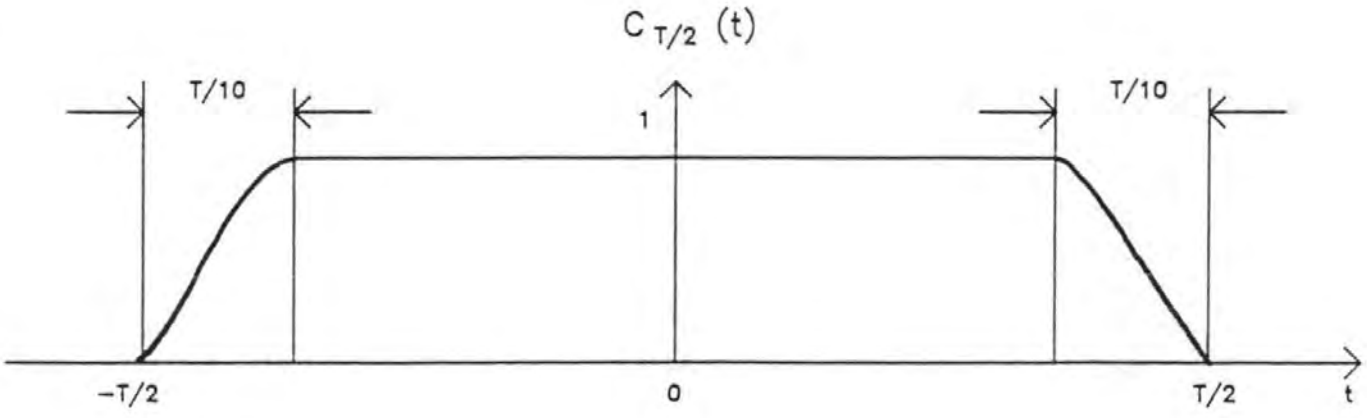

Figure D.1 Cosine Taper Window Function

D2.6. Daniall Window

$$\bar{W}_{j/2} = (2m+1)^{-1} \text{ for } j = m,(-m+1) \ldots\ldots (m-1), m$$
$$= 0 \text{ elsewhere}$$

$$\bar{W}(i/2-f) = (2m+1) \sum_{j=-m}^{m} \text{sinc}(i-2f-j)$$

D2.7. Modified Daniall window

Here $\bar{W}_{j/2} = \frac{1}{4}m$ for $(-m+1) \leqslant j \leqslant (m-1)$
$= \frac{1}{4}m$ for $j = \pm m$
$= 0$ elsewhere

$$\bar{W}(i/2-f) = (2m+1)^{-1} \sum_{j=-m}^{m} \text{sinc}(i-2f-j)$$

A full appraisal of all the above windows can be found in Digital Spectral Analysis by Yuen and Fraser[19].

APPENDIX E

VERTICAL ACCELERATION TERM

The 1-D momentum equation (10.2) is given with a term F_x to allow for the vertical acceleration. F_x is derived below: (Gopalakrishnan 1980).

The terms which account for vertical accelerations in the momentum equation are derived from considerations of pressure variation on a vertical section. An expression for the variation can be obtained from the momentum equation for the z-direction. Once this variation is established the corresponding effect can be introduced in the term

$$-\frac{1}{\rho}\frac{\partial p}{\partial x}$$ of the momentum equation for the x-direction equation.

Thus, we obtain an equation for the x-direction in which the effects of vertical accelerations are included. The steps are as follows:

$$U(x,z,t) = U(x,t) + U^*(x,z,t) \qquad (E.1)$$

Equation (E.1) describes the x-direction velocity as the combination of a mean and fluctuating velocity.

Applying (E.1) to the Eulerian equation of motion (E.2) below:

$$\frac{\partial U}{\partial t} + U\frac{\partial U}{\partial x} + w\frac{\partial U}{\partial z} = -\frac{1}{\rho}\frac{\partial p}{\partial x} \qquad (E.2)$$

we obtain:

$$\frac{\partial (U + U^*)}{\partial t} + (U + U^*)\frac{\partial (U + U^*)}{\partial x} + W\frac{\partial (U + U^*)}{\partial z} = -\frac{1}{\rho}\frac{\partial p}{\partial x} \qquad (E.3)$$

At this stage it is assumed that u^* is negligible compared to U i.e. the horizontal velocity is assumed to be uniform over a vertical section. This assumption has been found to introduce negligible errors in most shallow water motions. On removing terms containing u^*, equation (E.3) becomes:

$$\frac{\partial U}{\partial t} + U\frac{\partial U}{\partial x} + w\frac{\partial U}{\partial z} = -\frac{1}{\rho}\frac{\partial p}{\partial x} \qquad (E.4)$$

Since U is not a function of z,

$$\frac{\partial U}{\partial z} = 0$$

Thus:

$$\frac{\partial U}{\partial t} + \frac{U\partial U}{\partial x} = -\frac{1}{\rho}\frac{\partial p}{\partial x} \qquad (E.5)$$

The corresponding z-direction momentum equation is:

$$\frac{\partial w}{\partial t} + U\frac{\partial w}{\partial x} + w\frac{\partial w}{\partial z} = -\frac{1}{\rho}\frac{\partial p}{\partial z} - g \qquad (E.6)$$

Also the continuity equation becomes:

$$\frac{\partial U}{\partial x} + \frac{\partial w}{\partial z} = 0 \qquad (E.7)$$

Thus:

$$\frac{\partial w}{\partial z} = -\frac{\partial U}{\partial x} \qquad (E.8)$$

Integrating equation (E.8) with regard to z yields:

$$w = -\frac{\partial U}{\partial x}Z + k \qquad (E.9)$$

The constant of integration k can be evaluated using the bottom boundary conditions of which $w(-h) = -U\frac{\partial h}{\partial x}$:

$$w = -U\frac{\partial h}{\partial h} \quad \text{at } z = -h$$

where w is the vertical particle velocity at a point.

Therefore:

$$-U\frac{\partial h}{\partial x} = -\frac{\partial U}{\partial x}(-h) + k$$

$$k = -\frac{\partial}{\partial x}(Uh)$$

Hence:

$$w = -\frac{\partial U}{\partial x} Z - \frac{\partial}{\partial x}(Uh) \qquad \text{(E.10)}$$

Thus, w is a linear function of z under the assumption that u^* is negligible. Based on equation (E.10), the derivatives of w in the z direction momentum equation, equation (E.6) can be written as follows:

$$\left.\begin{aligned}
\frac{\partial w}{\partial t} &= -Z\frac{\partial^2 U}{\partial x \partial t} - \frac{\partial}{\partial x}\left\{ h\frac{\partial U}{\partial t} \right\} \\
\frac{\partial w}{\partial x} &= -\frac{\partial^2 U}{\partial x^2} Z - \frac{\partial}{\partial x}\left\{ U\frac{\partial h}{\partial x} - h\frac{\partial U}{\partial x} \right\} \\
&= -z\frac{\partial^2 U}{\partial x^2} - \left[U\frac{\partial^2 h}{\partial x^2} + 2\frac{\partial U}{\partial x}\frac{\partial h}{\partial x} + h\frac{\partial^2 U}{\partial x^2} \right] \\
\frac{\partial w}{\partial z} &= \frac{\partial U}{\partial x}
\end{aligned}\right\} \qquad \text{(E.11)}$$

Thus, the LHS of equation (E.6) can be expressed as a function Σ of U and its time and space derivatives, h and z, i.e. equation (E.6) can now be written as:

$$\Sigma \left[U,\ h,\ \frac{\partial U}{\partial x},\ \frac{\partial h}{\partial x},\ \frac{\partial^2 U}{\partial x^2},\ \frac{\partial U}{\partial t},\ Z \right] = -\frac{1}{\rho}\frac{\partial p}{\partial z} - g \qquad \text{(E.12)}$$

Integrating equation (E.12) with regard to z yields:

$$\int \Sigma\, dz = -\frac{P}{\rho} - gz + k \qquad \text{(E.13)}$$

At $z = \eta$, $p = 0$ therefore:

$$\int_o^{\eta} \Sigma\, dz = -g\eta + k \qquad \text{(E.14)}$$

Hence

$$\int \Sigma\, dz = -\frac{P}{\rho} - gz + g\eta + \int_o^{\eta} \Sigma\, dz \qquad \text{(E.15)}$$

or

$$-\frac{P}{\rho} = \int \Sigma dz + g\,(z + \eta) - \int_o^{\eta} \Sigma dz \qquad \text{(E.16)}$$

Differentiatng equation (E.16) with respect to x:

$$-\frac{1}{\rho}\frac{\partial p}{\partial x} = -g\frac{\partial \eta}{\partial x}\left[\int_o^{\eta} \Sigma dz - \int \Sigma dz \right] \qquad \text{(E.17)}$$

The last term on the RHS shows that

$\frac{\partial p}{\partial x}$ is a function of z, substituting for

$-\frac{1}{\rho}\frac{\partial p}{\partial x}$ from equation (E.17) in equation (E.15) yields:

$$\frac{\partial U}{\partial t} + U\frac{\partial U}{\partial x} = -g\frac{\partial \eta}{\partial x}\left[\int_o^{\eta} \Sigma dz - \int \Sigma dz \right] \qquad \text{(E.18)}$$

In order to remove the z dependence, equation (E.18) is integrated with regard to z from $-h$ to η.

$$\int_{-h}^{\eta} \left\{ \frac{\partial U}{\partial t} + U\frac{\partial U}{\partial x} \right\} dz = -\int_{-h}^{\eta} g\frac{\partial \eta}{\partial x}\, \partial z - \int_{-h}^{\eta} \frac{\partial}{\partial x}\left[\int_{-h}^{\eta} \Sigma dz - \int \Sigma dz \right] dz$$

i.e.

$$\left\{ \frac{\partial U}{\partial t} + U\frac{\partial U}{\partial x} \right\}(\eta + h) = -g\frac{\partial \eta}{\partial x}(\eta + h) - \int_{-h}^{\eta} \frac{\partial}{\partial h}\left[\int_o^{\eta} \Sigma d\bar{z} - \int \Sigma d\bar{z} \right] dz \qquad \text{(E.19)}$$

Dividing equation (E.19) throughout by $(\eta + h)$ we obtain:

$$\frac{\partial U}{\partial t} + U \frac{\partial U}{\partial x} = -g \frac{\partial \eta}{\partial x} - \frac{1}{\eta+h} \int_{-h}^{\eta} \frac{\partial}{\partial x} \left[\int_{o}^{\eta} \Sigma d\bar{z} - \int \Sigma d\bar{z} \right] dz \qquad (E.20)$$

Comparing equation E.20 with the vertically integrated or shallow water equation without friction, it is seen that the effect of vertical acceleration comes in through the term:

$$F_x = - \frac{1}{\eta+h} \int_{-h}^{\eta} \frac{\partial}{\partial k} \left[\int_{o}^{\eta} \Sigma d\bar{z} - \int \Sigma d\bar{z} \right] dz$$

As U and h are not functions of z, the integration involved can be easily carried out. For example the term:

$$\frac{\partial w}{\partial t}$$

which forms one of the terms in the function Σ undergoes the following operations during the integrations indicated above:

$$\int_{-h}^{\eta} \frac{\partial}{\partial h} \left[\int_{o}^{\eta} \frac{\partial w}{\partial t} d\bar{z} - \int \frac{\partial w}{\partial t} d\bar{z} \right] d\bar{z}$$

$$\int \frac{\partial w}{\partial t} dz = \int \left[- z \frac{\partial^2 U}{\partial x \partial t} - \frac{\partial}{\partial x} \left[\frac{h \partial U}{\partial t} \right] dz = \right.$$

$$\left. - \left[\frac{\partial^2 U}{\partial x \partial t} \frac{z^2}{2} + \frac{\partial}{\partial x} \left[h \frac{\partial U}{\partial t} \right] z \right] \right. \qquad (E.21)$$

Therefore:

$$\frac{\partial}{\partial x} \int \frac{\partial w}{\partial t} dz = - \left[\frac{z^{\eta}}{2} \frac{\partial}{\partial x} \left[\frac{\partial^2 U}{\partial x \partial t} \right] + z \frac{\partial^2}{\partial x^2} \left[\frac{h \partial U}{\partial t} \right] \right. \qquad (E.22)$$

and

$$\int_{-h}^{\eta} \frac{\partial}{\partial x} \int \left[\frac{\partial w}{\partial t} d\bar{z} \right] dz = - \left[\frac{z^3}{6} \frac{\partial}{\partial x} \left[\frac{\partial^2 U}{\partial x \partial t} \right] + \frac{z^2}{2} \frac{\partial^2}{\partial x^2} \left[\frac{h \partial U}{\partial t} \right] \right]_{-h}^{\eta} =$$

$$\left. - \left[\frac{(\eta^3 + h^3)}{6} \frac{\partial}{\partial x} \left[\frac{\partial^2 U}{\partial x \partial t} \right] + \frac{(\eta^2 + h^2)}{2} \frac{\partial^2}{\partial x^2} \left[\frac{h \partial U}{\partial t} \right] \right] \right. \qquad (E.23)$$

also:

$$\frac{\partial}{\partial x}\int_o^{\eta}\frac{\partial w}{\partial t}\,dz = -\left[\frac{\eta^2}{2}\frac{\partial}{\partial x}\left[\frac{\partial^2 U}{\partial x\partial t}\right] + \eta\frac{\partial^2}{\partial x^2}\left[\frac{h\partial U}{\partial t}\right]\right] =$$

$$-\left[\frac{2\eta}{2}\frac{\partial\eta}{\partial x}\frac{\partial}{\partial x}\left[\frac{\partial^2 U}{\partial x\partial t}\right] + \frac{\eta^2}{2}\frac{\partial^2}{\partial x^2}\left[\frac{\partial^2 U}{\partial x\partial t}\right] + \frac{\partial\eta}{\partial x}\frac{\partial^2}{\partial x^2}\left[\frac{h\partial U}{\partial t}\right] + \right.$$

$$\left.\frac{\eta\partial^3}{\partial x^3}\left[\frac{h\partial U}{\partial t}\right]\right] \qquad \text{(E.24)}$$

Therefore:

$$\int_{-h}^{\eta}\frac{\partial}{\partial x}\left[\int_o^{\eta}\frac{\partial w}{\partial t}\,\partial\bar{z} = -(h+\eta)\left[\eta\frac{\partial\eta}{\partial x}\frac{\partial}{\partial x}\left[\frac{\partial^2 U}{\partial x\partial t}\right] + F_x \qquad \text{(E.25)}\right.$$

where $F_x = \frac{\eta^2}{2}\frac{\partial^2}{\partial x^2}\left[\frac{\partial^2 U}{\partial x\partial t}\right] + \frac{\partial\eta}{\partial x}\frac{\partial^2}{\partial x^2}\left[\frac{h\partial U}{\partial t}\right] + \eta\frac{\partial^3}{\partial x^3}\left[h\frac{\partial U}{\partial t}\right]\Big]$

Equation (E.25) is thus the 1-D momentum equation which accounts for vertical accelerations and hence may be called the "quasi 2-D equation". It is evident from the above development of the quasi 2-D momentum equation that the consideration of vertical accelerations does not affect the form of the 1-D continuity equation.

Together with equation (10.1), equation (E.25) is used in the solution system of the numerical model.

REFERENCES

AAGE C. and SAND S. 1984
"Design and Construction of the DHI 3-D Wave Basin"
Proc. Symp. on Description and Modelling of Directional Seas pp20.

AHRENS J.P. 1983
"Wave run-up on idealized structures"
Proc. Int. Conf. on Coastal Structures '83 pp925-938.

ALLSOP N.W.H. and OJA S.I.A.
"Low-crest Rubble Mound Breakwaters"
Proc. Conf. on Hydraulic Modelling of Civil Engineering structures.

ALLSOP N.W.H. 1985
"Low-crest breakwaters - Studies in random waves"
Proc. of Speciality Conf. on Design, Maintenance and Performance of Coastal Structures pp94-107.

ALLSOP N.W.H. 1985
"Probability Distributions and levels of Wave run-up on Armoured Rubble Slopes"
Int. Conf. on Numerical and Hydraulic Modelling of Ports and Harbours pp339-347.

AUSTIN D.I. and SCHLEULER R.S. 1982
"Numerical model of wave/breakwater interactions"
Coastal Engineering Vol III 1982.

ARIS R.
"Mathematical Modelling Techniques"
Pitman 1980.

BENDAT J.S. and PIERSOL A.G. 1971
"Random data : Analysis and Measurement Procedures"
Wiley-Interscience.

BINGHAM G., GODFREY M.D. and TUKEY J.W. 1967
"Modern Techniques of Power Spectrum Estimates"
I.E.E.E. Trans on Audio and Electroacoustics Vol AA-15 pp56-66.

BLACKMAN and TUKEY J.W.
"The Measurement of Power Spectra"
Dove Publications Inc. 1958.

BRACEWELL R.N. 1977
"The FFT and it's application"
McGraw-Hill 1977.

BRIGGS M.J. 1984
"Calculation of Directional Wave Spectra by the MEM of Spectral Analysis"
PCCE Vol 1 1984, 00484-500.

BRITISH STANDARDS BS 6349 PART 1
"Maritime Structures"

BULLOCK G.N. and MURTON G.J. 1987
"Wave Testing of Reflective Coastal Structures"
Advances in Wate Modelling and Measurement BHRA pp353-366.

BULLOCK G.N. and MURTON G.J. 1989
"Performance of a Wedge-Type Absorbing Wave Maker"
Journal of Waterway, Port, Coastal and Ocean Engineering. ASCE ppl-17.

BUHR HANSEN J., SCHILLTER P. and SVENDSEN I.A. 1975
"Laboratory Generation of Waves of Constant Form"
Inst. of Hydrodynamics and Hydraulic Engineering.

CARLSEN C.T. 1984
"Field studies of run-up on dissapative beaches"
PCCE Vol 1 1984 pp399-414

CHAE J. 1979
"The Analysis of Ocean Wave Data - Characteristic Wave Parameters and Design Wave Height"
MSc Thesis, Salford University 1979.

CLARKE P. and FEDLING P. 1981
"MLM Estimation of Direction Wave Spectra"
Proc. Conf. on Directional Wave Spectra Applications pp21-41.

COOLEY J.W. and TUKEY J.W. 1965
"An Algorithm for the Machine Calculation of Complex Fourier Series"
Math. of Computations V Vol 19, pp297-301.

DAKE J.M.K. 1983
"Essentials of Engineering Hydraulics"
Macmillan Press.

DAUBERT O., HAUGEL A. and CABOUET J. 1982
"Waterwaves Calculations by Navier-Stokes Equations"
PCCE Vol 1 1982, pp832-845.

DEACON G.E.R. 1952
"Analysis of Sea Waves in Gravity Waves"
Natl. Bureau Stds. circ. 521 pp209-214.

DOUGLASS S.L. 1984
"Irregular Wave Overtopping Rates"
PCCE Vol 1 1984 pp316-327.

ESTEUA D. 1976
"Wave Direction Computations with 3 Gauge Arrays"
PCCE Vol 1 1976 pp349-367.

GAILLARD P., GAUTHIER M. and HOLLY F. 1980
"Methods of Analysis of Random Wave Experiments with Reflecting Coastal Structures"
PCCE Vol 1 1980 pp204-220.

GILBERT G. and THOMPSON D.M. 1978
"Reflections in Random Waves; the Frequency Response Function Method"
HRS Report IT 173, March 1978.

GILBERT G. 1978
"Absorbing Wave Generators"
HRS Notes No. 20 May 1978.

GODA Y. 1967
"Travelling Wave Crests in Wave Channels"
Appendix to Report 13 Port and Harbours Research Inst.
Ministry of Transport, Japan 1967.

GODA Y. 1974
"Estimation of Wave Statistics from Spectral Information'
Proc. Int. Symp. on Ocean Wave Measurement and Analysis Vol 1.

GODA Y. 1970
"Estimation of Incident and Reflected Waves in Random Wave Experiments"
PCCE Vol 1 1976 pp828-845

GODA Y. 1970
"Numerical Experiments on Wave Statistics with Spectral Simulation"
Report of Ports and Harbours Institute 1970.

GOPALAKRISHNAN T.C. and TUNG C.C. 1980
"Run-up due to Non-breaking Waves - A Finite Element Approach"
Coastal Engineering Vol III 1980 pp3-22.

GRAVESEN H., FREDERIKSEN E. and KIRKEGAORD J. 1974
"Model Tests with Directly Reproduced Nature Wave Trains"
PCCE Vol 1 1974 pp372-385.

HAMER F. and HAMER P. 1982
"Laboratory Experiments on Wave Transmission by Wave Overtopping"
Coastal Engineering Aug. 1982.

HAUGEL A,. LABODIE G. and LATTEUX B. 1982
"A Finite Element Method for the Shallow Water Equation"
PPCE Vol 1 1982 pp617-635.

HAUGEL A. and PECHON P. 1982
"Applications of a Numerical Shallow Water Wave Model"
PPCE Vol 1 1982 pp846-861.

HYDRAULICS RESEARCH LTD., 1980
"Wave Spectrum Synthesisers"

ISOBE M., KONDO J. and HORIKAWA K. 1984
"Extension of MLM for Estimating Directional Spectrum"
Symp. on Description and Modelling of Directional Seas pp14.

IWAGAKI Y. and SAKAI T. 1970
"Horizontal Water Particle Velocity of Finite Amplitude Waves"
PCCE Vol 1 1970 pp304-325.

JEFFERYS E.R., WAREHAM G., RAMSDEN N. and PLATTS M. 1981
"Measuring Directional Spectra with the MLM"
Proc. Conf. on Directional Wave Spectra Applications pp203-219.

JENNINGS D.J. 1978
"The Run-up of Constant Form Sinewaves on Uniform Slopes"
MSc Thesis Salford University 1978.

JENSEN O.J. and SORENSEN T. 1982
"Overspilling /Overtopping of Rubble Mound Breakwaters: Results of Studies useful in Design Procedures"
Coastal Engineering Vol III 1982 pp51-66.

KAJIMA R. 1969
"Estimation of an Incident Wave Spectrum in the Sea Area Influenced by Reflection"
Coastal Engineering in Japan Vol 12 1969 pp9-16.

KAMPHOIS J.W.
"Practical Scaling of Coastal Models"
PCCE 1974

KATAPODES A.M.
"2-D Shallow Water-wave Models"
Jnl Eng. Mech. Div. ASCE. Vol 105 1979.

KIMURA A. and IWAGAKAI Y. 1976
"Random Wave Simulation in an Laboratory Wave Tank"
PPCE Vol 1 1976 pp368-387.

LARSEN J., MADENS P. and ABBOTT M.B. 1984
"Numerical Modelling of Directional Seas in Deep Water"
Int. Symp. on Description and Modelling of Directional Seas.

LAX P. and WENDROFF B.
"Systems of Convolution Labs Comm. in Pure and Applied Mathematics"
Vol 13 1960, pp217-237.

LEMEHAUTE B., DIVEKY D. and LIN A. 1968
"Shallow water waves : A comparison of theories and experiments"
PCCE Vol 1 1968 pp86-106.

LEMEHAUTE B. 1976
"Similitude in Coastal Engineering"
Jnl. of ASCE, Waterways, Harbours and Coastal Engineering Division,
No. 102, pp317-335.

MANSARD E. and FUNKE K. 1986
"A Comprehensive Wave Data Analysis package"
Int. Conf. on Measuring Techniques pp61-74.

MANSARD E. and FUNKE K. 1980
"The Measurement of Incident and Reflected Spectra using a Least Squares Method"
PCCE Vol 1 1980, pp154-172.

MASE H. and IAWAGAKI Y. 1984
"Run-up of Random Waves on Gentle Slopes"
PCCE Vol 1 1984 pp593-609.

MATHAI and RATHIE
"Probability and Statistics"
Macmillan Press 1977

MURTON G.J. 1986
"An Appraisal of a Wave Absorption System"
Report; Deprt. of Civil Engineering Plymouth Polytechnic 1986.

NAGAI J. and TAKODA A. 1982
"Relations between the Run-up and Overtopping of Waves"
Coastal Engineering Vol III 1982 pp 1975-1992.

NUSSBAUMER N.J. 1981
"FFT's and Convolution Algorithms"
Springer-Verby

OCEAN WAVE MEASURE AND ANALYSIS
Int. Sym. on Vol I and II ASCE

OUELLET Y. and EUBANKS P. 1976.
"Overtopping of Rubblemound Breakwaters by Irregular Waves"
PCCE Vol 3 1976 pp2756-2776.

PANICKER N.N. and BORGMAN L.E. 1974.
"Enhancement of Directional Wave Spectrum Estimates"
PCCE Vol 1 1974, pp255-279.

PINKSTER J.A. 1984
"Numerical Modelling of Directional Seas"
Symp. on Description and Modelling of Directional Seas.

PLOEG J. and FUNKE E. 1980
"A Survey or 'Random' Wave Generation Techniques"
PCCE Vol 1 1980 pp135-153.

POLYA G. and LATTA G. 1974
"Complex Variables"
Wiley

RAICHLEN F. and HAMMACK J. 1974
"Run-up due to Breaking and Non-breaking Waves"
PCCE Vol 3 1974 pp1937-1955.

RAYNER R.F. 1983
"Aspects of the Oceanography of Two Mid-Indian Ocean Atolls"
PhD Thesis, Salford University 1983.

ROOS A. and BATTJES J.A. 1976
"Characteristics of Flow in Run-up of Periodic Waves"
PCCE Vol 1 1976 pp781-795.

SAKAI T. and IWAGAKAI Y. 1974
"Transformation of Irregular Waves in Shoaling Water"
PCCE Vol 1 1974 pp412-430.

SALTER S. 1984
"Physical Modelling of Directional Seas"
Symp. on Description and Modelling of Directional Seas.

SALTER S 1981
"Absorbing Wavemakers and Wide Tanks"
Conf. on Directional Wave Spectra Applications pp185-202.

SANDSTRON A. 1974
"Measurement of Incident Wave heights in Composite Wave Trains"
PCCE Vol 1 1974 pp386-391.

SEELIG W.N. 1983
"Wave Reflections from Coastal Structures"
Conf. on Coastal Structures '83 pp961-973.

SEELIG W.N. 1979
"Effects of Breakwaters on Waves: Laboratory Tests of Wave Transmission by Overtopping"
Conf. on Coastal Structures '79.

SEI-IGAI H. and RANG-CHANG H. 1977
"An Analytical and Computer Study of Overtopping"
Coastal Engineering Vol 1 1977 pp221-241.

SHORE PROTECTION MANUAL
U.S. Army Coastal Engineering Research Centre 1977

SILVESTER R.
Coastal Engineering
Elsevier 1974.

SOLLIT D. and DEBOK 1976
"Large-scale Model Tests of Placed Stone Breakwaters"
PCCE Vol 3 1976 pp2572-2588.

SVENDSEN I.A. 1984
"Wave Attenuation and Set-up"
PCCE Vol 1 1984 pp54-69.

SUTHERLAND A.J., SHARMA J.N. and SHEMDIN D.H. 1976
"Wave Run-up on a Simulated Beach"
PCCE Vol 1 1976 pp752-766.

TAKADA A. 1974.
"Estimation of Wave Overtopping Quantities over Seawalls"
PCCE Vol 3 1984 pp1996-2005

TAYLOR C., HUGHES I.E.
"FE Programming of the Navier-Stokes Eqns"
Pineridge Press 1981.

THOMPSON D.M., GILBERT G. and BREWER A.J. 1970
"Design Curves for Regular and Random Wave Generators"
HRS Progress Report 1972.

THOMPSON D.M. and SHUTTLER R.M. 1972
"Signal Generation for Random Wave Generators"
HRS Progress Report 1972.

TUCKER M.J. 1979
"The Analysis and Interpretation of records of Sea Waves Part 2: The Spectral Analysis of 1-D records"
I.O.S. Internal Report 50 1979.

TUCKER M.J. 1984
"Numerical Simulation of a Random Sea : A Common Error and the Effect Upon Wave Group Statistics"
Applied Ocean Research Vol 6 No. 2 pp118-122.

TUCKER M.J.
"The Analysis of Finite Records of Fluctuating Signals"
British Journal of Applied Physics Vol 8 pp137-142.

WANG F.C. and PURPURA J.A. 1974
"Computer Algorithm of Wave Run-up on Beaches"
PCCE Vol 3 1974 pp 1956-1975.

WEBBER N. and CHRISTIAN C. 1974
"A Programmable Irregular Wave Generator"
PCCE Vol 1 1974 pp340-347

WILSON B., SUBRATA K. and SNIDER R. 1974
"Spectrum Analysis of Ocean Wave Records"
Int. Conf. on Wave Data Measurement and Analysis '74 pp87-106

YAMAGUCHI M. and ISOCHUYA Y. 1976
"Wave Shaoling of Finite Amplitude Waves"
PCCE Vol 1 1976 pp497-506

YUEN C.K. and FRASER D. 1979
"Digital Spectral Analysis"
Pitman 1979.

ZIELKE W. 1984
"A Numerical Solution of Boussinesq Type Wave Equations"
PCCE Vol 1 1984 pp1057-1072.

ARIS R.
"Mathematical Modelling Techniques"
Pitman

BOWDEN A.J. et al 1968
"Wave 'set-down' and 'set-up'"
Journal of Geophysical Research No. 73 pp2569-2577

BREBBIA C.A., FERRANTE A.J. 1978
"Computational Methods for the Solution of Engineering Problems"
Pentech Press Plymouth

BAKER A.J. 1983
"Finite Element Computational Fluid Mechanics"
McGraw-Hill New York

INSTITUTION OF CIVIL ENGINEERS 1983
"Breakwaters - Design and Construction"
Thomas Telford London

BULLOCK G.N. and SHORT I. 1985
"The Characteristics of Laboratory Generated Waves"
Waterway, Port, Coastal and Ocean Engieering ASCE.

BRIGHAM E.O.
"The Fast Fourier Transform"
Prentice-Hall New Jersey

DESAI C.S. 1979
"Elementary Finite Element Method"
Prentice-Hall New Jersey

FRYER D.K., GILBERT G. and WILKIE M.J. 1973
"A Wave Spectrum Synthesiser"
Jnl. of Hydraulics Research Vol 2 No. 3 pp193-204.

BRIGHAM E.O.
"The Fast Fourier Transform"
Prentice-Hall, New Jersey

DESAI C.S. 1979
"Elementary Finite Element Method"
Prentice-Hall, New Jersey

FRYER D.K., GILBERT G. and WILKIE M.J. 1973
"A Wave Spectrum Synthesiser"
Jnl of Hydraulics Research Vol 2 No. 3 pp193-204

HERSCHY R.W. 1985
"Streamflow Measurement"
Elsevier Applied Science Publishers.

HAWKES P.J. 1982
"Experimental Study and Computer Simulation of Waves on Beaches"
Ph.D. Thesis University of Liverpool

HIBBERD S. and PEREGRINE D.H. 1979
"Surf and Runup on a beach - a uniform bore"
Jnl of Fluid Mechanics Vol 95 pt 2.

HINTON E. and OWEN D.R.J. 1979
"An Introduction to Finite Elements"
Pineridge Press, Swansea.

KIRKGOZ M.S. 1981
"A theoretical study of plunging breakers and their runup"
Coatal Engineering Vol 5. No. 4

KOBAYASKI N. and REECE A.M. 1983
"Irregular Wave Overtopping on gravel islands"
Jnl. of Waterways, Ports, Coastal and Ocean Eng. Vol 109 No. 4

MILGRAM J.H. 1970
"Active Water-wave Absorbers"
Jnl of Fluid Mechanics Vol 42 pt 4 pp845-859.

MOSKOWITZ L.
"Estimates of the Power Spectrums for Fully Developed Seas for Wind Speeds of 20-40 Knots"
Jnl of Geophysical Research Vol 69 No. 24

OWEN M.W. 1982
"Overtopping of Sea Defences"
HRL Report EX 924.

PACKWOOD A.R. 1980
"Surf and Run-up on Beaches"
PhD University of Bristol

PIERSON W.J.
"The Interpretation of Wave Spectrums in Terms of Wind Profile instead of the Wind Measured at a Constant Height"
Jnl of Geophysical Research, Vol 69 No. 24

PIERSON W.J. and MOSKOWITZ L
"A proposed spectral form for fully developed wind seas based on the similarity theory of S.A.Kitaigorodskii"
Jnl. of Geophysical Research Vol 69 No. 24.

SAND S.E. 1982
"Optimisation of absorbers for DHI's Offshire Basin by means of 3 gauge reflection procedure"
Int. Report Danish Hydraulics Institute.

SORENSEN T
"Model testing with Irregular Waves"
The Dock and Harbour Authority 54 No. 631.

STIVE M.J.F. 1984
"Energy Dissipation in Waves breaking on gentle slopes"
Coastal Eng. Vol 8 No. 12

TAYLOR C. and HUGHES T.G. 1981
"Finite Element Programing of Navier Stokes Equations"
Pineridge Press, Swansea.

BURNETT D.S.
"Finite Element Analysis from concepts in application"
A T T Bell Laboratories 1987.

JOHNSON L.W. and REISS R.D.
"Numerical Analysis"
Addison-Wesley Publishing Company Inc. 1982.

STEPHENS R.V., SMALLMAN, J.V. and ALLSOP N.W.H.
"Development and applications of a Mathematical Model of Wave action on steep slopes"
HRL 1988.